Aus dem Adolf-Butenandt-Institut der Ludwig-Maximilians-Universität München
Lehrstuhl für Stoffwechselbiochemie
Vorstand: Prof. Dr. rer. nat. Dr. h.c. Christian Haass

Generation of Granulin knock out zebrafish models for frontotemporal lobar degeneration and related disorders by genome editing

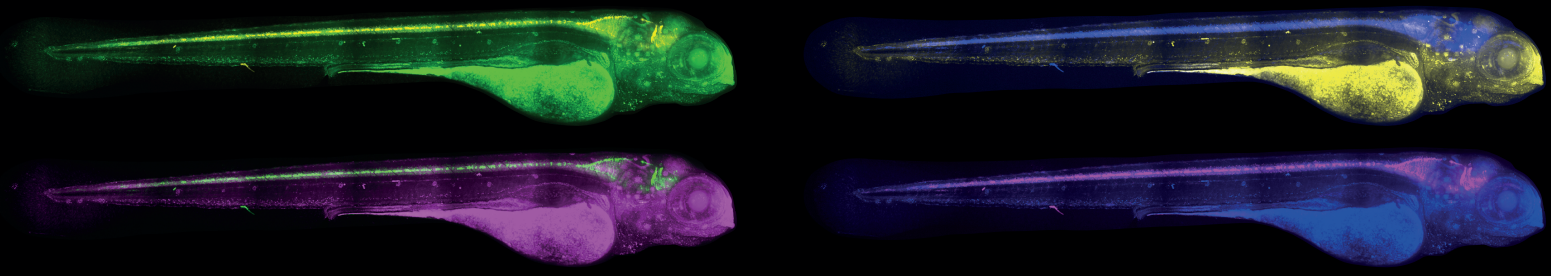

Dissertation
zum Erwerb des Doktorgrades der Naturwissenschaften (Dr. rer. nat.)
an der Medizinischen Fakultät der
Ludwig-Maximilians-Universität München

Vorgelegt von
Barbara Solchenberger
aus Dachau

2014

Gedruckt mit Genehmigung der Medizinischen Fakultät
der Ludwig-Maximilians-Universität München

Betreuer:	Prof. Dr. rer. nat. Dr. h.c. Christian Haass
Zweitgutachter:	Priv. Doz. Dr. rer. nat. Reinhard Obst
Dekan:	Prof. Dr. med. Dr. h.c. Maximilian Reiser, FACR, FRCR
Tag der mündlichen Prüfung:	27.11.2014

Eidesstattliche Versicherung

Ich, Barbara Solchenberger, erkläre hiermit an Eides statt, dass ich die vorliegende Dissertation mit dem Thema

'Generation of Granulin knock out zebrafish models for frontotemporal lobar degeneration and related disorders by genome editing'

selbstständig verfasst, mich außer der angegebenen keiner weiteren Hilfsmittel bedient und alle Erkenntnisse, die aus dem Schrifttum ganz oder annähernd übernommen sind, als solche kenntlich gemacht und nach ihrer Herkunft unter Bezeichnung der Fundstelle einzeln nachgewiesen habe.

Ich erkläre des Weiteren, dass die hier vorgelegte Dissertation nicht in gleicher oder ähnlicher Form bei einer anderen Stelle zur Erlangung eines akademischen Grades eingereicht wurde.

München, den 14.07.2014

(Barbara Solchenberger)

Für meine Eltern

Table of contents

List of figures

List of tables

List of abbreviations

aa	amino acid
AABA	α-aminobutyric acid
AD	Alzheimer's disease
AGM	dorsal aorta in the aorta-gonad-mesonephros
ALM	anterior lateral plate mesoderm
ALS	amyotrophic lateral sclerosis
AO	acridine orange
ApoA-I	apolipoprotein A-I
Apoeb	apolipoprotein Eb
APS	ammonium persulfate
ATP13A2	ATPase type 13A2
bp	base pair
bvFTD	behavioural variant frontotemporal dementia
C. elegans	*Caenorhabditis elegans*
$CaCl_2$	Calcium chloride
Cas9	CRISPR-associated 9
ChIn	chemically induced inflammation
CHMP2B	chromatin-modifying protein 2B
CHT	caudal hematopoietic tissue
CLEAR	coordinated lysosomal expression and regulation
CLN	ceroid lipofuscinosis neural protein
CNS	central nervous system
CO_2	carbon dioxide
CRISPR	clustered regularly interspaced short palindromic repeats
crRNA	CRISPR RNA
CTSD	cathepsin D
CTSF	cathepsin F
$CuSO_4$	copper sulfate
DA	dorsal aorta
dATP	deoxyadenosine triphosphate
dCTP	deoxycytosine triphosphate
DEPC	diethylpyrocarbonate
dGTP	deoxyguanosine triphosphate
DLAV	dorsal longitudinal anastomotic vessels
DMEM	Dulbecco's Modified Eagel's Medium
DMSO	dimethyl sulfoxide

DNA	deoxyribonucleic acid
DNAJC5	DnaJ homolog subfamily C member 5
dNTP	deoxynucleoside triphosphates
DTT	dithiothreitol
dTTP	deoxytyrosine triphosphate
dpf	days post-fertilization
DPR	dipeptide-repeat
DSB	double-strand breaks
ECs	endothelial cells
EDTA	ethylenediaminetetraacetic acid
EGFP	enhanced GFP
Eif4a1b	eukaryotic translation initiation factor 4A, isoform 1B
Eif5	eukaryotic translation initiation factor 5
ELISA	enzyme-linked immunosorbent assay
EMPs	erythromyeloid progenitors
ENU	N-ethyl-N-nitrosouresa
ER	endoplasmic reticulum
ERK	extracellular regulated kinase
EST	expressed sequence tag
EWS	Ewing's sarcoma
FACS	fluorescence-activated cell sorting
FBS	fetal bovine serum
Fli1a	friend leukemia integration 1a
FLNC	filamin C
Flnca	filamin Ca
Flncb	filamin Cb
FTLD	frontotemporal lobar degeneration
FTLD-TDP	FTLD with TDP43-positive inclusions
FUS	fused in sarcoma
Gal4	yeast transcription activator protein Gal4
Gfap	glial fibrillary acidic protein
GFP	green fluorescent protein
GRN	granulin
Grn1	granulin 1
Grn2	granulin 2
Grna	granulin A
Grnb	granulin B
gRNA	guide RNA

GSK-3β	glycogen synthase kinase-3 β
GuHCl	guanidine hydrochloride
H_2O_2	hydrogen peroxide
HDL	high density lipoprotein
HDR	homology-directed repair
H_2O	water
hpa	hours post amputation
hpf	hours post-fertilization
HRP	horseradish peroxidase
HSCs	hematopoietic stem cells
IGF-1	insulin-like growth factor 1
IL-6	interleukin 6
IMC	intermediate cell mass
IMI	Institute of Molecular Immunology
ISV	intersegmental blood vessels
KCl	potassium chloride
KCTD7	potassium channel tetramerization domain containing 7
kDa	kilo-Dalton
KD	knock-down
KH_2PO_4	Monopotassium phosphate
KI	knock-in
KO	knock-out
LAMP	lysosomal-associated membrane protein
liq. N_2	liquid nitrogene
LPM	lateral plate mesoderm
Luc	luciferase
lynEGFP	membrane-localized variant of EGFP
Lyz	lysozyme
mAb	monoclonal antibody
MAPK	mitogen activated protein kinase
MAPT	microtubule-associated protein tau
Met	methionine
MFSD8	major facilitator superfamily domain containing 8
$MgCl_2$	magnesium chloride
$MgSO_4$	magnesium sulfate
MMP	matrix metallopeptidase
MND	motor neuron disease
MO	morpholino

MPC	myogenic progenitor cells
Mpeg1	macrophage-expressed gene 1
MPX	myeloid-specific peroxidase
mRNA	messenger RNA
mTORC1	mammalian target of rapamycin complex 1
MW	molecular weight
NaCl	sodium chloride
Na_2HPO_4	disodium hydrogen phosphate
NaN_3	sodium acid
NaOAc	sodium acetate
NCL	neuronal ceroid lipofuscinosis
NCS	newborn calf serum
ND	neurodegnerative disease
NHEJ	non-homologous end joining
NMD	nonsense mediated mRNA decay
o/n	overnight
OPTN	optineurin
ORF	open reading frame
OVA	ovalbumin
PAGE	polyacrylamide gel electrophoresis
PAM	protospacer adjacent motif
PAS	Periodic acid-Schiff
PB	phosphate buffer
PBI	posterior blood island
PBS	phosphate buffered saline
PCR	polymerase chain reactions
preTT	premature translation termination
PFA	paraformaldehyde
PI	protease inhibitor
PI3K	phosphatidyl inositol-3 kinase
PLM	posterior lateral plate mesoderm
PNFA	progressive nonfluent aphasia
PPA	primary progressive aphasia
PPT1	palmitoyl protein thioesterase 1
PTU	phenylthiourea
PTZ	pentylenetetrazole
qPCR	quantitative PCR
RAN	repeat-associated non-ATG

RBI	rostral blood island
RE	restriction endonucleases
RGEN	RNA-guided endonuclease
RNA	ribonucleic acid
ROS	reactive oxygen species
RT	room temperature
Saposin	sphingolipid activator protein
SCMAS	subunit c of mitochondrial ATP synthase
SD	semantic dementia
SD	standard deviation
SDS	sodium dodecyl sulfate
S.E.M.	standard error of the mean
SFFV	spleen focus forming virus
SLPI	secretory leukocyte protease inhibitor
SORT1	sortilin 1
SP	signal peptide
spi1b	spleen focus forming virus (SFFV) proviral integration oncogene spi1b
SQSTM1	sequestosome 1
STAT3	signal transducer and activator of transcription 3
TAF15	TATA-binding protein-associated factor
TALE	transcription activator-like effector
TALEN	transcription activator-like effector nuclease
TAR	transactive response
TARDBP	TAR-DNA-binding protein
TARDBPL	TAR-DNA-binding protein like
TBP	TATA-binding protein
TDP-43	TAR-DNA-binding protein of 43kDa
TEMED	tetramethylethylenediamine
TFEB	transcription factor EB
TILLING	targeted induced local lesions in genomes
TMEM106b	transmembrane protein 106B
TNFα	tumor necrosis factor α
TNFR	TNF receptor
TPP1	tripeptidyl peptidase 1
tracrRNA	trans-activating crRNA
TREM2	triggering receptor expressed on myeloid cells 2
UBQLN2	ubiquilin 2
UAS	upstream activation sequence

VCP	valosin-containing protein-1
VDA	ventral wall of the dorsal aorta
wpf	weeks post-fertilization
wt	wildtype / wildtypic
zf-Grn's	zebrafish granulins (Grna, Grnb, Grn1 and Grn2)
ZF	zinc-finger
ZFN	zinc-finger nuclease

1 Abstract

The neurodegenerative disease frontotemporal lobar degeneration (FTLD) is characterized by a progressive loss of neurons in the frontal and temporal lobes leading to behavioural abnormalities and language impairment. Granulin (GRN), a secreted glycoprotein, is genetically linked to FTLD with cytosolic TAR-DNA-binding protein 43 (TDP-43) and ubiquitin-positive deposits. FTLD patients carry heterozygously a loss of function mutation in *GRN* and interestingly, homozygous mutation carrier that lack GRN completely, develop neuronal ceroid lipofuscinosis (NCL), a lysosomal storage disorder and neurodegenerative disease. Despite great efforts in the last years, the role of GRN in health and disease is still largely elusive.

To unravel GRN's physiological function, this study aimed to establish a zebrafish GRN loss of function animal model. I generated mutants in both zebrafish GRN orthologues, *granulin a* (*grna*) and *granulin b* (*grnb*), using the zinc finger nuclease technology for genome editing. I confirmed that all *grna* and *grnb* mutant alleles generated result in a strong reduction of mRNA expression and a complete loss of protein.

Grna and Grnb single and double knock out (KO) zebrafish are viable and fertile, lack obvious morphological phenotypes, and develop normally. Examination of the mutants for previously reported knock down phenotypes did not confirm spinal motor neuron axonopathies or a reduced number of myogenic progenitor cells. Moreover, there are no signs of phenotypic alterations in the developing vasculature. Analysing the Grna;Grnb double KO zebrafish for disease-related phenotypes and molecular changes known from FTLD patients or Grn-deficient mice like neurodegeneration, microgliosis, lipofuscinosis, lysosomal dysfunction, or behavioural phenotypes did not reveal any phenotypic or molecular alterations in the mutants. Like mammalian GRN, zebrafish *granulins* are increased after an injury, but despite this increase, the regeneration as well as the immune response after tail fin amputations were not affected in Grna;Grnb KO zebrafish larvae.

In summary Grna and Grnb loss of function mutants were successfully generated. Phenotypes described in Grna or Grnb morphants as well as GRN-deficient mammals and patients were absent in Grna;Grnb KO zebrafish. Investigations of injured, adult Grna;Grnb-deficient zebrafish brains might suggest a novel physiological function of Grna and Grnb.

2 Zusammenfassung

Die neurodegenerative Erkrankung Fronto-Temporal-Lappen-Degeneration (FTLD) zeichnet sich durch einen progressiven Verlust von Neuronen im Frontal- und Temporal-Lappen aus. Dies führt zu Verhaltensauffälligkeiten und Sprachstörungen. *Granulin* (*GRN*), ein sezerniertes Glykoprotein, wird genetisch mit einer Form der FTLD in Verbindung gebracht, die sich durch TAR-DNA-bindendes Protein 43 (TDP-43) sowie Ubiquitin-positive Ablagerungen im Zytosol auszeichnet. Patienten mit FTLD tragen heterozygot eine Funktionsverlust (KO)-Mutation in ihrem Genom. Interessanterweise entwickeln homozygote Träger einer KO-Mutation, die lysosomale Speicherkrankheit neuronale Zeroidlipofuszinose, die auch eine neurodegenerative Erkrankung ist. Trotz intensiver Forschung in den letzten Jahren ist die Rolle von GRN im gesunden Menschen und bei den genannten Erkrankungen noch weitgehend unklar.
Das Ziel dieser Arbeit war es, ein GRN defizientes Zebrafisch-Tiermodell zu entwickeln und die physiologische Funktion von GRN zu ermitteln. Zur Generierung GRN defizienter Zebrafishmutanten habe ich die Orthologen von GRN, *granulin a* (*grna*) und *granulin b* (*grnb*), mit Hilfe der Zinkfinger Nuklease Technologie gezielt genetisch modifiziert. Ich konnte zeigen, dass alle generierten mutierten Allele zu einer starken Reduktion der mRNA und zum Verlust des jeweiligen Proteins führen.
Die Grna und Grnb Einzel- wie auch Doppelmutanten sind lebens- und vermehrungsfähig, und sie entwickeln keine offensichtlichen morphologischen Auffälligkeiten. Nach einem partiellen, temporären Funktionsverlust (KD) beschriebene Phänotypen, wie ein verändertes Auswachsen der Motoneuronaxone oder eine reduzierte Anzahl von Muskelvorläuferzellen, konnten bei Untersuchungen in den Einzel- und Doppelmutanten nicht bestätigt werden. Auch die Struktur der Blutgefäße ist nicht verändert. Phänotypische und molekulare Veränderungen, die in FTLD Patienten und Grn-defizienten Mäusen beschrieben wurden, wie Neurodegeneration, Mikrogliose, Lipofuszinose, lysosomale Dysfunktion und Verhaltensveränderungen, treten in den Grna;Grnb KO-Mutanten nicht auf. Wie auch in Säugetieren werden die Zebrafisch *granuline* nach einer Verletzung verstärkt exprimiert. Trotz dieses Anstiegs ist die Regeneration und die Immunantwort nach einer Schwanzflossenamputation in Grna;Grnb Doppelmutanten nicht verändert.
Im Rahmen dieser Doktorarbeit wurden erfolgreich Grna und Grnb KO-Mutanten generiert. Bereits in Patienten, Grn-defizienten Mäusen und KD Zebrafischen beschriebene Phänotypen treten in diese KO-Mutanten nicht auf. Untersuchungen in Gehirnen von erwachsenen Grna;Grnb Doppelmutanten nach Verletzung deuten jedoch auf eine bisher unbekannte physiologische Funktion von Grna und Grnb hin.

3 Introduction

Neurodegenerative diseases like Alzheimer's disease (AD) and frontotemporal lobar degeneration (FTLD) are characterized by a progressive loss of neurons leading to a loss of memory or changes in behaviour, respectively. Amongst the main risk factors to develop neurodegenerative diseases is ageing. According to a collaborative analysis by Alzheimer Europe, the prevalence to be diagnosed with a neurodegenerative disease is 0.6% for people between 60-64 years of age and 41.0% in the age group of 90-94 (http://www.alzheimer-europe.org/Research/European-Collaboration-on-Dementia/Prevalence-of-dementia/Prevalence-of-dementia-in-Europe) . Therefore, all ageing societies are facing a tremendous medical, social, and economical burden, as the rate of neurodegenerative disease incidence rises in the decades ahead. For 2008 it was estimated that 10.11 million people in Europe suffered from dementia generating total costs of illness estimated to 177 billion euro (Wimo et al., 2011). The awfulness of neurodegenerative diseases and the increasing financial burden urge scientists and societies all over the world to learn more about these, so far incurable diseases, to find treatments and one day a cure.

Understanding the underlying pathomechanisms is of tremendous importance when seeking for a cure. To understand what is happening in patients suffering from a disease model systems are used. Amongst these animal models, with all cell types present, fill a major gap between cell culture model systems and human patients. In the past animal models have proven to provide useful insights in disease pathomechanisms (e.g.Gutierrez et al., 2014; Mahmood et al., 2013a; Partanen et al., 2008; Ralph et al., 2005). Moreover, they offer the opportunity to disclose possible adverse events upon pharmacological treatment also in body tissues that are not directly affected by the disease (e.g.Strähle and Grabher, 2010). A unique feature of (neuro)degenerative diseases is the progressive degradation of the affected tissue precluding a detailed examination at the time of death. Therefore, animal models that mimic disease progress, disease-related phenotypes, and biochemical changes are of vital importance in understanding triggers and courses of neurodegenerative diseases in humans.

3.1 Aim of the project

The aim of this PhD thesis is to establish an animal model for the neurodegenerative diseases FTLD and neuronal ceroid lipofuscinosis (NCL) providing a model to decipher pathomechanisms and identify drugs that ameliorate or cure these diseases. FTLD and NCL have in common that they are both genetically linked to loss of function mutations in *Granulin* (*GRN*) (Baker et al., 2006; Cruts et al., 2006; Shankaran et al.,

2008; Smith et al., 2012). To mimic the partial loss of GRN-function in FTLD and the complete loss of function in NCL, I will generate a GRN loss of function animal model. I will work in this study with the zebrafish a frequently used vertebrate model organism that is genetically modifiable and due to the high number of offspring very suitable for large-scale compound screens (Esterberg et al., 2013; Gutierrez et al., 2014). To provide a basis for this study, tools for the detection of zebrafish Granulin e.g. zebrafish specific antibodies should be developed. A basic characterization of the expression pattern of zebrafish *granulin* should follow. Thereafter, zebrafish Granulin loss of function mutants should be generated by genome editing using the zinc finger nuclease technology. After successful generation of loss of function mutants, these should be analysed for phenotypical and biochemical alterations. Thereby the focus will be on the validation of phenotypes and molecular changes that were previously reported from patients suffering from FTLD or NCL with underlying *GRN* mutations or other GRN-deficient animal models. Moreover, the expression pattern of zebrafish *granulin* should be considered in the analysis of the mutants. Apart from being an animal model for FTLD and NCL caused by GRN-deficiency, these zebrafish mutants will also provide insights in the physiological function of zebrafish Granulin.

In the following the two neurodegenerative diseases important for this project, FTLD and NCL, are briefly described. Then the protein central to this study, GRN, is introduced and data available from GRN-deficient patients and model organisms is summarised. Thereby, the data provided by the literature about (zebra)fish Granulin will be explained in detail. Subsequently, the immune cells present during zebrafish development and available transgenic zebrafish lines as well as wounding assays performed in this study are introduced. Finally, genome editing technologies in zebrafish are described.

3.2 Frontotemporal lobar degeneration

The term FTLD summarises brain atrophies in the frontal and temporal lobes that can manifest in heterogeneous clinical symptoms including behaviour and language dysfunction (Premi et al., 2012). FTLD accounts for 5-15% of all dementias and in individuals younger than 65 it is the second most common cause of dementia after AD (Pan and Chen, 2013; Rademakers et al., 2012). Duration of illness depends mostly on the underlying pathologies and varies from 2-20 years (Hodges et al., 2003; Pan and Chen, 2013). Until today there is no cure for FTLD. Treatment of patients with FTLD symptoms involves a combination of symptomatic pharmacological therapy with e.g. behavioural and physical modification techniques (Seltman and Matthews, 2012).

3.2.1 FTLD clinical classification and characteristics

Clinically the FTLD syndrome is divided into the following subtypes: behavioural variant frontotemporal dementia (bvFTD), progressive nonfluent aphasia (PNFA), and semantic dementia (SD) (Premi et al., 2012; Seltman and Matthews, 2012). Additionally, FTLD and motor neuron diseases (MND) / amyotrophic lateral sclerosis (ALS) (FTLD-MND or FTLD-ALS) as well as extrapyramidal movement disorders (parkinsonism or corticobasal syndrome) show a significant clinical, pathological, and genetic overlap with FTLD (Rademakers et al., 2012; Seltman and Matthews, 2012). The most common variant amongst all FTLD cases is bvFTD. Patients show progressive changes in personality and behaviour e.g. disinhibition and decline in executive function. The atrophy in bvFTD occurs predominantly in the frontal lobe. In PNFA and SD, which can be summarised by the umbrella term primary progressive aphasia (PPA), atrophy occurs primarily in the temporal lobe and is at first asymmetrical. Patients diagnosed with PNFA have difficulties expressing themselves using language and/or motor speech deficits, but language comprehension is largely retained. In SD cases, the latter is impaired, whereas speech production remains unaffected. A clear clinical classification of bvFTD, PNFA, and SD can be difficult due to considerable overlap, especially in advanced stages of the disease (Pan and Chen, 2013; Seltman and Matthews, 2012).

3.2.2 FTLD neuropathology and associated genes

The aggregation of specific proteins is a common feature of neurodegenerative diseases and allows to distinguish different neurodegenerative diseases sometimes not possible after a clinical examination only. FTLD can also be subclassified into categories according to the proteins that are predominantly found in pathological brain deposits. These proteins are microtubule-associated protein tau (MAPT), TAR-DNA-binding protein 43 (TDP-43), and the FET family proteins, Fused in sarcoma (FUS), Ewing's sarcoma (EWS), and TATA-binding protein-associated factor (TAF15). Accordingly, the corresponding categories are: FTLD-TAU, FTLD-TDP, and FTLD-FET/FTLD-FUS (Pan and Chen, 2013; Seltman and Matthews, 2012). 25-50% of FTLD cases present a positive family history (Rademakers et al., 2012) and the proteins aggregating correlated with the underlying genotype. Mutations in *MAPT* were the first identified to cause FTLD. They account for 5-20% of familial FTLD and patients carry tau aggregates in their brain, which are toxic to the cell (Hardy and Rogaeva, 2013; Rademakers et al., 2012). Interestingly, tau deposits are also found to aggregate in the brain of AD patients (Selkoe, 2011). A haploinsufficency in *GRN* accounts for 5-20% of familial and 1-5% of sporadic FTLD cases (Baker et al., 2006; Cruts et al.,

2006; Rademakers et al., 2012). In these patients ubiquitin-positive TDP-43 deposits are characteristic (Neumann et al., 2006). Rare missense mutations or truncations are also found in *valosin-containing protein-1* (*VCP*), *chromatin-modifying protein 2B* (*CHMP2B*), *sequestosome 1* (*SQSTM1*) (p62), *optineurin* (*OPTN*) and *ubiquilin 2* (*UBQLN2*) (Deng et al., 2011; Holm et al., 2007; Ito et al., 2011; Kamada et al., 2013; Le Ber et al., 2013; Rubino et al., 2012; Watts et al., 2004). Mutations is all these genes lead, like mutations in *GRN*, to TDP-43 and/or ubiquitin binding protein p62-positive aggregates and the pathomechanism is likely linked to autophagy or lysosomal pathways (Hardy and Rogaeva, 2013; Pikkarainen et al., 2008; Rademakers et al., 2012). TDP-43 is a nuclear DNA/RNA binding protein that shuttles between the nucleus and the cytosol. In healthy patients TDP-43 is predominantly found in the nucleus (Dormann and Haass, 2011). Under pathological conditions some cells, however, show abnormal TDP-43 deposits in the cytosol combined with a nuclear clearance of TDP-43 (Neumann et al., 2006, 2009). Additionally, it was demonstrated that pathological TDP-43 is hyperphosphorylated, ubiquinated, and N-terminally truncated (Dormann and Haass, 2011; Neumann et al., 2006). Until today it is not completely solved how mutations in such diverse genes can result all in the same neuropathology, namely TDP-43 deposits. In 2011, two groups reported independently that a GGGGCC hexanucleotide repeat expansion in the non-coding region of *C9ORF72* is a disease-causing alteration on chromosome 9p21 in ALS and FTLD (Dejesus-Hernandez et al., 2011; Renton et al., 2011). *C9ORF72* repeat expansions account for 21% of familial and 6% of sporadic FTLD cases and are, together with mutations in *GRN*, the most common genetic cause of FTLD (Rademakers et al., 2012). As possible disease-causing mechanisms of the *C9ORF72* repeat expansion, several hypotheses are currently discussed. One possibility is a toxic gain of function by the sequestration of RNA binding proteins in RNA foci (Dejesus-Hernandez et al., 2011; Lee et al., 2013) or repeat-associated non-ATG (RAN) translation of the GGGGCC expansion in dipeptide-repeat (DPR) proteins (Ash et al., 2013; Mori et al., 2013). The other possibility is a loss of function mechanism, as the *C9ORF72* mRNA is reduced to 50% in mutation carrier (Dejesus-Hernandez et al., 2011). Besides genes, which carry mutations that are causative for FTLD, there are also mutations in genes that increase the risk to develop FTLD. Among these are mutations in *transmembrane protein 106B* (*TMEM106b*) a protein that localises to late endosomes/lysosomes (Lang et al., 2012; van der Zee et al., 2011) and the recently identified mutations in the *triggering receptor expressed on myeloid cells 2* (*TREM2*) gene, which is involved in the immune response (Borroni et al., 2014; Guerreiro et al., 2013).

3.3 Neuronal ceroid lipofuscinosis

Besides FTLD-TDP loss of function mutations in *GRN* were also identified to cause NCL. In contrast to FTLD-TDP patients with *GRN* mutations (FTLD-TDP/*GRN*), NCL patients carrying a mutation in *GRN* (NCL/*GRN*) are homozygous for the loss of function mutation (Smith et al., 2012).
The term NCL summarises a group of inherited disorders that are on the one hand characterized by neuronal loss in brain and retina, and on the other hand by the accumulation of intracellular lipopigments. In childhood NCL is the most frequent neurodegenerative and lysosomal disease, whereas in adulthood it accounts for only a minor amount of these two diseases (Anderson et al., 2013). Until today there is no cure for NCL and therapies for NCL patients are so far only palliative (Schulz et al., 2013).

3.3.1 NCL clinical classification and characteristics

Previously, NCL was classified depending on the disease onset into congenital, infantile, late infantile, juvenile, and adult NCL or according to the person who first described it e.g. Batten disease (Schulz et al., 2013; Warrier et al., 2013). Since it became more and more obvious that NCL is genetically quite heterogeneous, the current nomenclature considers the mutated gene and the disease onset (Schulz et al., 2013). The main symptoms are visual failure, dementia, motor deterioration, and epilepsy, due to the massive neuronal loss, leading finally to premature death (Schulz et al., 2013; Warrier et al., 2013). The order of symptom occurrence is variable and depends on the genes involved as well as the disease onset (Schulz et al., 2013).

3.3.2 NCL neuropathology and associated genes

One of the hallmarks of NCL is the accumulation of intracellular, autofluorescent storage material that resembles the lipopigments ceroid and lipofuscin. These storage bodies contain subunit c of mitochondrial ATP synthase (SCMAS) or sphingolipid activator proteins (Saposin) A and D as well as lipids of lysosomal/endosomal origin (Palmer et al., 2013). Since storage bodies do also occur in extracerebral tissues, storage bodies in biopsies from NCL patients are visualized by microscopy for diagnosis and characterization (Anderson et al., 2013). NCL is mostly inherited in an autosomal recessive manner (Warrier et al., 2013). The genes known that carry mutations that are causative for NCL are: *palmitoyl protein thioesterase 1* (*PPT1*), *tripeptidyl peptidase 1* (*TPP1*), *ceroid-lipofuscinosis, neuronal 3* (*CLN3*), *DnaJ homolog subfamily C member 5* (*DNAJC5*), *CLN5*, *CLN6*, *major facilitator superfamily domain containing 8* (*MFSD8*),

CLN8, *cathepsin D* (*CTSD*), *GRN*, *ATPase type 13A2* (*ATP13A2*), *cathepsin F* (*CTSF*), and *potassium channel tetramerization domain containing 7* (*KCTD7*). These genes code for proteins that are very heterogenous in their functions. For example PPT1, TPP1, CTSD, and CTSF are lysosomal enzymes and *CLN3*, *CLN6*, *CLN7*, and *CLN8* code for transmembrane proteins. How these genetic defects in genes coding for such diverse proteins can lead to such similar clinical manifestation, is still not understood. Despite the identification of NCL causing genes the disease mechanisms underlying NCL remain to be solved (Palmer et al., 2013; Schulz et al., 2013; Warrier et al., 2013).

3.4 Granulin and its diverse functions

The protein central to this study is GRN, a pleiotrophic protein that was discovered independently in several processes in the early 1990s. Therefore, it is also known as proepithelin, progranulin, 88kDa glycoprotein, and PC cell-derived growth factor (Bateman et al., 1990; Kleinberger et al., 2013). The 593 amino acid secreted glycoprotein with seven and a half granulin domains is encoded by the *GRN* gene on chromosome 17 (De Muynck and Van Damme, 2011). Due to complex glycosylation it migrates in a denaturing gel electrophoresis at 75-90kDa, which is higher than the calculated molecular weight (MW) of 68.5kDa (Kleinberger et al., 2013). The unique nature of the granulin domains is their 10-12 cysteine-containing motif (X_{2-3} CX_{5-6} CX_5 CCX_8 CCX_6 CCX_5 CCX_5 CX_{5-6} CX) (Nguyen et al., 2013). GRN is a proprotein that can be cleaved in the linker regions between the granulin domains into individual granulin peptides by proteases, like neutrophil elastase, proteinase 3, and matrix metallopeptidases (e.g. MMP-9). This proteolytic processing can be inhibited by binding of secretory leukocyte protease inhibitor (SLPI) or high density lipoprotein (HDL)/apolipoprotein A-I (ApoA-I) (Okura et al., 2010). It is believed that GRN and the granulin peptides are both functional (De Muynck and Van Damme, 2011; Kleinberger et al., 2013; Nguyen et al., 2013). It was shown, for example, that GRN exhibits anti-inflammatory, whereas the granulin peptides exhibits pro-inflammatory properties (Zhu et al., 2002).
Even though altered GRN levels are reported from several pathologic conditions, e.g. cancer, inflammation, or neurodegeneration (Baker et al., 2006; Cruts et al., 2006; Ong and Bateman, 2003; Toh et al., 2011), its exact role and signaling mechanisms are still elusive. An overview of the diverse possible functions of GRN is given below.

3.4.1 GRN in neurodegenerative diseases

Genetic linkage studies comparing case and control groups, genetically linked mutations in *GRN* to FTLD. Haploinsufficiency was suggested as the underlying disease mechanism

since all FTLD patients are heterozygous for loss of function mutations in *GRN* (Baker et al., 2006; Cruts et al., 2006; Shankaran et al., 2008). A total of 149 mutations, distributed over the whole *GRN* gene, were identified so far. 69 of these mutations are documented loss of function mutations that lead to FTLD (http://www.molgen.ua.ac.be/ADMutations/default.cfm?MT=0&ML=0&Page=Home) (Cruts et al., 2012). FTLD-TDP/*GRN* patients show ubiquitin-positive TDP-43 inclusions in affected brain regions (Neumann et al., 2006). Another linkage analysis identified a previously described loss of function mutation in *GRN* in two siblings suffering from NCL. In contrast to the FTLD-TDP/*GRN* patients, the NCL/*GRN* patients were homozygous for the loss of function mutation in *GRN* (Smith et al., 2012). Moreover, it was shown that some missense mutations in *GRN* increase the risk to develop AD and maybe also ALS (Brouwers et al., 2008; Del Bo et al., 2011; Lee et al., 2011; Sleegers et al., 2008). Despite vast efforts in the last years, it is still unclear how less or no GRN can cause neurodegenerative diseases. On the contrary, GRN is upregulated in activated microglia in a number of neurodegenerative diseases including Creutzfeldt-Jakob disease, MND, multiple sclerosis, and AD (Baker and Manuelidis, 2003; Baker et al., 2006; Malaspina et al., 2001; Vercellino et al., 2011). The reasons for that and if this increase has an influence on disease progress are still unknown.

3.4.2 GRN a mitogenic and neurotrophic growth factor

Also many tumor types including liver, renal, brain, breast, prostate, ovarian, and colorectal cancer have in common that the *GRN* expression is elevated (DeMorrow, 2013; He and Bateman, 2003). GRN was shown to have an influence on cell survival, invasiveness, and aggressiveness of the tumor (Frampton et al., 2012; He et al., 2002; Monami et al., 2006). Since increased GRN levels in the plasma correlate with an increased recurrence risk and a decreased overall survival, GRN is discussed as a potential prognostic biomarker in cancer research (Carlson et al., 2013; Han et al., 2011; Serrero et al., 2012). Moreover, it was demonstrated that GRN can stimulate cell growth in the absence of insulin-like growth factor 1 (IGF-1) receptor, confirming that GRN is a potent mitogenic growth factor (Zanocco-Marani et al., 1999). Although it is unclear which receptor mediates GRN signaling in this respect, it was shown that GRN promotes its growth factor activities via the common cell proliferation signaling pathways including mitogen activated protein kinase (MAPK)/extracellular regulated kinase (ERK) and phosphatidyl inositol-3 kinase (PI3K) pathways (Cenik et al., 2012). Despite the numerous studies that observed elevated GRN levels in many tumor types, the reasons remain elusive.

It was furthermore demonstrated in neuronal cell culture that GRN and also some

granulin peptides enhance neurite outgrowth and branching as well as overall neuronal survival (De Muynck et al., 2013; Gass et al., 2012; Van Damme et al., 2008). These neurotrophic activities of GRN that seem to be independent of the possible GRN-receptor Sortilin 1 (SORT1) are mediated via the MAPK/ERK, PI3K/Akt, and glycogen synthase kinase-3 β (GSK-3β) signaling pathways (De Muynck et al., 2013; Gao et al., 2010; Gass et al., 2012; Nedachi et al., 2011; Xu et al., 2011). Additionally, GRN is secreted at the synapse in an activity-dependent manner, thereby regulating synapse number and structure (Petoukhov et al., 2013; Tapia et al., 2011). Whether especially the last function of GRN plays a role in FTLD-TDP/*GRN* or NCL/*GRN* and whether the increased GRN levels in AD are beneficial because of GRNs neurotropic potential remain to be solved.

3.4.3 GRN an anti-inflammatory factor

Amongst other tissues, granulin peptides, the processed form of GRN, were initially purified from human immune cells suggesting roles in inflammation, wound repair, and tissue remodeling (Bateman et al., 1990). Several studies demonstrated that GRN is upregulated after acute or in chronic inflammation in the central nervous system (CNS) and in the periphery (Jian et al., 2012; Lim et al., 2012; Moisse et al., 2009; Naphade et al., 2010; Qiu et al., 2013; Qu et al., 2013; Tanaka et al., 2012; Ungurs et al., 2014; Wang et al., 2011; Youn et al., 2009). These elevated GRN levels are largely assigned to an increase in expression in macrophages or microglia (Moisse et al., 2009; Naphade et al., 2010; Tanaka et al., 2012). Analysis of neurons after an axotomy revealed a slight decrease in GRN levels (Moisse et al., 2009). Administration of GRN to the injured or wounded tissue did improve wound healing and reduced the scar size (Egashira et al., 2013; Guo et al., 2012; He et al., 2003; Kojima et al., 2009). Reduced Grn levels cause, in contrast, an exaggerated inflammatory response and increased levels of the proinflammatory cytokine interleukin 6 (IL-6) (Bossù et al., 2011; Yin et al., 2010a). Moreover, the inflammatory response to a traumatic brain injury in Grn-deficient mice is augmented, when compared to wildtype animals and fractured bones heal slower (Tanaka et al., 2012; Zhao et al., 2013). The strengthened inflammatory boost in injured brains from Grn knock out (KO) mice seems to be caused by an increased lysosomal biogenesis in CD68-positive activated microglia (Tanaka et al., 2012, 2013). Additionally, it was shown that macrophages from Grn KO mice are more phagocytic and Grn-deficient microglia were more toxic to neurons in cell culture, which is probably due to the increased release of pro-inflammatory cytokines of these microglial cells (Kao et al., 2011; Martens et al., 2012). The GRN proprotein was demonstrated to have anti-inflammatory properties, whereas the granulin peptides

have the attribute to be pro-inflammatory. Shifting the equilibrium to one side, has therefore a direct effect on wound healing (Kessenbrock et al., 2011; Ungurs et al., 2014; Zhu et al., 2002). GRN is also capable of blocking tumor necrosis factor α (TNFα) signaling (Okura et al., 2010; Tang et al., 2011; Zhao et al., 2013; Zhu et al., 2002). Whether this is mediated by direct binding to TNF receptor (TNFR) 1 and 2 or indirect is discussed controversially, since the direct binding of GRN to TNFR1 or TNFR2 was not reproduced so far (Chen et al., 2013b; Etemadi et al., 2013; Jian et al., 2013; Tang et al., 2011). It is conceivable that anti-inflammatory and pro-inflammatory properties of GRN and the granulin peptides, respectively, play a role in FTLD-TDP/*GRN* and NCL/*GRN* but how this occurs is still elusive.

3.4.4 GRN an angiogenic factor

Besides being a mitogenic growth factor and involved in inflammation, administration of Grn to transcutaneous wounds did increase the size and number of blood vessels in the wound. Therefore, it was concluded that GRN has angiogenic properties (He et al., 2003). An anti-GRN antibody was demonstrated to reduce the number of microvessels in a hepatocellular tumor model (Ho et al., 2008) indicating an influence in tumor vessel growth. During development *Grn* is expressed in the developing cerebral microvasculature, but apparently not in established blood vessels (Daniel et al., 2003; Petkau et al., 2010). Grn KO mice were shown to be more susceptible to disruptions of the blood brain barrier (BBB) and it was suggested that this is due to cardinal alterations in the microvasculature (Jackman et al., 2013). Even though there are several indications that link GRN to the vasculature, the exact role of GRN in angiogenic processes and vessel stability remain to be clarified. In respect to FTLD-TDP/*GRN* and NCL/*GRN* it is of special interest to learn more about the role of GRN in the microvasculature of the brain and the exact role of GRN on BBB function.

3.4.5 GRN involved in lysosomal function?

Apart from the finding that a lack of GRN in humans leads to NCL/*GRN* (Smith et al., 2012), it was shown that *Grn* expression and protein levels are increased in mouse models of two other lysosomal storage disorders, CLN10 and mucopolysaccharidosis I and IIIB (Götzl et al., 2014; Ohmi et al., 2003). Treating cells with compounds that alkalise the pH of the lysosome or inhibition of the vacuolar ATPase, increased GRN levels, too (Capell et al., 2011). A lysosomal function of GRN was also indicated in other studies. GRN showed up in a proteom analysis for mannose 6-phosphate (M6P) containing lysosomal matrix proteins but a direct binding of GRN to M6P-receptor (M6PR) was not confirmed (Kollmann et al., 2005). These findings are supported

by a second proteom analysis that did indicate a possible binding of GRN to the cation independent M6PR (CIM6PR) (Qian et al., 2008). Interestingly, this CIM6PR also mediates endocytosis of the secreted protein insulin-like growth factor II from the bloodstream (MacDonald et al., 1988). Moreover, a lysosomal function of GRN was proposed in a function prediction model and it was demonstrated that GRN overexpression leads to enlarged lysosomes (Belcastro et al., 2011). The *Grn* promoter region contains two coordinated lysosomal expression and regulation (CLEAR) binding motifs and *Grn* expression is induced upon translocation of transcription factor EB (TFEB) to the nucleus, a key regulator of lysosomal biogenesis (Belcastro et al., 2011; Sardiello et al., 2009; Tanaka et al., 2013). Moreover, it was shown that GRN binds to sortilin (SORT1), a cell surface clearance receptor of neurons, also involved in intracellular protein trafficking (Willnow et al., 2008). It was suggested that upon binding, GRN is endocytosed, and targeted to the lysosomes (Hu et al., 2010; Nykjaer and Willnow, 2012; Zheng et al., 2011). Recent data reveals that lysosomal gene expression and protein levels are increased in Grn KO mice (Götzl et al., 2014; Tanaka et al., 2013), especially after traumatic brain injury (Tanaka et al., 2013). It was postulated that GRN is a negative regulator of excessive lysosomal biogenesis and the following mechanism was suggested: GRN is targeted to the lysosome via SORT1-mediated endocytosis, where it activates mammalian target of rapamycin complex 1 (mTORC1). Thereby, TFEB is phosphorylated and can not translocate to the nucleus. Consequently, lysosomal gene expression is not induced (Tanaka et al., 2013). In neuronal dentrites and axons GRN colocalises with dense-core vesicles, lysosome-related organelles and it was shown that GRN levels have an influence on the secretory vesicle density at the synapse (Marks et al., 2013; Petoukhov et al., 2013; Tapia et al., 2011). Despite the increasing evidence that GRN seems to have a lysosomal function, the exact role of GRN in lysosomal biology and its contribution to the diseases FTLD-TDP/*GRN* or NCL/*GRN* still has to be clarified.

3.5 GRN deficiency in men and mice

If an animal model should be generated to model a human disease as much information from the human pathology as possible is advantageous and also a comparison to phenotypes published in other model systems is of importance in validating the animal model. In the following the phenotypes and biochemical alterations found in GRN-deficient men and mice are summarised.

3.5.1 Neuropathology of GRN-deficient FTLD-TDP and NCL patients

In humans partial GRN deficiency leads to FTLD-TDP and a complete GRN deficiency results in NCL. These two distinct neurodegenerative diseases were not connected until recently. Now there is increasing evidence that also in FTLD-TDP/*GRN* a lysosomal dysfunction is involved the manifestation of pathology (Götzl et al., 2014; Smith et al., 2012).

Patients with FTLD-TDP/*GRN* present clinically a quite heterogenous group with much phenotypic variation of the FTLD symptom spectrum and sometimes overlap of symptoms that are distinctive of other neurodegenerative diseases. Least common features are a frequently asymmetric disease onset and a more pronounced atrophy in the frontal cortex (Kleinberger et al., 2013; van Swieten and Heutink, 2008). Neuropathologically FTLD-TDP/*GRN* patients are characterized by extensive micro- and astrogliosis as well as ubiquitin-positive TDP-43 cytoplasmatic inclusions (Götzl et al., 2014; Mackenzie, 2007; van Swieten and Heutink, 2008). In one study it was shown, that the number of synaptic vesicles at the synapse was increased in the hippocampus of FTLD-TDP/*GRN* patients (Tapia et al., 2011). Frontal cortex sections from mutation carriers revealed an upregulation of Saposin D, CTSD, and lysosomal-associated membrane protein 1 (LAMP1) in neurons and glia, and an upregulation of SCMAS as well as TMEM106B in neurons. Interestingly, all of these are lysosomal proteins (Chen-Plotkin et al., 2012; Götzl et al., 2014). Biochemical studies revealed additionally that *filamin C* (*FLNC*) and *signal transducer and activator of transcription 3* (*STAT3*) expression were increased in brain samples from FTLD-TDP/*GRN* patients and protein levels of FLNC, phospho-TDP-43, Saposin D, LAMP1, LAMP2, and TMEM106B were elevated (J. Banzhaf-Strathmann and J. Janssens, unpublished; Chen-Plotkin et al., 2012; Götzl et al., 2014). The latter are all lysosomal proteins, which indicates lysosomal dysfunction and provides a link to the lysosomal storage disorder NCL.

Clinically the two NCL/*GRN* patients presented typical NCL symptoms and an electron micrograph of a skin biopsy revealed the typical fingerprint profile of intracellular storage material (Smith et al., 2012). In NCL extracerebral tissue is frequently used for diagnosis, as lysosomes throughout the body are dysfunctional and lead to an accumulation of lipofuscin deposits in all cells of the body. Brain samples from NCL/*GRN* patients for neuropathological analysis are not available (Smith et al., 2012).

3.5.2 Phenotypes and biochemical alterations in Grn KO mice

To learn more about FTLD-TDP/*GRN* and NCL/*GRN* and the underlying pathomechanisms, several Grn KO mouse models have been generated independently (Kao

et al., 2011; Kayasuga et al., 2007; Petkau et al., 2012; Wils et al., 2012; Yin et al., 2010a). The mouse orthologue, *Granulin* (*Grn*), codes for a 602 amino acid protein with 7 granulin domains and 79% sequence identity to GRN (Petkau et al., 2012). It was demonstrated that *Grn* is expressed in epithelia, especially in these with a high proliferation rate, and immune cells. In the murine brain it is expressed at high levels by activated microglia and specific neurons, including pyramidal cells of the hippocampus, some cerebral cortical neurons, and cerebellar Purkinje cells, and at low levels in astrocytes and ependymal cells (Ahmed et al., 2007, 2010; Daniel et al., 2000; Petkau et al., 2010). All Grn KO mice are viable, fertile, and produce offspring according to the Mendelian rules (Kleinberger et al., 2013). A reduced lifespan in aged mice was observed in some studies (Ghoshal et al., 2012; Wils et al., 2012), but was not confirmed in other Grn KO mice (Petkau et al., 2012; Yin et al., 2010a). FTLD-related behavioural phenotypes were addressed by behavioural tests. The observed phenotypes in the different KO mice were, however, not consistent (Kleinberger et al., 2013). Some studies agreed on a reduced social interaction in Grn KO mice (Ghoshal et al., 2012; Petkau et al., 2012; Yin et al., 2010b) and it was shown that they have a slightly poorer performance in tests for motor function (Ghoshal et al., 2012; Petkau et al., 2012; Wils et al., 2012). Neuropathological examinations of the different mouse lines revealed more overlap. A pronounced micro- and astrogliosis and the accumulation of ubiquinated proteins as well as increased lipofuscinosis were described in several studies (Ahmed et al., 2010; Ghoshal et al., 2012; Petkau et al., 2012; Wils et al., 2012; Yin et al., 2010a,b). In contrast to human FTLD-TDP/*GRN* patients no cytosolic TDP-43 aggregates were observed in Grn KO mice, but two groups described enhanced phospho-TDP-43 immunoreactivity (Ahmed et al., 2010; Wils et al., 2012; Yin et al., 2010a,b). Furthermore, only one study did observe neurodegeneration in aged Grn KO mice (Ahmed et al., 2010), this was, however, not confirmed in others (Ghoshal et al., 2012; Petkau et al., 2012; Wils et al., 2012). In cortical, hippocampal, as well as thalamic sections from Grn KO mice, neurons and glia were labeled more intensely for Ctsd, Saposin D, and SCMAS (neurons only) (Götzl et al., 2014). Biochemically, Grn homozygous but not Grn heterozygous KO mice had increased *Ctsd*, *Stat3*, and *Flnc* mRNA expression levels and increased Flnc, Saposin D, Ctsd, and TMEM106b protein levels (J. Janssens, unpublished; Götzl et al., 2014; Wils et al., 2012). The accumulation of lysosomal proteins - Saposin D, Ctsd, and TMEM106b - as well as the stronger staining for lysosomal proteins on sections points towards a lysosomal dysfunction typical for NCL models (Götzl et al., 2014). Interestingly, *Flnc*, *Stat3*, *Ctsd*, *Grn*, and *Sort1* were also identified to be upregulated or differentially spliced in a mouse model, where TDP-43 was depleted in the adult brain (Polymenidou et al., 2011), and filamin

Ca (Flnca) and Stat3 were upregulated in *TAR DNA binding protein* (*tardbp*); *tardbp like* (*tardbpl*) double mutant zebrafish (Schmid et al., 2013). Indicating that a lack of functional TDP-43, which is partially trapped in aggregates in FTLD-TDP/*GRN*, might enhance the biochemical alterations in the patients. All observations from Grn KO mice have in common, that they become more pronounced with ageing. Furthermore, neuropathological and biochemical changes were only observed in homozygous Grn KO mice, so far, and not in heterozygous Grn KO mice (Filiano et al., 2013; Götzl et al., 2014). The reasons for the discrepancies between heterozygous FTLD-TDP/*GRN* loss of function carrier and the heterozygous Grn KO mice are still elusive but the fact that human beings become older might play a role. The only observations that were consistent in homozygous and heterozygous Grn KO mice are age-dependent social and emotional deficits (Filiano et al., 2013). Taken together, the homozygous Grn KO mice model some aspects of NCL/*GRN* and it remains to be clarified, if they are also a powerful model for FTLD-TDP/*GRN*. The most recent studies indicate that also in FTLD-TDP/*GRN* a lysosomal dysfunction contributes to the pathology (Götzl et al., 2014; Tanaka et al., 2013), but further studies are needed to clarify the exact pathomechanisms and a model suitable for medium- to high-throughput compound screens is still missing.

3.6 GRN in zebrafish and other non-mammalian models

Since GRN is a secreted protein, it is of great interest to study GRN in the context of multi-cellular model organisms. Mice are the most commonly used model organism to study human diseases, but zebrafish for example are much more suitable for large-scale compound screens, due to their high number of offspring that can be produced from one spawning and their small size. Moreover, zebrafish larvae are translucent and a great model to analyse processes by *in vivo* imaging. *GRN* has evolved early during evolution and genes encoding proteins with granulin motives have been described in commonly used model organisms besides *Mus musculus*, like *Xenopus leavis*, *Caenorhabditis elegans* (*C. elegans*) and *Danio rerio* (Bucan et al., 1996; Cadieux et al., 2005; Kao et al., 2011; Pera et al., 2005).

3.6.1 Phenotypes of GRN-deficient *C. elegans*

The *C. elegans* genome encodes for one GRN, *pgrn-1*, with three granulin domains. Mutants lacking *pgrn-1* produce less progeny and have fewer apoptotic corps. This seems to be due to a more rapid clearance of dying cells (Kao et al., 2011). Moreover, the same mutants are more resistant to osmotic, heat, and endoplasmic reticulum (ER) stress, whereas their response to oxidative or genotoxic stress and pathogen exposure is

not altered (Judy et al., 2013). The mechanisms for that and the translation of these findings to FTLD-TDP/*GRN* or NCL/*GRN* are pending.

3.6.2 GRN and possible functions in fish

In teleost fish granulin-like peptides, which contain $1\frac{1}{2}$ granulin domains, were isolated for the first time from haematopoietic tissue of carp (*Cyprinus carpio*) (Belcourt et al., 1993). One of them, granulin-1, was shown to be produced and to be elevated in carp and goldfish macrophages/monocytes of spleen, head kidney, and peripheral tissues, involved in host defence (Belcourt et al., 1995). Moreover, granulin was identified to be a candidate involved in goldfish macrophage haematopoiesis and macrophage development *in vitro*. The growth factor, *granulin*, is expressed at high levels during the proliferative phase and was suggested to be a positive modulator of macrophage differentiation (Barreda et al., 2004; Hanington et al., 2006). Additionally, *in vitro* treatment of carp head kidney cells with immunostimulants led to increased levels of granulin-like peptides (Sakai et al., 2005).

3.6.2.1 Four GRNs in *Danio rerio*

In contrast to carp and goldfish, the zebrafish (*Danio rerio*) genome harbors four zebrafish *granulins* (zf-*grns*), two short ones, *granulin 1* (*grn1*) and *granulin 2* (*grn2*), and two long ones, *granulin A* (*grna*), *granulin B* (*grnb*), of which the latter are the orthologues of the human and rodent *GRN* (see Fig. 5.1). It was shown that *grna* and *grnb* are maternally provided and expressed throughout development. *grn1* and *grn2* seem not to be maternally provided and expression was only detectable from 30 hours post-fertilization (hpf) onward (Cadieux et al., 2005). All four zf-*grns* are expressed in all adult tissues analysed (Cadieux et al., 2005). *In situ* hybridisation demonstrated that the zf-*grns* are expressed in several tissues of the endoderm and each of them shows a distinct expression pattern (Cadieux et al., 2005). In the CNS, *grna* seems to be expressed around 24hpf at the midbrain-hindbrain boundary, in the tectum, in some structures in the eye (Cadieux et al., 2005) and at 27hpf also by caudal primary motoneurons (Chitramuthu et al., 2010). At these stages and later *grnb* is strongly expressed in forebrain, midbrain, hindbrain, and the eyes and was described to resemble the murine *Grn* expression pattern in the brain (Cadieux et al., 2005). *grna*, *grn1*, and *grn2* but not *grnb* expression can be detected in haematopoietic tissues, like the intermediate cell mass, the pronephric ducts, and leukocytes (Cadieux et al., 2005). *grna* expression is furthermore elevated in cells of the myeloid lineage including microglia when compared to non-myeloid cells (Craig et al., 2008; Zakrzewska et al., 2010). Therefore, *grna* was also used as a microglia specific marker (Huang et al., 2012).

3.6.2.2 A function of zf-*grns* in injury and infection?

grna might be involved in regenerative processes after injuries since it is upregulated after ventricular resection of the adult zebrafish heart (Lien et al., 2006), retinal injury (Craig et al., 2008), and tail fin amputation in zebrafish larvea (Mathew et al., 2009). In adult zebrafish *Mycobacterium marinum*- and *Streptococcus equi ssp zooepidemicus*-infection models, a *granulin* was strongly increased but it remains unclear, which of the four zf-*grns* (Borst et al., 2013; Meijer et al., 2005). All these studies have in common that they describe an upregulation of one or more zf-*grns* after injury or infection but none of them did further address the role of zf-*grns*, especially *grna*, in those processes. These findings clearly indicate a possible function of zf-*grns* in injury, infection, or wound healing and therefore need to be considered in the analysis of the zf-Grn loss of function mutants.

3.6.2.3 Phenotypes of transient zf-Grn deficiency

Several knock down (KD) studies using *grna* or *grnb* morpholinos (MO) are published in zebrafish (Chitramuthu et al., 2010; De Muynck et al., 2013; Laird et al., 2010; Li et al., 2010, 2013; Shankaran et al., 2008). Table 3.1 provides an overview of the transient KD studies published so far. KD of Grnb did not lead to an obvious morphological phenotype and Tardbp/Tardbpl were not mislocalised to the cytosol in injected embryos (Shankaran et al., 2008). Two groups reported independently, that a KD of Grna as well as Grnb results in spinal motor neuron (SpMN) axonopathy (Chitramuthu et al., 2010; De Muynck et al., 2013; Laird et al., 2010). In one of the studies it was stated that the SpMN axons also show premature branching and that *grna* MO-injected embryos have swimming defects in a touch response assay. Interestingly, overexpression of *grna* did also stimulate SpMN axon branching (Chitramuthu et al., 2010). These studies suggest, that especially Grna is required for proper SpMN axon development. Futhermore, KD of Grna decreased the trunk muscle size and the number of myogenic progenitor cells (MPCs) in embryos. Grnb KD decreases the number of embryonic MPCs, too, but to a lower extent. Additionally, muscle-specific overexpression of Grna did increase the myofibre size and enhanced MPCs activation after toxin-induced muscle injury in zebrafish larvae (Li et al., 2013). A KD of Grna results also in an impaired liver morphogenesis (Li et al., 2010). The latter studies suggested that Grna signals via the hepatocyte growth factor receptor, also known as met proto-oncogene (Li et al., 2010, 2013).

Taken together, only the studies describing an hepatic or a muscular phenotype addressed underlying molecular pathways. Signaling mechanisms were not approached in the

Table 3.1 – Overview of GRN deficient zebrafish models and phenotypes described.

Publication	Modification (control of KD)	Phenotype	Rescue by over-expression
Shankaran et al., 2008	Grnb KD, splice grip (RT-PCR)	- no morphological phenotype - no mislocalisation of Tardbp or Tardbpl	n.d.
Li et al., 2010	Grna KD, 5'UTR MOs (control MO, reporter construct, protein expression)	- reduced liver size - reduced proliferation and enhanced apoptosis of liver cells - hepatic MET signaling reduced	Yes - *grna*
Laird et al., 2010	- Grna KD, ATG and 5'UTR MO - Grnb KD, ATG and 5'UTR MO - Grna and Grnb KD, ATG MOs (control MO)	- reduced length of SpMN axons - no mislocalisation of TDP-43	Yes (Grna KD) - human *GRN*
Chitramuthu et al., 2010	- Grna KD, ATG and 5'UTR MO - Grnb KD, 5'UTR MO (Grna: control MO, protein expression)	Grna KD: - neuronal structures in the head disrupted - reduced length of SpMN axons - extended branching of SpMN axons - swimming defects Grnb KD: - severe phenotype - reduced head size	Yes (Grna KD) - *grna* - human *GRN* only SpMN truncation
Li et al., 2013	- Grna KD, 5'UTR MOsLi et al., 2010 - Grnb KD, n.a. (Grna: control MO, protein expression)	Grna KD: - impaired muscle growth - reduced number of MPCs - impaired proliferation and enhanced apoptosis of MPCs Grnb KD: reduced number of MPCs	Yes - *grna*
De Muynck et al., 2013	Grna KD, 5'UTR MO, Laird et al., 2010 (control MO)	reduced length of SpMN axons	No

studies that characterised a SpMN axonopathy. As these studies are only descriptive, the underlying molecular pathways still await to be discovered. In line with the expression pattern of zf-Grns it is suggested to consider also possible immunological or regenerative phenotypes in zebrafish deficient for zf-Grns, which has not been done so far. Unfortunately, KD approaches are limited to early development and all phenotypes in GRN-deficient patients suffering from FTLD-TDP or NCL are medium to late onset and progressive. These kind of phenotypes can only be revealed in stable KO mutants in zebrafish, since only stable mutants allow an analysis in late larval stages and in aged adult zebrafish. Therefore the generation of stable zf-Grn loss of function mutants modeling FTLD-TDP/*GRN* and NCL/*GRN* is urgently needed and of high relevance.

3.7 Zebrafish - a model to study inflammation and regeneration

The expression pattern of zf-*grns* (Borst et al., 2013; Cadieux et al., 2005; Craig et al., 2008; Lien et al., 2006; Mathew et al., 2009; Meijer et al., 2005; Zakrzewska et al., 2010) and data from other teleost fish (Barreda et al., 2004; Belcourt et al., 1993, 1995; Hanington et al., 2006; Sakai et al., 2005) indicate a possible function of zf-Grns in inflammation, wound healing, or regeneration. Moreover, it is known that activated microglia in the mouse brain show elevated Grn levels (Moisse et al., 2009; Naphade et al., 2010; Tanaka et al., 2012). Mammalian and zebrafish immunity have many aspects in common. For example, the crucial genes in haematopoiesis and blood/immune cell types are highly similar, making zebrafish an ideal organism to study the inflammatory response (Jing and Zon, 2011; Renshaw and Trede, 2012). However, in contrast to mammals the zebrafish has, like other non-mammalian vertebrates, the potential to regenerate tissues, like fin, brain, or heart, even as an adult organism. Therefore, zebrafish is an ideal model organism to learn more about the regenerative capacity of vertebrates (Gemberling et al., 2013; Yoshinari and Kawakami, 2011). Zebrafish-specific tools and assays to study the inflammatory response after an injury and the subsequent regeneration are established and some will be introduced here later.

3.7.1 The development of zebrafish immune cells

Blood cells and immune cells are not present during the first hours of the life of a zebrafish embryo. These arise gradually from haematopoietic stem cells (HSCs) in a process termed haematopoiesis, which is defined as the generation of cellular blood from HSCs. Like in mammals, zebrafish haematopoiesis occurs in consecutive waves - the primitive, transient-definitive, and definitive wave (Fig. 3.1). In contrast to mammalian vertebrates, the sites of haematopoiesis are distinct. HSCs in mammals reside, for example, in the bone marrow, whereas HSCs in zebrafish reside in the

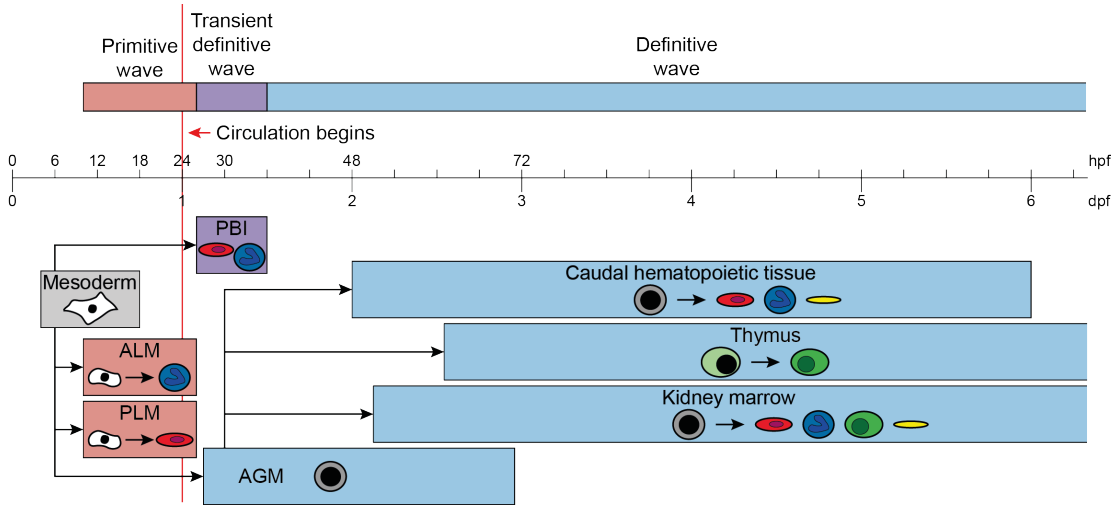

Figure 3.1 – Graphic illustration of the timeline of haematopoiesis in zebrafish. The consecutive waves of zebrafish haematopoiesis are illustrated. Haemangioblasts (white), erythroid cells (red), myeloid cells (blue), definitive HSCs (grey), thromboid cells (yellow), lymphoid progenitor cells (light green), and lymphoid cells (green). ALM: anterior lateral plate mesoderm. PLM: posterior lateral plate mesoderm. PBI: posterior blood island. AGM: dorsal aorta in the aorta-gonad-mesonephros. Modified from Jing and Zon (Jing and Zon, 2011)

kidney marrow, the main haematopoietic tissue in zebrafish (Jing and Zon, 2011; Sood and Liu, 2012). All haematopoietic cells in zebrafish are of mesodermal origin (Fig. 3.1, grey box). Primitive haematopoiesis starts around 12hpf in the lateral plate mesoderm (LPM). Uni-potent haemangioblasts populate the anterior LPM, which later becomes the rostral blood island (RBI), and the posterior LPM, which gives later rise to the intermediate cell mass (ICM) (Fig. 3.2, 24hpf). Haemangioblasts in the anterior LPM/RBI differentiate predominantly into primitive macrophages and those in the posterior LPM/ICM differentiate predominately into primitive erythrocytes (Fig. 3.1, red boxes) (Ellett and Lieschke, 2010; Jing and Zon, 2011; Kanther and Rawls, 2010; Sood and Liu, 2012). From 16hpf to 48hpf multi-potential erythromyeloid progenitors (EMPs) can be detected in the posterior blood island (PBI) and in the caudal haematopoietic tissue (CHT) (Fig. 3.2, 48hpf). EMPs of the transient-definitive wave can differentiate into erythroid and myeloid cells (Fig. 3.1, purple box) (Jing and Zon, 2011; Kanther and Rawls, 2010; Xu et al., 2012). In parallel, definitive haematopoiesis starts from approximately 26hpf onwards. Haemogenic endothelial cells from the ventral wall of the dorsal aorta in the aorta-gonad-mesonephros (AGM) differentiate into HSCs. These HSCs first colonize the CHT, a transient haematopoietic tissue in zebrafish embryos, and can differentiate to erythroid, myeloid, and thromboid cells (Ellett and Lieschke, 2010; Jing and Zon, 2011; Xu et al., 2012). From 2 days post-fertilization (dpf) HSCs finally populate the kidney, where they give rise to erythroid, myeloid, and

thromboid cells as well as eosinophiles (Fig. 3.2, 6dpf) (Jing and Zon, 2011; Kanther and Rawls, 2010). Lymphopoiesis starts from 3dpf when lymphoblasts colonize the thymus (Fig. 3.1, blue boxes; Fig. 3.2, 48hpf/6dpf) (Jing and Zon, 2011; Kanther and Rawls, 2010). However, the adaptive immune system in zebrafish seems to become functional at approximately 4 weeks post-fertilization (wpf), only. Heretofore, the zebrafish relies on its innate immune system, which makes zebrafish larvae an ideal organism to study the innate immune response in the absence of adaptive immunity (Ellett and Lieschke, 2010; Kanther and Rawls, 2010; Sood and Liu, 2012). Microglia, the resident phagocytes

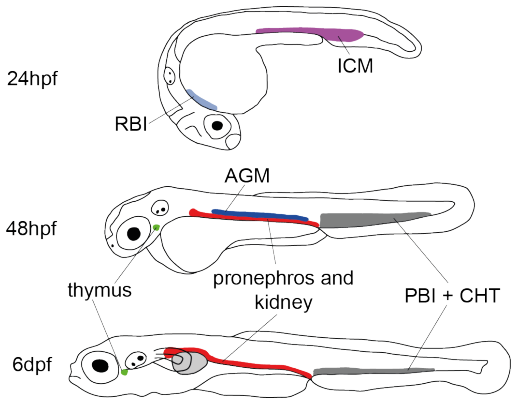

Figure 3.2 – Graphic illustration of the spatial distribution of haematopoietic tissues during zebrafish development. Rostral blood island (RBI): light blue. Intermediate cell mass (ICM): purple. Dorsal aorta in the aorta-gonad-mesonephros (AGM): blue. Posterior blood island (PBI) and caudal haematopoietic tissue (CHT): grey. Pronephros and kidney: red. Thymus: green. Modified from Kanther and Rawls (Kanther and Rawls, 2010)

in the brain, derive from primitive macrophages from the yolk sac and colonize the larval brain from 60hpf onwards (Herbomel et al., 2001; Shiau et al., 2013). During development they pass a morphological transition from highly motile amoeboid cells to mature ramified microglia (Svahn et al., 2013).

3.7.2 Visualizing the immune response - zebrafish transgenic lines

A big advantage of zebrafish compared to other model organisms is their transparency during development providing the potential to visualize processes like the immune response *in vivo*. Additionally stable, inheritable labeling of specific cells by the expression of fluorescent proteins driven by cell-specific promoters is possible. To visualize and examine the immune cell behaviour after an inflammatory stimulus such transgenic zebrafish lines were generated. In these transgenic lines specific immune cell populations are selectively labeled using immune cell specific promoters. Apart from *in vivo* imaging in larvae, these transgenic lines allow also fluorescence-activated cell sorting (FACS) of zebrafish immune cells. In the following a few transgenic

lines available to label immune cells are briefly described. Zebrafish myeloid lineage precursors express *spleen focus forming virus (SFFV) proviral integration oncogene spi1b* (*spi1b*) (Bennett et al., 2001; Lieschke et al., 2002). Therefore, the *spi1b* promoter drives myeloid-specific expression in transgenic zebrafish (Ward et al., 2003). Since microglia derive from *spi1b*-positive cells, they are together with myeloid precursor cells, macrophages, and neutrophils, green fluorescent protein (GFP)-positive in the transgenic line Tg(*spi1b*:Gal4/UAS:EGFP) (Herbomel et al., 2001; Peri and Nüsslein-Volhard, 2008). Neutrophils in zebrafish express *myeloid-specific peroxidase* (*mpx*) an orthologue to the mammalian myeloperoxidase (Bennett et al., 2001; Lieschke et al., 2001). In the transgenic line Tg(*mpx*:GFP) neutrophils are GFP-positive (Mathias et al., 2006; Renshaw et al., 2006). Interestingly, low levels of *mpx* are expressed by some inflammatory macrophages, too. Therefore, these are also labeled in the Tg(*mpx*:GFP) (Mathias et al., 2009). The antibacterial enzyme lysozyme (Lyz) was proposed to be a macrophage-specific protein (Liu and Wen, 2002). However, a more precise evaluation of the Tg(*lyz*:EGFP) revealed that GFP is expressed initially in macrophages and neutrophils but at later stages GFP expression is more or less restricted to neutrophils (personal communication A. Meijer; Feng et al., 2010; Hall et al., 2007). A microarray approach to identify genes that are specifically expressed by macrophages identified *macrophage-expressed gene 1* (*mpeg1*). The transgenic line using the *mpeg1* promoter, Tg(*mpeg1*:mCherry), shows mCherry expression in macrophages but also in microglia, making it a great transgenic line to study these two cell types (Ellett et al., 2011; Svahn et al., 2013; Zakrzewska et al., 2010). *In situ* hybridization in zebrafish larvae demonstrated that *apolipoprotein Eb* (*apoeb*) is a marker for microglia in zebrafish, but in the transgenic line Tg(*apoeb*:lynEGFP) microglia and additionally some radial glia cells are positive for GFP (Herbomel et al., 2001; Peri and Nüsslein-Volhard, 2008). The set of transgenic lines described here labels the myeloid lineage, macrophages, neutrophils, and microglia and provides great tools to study the immune response by *in vivo* imaging.

3.7.3 Assays to study wound healing and regeneration in zebrafish

Immune cells are present in healthy, uninjured models but for the examination of an immune cell response an injury or other inflammatory stimulus is needed that triggers an inflammatory response. After an injury, for example, a wound is repaired by diverse processes that take place simultaneously and involve various cell types. First, cutaneous wounds are sealed. Then, chemotactic signals from the wound lead to an inflammatory response, recruiting neutrophils and macrophages or microglia to the lesion site. Neutrophils quickly infiltrate the damaged tissue and phagocytose, degranulate,

produce and release reactive oxygen species (ROS), or participate in the formation of extracellular nuclear traps. Macrophages follow the neutrophils to the wound site. They ingest foreign substances and apoptotic debris, but they also secret chemotactic substances like chemokines. Moreover, macrophages play a role in tissue rearrangement and regeneration (Deng and Huttenlocher, 2012; Ellett et al., 2011; Li et al., 2012). In the brain microglia fulfil the role of peripheral macrophages (Schlegelmilch et al., 2011; Sieger and Peri, 2013). After the recruitment of immune cells, the wound is repaired by various processes, the inflammation is resolved, and either the tissue is regenerated or a scar is formed. In contrast to mammals, where scar formation is the usual outcome, zebrafish have a very high regenerative capacity. They can regenerate injuries in the brain and amputations of appendices in size and shape without the formation of a scar, even as an adult organism (Gemberling et al., 2013; Murawala et al., 2012; Yoshinari and Kawakami, 2011). To analyse the inflammatory response and regeneration in zebrafish various assays in larvae and adult zebrafish have been established.

3.7.3.1 Larval injury and wounding assays

In zebrafish larvae tail fin amputation or laser ablation of cells in the periphery or the larval brain are often used to study inflammatory processes and regeneration (Fig. 3.3) (Cvejic et al., 2008; Sieger et al., 2012; Yoshinari and Kawakami, 2011). After tail fin amputation in embryos or larvae the epithelial cells contract and seal the

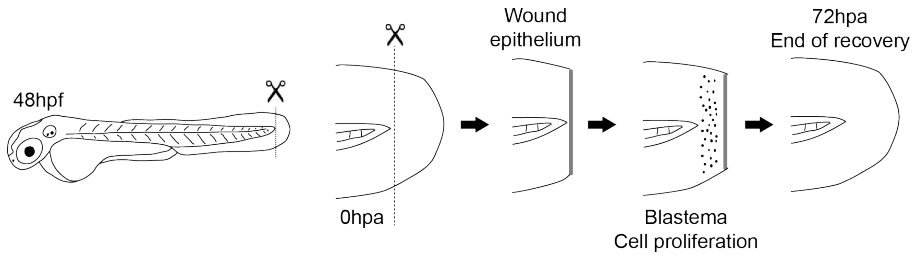

Figure 3.3 – Schematic illustration of the tail fin amputation and regeneration in zebrafish embryo/larvae. After amputation of the tail fin at 48hpf, the epithelial cells contract and seal the wound (wound epithelium). Then a blastema forms and cells start to proliferate. By 72 hours post amputation the tail fin has recovered. Modified from Yoshinari and Kawakami (Yoshinari and Kawakami, 2011).

wound (wound epithelium) (Yoshinari and Kawakami, 2011). In parallel, a hydrogen peroxide (H_2O_2) gradient forms, which is required for the recruitment of neutrophils and macrophages to the wound (Niethammer et al., 2009). By *in vivo* imaging it was shown that neutrophils arrive first at the wound site and that they migrate faster to the wound, but with less directionality than macrophages. Macrophages arrive at the wound from 6 hours post amputation (hpa) onwards and persist longer at the wound margin. A lack

of neutrophils enhances regeneration slightly, whereas a lack of macrophages impairs the regenerative process (Ellett et al., 2011; Li et al., 2012). After approx. 12hpa a blastema forms next to the stump surface. Proliferating cells from this region differentiate into all kinds of cell types, needed to regenerate the finfold in size and shape and by 72hpa, the larval fin is restored (Kawakami et al., 2004; Li et al., 2012; Yoshinari et al., 2009). Mechanical induction of wounding/injuries is time-consuming and a rate-limiting step. This makes tail fin amputation assays not suitable for medium- to high-throughput screens. To circumvent this a chemically induced inflammation (ChIn) assay was established. Zebrafish larvae are soaked in copper sulfate ($CuSO_4$) solution. This treatment causes rapidly cell death of sensory hair cells in the lateral-line system. Neutrophils respond to the cell death and are quickly recruited to the damaged neuromasts. This migration can be visualized in transgenic neutrophil-labeled zebrafish lines, also by automated imaging. Therefore, this assay is suitable for high throughput pharmacological and genetic screens (d'Alençon et al., 2010; Wittmann et al., 2012).

3.7.3.2 Adult zebrafish injury models

Zebrafish larvae and embryos are suitable for a whole range of experiments but sometimes an issue precludes an analysis during developmental stages. If, for example, the regenerative potential in adult zebrafish should be addressed it is apparent that injury experiments in adult zebrafish are more suitable (Gemberling et al., 2013). Due to its simplicity and accessibility the amputation of the tail fin is a frequently used regeneration assay in adult zebrafish. It was shown that the fin is reconstituted in size and shape within approx. 10 days after amputation (Yoshinari and Kawakami, 2011). Despite some differences in the larval and adult finfold, the cellular and molecular mechanism involved seem to be similar (Kawakami et al., 2004).
Another regeneration assay that gained interest in the recent years is the stab wound injury in the adult zebrafish telencephalon, a model for traumatic brain lesions (Ayari et al., 2010; Baumgart et al., 2012; Kroehne et al., 2011; März et al., 2011). Soon after the injury a strong inflammatory response can be observed. The number of microglia and leukocytes increases in the injured hemisphere and the expression levels of proinflammtory cytokines are elevated. After only a few days the acute inflammatory response is resolved. Cells of radial glia origin from the ventricular zone populate the lesion site and differentiate into functional neurons. In contrast to mammals, no permanent glial scarring can be observed, highlighting the regenerative potential of the zebrafish brain (Kroehne et al., 2011; Kyritsis et al., 2012; März et al., 2011). In future, a detailed knowledge of the mechanisms involved as well as a possible transfer into therapies for patients suffering from neurodegenerative diseases might be of fundamental

importance.
For both assays the morphological changes and cells that participate in inflammation and regeneration have been described. Nevertheless, the complex processes of regeneration are still poorly understood and only a few signaling molecules involved are described so far (Gemberling et al., 2013; Yoshinari and Kawakami, 2011).

3.8 Generation of loss of function zebrafish

When modeling the effect of disease-related mutations in a model organism it is very useful to carefully evaluate beforehand if the disease might be triggered by a loss of the functional protein or by the aggregation of an aberrant protein. These reflections should have a direct impact on the approach chosen for the generation of the model. In both FTLD-TDP/*GRN* and NCL/*GRN* the mutations result in a reduction or depletion of GRN, respectively (Baker et al., 2006; Cruts et al., 2006; Shankaran et al., 2008; Smith et al., 2012). Therefore, a zebrafish GRN model should be a loss of function model, too. In the following, targeted genome editing, which was used for the generation of the zebrafish GRN mutants, is discussed in the context of earlier strategies to perform mutagenesis in zebrafish, as targeted genome editing became feasible only a few years ago.

3.8.1 History of forward and reverse genetics in zebrafish

To gain insights into gene function *in vivo*, one can either mutate a specific gene of interest and analyse the organism for resulting phenotypes (reverse genetics), or one observes a phenotype and searches for the mutated gene responsible for the observed phenotype (forward genetics) (Fig. 3.4). In the early days of molecular genetics forward genetics using mutagens was the state-of-the-art since tools to perform reverse genetics were still lacking. In zebrafish unbiased forward genetic screens were performed using e.g. γ-irradiation, retroviruses, or chemicals like N-ethyl-N-nitrosouresa (ENU) as mutagens. Depending of the breeding scheme the F2 or F3 generation was analysed for phenotypes, followed by the identification of the causative mutation (Fig. 3.4A) (Lawson and Wolfe, 2011). In contrast to other organisms reverse genetics using targeted mutagenesis was not feasible in zebrafish due to a lack of zebrafish embryonic stem cell cultures. For some years the solution was either to perform a targeted KD or to do a forward random mutagenesis screen. For the first approach, the anti-sense KD, e.g. MO that inhibit either translation or splicing of a gene of interest can be used. This technology is very popular, cheap, and quick. Nevertheless, it often leads only to a partial and transient loss of the protein of interest (Bill et al., 2009) and suffers sometimes from off-target effects or toxicity. One of the first approaches used for reverse genetics in zebrafish

was TILLING (targeted induced local lesions in genomes) (Wienholds et al., 2002). TILLING combines random mutagenesis by e.g. ENU in the whole genome with specific screening for mutations in a previously selected gene of interest in the F1 generation (Fig. 3.4B). This approach provides an inheritable loss of function mutation, but is time, labor, and cost intensive (Moens et al., 2008). In 2008 zinc finger nucleases (ZFNs) were shown to be functional in zebrafish and the introduction of targeted, inheritable lesions in the zebrafish genome became possible for the first time (Fig. 3.4C) (Doyon et al., 2008; Meng et al., 2008).

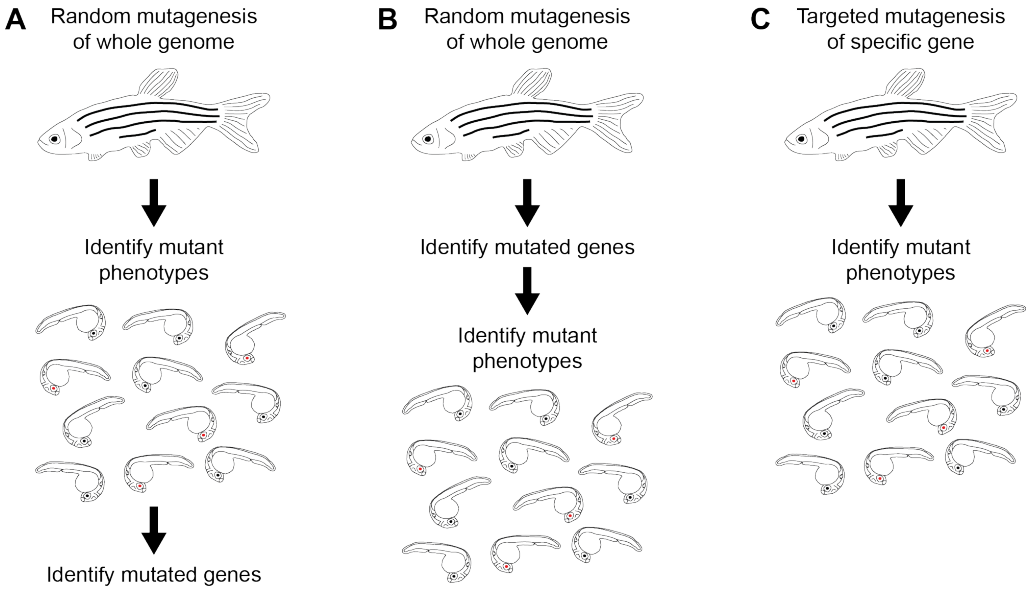

Figure 3.4 – Forward and reverse genetics in zebrafish. There are three possible approaches to link a phenotype to a gene. **A**: In forward genetics, first random mutagenesis is performed, then phenotypic alterations are identified, and finally the genome is analysed for the causative mutation. **B**: In for example TILLING, random mutagenesis is performed and offspring are screened for mutations in a gene of interest. Mutation carriers are then analysed for phenotypic alterations. **C**: Targeted mutagenesis or genome editing induces mutations in pre-selected genes. The offspring are then analysed for phenotypic alterations. Modified from Schier (Schier, 2013).

3.8.2 Targeted mutagenesis in zebrafish by genome editing

ZFN, transcription activator-like effector nucleases (TALENs), and the clustered regularly interspaced short palindromic repeats/CRISPR-associated 9 (CRISPR/Cas9) system (Gaj et al., 2013), induce double-strand breaks (DSB) in the genome, which are either repaired by homology-directed repair (HDR) or non-homologous end joining (NHEJ) (Schmid and Haass, 2013). NHEJ is in comparison to other cellular repair mechanisms error-prone and induces insertions, deletions, or a combination of both, which can lead to loss of function mutations in the selected gene of interest (Fig. 3.5) (Schmid

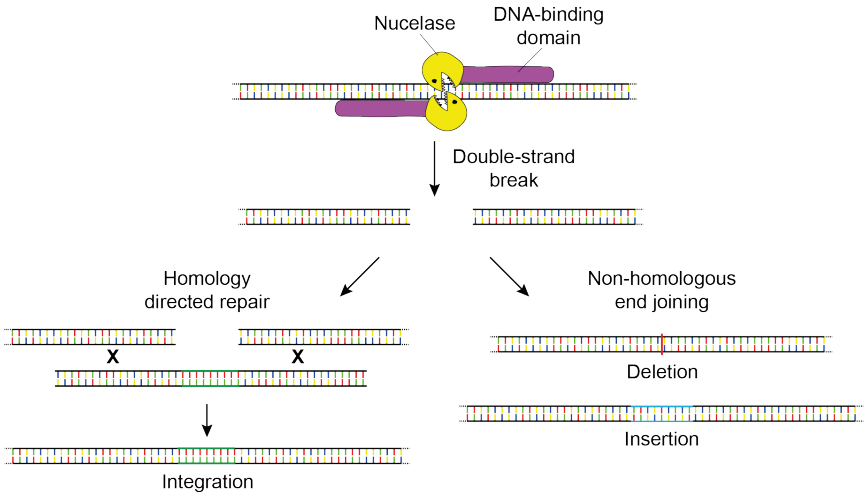

Figure 3.5 – Graphic illustration of genome editing and possible results - integration, deletion, and insertion. Nucleases induce double-strand breaks at a pre-selected target sequence. The nucleases are targeted to their target site by sequence-specific DNA binding elements. The DSB can either be repaired by homology directed repair (HDR), which can lead to the integration of foreign DNA, when the DNA is flanked by homologous sequences, or by non-homologous end joining (NHEJ), an error-prone repair mechanism that can generate deletions or insertions.

and Haass, 2013). Potential loss of function mutations are mutations that cause a shift in the reading frame of the targeted gene of interest. If a premature translation termination (preTT) codon is introduced by the mutation, the aberrant mRNA is most likely recognised and efficiently degraded by the cell's own nonsense-mediate mRNA decay (NMD) machinery resulting in a loss of protein (Vicente-Crespo and Palacios, 2010; Wittkopp et al., 2009). In the last years several genome editing technologies emerged, which are summarised herein.

3.8.2.1 Zinc finger nucleases

ZFNs, which were the first technology to perform genome editing in zebrafish, are composed of an engineered tandem array of DNA binding Cys_2His_2 zinc-finger (ZF) fused to the nuclease domain of a type IIS *FokI* endonuclease (Kim et al., 1996). The DNA-binding ZF moiety of the chimeric ZFN guides the nonspecific nuclease moiety to a specific, pre-selected target site in the DNA (Cathomen and Joung, 2008; Hafez and Hausner, 2012). ZF DNA-binding domains consist of three to six ZFs, each recognizing three DNA base pairs (bp) (Hafez and Hausner, 2012; Urnov et al., 2010). Since the *FokI* nuclease domain is only enzymatically active as a dimer, two ZFN monomers need to recognize their 9bp to 18bp target sequence in the DNA in close vicinity to form an active dimer. ZFN monomers are designed to bind the DNA in a tail-to-tail conformation to form a nuclease dimer, which is able to induce a DSB in the 4bp

to 6bp nucleotide spacer between the ZFN binding sites (Fig. 3.6) (Cathomen and Joung, 2008; Porteus and Carroll, 2005). Site-specific DNA DSBs are then repaired by the cell endogenous repair mechanisms NHEJ or HDR (Fig. 3.5) (Urnov et al., 2010). One challenge with ZFNs is the construction and evaluation of the ZF DNA-binding

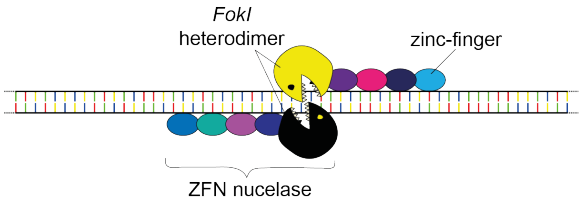

Figure 3.6 – Graphic illustration of ZFNs binding to DNA enabling DNA cleavage. Two ZFNs with four ZFs (multi-coloured) bind sequence specific to the DNA on the forward and the reverse strand allowing the *FokI* nucleases to form a heterodimer (yellow and black) and cleave the DNA.

domains, as the binding affinities of a single ZF moiety is context dependent. ZFNs and ZF DNA-binding domains can either be generated in-house by the modular assembly method, which has a low success rate, or by a combinatorial selection of engineered multifinger proteins, which requires some expertise and is labor-intensive. Another option is to outsource the generation of the whole ZFNs to e.g. Sigma-Aldrich with their proprietary ZF design platform. This is cost-intensive but was shown to produce very efficient ZFNs (Cathomen and Joung, 2008; Leong et al., 2011). To date ZFNs were used successfully in cell culture systems and in many model organisms for gene disruption, correction, and addition (Urnov et al., 2010). In zebrafish, ZFNs were so far only used for gene disruption, since HDR is a very rare event in this context (Doyon et al., 2008; Meng et al., 2008). The on- to off-target ratio of ZFN-induced lesions is high. Nevertheless, there are possibilities to enhance the specificity of ZFNs. By using obligatory heterodimeric *FokI* nucleases a DNA binding and cleavage of two identical (e.g. forward only) ZFNs is prevented (Miller et al., 2007) and also an increased number of ZFs reduces the amount of potential off-target sites in the genome (Gupta et al., 2011). Moreover, decreasing the injection dose is reducing off-target induced toxicity in zebrafish (Doyon et al., 2008; Gupta et al., 2011). Additionally, it was shown in one of the first publications that in outcrossing of ZFN-injected zebrafish (P0) no off-target lesions could be identified in the F1 generation (Gupta et al., 2011). Therefore, extensive, time-consuming outcrossings that were necessary after ENU mutagenesis are no longer required using this technology.

3.8.2.2 Transcription activator-like effector nucleases

The second genome editing technology is similar to ZFNs. Like ZFNs, TALENs are composed of a DNA binding domain and a nuclease domain. The DNA binding domain, transcription activator-like effector (TALE), was identified in the plant pathogen *Xanthomonas* and in contrast to ZF each of the tandem repeats (as many as 30) binds to 1bp in the DNA target site via two hypervariable amino acids (Boch et al., 2009; Moscou and Bogdanove, 2009). When fusing the TALE with a *FokI* nuclease domain (TALEN), two TALENs can induce DSB like it was previously reported for ZFNs (Fig. 3.7) (Christian et al., 2010). Soon after the description that TALENs were

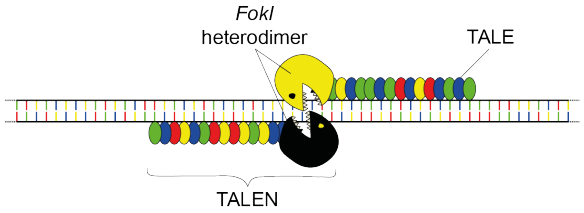

Figure 3.7 – Graphic illustration of TALENs binding to DNA enabling DNA cleavage. Two TALENs bind with their TALEs (multi-coloured) sequence specific to the DNA on the forward and the reverse strand allowing the *FokI* nucleases to form a heterodimer (yellow and black) and cleave the DNA. TALE array (multi-coloured).

effectively used in human cell culture for targeted genome editing, TALENs were also used for targeted genome editing in zebrafish (Huang et al., 2011; Miller et al., 2010; Sander et al., 2011). The big advantage of TALENs is that the generation of the DNA binding domain is faster and easier than that of the ZF DNA-binding domains of ZFNs. Contrary to ZFs, TALE binding is not context dependent and DNA binding is easier to predict. Therefore, TALE DNA-binding domains can be done in-house by more or less simple cloning. Moreover, TALENs are equally or more mutagenic than ZFNs (Chen et al., 2013a; Moore et al., 2012). Additionally, TALENs and single-stranded DNA oligonucleotides or linearized donor DNA were used for precise targeted insertions in the zebrafish genome by HDR, which was not achieved before with this efficiency (Bedell et al., 2012; Zu et al., 2013). Another advantage of TALENs is that the nuclease-associated toxicity of TALENs is lower than that of ZFNs (Mussolino et al., 2011). TALENs are now preferred over ZFNs for targeted genome editing.

3.8.2.3 CRISPR/Cas9 system

The latest tool for genome editing, the CRISPR/Cas9 system, differs from ZFNs and TALENs in the facts that the DNA is recognized by Watson-Crick base pairing by a guide RNA (gRNA) and that the RNA-guided endonuclease (RGEN), Cas9, functions

as a monomer (Cho et al., 2013; Schmid and Haass, 2013). The CRISPR/Cas system is derived from bacteria and archaea and is used as an adaptive immune system, protecting them from infections by viruses and plasmids (Bhaya et al., 2011). There are at least three types of those prokaryotic CRISPR/Cas systems and of these the type II systems are best established for RGEN genome editing. Among these the CRISPR/Cas9 system of *Streptococcus pyogenes* is the best studied. Originally it requires a CRISPR RNA (crRNA), a trans-activating crRNA (tracrRNA), and the endonuclease Cas9. The crRNA is binding with its 5' end to a 20 nucleotide DNA sequence, next to a NGG protospacer adjacent motif (PAM) on the opposite strand. The tracrRNA base-pairs

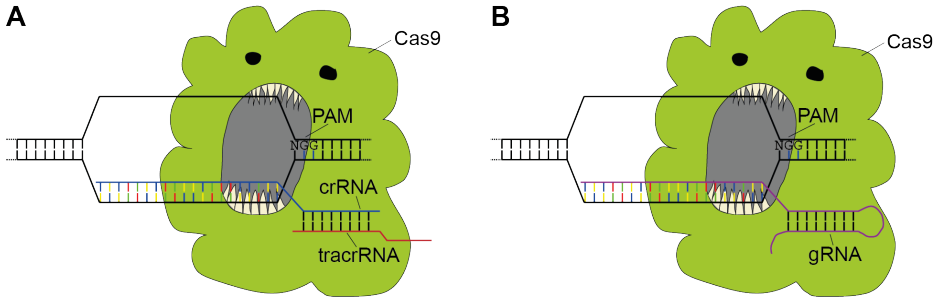

Figure 3.8 – Graphic illustrations of the CRISPR/Cas9 system. **A**: The original CRISPR/Cas9 system. a crRNA (blue) base-pairs sequence specific to a selected DNA sequence. The only requirement is a nearby NGG protospacer adjacent motif (PAM) on the opposite strand. tracrRNA (red) is binding to the crRNA and the complex is recognised by the nuclease Cas9 (green), which can induce a DSB upon binding. **B**: The modified CRISPR/Cas9 system. Instead of a crRNA a gRNA (purple) that is a fusion of the crRNA and the tracrRNA binds to the DNA. This DNA-gRNA complex is recruits the Cas9 (green) to the DNA.

with the crRNA and both form a specific structure, that is recognized by the Cas9 endonuclease, which is then inducing DSBs (Fig. 3.8A). To reduce the complexity of the system the two RNAs, tracrRNA and crRNA, were engineered to a single RNA chimera, termed gRNA, which is still efficiently recruiting Cas9 for site-specific DNA cleavage (Fig. 3.8B) (Jinek et al., 2012). The CRISPR/Cas9 system was quickly applied in eukaryotic cells for targeted genome editing. To enhance the nuclear localisation of Cas9 and improve the efficiency, a nuclear localisation sequence was added to Cas9 (Cong et al., 2013; Jinek et al., 2013; Mali et al., 2013). In zebrafish the CRISPR/Cas9 system was also used successfully to induce mutations at a selected genomic locus and for knock in by HDR (Chang et al., 2013; Hruscha et al., 2013; Hwang et al., 2013a,b; Xiao et al., 2013). Like all genome editing technologies, the CRISPR/Cas9 system can induce mutations at off-target sites, too. The advantage of this genome editing system is, however, that the off-target sites are easier to predict as they rely on Watson-Crick base pairing as well (Cho et al., 2014). The on- to off-target ratio of the CRISPR/Cas9

system seems to be comparable to ZFNs and TALENs and targeting off-targets can be reduced in zebrafish by using lower mRNA concentrations of *Cas9* (Cho et al., 2013; Fujii et al., 2013; Hruscha et al., 2013). Compared to ZFNs and TALENs, the CRISPR/Cas9 system is less time- and cost-consuming, but still displays comparable efficiencies (Schmid and Haass, 2013). Therefore, the CRISPR/Cas9 system is now widely used for genome editing in cell culture as well as in animal and plant models and still offers many applications and modifications to be discovered.

4 Material and Methods

4.1 Material

4.1.1 Zebrafish lines

The zebrafish lines used in this study are listed below. ZFN mutants were generated by injections into the wildtype-line AB.

Zebrafish line	**Origin (Reference)**
wildtype-line AB	G. Streisinger, Institute of Neuroscience, University of Oregon, Eugene, USA
wildtype-line TLF	C. Nüsslein-Volhard, MPI for Developmental Biology, Tübingen, Germany
Tg(*apoeb*:lynEGFP)^{zf147Tg}	F. Peri, EMBL, Heidelberg, Germany (Peri and Nüsslein-Volhard, 2008)
Tg(*fli1a*:EGFP)^{y1Tg}	J. Bussmann, MPI for Molecular Biomedicine, Münster, Germany (Lawson and Weinstein, 2002)
Tg(*kdrl*:HRAS-mCherry)^{s896Tg}	P. Hammerl, Helmholtz Center Munich, Munich, Germany (Chi et al., 2008)
Tg(*lyz*:EGFP)^{nz117Tg}	A. Mahagaonkar, Molecular Medicine and Pathology, University of Auckland, Auckland, New Zealand (Hall et al., 2007)
Tg(*mpeg1*:mCherry)	used in the laboratory of A. Meijer, Institute of Biology, Leiden University, Leiden, Netherlands (generated in the laboratory of George Lutfalla, unpublished)
Tg(*mpx*:GFP)^{i114Tg}	used in the laboratory of A. Meijer, Institute of Biology, Leiden University, Leiden, Netherlands (Renshaw et al., 2006)
Tg(*spi1b*:Gal4/UAS:EGFP)^{zf149Tg}	F. Peri, EMBL, Heidelberg, Germany (Peri and Nüsslein-Volhard, 2008)

4.1.2 Cell lines

Cell line	**Origin**
HEK293T	ATCC-Nr. CRL-1573

4.1.3 Vectors and plasmids

The following vectors and plasmids were used, # indicates the number in the Schmid laboratory plasmid database:

Vector	**Insert**	**Origin**	#
pCR8/GW/TOPO	-	Invitrogen	-
pCRII TOPO	-	Invitrogen	-
pCS2+GW-A	GW-Reading Frame A	M. Teucke	E04
pCS2+GW-A (vice versa)	GW-Reading Frame A	M. Teucke	E03
IRBOp991G0282D	*grn1* cDNA	imaGenes	I24
IRBOp991A1165D	*grn2* cDNA	imaGenes	I25
pZFN1_grnb set1	ZFN1 grnb set1	Sigma-Aldrich	H21
pZFN2_grnb set1	ZFN2 grnb set1	Sigma-Aldrich	H22
pZFN3_grnb set2	ZFN3 grnb set2	Sigma-Aldrich	H23
pZFN4_grnb set2	ZFN4 grnb set2	Sigma-Aldrich	H18
pZFN5_grnb set3	ZFN5 grnb set3	Sigma-Aldrich	H19
pZFN6_grnb set3	ZFN5 grnb set3	Sigma-Aldrich	H20
pZFN1_grna set1	ZFN1 grna set1	Sigma-Aldrich	H55
pZFN2_grna set1	ZFN2 grna set1	Sigma-Aldrich	H56
pZFN3_grna set2	ZFN3 grna set2	Sigma-Aldrich	H57
pZFN4_grna set2	ZFN4 grna set2	Sigma-Aldrich	H58
pCS2+GW-A_*grna*	*grna*	B. Solchenberger	L24
pCS2+GW-A_*grna+MYC*	*grna+MYC*	B. Solchenberger	L25
pCS2+GW-A_*grna*_wt(AB)	$grna^{\text{wt (AB)}}$	B. Solchenberger	M51
pCS2+GW-A_*grna*_wt(TLF)	$grna^{\text{wt (TLF)}}$	B. Solchenberger	M52
pCS2+GW-A_*grnb*	*grnb*	B. Solchenberger	H25
pCS2+GW-A_*grnb+MYC*	*grnb+MYC*	B. Solchenberger	H63
pCS2+GW-A_*grn1*	*grn1*	B. Solchenberger	I29
pCS2+GW-A_*grn1+V5*	*grn1+V5*	B. Solchenberger	L03
pCS2+GW-A_*grn2*	*grn2*	B. Solchenberger	I43
pCS2+GW-A_*grn2+V5*	*grn2+V5*	B. Solchenberger	I41

4.1.4 Oligonucleotides

Oligonucleotides were synthesized by Thermo Scientific or Sigma-Aldrich. Sequences are given in 5'-3' orientation. Abbreviation and number in the oligonucleotide name refer to the Schmid laboratory oligonucleotide database.

Primer for cloning:

BS-E21 grnb+MYC R	TTATTCATTCAAGTCCTCTTCAGAAATGA GCTTTTGCTCCATGAGAGAATTATTCCAC CACGT
BS-E27 grn2 F long	ATGTTCCCAGTGTTGATGTTACTCATGGC GGCTCTGGTGGCTGCA
BS-E28 grn1+Myc R	TTATTCATTCAAGTCCTCTTCAGAAATGA GCTTTTGCTCCATCCCCAACTCCAACCCG CTG
BS-E29 grn2+V5 R	TCACGTAGAATCGAGACCGAGGAGAGGGT TAGGGATAGGCTTTCCACCCCCCAACTCC AACTCGCTGCAGC
BS-E32 grna STOP XbaI R	GCTCTAGAGCTTATAGAGTTAGGGCTCGT TTC
BS-E33 grna+Myc XbaI R	GCTCTAGAGCTTATTCATTCAAGTCCTCT TCAGAAATGAGCTTTTGCTCCATCCCTAG AGTTAGGGCTCGTTTC
BS-E35 grn2 R	TTTGCTTACAACTCCAACTCG
BS-E36 grna F in	TCCACCTGCTCAAAAAATGT
BS-E37 grna F out	CCGCTGTTCACAAATCCA
BS-E38 grna R in	GTGCTGCTGTGATGTTTATA
BS-E39 grna R out	CTTGAGCATGTAAGTGTC
BS-F36 grn1+V5 R	TCACGTAGAATCGAGACCGAGGAGAGGGT TAGGGATAGGCTTTCCACCCCCCAACTCC AACCCGCTG
oA01 M13 F	TGTAAAACGACGGCCAGT
oA02 M13 R	CAGGAAACAGCTATGACC
oC48 grnb F	ATGGTGCGTGCAGCTTTCAT
oC49 grnb R	TTAGAGAGAATTATTCCACCACGT

oC54 grn1 F	ATGTTCCCAGTGTTGATGTTAC
oC55 grn1 R	TTACAACTCCAACCCGCTG
oC70 grna UTR F	CTGCTCAAAAAATGTTGAGACTG

Primer for sequencing:

BS-A05 grna E9-10 F	AGCCTGAAACTCAACGCACT
BS-A35 GRnARTPCRex6FORself2	GCTGTATGCTGTGATGACAA
BS-A11 grnb E9-10 F	CAAAAGCACTGCTGTCCAGA
BS-A18 zfGRNBseqCxRev	GCACACGGCATTTTTCATAGG
BS-A40 zfGRNBRTPCRex2For	ACTGCTGTTATCAGGGAACTTTGT
BS-B01 zfGRNRTPCRBex6Bfor	TACTAGAGACCGGTAGTTACGGATG
BS-B02 zfGRNBexon7Brev	CTGACAAACACGTACTATGGATGAG
BS-B05 zfGRNBgATCpos1301For	CGTGTCCAACCGGGACCACCTGCTG
BS-B07 zfGRNBgATCpos1901For	GCTACATCTGTAAGCTGGAGTTAGG
BS-B10 grnb E6-7-gen E6 R	TACACGATTTTGCCGTTGAA
BS-B11 grnb E6-7-gen E7 F	CAGAATTCGCCACAGTGAAA
BS-B12 grnb E6-7-gen E7 R	GCATCCGTAACTACCGGTCT
BS-B13 grnb E9-10-gen E9 R	CAAAAGCACTGCTGTCCAGA
BS-B14 grnb E9-10-gen E10 F	CCCCATTTTCCCCTGTTATT
BS-B15 grnb E9-10-gen E10 R	GCACAAAGCATGACTGACCA
BS-B16 grna E9-10-gen E9+10 R	GCTGCGTTCCAGACACAGTA
BS-B17 grna E13-14-gen E13+14 F	CGGCACCATGAAACAGTAGA
BS-B18 grna E13-14-gen E13+14 R	TTCACGCTTACCTTTGCTTG
BS-C07 ZfGRNaENS5'UTR6	GGAGATCATCTGCCTCCAAT
BS-C18 zfgrnBENSexon3Rev	ATTTTTCATAGGACAGCAGCCCCAG
BS-C24 ZFGRNb5'UTR5BRev	AAGTGAGATCTGTGAGGGGTGT
BS-D38 grna_ex3R	GCGTGGATGTGTAAATGGTG
BS-D39 grna_ex4+5F	CCTCTTGCCTCAACACACCT
BS-D40 grna_ex4+5R	GGTGCCAGATACCAGCATTT
BS-E01 grna_ex6+7F	CTGCTGGCCACATATCTTCA
BS-E02 grna_ex6+7R	GGCATTACTGCGTGGAGTTT

BS-E03 grna_ex8+9F	ACCACCATAAAATGCCAAGG
BS-E04 grna_ex8+9R	GCAAAACTTGCCTGACATGA
BS-E05 grna_ex11+12F	CAGGAAAATTAGCGCAGAGC
BS-E06 grna_ex11+12R	CTCAAGCTTTCCCAGAGCAC
BS-E07 grna_ex16/17F	GGGCTAGTTGGGATGGGTAT
BS-E08 grna_ex16/17R	CCAGAAAATCATCCAGAAAATCA
BS-E09 grnb_ex3F	TTTCTCACCACTTAGCGAATGTA
BS-E10 grnb_ex4F	TGTAAAGTGTTACCGTTTATTCCTT
BS-E11 grnb_ex5+6F	CCGAAACACTGCACACACTC
BS-E12 grnb_ex8+9F	TTGAAACTGACACCTCAGTATGTG
BS-E13 grnb_ex11F	TTTCAAATCCGTTGTGTTGG
BS-E14 grnb_ex11R	TGGCAGGGCAAGTAAAAATC
BS-E15 grnb_ex12F	TTTGCGTGTACTAGTTTTTAGATCG
BS-E16 grnb_ex12R	TTTCCCAAAGGGTTATCGAA
BS-E26 grna Seqcheck	CATTCTCCAGCAATGTTCTTACAG
BS-F60 grna F for Seq. ROI1	ACACCTGTGCAATCAACTACTA
BS-F61 grna R for Seq. ROI2	CTCGACTGTTCATCGCATTTA
GATC grnb F V7	TTTGCACTGCCACACAC
GATC M13-FP	TGTAAAACGACGGCCAGT
GATC M13-RP	CAGGAAACAGCTATGACC
GATC SP6	ATTTAGGTGACACTATAGAA
GATC T7-981079	TAATACGACTCACTATAG

Primer for genotyping:

BS-E22 grnb ZFN F	AATGACACAAGACGTCCTCATAAA
BS-E23 grnb ZFN R	AAAAATAATAACCACAGCGCAACT
BS-E24 grna ZFN F	TTCAGTCATTGTTTCAGAGGTCA
BS-E25 grna ZFN R	TTCCTCTGATCCACTTTCTACCA

Primer for quantitative PCR:

BS-F72 FLNCa E4748 F	CCTTCGTGGGTCAGAAGAAC

BS-F73 FLNCa E4748 R	GGAGTTCTAGGACCGTGGAC
BS-G06 grn1/grn2 ex34 Fa	CCACCAGAACCTTCCAGAAA
BS-G07 grn1/grn2 ex34 Ra	TGGCCAGTTCTAGTCTTGCAG
BS-G20 ctsd ex23 F	GAAATACAACCTGGGCTTCC
BS-G21 ctsd ex23 R	GAAGGTCTGGACAGGAGTGC
BS-G46 grnb ex68 F	GTCGCAGGAAGCCATTAGAG
BS-G47 grnb ex68 R	CAGCATGTTGTATCTTCTGGACA
BS-G62 ctsba ex78 F	ACAGCCCCTCTTACAAGCAA
BS-G63 ctsba ex78 R	TCCCTCTACTGGACCGTTCTT
BS-G68 ctsbb ex45 F	GCCGAACTGTAAGACCCTCA
BS-G69 ctsbb ex45 R	TGCTTCCCTTTACTGTGGATG
BS-G74 actb1 ex12a F	GATCTTCACTCCCCTTGTTCA
BS-G75 actb1 ex12a R	AAAACCGGCTTTGCACATAC
BS-H01 tbp ex23a F	TCAGCATGGAGCAGAACAAC
BS-H02 tbp ex23a R	CCCATACGGCATCATAGGAC
BS-H14 grna ex2324 F	ACCACATGGGGATGTTGC
BS-H15 grna ex2324 R	CCAAGTCTCCGGCTGAAATA
BS-H22 aldh1a2 ex1112 F	GGCCGTCTTCACCAGAGATA
BS-H23 aldh1a2 ex1112 R	TGAATCCTCCGAAAGGACAC
BS-H24 apoeb ex13 F	GCTCCACACGGAGAAAAATC
BS-H25 apoeb ex13 R	GCCTGGAACAGGCTACGAG
BS-H42 stat3 ex1112 F	CCAGCTCAAAATCAAAGTGTG
BS-H43 stat3 ex1112 R	TTGGATTCCTCCATGTTCATC
BS-H44 mmp9 ex23 F	GGAGACCTGAAGTGGGATCA
BS-H45 mmp9 ex23 R	AGCTCTGGCAAAAGCATCAT
BS-H50 flncb ex1213 F	GGCCCTACAAAGTGGACATC
BS-H51 flncb ex1213 R	CTTCAAACCAGGCCCATAAG
oA03 β-actin F	TGTTTTCCCCTCCATTGTTGG
oA04 β-actin R	TTCTCCTTGATGTCACGGAC
eif4a1b FW	TTCAGAAACTCAGTACTAGCATACA
eif4a1b RV	GTGACATCCAACACCTCTGC

Eif5 FW	CAAGTTTGTGCTGTGTCCCG
Eif5 RV	AGCCTTGCAGGAGTTTCCAA

4.1.5 Bacteria

DH5α *E. coli* competent cells	Hanahan (Hanahan, 1983)
One Shot TOP10 Chemically Competent *E. coli*, C4040	Invitrogen

4.1.6 Antibodies

The following antibodies were used for whole mount immunofluoresecence stainings (IF) and Western blotting (WB).

Primary antibodies:

Antibody (Species)	**Dilution**	**Origin (Reference)**
α-actinin, A7811 (mouse)	IF: 1:500	Sigma-Aldrich (Schmid et al., 2013)
α-tubulin, T6199 (mouse)	WB: 1:10000	Sigma-Aldrich
Calnexin, SPA-860 (rabbit)	WB: 1:10000	Stressgen
Cathepsin D (rabbit)	WB: 1:8000	C. Follo, Department of Medical Sciences, University of Piemonte Orientale "Amedeo Avogadro", Novara, Italy (Follo et al., 2011)
F59 (mouse)	IF: 1:100	DSHB (Hammond et al., 2007)
FLAG M2-Peroxidase, A8592	WB: 1:2000	Sigma-Aldrich
MYC 9E11 (mouse)	WB: 1:50	Institute of Molecular Immunology (IMI), Helmholtz Center Munich
Pax7 (mouse)	IF: 1:100	DSHB (Feng et al., 2006)
V5, AB3792 (rabbit)	WB: 1:2000	Chemicon
ZE-BO 1F4 (rat IgG2a)	IF: 1:50	E. Kremmer (Prengel, 2000)
zn1 (mouse)	IF: 1:100	DSHB (Trevarrow et al., 1990)
znp1 (mouse)	IF: 1:100	DSHB (Trevarrow et al., 1990)

Primary peptide antibodies generated by the IMI, Helmholtz Center Munich:

Antibody (Species)	Dilution	Epitope
grna 12E7-111 (rat IgG2b)	WB: 1:1	KQKKPETQRTTTRPTGTTS
grnb 11F4-11 (rat IgG2c)	WB: 1:1	CTKSSSSTWWNNSL

Secondary antibodies:

Antibody	Dilution	Origin
anti-mouse IgG, HRP conj., W4021	1:5000	Promega
anti-rabbit IgG, HRP conj., W4011	1:10000	Promega
anti-mouse IgG1, HRP conj.	1:12000	IMI, Helmholtz Center Munich
anti-mouse IgG2a/b, HRP conj.	1:12000	IMI, Helmholtz Center Munich
anti-mouse IgG3, HRP conj.	1:12000	IMI, Helmholtz Center Munich
anti-rat IgG1, HRP conj.	1:8000	IMI, Helmholtz Center Munich
anti-rat IgG2a, HRP conj.	1:12000	IMI, Helmholtz Center Munich
anti-rat IgG2b, HRP conj.	1:2000	IMI, Helmholtz Center Munich
anti-rat IgG2c, HRP conj.	1:32000	IMI, Helmholtz Center Munich
Alexa Fluor 488 anti-mouse, A-11029	1:500	Invitrogen
Alexa Fluor 555 anti-rat, A-21434	1:500	Invitrogen

4.1.7 Chemicals

4.1.7.1 Chemicals and reagents

Acetic acid, 100063.2511	Merck
Acridine orange (AO), 235474	Sigma-Aldrich
Acrylamide / bis solution, 10681.03	Serva
Agarose, 15510-027	Invitrogen
Ammonium persulfate (APS), 9592.2	Roth
Ampicillin, K029.2	Roth
Amplify fluorographic reagent, NAMP100	Amersham Biosciences
β-Mercaptoethanol, 4227.1	Roth

Bacto agar, 214030	BD
Bacto trypton, 211699	BD
Boric acid, 100165.1000	Merck
Bovine serum albumin (BSA), A8022	Sigma-Aldrich
Bromophenol blue, 18030	Fluka
Calcium chloride ($CaCl_2$), 102382.0500	Merck
Chloroform/isoamylalcohol, X984.1	Roth
Collagenase, C9891	Sigma-Aldrich
Copper(II) sulfate ($CuSO_4$) 102790.0250	Merck
DanKlorix	Colgate-Palmolive
DePex mounting medium	e.g. Sigma-Aldrich
Deoxynucleoside triphosphates (dATP, dCTP, dGTP, dTTP)	Thermo Scientific
Diethylpyrocarbonate (DEPC), D5758	Sigma-Aldrich
Dimethyl sulfoxide (DMSO), 317275	Merck
Disodium hydrogen phosphate (Na_2HPO_4), 106580.5000	Merck
Dithiothreitol (DTT) (100mM), Y00147	Invitrogen
6x DNA loading dye, R0611	Thermo Scientific
Deoxynucleoside triphosphate (dNTP), 11819362001	Roche
Dry ice	-
dT16 Oligo	gift from D. Edbauer
dT20 Oligo	gift from D. Edbauer
Ethylenediaminetetraacetic acid (EDTA), 108418.1000	Merck
80% ethanol, UN1170	CLN
Ethanol p.a., 100989.1011	Merck
Ethidium bromide, 2218.2	Roth
FastRuler high range DNA ladder, 500-10000bp, SM1123	Thermo Scientific
FastRuler middle range DNA ladder, 100-5000bp, SM1113	Thermo Scientific
FastRuler low range DNA ladder, 50-1500bp, SM1103	Thermo Scientific
Fetal bovine serum (FBS), F7524	Sigma-Aldrich
Gelatin, 104080.0100	Merck
GeneRuler DNA ladder mix, SM0331	Thermo Scientific

GeneRuler express DNA ladder, SM1553	Thermo Scientific
Glycerol p.a., 3783.2	Roth
Glycine p.a., 04943	Biomol
5x GoTaq buffer, M791A or M792A	Promega
GoTaq DNA polymerase, M830B	Promega
Guanidine hydrochloride, G4505	Sigma-Aldrich
Immersol W 2010	Zeiss
Isopropanol p.a., 109634.2511	Merck
Lipofectamine, 11668-019	Invitrogen
Liquid nitrogene (liq. N_2)	Linde
Loeffler's methylene blue solution, 101287	Merck
LysoTracker Red DND-99, L7528	Molecular Probes
Magnesium chloride ($MgCl_2$), 105833.1000	Merck
Magnesium sulfate ($MgSO_4$), 105886.1000	Merck
Methanol p.a., 106059.2511	Merck
Methionine [S35]-label	Hartmann Analytik
Methyl cellulose, M0387	Sigma-Aldrich
Meyer's haematoxylin stain	e.g. Sigma-Aldrich
Milk powder, T145.2	Roth
Monopotassium phosphate (KH_2PO_4), 104877.1000	Merck
Neutral red, 861251	Sigma-Aldrich
Newborn calf serum (NCS), N4762	Sigma-Aldrich
Nonidet P40 / NP40 / IGEPAL, 19628	USB
Orange G, O3756	Sigma-Aldrich
Paraformaldehyde (PFA), P6148	Sigma-Aldrich
Penicillin-Streptomycin, 15140-122	Gibco
Pentylenetetrazole (PTZ), P6500	Sigma-Aldrich
Periodic acid	e.g. Sigma-Aldrich
Phenylthiourea (PTU), P7629	Sigma-Aldrich
Phenol/chloroform/isoamylalcohol, A156.1	Roth
Potassium chloride (KCl), 104936.1000	Merck

Protease inhibitor (PI) mix, 05056489001	Roche
Pronase, 11459643001	Roche
Proteinase K (PK), 03115852001	Roche
Precision plus protein all blue standard, 161-0373	Bio-Rad
Pwo Polymerase, 01-5010	peqlab
Random hexamere primer, S0142	Thermo Scientific
Random primer mix, S1330S	NEB
Restriction endonucleases	NEB, Thermo Scientific
RiboLock RNase inhibitor (40U/µl), EO0382	Thermo Scientific
RNase H, 18021071	Invitrogen
RNAlater , AM7024	Ambion
Schiff Reagent	Raymond A. Lamb
SeeBlue Plus2 pre-stained standard, LC5925	Invitrogen
Sodium acid (NaN_3), 106688.0100	Merck
Sodium acetate (NaOAc), 6779.1	Roth
Sodium chloride (NaCl), 3975.2	Roth
Sodium dodecyl sulfate (SDS), 20765.03	Serva
SP6 polymerase, EP0131	Fermentas
Spectinomycin, 85555	Fluka
Sucrose, S1888	Sigma-Aldrich
T7 polymerase, EP0111	Fermentas
Tetramethylethylenediamine (TEMED), 2367.3	Roth
TissueTek O.C.T., 25608-9300	VWR
Tricain, A5040	Sigma-Aldrich
Tris, 08003	AppliChem
Triton X-100, 108603.1000	Merck
Tropix I-Block, T2015	Applied Biosystems
Tween 20, 822184.0500	Merck
Xylene, 108681.1000	Merck
Yeast extract, 212720	BD

4.1.7.2 Solutions and buffer

For all solutions and buffers H_2O was used that was purified and desalted by a Milli-Q system (electric resistance 18.2MΩcm at 25°C).

Acridine orange stock solution	3mg/ml in dH_2O
1%-2% agarose	1%-2% agarose 1x TBE
Ampicillin stock	100mg/ml dissolved in dH_2O and sterile filtered
10% APS (stock)	10% APS in dH_2O stored at -20°C
Bleaching solution	1l tap water, 380µl DanKlorix
10x BSA stock	0.1g/ml
DEPC dH_2O	200µl DEPC per 100ml dH_2O incubate o/n at 37°C and autoclave
Destain solution	25% isopropanol 7% acetic acid in H_2O
GuHCl-stripping buffer	6M guanidine hydrochloride 20mM Tris 0.2% Triton X-100/NP40 adjust to pH7.5
I-Block	0.2% Tropix I-Block 0.1% Tween in 1xPBS
4x Lämmli sample buffer	4ml 20% SDS 4ml glycerol 1ml β-mercaptoethanol 1.25ml 1M Tris, pH7.6 1 pinch bromophenol blue
Lysis buffer	10% PK stock in TE, pH8.0
6x Loading dye orange or blue	0.5% SDS 25% glycerol 25mM EDTA in dH_2O pinch of Orange G or Bromophenol blue
3% methyl cellulose	3% methyl cellulose in prewarmed H_2O 70°C shake o/n at 4°C and centrifuge until every bubble is gone

NCST	10% NCS stock 0.1% Tween in 1xPBS
Neutral red stock solution	10mg/ml neutral red in E3
0.1M PB pH7.4	19ml 0.2M KH_2PO_4 81ml 0.2M Na_2HPO_4 ad 200ml dH_2O
10x PBS	80g NaCl 17.8g $Na_2HPO_4x2H_2O$ 2.4g KH_2PO_4 2g KCl ad 1l with dH_2O
PBST	0.1% Tween in 1x PBS
PBST milk	3% milk powder 0.1% Tween in 1x PBS
10x PCR buffer	100mM Tris, pH8.3 500mM KCl 15mM $MgCl_2$ 0.1% (w/v) gelatin in dH_2O
PCR mix	60µl 100mM dATP 60µl 100mM dCTP 60µl 100mM dGTP 60µl 100mM dTTP 6ml 10x PCR buffer 36.3ml dH_2O
0.5% periodic acid solution	0.5g periodic acid in 100ml dH_2O
4% PFA	4% PFA in 1x PBS incubate approx. 5min at 80°C until PFA is dissolved cool to 4°C prior to usage or store at -20°C
PK stock	17mg/ml PK in dH_2O
Pronase stock	30mg/ml pronase in dH_2O
10x PTU	0.3mg/ml in E3
PTZ stock solution (150mM)	5.18mg PTZ 10% DMSO in 250ml E3

Running gel buffer	1.5M Tris, pH8.8
10x running buffer	29g Tris 144g glycine ad 1l with dH_2O and autoclave
SDS running buffer	0.1% SDS in 1x running buffer
Spectinomycin stock	30mg/ml dissolved in dH_2O and sterile filtered
Stacking gel buffer	1M Tris, pH6.8
STEN lysis buffer	50mM Tris, pH7.6 150mM NaCl 2mM EDTA 1% NP-40
Stripping buffer	62.5mM Tris 2% SDS adjust to pH6.7
10x TBE	1080g Tris 550g Boric acid 400ml 0.5M EDTA, pH8.0 ad 10l dH_2O
10x TBS	1.25M NaCl 0.5M Tris adjust to pH7.6 and autoclave
TBST	0.1% Tween in 1x TBS
TBST milk	3% milk powder 0.1% Tween in 1x TBS
TE pH8.0	10mM Tris 1mM EDTA adjust to pH8.0 and autoclave
10x transfer buffer	30.3g Tris 144g glycine ad 1l with dH_2O adjust to pH8.3 and autoclave
50x tricain	2g tricain 10.5ml 1M Tris pH9.0 ad 500ml with dH_2O adjust to pH7.0

4.1.7.3 Media

Media used for the cultivation of bacteria were autoclaved to prevent the growth of undesired organisms. After cooling sterile filtered antibiotics in the indicated concentrations were added.

Cell culture medium	DMEM 10% FBS 1% Penicillin-Streptomycin
Dulbecco's Modified Eagel's Medium (DMEM), 61965-026	Gibco
E3	5mM NaCl 0.17mM KCl 0.33mM $CaCl_2$ 0.33mM $MgSO_4$
E3 Methylene blue	5mM NaCl 0.17mM KCl 0.33mM $CaCl_2$ 0.33mM $MgSO_4$ 0.002% Loeffler's methylene blue solution)
LB-Agar	1.5% Bacto Agar 1% Bacto Trypton 0.5% Yeast extract 17.25mM NaCl in dH_2O Ampicillin 100µg/ml or Spectinomycin 100µg/ml
LB-Medium	1% Bacto Trypton 0.5% Yeast extract 17.25mM NaCl in dH_2O Ampicillin 100µg/ml or Spectinomycin 100µg/ml
Opti-MEM, 51985-026	Gibco
SOC-Medium, 15544-034	Invitrogen

4.1.8 Kits

A-Plus Poly(A) Polymerase Tailing Kit, PAP5104A	Epicentre
BC Assay Protein Quantitation Kit, UP40840A	Uptima
Gateway LR Clonase II Enzyme Mix, 11791-020	Invitrogen
GoTaq DNA Polymerase, M3175	Promega
iProof High-Fidelity DNA Polymerase, 172-5300	BioRad
iScript cDNA Synthesis Kit, 170-8891	BioRad
iQ SYBR Green supermix, 170-8880	BioRad
M-MLV Reverse Transcriptase, 28025-013	Invitrogen
MEGAClear Kit, AM1908	Ambion
mMESSAGE mMACHINE SP6 Kit, AM1340	Ambion
mMESSAGE mMACHINE T7 Kit, AM1344	Ambion
MessageMAX T7 mRNA transcription kit	Epicentre
NucleoBond Xtra Midi, 740410	Macherey-Nagel
NucleoSpin Gel and PCR Clean-up, 740609	Macherey-Nagel
NucleoSpin Plasmid, 740588	Macherey-Nagel
pCR8/GW/TOPO TA Cloning Kit, K250020	Invitrogen
Pierce ECL Plus Western Blotting Substrate, 32132	Thermo Scientific
RNAqueous-Micro Kit, AM1931	Ambion
RNase-free DNase Set, 79254	Qiagen
RNeasy Mini Kit, 74104	Qiagen
SsoFast Eva Green Supermix, 172-5204	BioRad
TnT SP6 Coupled Reticulocyte Lysate System, L4601	Promega

4.1.9 Consumables

0.2ml Strip tubes, AB-0266	Thermo Scientific
96-Well PCR Plate, AB-0600	Thermo Scientific
Blotting Paper, MN 218 B	Macherey-Nagel
Borosilicate glass capillaries, 1B120F-4	World Precision Instruments

Centrifuge tubes 15ml, 50ml	Sarstedt
Combitips Plus 0.5ml, 5ml	Eppendorf
Cover slip	Thermo Scientific
Fluorodish Cell Culture Dish - 35mm, FD3510-100	World Precision Instruments
Hard-Shell 384-Well PCR Plates, HSP-3805	BioRad
Microcentrifuge tubes 1.5ml, 2.0ml	Sarstedt
Microscope slide	Thermo Scientific
Microscope slide with wells	Thermo Scientific
Microseal B Film, MSB1001	BioRad
Multi-well plates (6, 12, 24, 48, 96)	Thermo Scientific
PCR Film , AB-0558	Thermo Scientific
Petri dishes 60mm, 100mm	Sarstedt
Pipette tips 10µl, 10µl long, 200µl, 1000µl	Sarstedt
Pipette tips with filter (10µl, 10µl long, 20µl, 100µl, 300µl, 1000µl)	Sarstedt
Phase Lock Tubes 1.5ml	Eppendorf
PVDF Membrane, Immobilon-P, IPVH00010	Millipore
sterile serological pipetts 5ml, 10ml, 25ml	Sarstedt
Superfrost Plus slides, J1800AMN3	Thermo Scientific
Transfer pipettes	Sarstedt
X-ray films Kodak, BioMax MR Film, Cat8701302	Sigma Aldrich
X-ray films Super RX, 47410 19236	Fujifilm

4.1.10 Equipment

Accu jet pro	Brand
Agarose gel documentation device	Intas
Agarose gel systems	Peqlab
Benchtop centrifuge 5415D	Eppendorf
Benchtop cool centrifuge Biofuge fresco	Heraeus
Bio-ice cooling unit, 170-3934	Bio-Rad

C1000 Thermal Cycler	Bio-Rad
Cassette for x-ray film exposure	Radiographic Products
Casting stands	Bio-Rad
Casting frames	Bio-Rad
Centrifuge multifuge 3 S-R	Heraeus
CO_2 Incubator	Binder
Cold-light source KL 1500 LCD	Zeiss
Dumont Forceps # 5 Titanium	Fine Science Tools
DMZ-Universal (needle) Puller	Zeitz-Instrumente
Foam Pads	Bio-Rad
Freezer -20°C	Liebherr
Freezer -80°C	Heraeus
Fridge	Liebherr
Gel Releaser, 165-3320	Bio-Rad
Gel dryer, model583	Bio-Rad
iCycle-MyiQ	BioRad
Incubator 28°C, 37°C, 55°C	Binder
Kontes Pellet Pestle, 1.5ml	Fisher Scientific
Kontes Pellet Pestle Cordless Motor, K749540-0000	Fisher Scientific
Microwave	Sharp
Microinjector (Femto Jet)	Eppendorf
Microinjection molds	e.g. Eppendorf
Micro scales BP2215	Sartorius
MilliQ academics	Millipore
Mini gel holder cassette, 170-3931	Bio-Rad
Mini-PROTEAN Comb, 10-well and 15-well	Bio-Rad
Mini-PROTEAN 3 cell	Bio-Rad
Mini-PROTEAN Tetra cell	Bio-Rad
Mini trans-blot central core, 170-3812	Bio-Rad
Multipipette plus	Eppendorf
Nano Photometer	IMPLEN

Needles	Kaut-Bullinger
OTF5000 Cryostat	Bright
PCR Plate Sealer	Eppendorf
PCR Thermocycler	Eppendorf, BioRad
pH Meter	WTW
Pipette 10µl, 100µl, 200µl and 1000µl	Eppendorf
Plate reader PowerWaveXS	BioTek
PowerPac Basic Power Supply, 164-5050	Bio-Rad
PowerPac HC Power Supply, 164-5052	Bio-Rad
Preserving boiler EKO 620	Petra
Scales BP3100S	Sartorius
Schott bottles	Schott
Sonifier (Cell Disruptor B15)	Branson
Shaker Duomax 1030	Heidolph
Shaker cold room	Bachofer
Short plates, 165-3308	Bio-Rad
Spacer plates 0.75mm, 165-3310 and 1.5mm, 165-3312	Bio-Rad
Spring Scissors, 3mm Blades, Straight	Fine Science Tools
Spring Scissors, 5mm, Blades Angled to the Side	Fine Science Tools
Stereo Microscope Stemi 2000	Zeiss
Tea nets	-
Thermomixer comfort	Eppendorf
Thermomixer compact	Eppendorf
UV Detectionsystem	Intas
Vortexgenie2	Scientific Industries
Waterbath	GLF
X-ray detection system (Curix 60)	Afga

4.1.11 Microscopes

Axiovert 135 (inverted) DIC	Zeiss
Cell Observer CSU-X1 Yokogawa Spinning Disk AxioCam MRm and Evolve 512	Zeiss
Confocal laser scanning microscope LSM 710	Zeiss
Fluorescence-Stereomicroscope MZ 16F	Leica
Fluorescence-Stereomicroscope MZ 16FA	Leica
Mikroskop Zeiss Axioplan 2 imaging AxioCam HRc	Zeiss
Stereomicroscope Zeiss Stemi 2000-C	Zeiss
ZebraBox Revolution High sensitivity digital camera (30 frames/s)	ViewPoint

4.1.12 Hardware and software

Adobe Illustrator CS5	Adobe Systems Software
Adobe Photoshop CS5	Adobe Systems Software
Axiovision 4.0	Zeiss
Bio-Rad CFX Manager 2.0	Bio-Rad
CLC Main Workbench 6	CLC bio
Gen5	BioTek
GraphPad Prism 6	GraphPad Software
ImageJ/Fiji	NIH, USA
Leica Application Suite	Leica
MacBookPro	Apple
Microsoft Office for Mac 2011	Microsoft
Papers2	Mekentosj
Zebralab tracking software 3,22,3,9	ViewPoint
Zen Black 2011	Carl Zeiss Microimaging
Zen Blue 2011	Carl Zeiss Microimaging

4.2 Methods

4.2.1 Zebrafish specific methods

4.2.1.1 Zebrafish husbandry and handling of embryos

Husbandry, breeding, and mating of wildtype, transgenic, and mutant zebrafish was according to standard methods (Mullins et al., 1994). Embryos and larvae were kept at 28.5°C in E3 medium until 5dpf. Developmental stages were determined as described by Kimmel et al. (Kimmel et al., 1995). Zebrafish embryos and larvae used for *in vivo* imaging or whole mount immunofluorescence (IF) stainings were treated with 1xPTU to avoid pigmentation (Karlsson et al., 2001).

4.2.1.2 Bleaching of fertilized zebrafish eggs

Fertilized zebrafish eggs were bleached to prevent contamination of the zebrafish facility by pathogens that can reside at the outer side of the chorion. This procedure is possible after epiboly is finished, until approx. 1.5dpf. The fertilized zebrafish eggs were placed in a tea net and were exposed to bleaching solution for 5min. Then the embryos were washed for 5min in tap water. This procedure was repeated once. After that the fish eggs were transferred into a new petri dish using E3 without methylene blue. 10µl of Pronase stock solution were added to allow the embryos to hatch from the denatured chorion.

4.2.1.3 Mating of adult zebrafish

For mating a female and male zebrafish were transferred to a mating box filled with water from the zebrafish facility (afternoon/evening). If the eggs needed to be of the same developmental stage the mating pairs were separated overnight (o/n) by a divider in the mating box. In the morning the divider was removed to allow spawning. After spawning, eggs were collected and put in a petri dish with E3 methylene blue.

4.2.1.4 Microinjection into zebrafish eggs

Microinjections into zebrafish eggs were performed at one- to two-cell-stage. Before injections, injection needles and injection agar plates were prepared. Injection needles were pulled with a needle puller using the programme P(A)60. Microinjection molds were placed into a petri dish containing 1.5% agarose in E3 to generate injection agar plates. Half of the freshly spawned eggs were sorted into the cavities, created by the molds of the injection plates. The other half served as a control. 2-4pl of 0.4µg/µl/ZFN mRNA solution of ZFN pairs or 0.1µg/µl to 0.4µg/µl mRNA solution (diluted with 0.4M

KCl in DEPC or DEPC H_2O) were injected into the yolk. Afterwards eggs/embryos were transferred into a petri dish containing E3 methylene blue. All eggs/embryos were kept at 28°C and unfertilized eggs were sorted out after a few hours. The next days embryos were examined for phenotypic alterations. Only injected embryos/larvae that had a normal appearance were fixed for further analysis or were raised to adulthood in the fish facility.

4.2.1.5 Fin biopsies from adult zebrafish

Determination of the genotype of a single zebrafish was performed on tail fin biopsies. Adult zebrafish were anaesthetized in fish facility water containing 5-10% Tricain stock solution, until the gills stop moving. A little piece of tissue from the periphery of the tail fin was cut on a cutting board and fixed in 100% methanol. Afterwards the zebrafish was transferred immediately to a single box containing fish facility water to recover.

4.2.1.6 Tissue harvesting from adult zebrafish

Tissues from adult zebrafish were isolated as described by Gupta and Mullins (Gupta and Mullins, 2010) and Gerlach et al. (Gerlach et al., 2011).

4.2.1.7 Fixation and storage of zebrafish samples

Embryos, larvae, and tissues for protein analysis or mRNA isolation were transferred to microcentrifuge tubes. The liquid was completely removed and samples were shock frozen in liq. N_2. Microcentrifuge tubes containing samples were stored at -80°C until usage.
Embryos for whole-mount IF stainings were transferred to microcentrifuge tubes. The liquid was removed, replaced by 4% PFA and samples were fixed o/n at 4°C. The success of fixation was examined by stereo microscopy. PFA was removed and samples were rinsed once with 1xPBST. Then they were washed three times for 5min with PBST on a shaker at room temperature (RT). Finally, a set of methanol washes (30% methanol in PBST, 60% methanol in PBST, 100% methanol) was performed with 5min steps on a shaker at RT. Samples were stored in 100% methanol at -20°C until usage.
Adult brain samples for cryosections were harvested as described above, washed in 0.1M PB pH7.4 and fixed for 4h in cold 2% PFA in 0.1M PB pH7.4 at RT on a shaker. Then the PFA was removed and brains were washed three times, 5min in 0.1M PB pH7.4. Samples were kept in 0.1M PB pH7.4 at 4°C until further processing.

4.2.1.8 Whole mount immunofluorescence stainings

For whole mount IF stainings embryos previously fixed in 4% PFA and stored in methanol were used. First the samples were rehydrated stepwise by a methanol series (60% methanol in PBST, 30% methanol in PBST). After the 5min lasting rehydration steps on a shaker at RT, the samples were washed three times for 5min in PBST at RT. 24hpf embryos for stainings with ZE-BO 1F4, Pax7, F59, or α-actinin were used for IF stainings right after this step. 48hpf embryos for stainings with ZE-BO 1F4, Pax7, F59, or α-actinin were treated on the bench at RT for 20min with 10µg/ml PK in PBST to make them permeable for the antibodies. 28-29hpf embryos for stainings with Znp1 and Zn1 were treated for 6.5min with 1mg/ml collagenase in PBST instead. After removal of PK or collagenase the remaining proteases were inactivated by re-fixating the embryos for 20min in 4% PFA on a shaker at RT. After removing the PFA, samples were washed for three times 5min in PBST.
Blocking was performed for 1h in NCST on a shaker at RT. Then the primary antibody was added in NCST, 0.05% NaN_3 and samples were incubated on a shaker at 4°C o/n. The next day the primary antibody was removed and kept for further use at 4°C. Afterwards, the samples were rinsed with PBST and washed three times for 15min in PBST on a shaker at RT. Then they were blocked two times for 30min in NCST. The secondary antibody was applied in NCST on a shaker at 4°C o/n. After removal of the secondary antibody samples were rinsed with PBST and washed three to five times for 15min in PBST depending on the strength of the fluorescence signal. Samples were recorded by microscopy as soon as possible. For longer storage samples were transferred stepwise to 75% glycerol in PBST and stored at 4°C.

4.2.1.9 Lämmli lysis of zebrafish samples

For the isolation of proteins Lämmli lysis was used. Microcentrifuge tubes containing shock frozen embryos, larvae, or adult tissue were put on dry ice. Then the Lämmli buffer was added at RT and the tissue was immediately and completely disrupted by sonication or with the tissue homogenizer. Afterwards the samples, total lysates, were boiled for 5min, 750rpm at 95°C and centrifuged 15min at 13000rpm to remove debris. The supernatant was used for SDS-PAGE. Remaining Lämmli lysed samples were stored at -20°C. For reuse samples were boiled once again for 5min, 750rpm at 95°C and centrifuged 1min at 11000rpm.

4.2.1.10 Staging of zebrafish embryos

To address the issue of a developmental delay, zebrafish embryos were staged by somite counting (Kimmel et al., 1995). Wildtype and homozygous mutant embryos were produced by setting up incrosses of wildtype and homozygous mutants, respectively. Spawning was only allowed for a short time period. Then the embryos were collected, put to 28°C, sorted for fertilization. 50 embryos were put into a new petri dish containing fresh E3. O/n embryos were incubated at 21°C to slow down the development of the embryos. When wildtype embryos had reached the 14 somite stage, the somites were counted at 21°C in at least 30 embryos per genotype.

4.2.1.11 LysoTracker Red labeling

Acidic compartments, including lysosomes, were labelled using LysoTracker Red (He and Klionsky, 2010). An end concentration of 10µM in E3 was used and living, anaesthetized embryos were incubated for 30min in this solution, wrapped in aluminium foil to protect the dye from degradation by light. Embryos were then rinsed twice with E3, embedded in agarose for imaging and imaged immediately by spinning disk confocal microscopy using a 561nm laser (Mahmood et al., 2013a).

4.2.1.12 Neutral red staining

Neutral red staining was performed to estimate the number of microglia (Herbomel et al., 2001). An end concentration of 2.5µg/ml in E3 was used and living, anaesthetized larvae were incubated for 1-2h in this solution, wrapped in aluminium foil to protect neutral red from degradation by light. Larvae were then rinsed twice with E3 plus 1xTricain, embedded in agarose for imaging and imaged immediately by spinning disk confocal microscopy using a 561nm laser.

4.2.1.13 Acridine orange staining

To estimate the number of cell undergoing cell death acridine orange staining was performed (Paquet et al., 2009). Living, anaesthetized larvae were incubated for 30min in 3µg/ml in E3 containing 1xTricain. The plates were wrapped in aluminium foil to protect acridine orange from degradation by light. Then larvae were rinsed twice with E3 1x Tricain, embedded in agarose for imaging and imaged immediately by spinning disk confocal microscopy using a 488nm laser.

4.2.1.14 *In vivo* imaging of zebrafish embryos and larvae

In vivo imaging of living zebrafish embryos or larvae was done using brightfield, laser scanning confocal or spinning disk confocal microscopy. Animals were anaesthetized in 1xTricain in E3 and mounted in 3% Methyl cellulose for short recordings or 1.5% Agarose in E3 for long time *in vivo* imaging, both containing 1xTricain. Agarose embedded embryos were covered with 1xTricain in E3 to protect the sample from drying out.

4.2.1.15 Pentylenetetrazole treatment

Pentylenetetrazole (PTZ) is an agent known to induce seizures in zebrafish (Baraban et al., 2005). Larvae were treated in 800µl E3 containing 15mM PTZ 1%DMSO and their movement was tracked for 5min after an incubation period of 30min. Control larvae were incubated in 800µl E3 1%DMSO.

4.2.1.16 Locomotion analysis

Locomotion analysis was performed at 5dpf. For each experiment 6 larvae per genotype or treatment were analysed. Individual larvae were placed in a single well of a 24-well plate in 800µl E3 or a solution containing the respective agent. After an adaption period of 30min in the ZebraBox Revolution, movements were recorded at RT for 5min in this device using a high sensitivity digital camera (30 frames/s) in combination with the ZebraLab tracking software. Tracks were visualized by the ZebraLab tracking software (max 115, small/large: 0.6cm/s, inact/small: 0.2cm/s). To test whether the swimming response is changed upon a stimulus (darkness) in mutants compared to wildtype, larvae were adapted to the device for 40min in 100% light. Then their movement was tracked for 5min 100% light, 5min 0% light, 5min 100% light, 5min 0% light, and 5min 100% light with the setup described above and tracks were analysed.

4.2.1.17 Cryosections of zebrafish larvae or brain

PTU-treated embryos or adult brains that were fixed previously were impregnated o/n in 30% sucrose. Then the samples were mounted and frozen in TissueTek O.C.T. on dry ice. 10-12mm sequential slices were cut on a cryostat and collected on Superfrost PLUS slides (Mahmood et al., 2013a). Slides were stored at -80°C.

4.2.1.18 Periodic acid-schiff stain

For Periodic acid-schiff (PAS) stain freshly prepared cryosections are needed. Before staining the samples were rehydrated in dH_2O. Then the slides with sections were

immersed in 0.5% periodic acid solution at RT for 10min. Afterwards, the slides were rinsed three times in dH_2O, followed by 15min incubation in Schiff's reagent at RT in the dark. Then the sections were washed with tap water. Thereby, the sections turned immediately dark pink. Sections were rinsed till the pink water-colour was gone. A counterstain with Mayer's Haematoxylin was performed for 30s. Sections were washed in tap water for 5min. To dehydrate the sections the following series was done: 30s 70% EtOH in dH_2O, 30s 90% EtOH in dH_2O, twice 2min 100% EtOH and 3min 100% EtOH. Then slides with sections were incubated three times 5min in Xylene and mounted in DePex Mounting Medium. After drying samples were ready for imaging.

4.2.1.19 Tail fin amputation in zebrafish embryo/larvae

Tail fins in zebrafish embryo/larvae were dissected at 2dpf or 3dpf with micro spring scissors in 1xTricain in E3 (Yoshinari and Kawakami, 2011). For mRNA isolation from the dissected tail fin, tail fins were amputated and embryos were fixed in RNAlater at 3hpa, 24hpa, 48hpa, and 72hpa. By cutting the fixed larvae after the yolk extension tail fin tissue was enriched. This tissue was then used for mRNA extraction.
Tail fin dissected embryos used in the regeneration assay were kept in single wells and imaged by brightfield microscopy at 0hpa, 24hpa, 48hpa, and 72hpa.
Transgenics with labelled myeloid cells with tail fins dissected were imaged immediately by *in vivo* time-lapse spinning disk confocal microscopy.

4.2.1.20 Chemically induced inflammation assay

$CuSO_4$ was used to induce an inflammation as described in d'Alençon et al. (d'Alençon et al., 2010). Embryos were fixed for mRNA isolation after 1h of $CuSO_4$ treatment and after further 3h and 6h of recovery.

4.2.1.21 FACS of macrophages and neutrophils

Macrophages were FACS sorted from 150 to 200 Tg(*mpeg1*:mCherry) larvae at 6dpf and neutrophils from 150 to 200 Tg(*mpx*:GFP) larvae at 6dpf by Julien Rougeot at the Institute of Biology, Leiden University (J. Rougeot, unpublished). For the macrophage experiments 500000 cells were obtained for the negative background and around 60000 mCherry positive cells. For the neutrophils 500000 cells were obtained for the negative background and around 5000 to 11000 GFP positive cells.

4.2.1.22 Stab wound injury

Stab wound injuries in the adult zebrafish telencephalon were performed by Rossella di Giaimo and Jovica Ninkovic at the Institute of Stem Cell Research, Helmholtz Center Munich according to Baumgart et al. (Baumgart et al., 2012).

4.2.2 Cellbiological methods

Cellbiological experiments were performed in collaboration with Anja Capell and Katrin Fellerer from our institute to obtain tagged-proteins for monoclonal antibody testing.

4.2.2.1 Cell cultivation

HEK293T were kept in cell culture medium. Cells were incubated in cell culture flasks of different size at 37°C and 5% CO_2. For transfections cells were plated in 60mm or 100mm Petri dishes.

4.2.2.2 Transfection of cells

24h after plating (approx. 80% confluency) cells were transfected using the lipofectamine transfection kit according to the manufacturer's instructions. 8µg/60mm and 12µg/100mm expression plasmid/petri dish were used. To facilitate the analysis of secreted proteins, the cell culture medium was removed 6h post transfection by Opti-MEM. Cells and medium were harvested approx. 24h after transfection as described below.

4.2.2.3 Harvesting of cells and whole cell lysis

Grna, Grnb, Grn1, and Grn2 are secreted proteins, therefore the cell medium was collected, centrifuged for 15-20min at full speed and transferred to new microcentrifuge tubes. The cell medium was kept on ice until further use or was frozen at -20°C. In parallel, the cells were washed twice with 1xPBS and detached from the dish with 1xPBS. Then they were centrifuged at 3500xg. PBS was removed and cells were either kept on ice until further usage or were frozen at -20°C. Cells were resuspended in ice-cold STEN lysis buffer containing 1x PI mix and incubated 10-20min on ice. During this incubation step, cells were mixed a few times intensely on a vortex device. Afterwards the sample was centrifuged at 4°C for 20min, 13000rpm. The supernatant was collected in a new microcentrifuge tube and the pellet was washed once again in STEN lysis buffer containing 1x PI mix. For further experiments the first supernatant (cell lysate) and the pellet (cell pellet) were used. After determination of the protein concentration 4x Lämmli sample buffer was added to the cell lysate and cell medium, and samples

were boiled at 95°C, 750rpm for 5-10min. The cell pellet was boiled in 100µl 2x Lämmli sample buffer. Then the samples were centrifuged for 1min at 13000rpm and were used for Immunoblotting or stored at -20°C.

4.2.3 Molecular biological methods

4.2.3.1 Isolation of genomic DNA

For the isolation of genomic DNA from tissue, which was fixed beforehand in 100% methanol, the methanol was removed with a pipette. To remove the methanol completely, the tissue was dried at 55°C. Then 50µl of lysis buffer was added to the fin tissue (30µl to embryos) and the samples were digested at 55°C for at least 1h. The inactivation of PK was done at 95°C for 5-10min. Remaining debris was removed in a short centrifugation step. The supernatant contains the genomic DNA and was used for further analysis.

4.2.3.2 Isolation of RNA

RNA from zebrafish embryos, zebrafish larvae, and adult zebrafish tissue was extracted according to the protocol of the RNeasy Mini Kit including DNase treatment (RNase-free DNase Set). Microcentrifuge tubes containing shock frozen embryos, larvae, or tissues were put on dry ice. For all steps RNase free consumables and solutions were used. The tissue was disrupted with the tissue homogenizer in 350µl+350µl RLT buffer containing β-mercaptoethanol. RNA was eluted in 30-50µl RNase-free water. The RNA quality was examined by agarose gel electrophoresis and the concentration was determined using a NanoDrop device. RNA from FACS sorted cells was extracted with the RNAqueous-Micro Kit. DNase treatment was performed with the DNase included in the kit. RNA was eluted in 11µl RNase-free water. All RNA solutions were stored at -80°C.

4.2.3.3 cDNA synthesis

cDNA synthesis was performed as described in the M-MLV Reverse Transcriptase kit. RiboLock RNase Inhibitor was utilized as RNase inhibitor. For cDNA that was used in qRT-PCRs 0.8µg total RNA and Random Primer Mix was used. The Random Primer Mix is an optimized mixture of hexamers and anchored-dT primer and does already contain dNTPs. Therefore, the addition of dNTPs was not necessary. RNase H digest was applied to remove RNA-DNA hybrids. For cDNA that was used in RT-PCRs 0.5µg total RNA were used. cDNA used for cloning of *grna* was amplified with a mix of 0.5µl dT16 Primer (50µM) and 0.5µl dT20 Primer (50µM), 1µl dNTP mix 10mM and 1-3µg total RNA. For the synthesis of all other cDNA 1µl Random Hexamere

Primer (50ng/µl) and 1µl dNTP mix 10mM were used. cDNA synthesis from mRNA derived from FACS sorted cells was performed using 10µl mRNA with the iScript cDNA Synthesis Kit. A β-actin control PCR (see below) was used as a control for cDNA synthesis was efficiency.

4.2.3.4 Polymerase chain reaction

Polymerase chain reactions (PCR) were used to amplify a chosen DNA fragment from a DNA template. Oligonucleotides were designed as described below. If not stated otherwise, the following mastermix / reaction was used:

mastermix / reaction	17.5µl PCR mix
	0.5µl 10µM forward primer
	0.5µl 10µM reverse primer
	0.2µl GoTaq DNA Polymerase

An indicated volume of DNA or cDNA was mixed with 15µl Mastermix and the following PCR programme was used as a standard scheme:

Cycle Step	Temperature	Time	No. of cycles
Initial Denaturation	95°C	2min	1
Denaturation	95°C	30s	xz
Annealing	xx°C	30s	
Extension	73°C	xy min	
Final Extension	73°C	5min	1

The annealing temperature (xx), extension time (xy), and number of cycles (xz) were adjusted for each PCR reaction.

4.2.3.4.1 β-*actin* control PCR

A β-*actin* control PCR was performed on synthesized cDNA to proof that the synthesis was successful. The general mastermix mentioned above was used and primers for the amplification of β-*actin* were oA03 β-actin F and oA04 β-actin R. For one reaction 0.5µl cDNA and 15µl mastermix were used. The annealing temperature was 60°C, the extension time 1min and the number of cycles 35. PCR products were analysed by agarose gel electrophoresis.

4.2.3.4.2 PCRs for sequencing of *grna* and *grnb*

To analyse *grna* and *grnb* for SNPs or other sequence variations both genes were partially sequenced. To amplify parts of *grna* and *grnb*, PCRs with the following primer combinations were used:

Amplicon	F Primer	R Primer	Annealing Temp.
grna exon3	BS-C07	BS-D38	61.8°C
grna exon4+5	BS-D39	BS-D40	58.4°C
grna exon6+7	BS-E01	BS-E02	66.8°C
grna exon8+9	BS-E03	BS-B04	61.8°C
grna exon10	BS-A05	BS-B16	60.0°C
grna exon11+12	BS-E05	BS-E06	66.8°C
grna exon13+14+15	BS-B17	BS-B18	64.6°C
grna exon16+17	BS-E07	BS-E08	58.4°C
grnb exon3	BS-E09	BS-C24	61.8°C
grnb exon4	BS-E10	BS-C18	61.8°C
grnb exon5+6	BS-E11	BS-B10	58.4°C
grnb exon7	BS-B11	BS-B12	60.0°C
grnb exon8	BS-E12	BS-B02	50.0°C
grnb exon10	BS-B14	BS-B15	58.4°C
grnb exon11	BS-E13	BS-E14	64.6°C
grnb exon12	BS-E15	BS-E16	58.4°C

The general mastermix was used with the primer pair combinations are listed in the table. For each reaction 5µl genomic DNA and 15µl mastermix were used. The annealing temperature was selected as shown in the table, the extension time was 1min and the number of cycles was 40. PCR products were separated by agarose gel electrophoresis, purified and sent for sequencing to GATC.

4.2.3.4.3 Screening/genotyping PCR for *grna* and *grnb* ZFN mutants

For screening/genotyping PCRs the general mastermix was used with the primer pairs BS-E24 grna ZFN F and BS-E25 grna ZFN R for *grna* and BS-E22 grnb ZFN F

and BS-E23 grnb ZFN R for *grnb*. For each reaction 2-2.5µl genomic DNA and 15µl mastermix were used. The annealing temperature was 63°C, the extension time 1min and the number of cycles 35. 5µl of the PCR product were then used for restriction endonuclease (RE) screening/genotyping, the residual PCR product was kept at 4°C and separated by agarose gel electrophoresis together with the sample that was digested by RE (see below).
For sequencing of the mutant alleles the reaction volume was scaled up three times. This PCR product was digested by restriction endonuclease digest, separated on an agarose gel and the band of the mutant allele was purified by DNA gel electrophoresis and sent for sequencing to GATC.

4.2.3.4.4 PCRs for cloning wildtype and mutant *grna* and *grna+MYC*

For the amplification of wildtype and mutant *grna* and *grna*+MYC cDNA templates were used (see above) and the following protocols using iProof High-Fidelity DNA Polymerase were applied:

	*grna*I	*grna*II	*grna+MYC*	Final conc.
5x iProof HF Buffer	4µl	4µl	4µl	1x
dNTP mix 10mM	0.4µl	0.4µl	0.4µl	200µM each
BS-E36 10µM	0.5µl	-	-	0.25µM
BS-E37 10µM	0.5µl	-	-	0.25µM
BS-E38 10µM	0.5µl	-	-	0.25µM
BS-E39 10µM	0.5µl	-	-	0.25µM
oC70 10µM	-	1µl	1µl	0.5µM
BS-E32 10µM	-	1µl	-	0.5µM
BS-E33 10µM	-	-	1µl	0.5µM
cDNA	1µl	1µl	1µl	-
DMSO	0.5µl	0.5µl	0.5µl	2.5%
iProof DNA Polymerase	0.2µl	0.2µl	0.2µl	0.02U/µl
sterile H_2O	ad 20µl	ad 20µl	ad 20µl	

The PCR programme suggested in the iProof DNA Polymerase manual was used with 10s denaturation time, 65°C annealing temperature, 20s annealing time, and 1min:30s extension time. The number of cycles was 30 and final extension was done for 10min.

1µl of the PCR products was analysed by agarose gel electrophoresis. If the analysis was positive parts of the PCR product were used for TOPO cloning reactions.

4.2.3.4.5 PCR for cloning *grnb+MYC*

In order to add a MYC-tag to *grnb*, the primer pair oC48 grnb F and BS-E21 grnb R+MYC was used. Instead of GoTaq DNA Polymerase 2µl pwo Polymerase were used per reaction. For each reaction 1µl pCR8/TOPO/GW-grnb (10ng/µl) and 14.8µl mastermix were used and 0.6µl GoTaq DNA Polymerase were added for the last 5 cycles to obtain a PCR product with sticky adenosine overhang. The annealing temperature was 60°C, the extension time 2min and the number of cycles 36. 1µl of the PCR product was analysed by agarose gel electrophoresis. If the analysis was positive parts of the PCR product were used for TOPO cloning reactions.

4.2.3.4.6 PCR for cloning *grn1*, *grn1+V5*, *grn2*, and *grn2+V5*

To clone to *grn1*, *grn1+V5*, *grn2*, and *grn2+V5*, the primer pairs oC54 grn1 F and oC55 grn1 R, oC54 grn1 F and BS-F36 grn1+V5 R, BS-E27 grn2 F long and BS-E35 grn2 R, BS-E27 grn2 F long and BS-E29 grn2+V5 R were used, respectively. For all, the general mastermix without polymerase was set up. 14.8µl mastermix and 1µl of a 1:10 dilution of the *grn1* or *grn2* EST were combined. To all reactions 2µl pwo polymerase were added. The standard PCR programme was used with an annealing temperature of 55°C, an extension time of 1min:30s and 35 cycles. 1µl of the PCR products was analysed by agarose gel electrophoresis. If the analysis was positive parts of the PCR product were used for TOPO cloning reactions.

4.2.3.4.7 Gradient PCR

Gradient PCRs were performed to determine the optimal annealing temperature of a primer pair. The general mastermix was used. A temperature gradient range from 50-70°C was tested as possible annealing temperatures. The extension time was adjusted to the expected size of the PCR product. PCR products were analysed by agarose gel electrophoresis.

4.2.3.4.8 Colony PCR

For colony PCRs single clones were picked with pipette tips and 30µl LB medium with the appropriate antibiotic were inoculated. Prior to the PCR the bacterial colonies were incubated at RT on the bench for 30min and stored for short-terms at 4°C. The general mastermix was used. Primers were selected that allowed to determine, if the insert was

integrated in the plasmid and in which orientation. For one reaction 3µl colony LB culture and 15µl mastermix were used. Annealing temperature and extension time were adjusted according to the primers used and the expected size of the PCR fragment. PCR products were analysed by agarose gel electrophoresis.

4.2.3.4.9 Semiquantitative PCR for *grna*, *grnb* and *grn1/grn2*

Semiquantitative PCR for *grna*, *grnb*, and *grn1/grn2* were done with the primer pairs BS-H14 grna ex2324 F and BS-H15 grna ex2324 R, BS-G46 grnb ex68 F and BS-G47 grnb ex68 R, BS-G06 grn1/grn2 ex34 Fa and BS-G07 grn1/grn2 ex34 Ra, respectively. The primer pair BS-H01 tbp ex23a F and BS-H02 tbp ex23a R was used to amplify the control *TATA binding protein* (*tbp*). 1µl cDNA and 15µl mastermix were used. The mastermix of one reaction contained 3.2µl 5x Green GoTaq Reaction Buffer, 0.3µl dNTPs (10mM), 0.5µl 10µM forward primer, 0.5µl 10µM reverse primer, 11.4µl dH_2O and 0.1µl GoTaq DNA Polymerase. The annealing temperature was 69°C, the extension time 30s and the number of cycles 30. For all PCR products the same volume was loaded on an agarose gel for agarose gel electrophoresis.

4.2.3.4.10 Quantitative PCR

All primer pairs for quantitative PCR (qPCR) spanned an exon-exon junction with an intron larger than 1kb to exclude amplification of genomic DNA. Specificity of the primers was tested by qPCR on wildtype cDNA and verified by a single peak in the melting curve analysis and one single band of the predicted size in agarose gelelectrophoresis. Additionally, the qPCR product was sequenced. qPCR was performed in 384-well format on a C1000 Thermal Cycler. For one reaction 2µl 1:3 to 1:10 cDNA dilution plus 3µl mastermix, composed of 2.5µl SsoFast Eva Green Supermix, 0.25µl 10µM forward primer and 0.25µl 10µM reverse primer were used. Each reaction was performed in triplicates. The PCR programme was 30s at 95°C, 50 cycles of 5s at 95°C and 10s at 60°C and a melting curve from 60°C to 95°C with increases of 0.5°C every 5s. qPCR on cDNA from FACS sorted macrophages or neutrophils was performed in 96-well format on a iCycle-MyiQ. For one reaction 5µl 1:10 cDNA dilution plus 15µl mastermix, composed of iQ SYBR Green supermix, forward primer and reverse primer were used. Each reaction was performed in duplicates. The PCR programme was 3min 95°C, 40 cycles of 15s at 95°C and 45s at 60°C and a melting curve from 95°C to 65°C with decreases of 0.5°C every 10s. The relative expression of each gene was calculated using the ΔΔCT-method and the normalized fold expression was calculated by normalisation to the reference gene(s) mentioned in the figure legend.

4.2.3.5 Agarose gel electrophoresis

Agarose gel electrophoresis was performed to analyse and separate PCR products, to analyse RE digests or to control RNA quality. Dependent on the size of the expected product 0.8-2% agarose gels containing ethidium bromide (approx. 1:50000) were used. Samples containing loading dye and a suitable DNA ladder were transferred to the gel. Electophoresis was performed in 1xTBE buffer until a clear separation of the bands of interest could be documented with a UV detection and documentation device.

4.2.3.6 DNA gel extraction and PCR purification

For the purification of PCR amplicons two methods were used. Either the PCR products were purified directly according to the NucleoSpin PCR Clean-up protocol or they were separated on an agarose gel, cut out and purified as described in the NucleoSpin Gel Clean-up protocol. Purified DNA was eluted in 30-50µl elution buffer NE and was either analysed by sequencing or used for cloning.

4.2.3.7 TOPO cloning

For molecular cloning the pCR8/GW/TOPO TA Cloning Kit or the TOPO TA Cloning Kit, Dual Promoter were used. Proof-reading polymerases do not generate sticky adenosine ends, which are required for both kits. The sticky adenosine ends were added as described in the following reaction: 20µl purified PCR product, 5µl 5x GoTaq Buffer, 0.5µl 10mM dATP and 0.3µl GoTaq DNA Polymerase were incubated for 15min at 72°C. Then 1-4µl PCR product were used in a TOPO Cloning reaction following the manual of the respective Cloning Kit. Instead of 1µl TOPO Vector 0.5µl were used. The TOPO cloning reaction was incubated for up to 30min. Afterwards the TOPO cloning reaction was used for transformation in chemically competent *E. coli* cells.

4.2.3.8 Gateway cloning

To transfer DNA fragments into expression clones the Gateway cloning system was used. 100ng/µl pCR8/GW/TOPO vector containing the DNA fragment of interest served as entry clone and 150ng/µl pCS2+ vector containing the Gateway cassette as destination vector. The Gateway cloning reaction was conducted as described in the user manual of the Gateway LR Clonase II Enzyme Mix. 1-5µl LR Clonase reaction were subsequently used for transformation in chemically competent *E. coli* cells.

4.2.3.9 Chemical transformation of bacteria

To transform plasmid DNA in bacteria, chemically competent DH5α or TOP10 *E. coli* cells were used. Cells were thawed on ice and 2-4µl of TOPO cloning reactions, 2µl of LR cloning reactions or 10pg- 100ng plasmid DNA were added and incubated on ice for 30min. Then a heat-shock at 42°C for 30s was done and microcentrifuge tubes were placed on ice again for 3min. To allow the bacteria to synthesise the antibiotics, 250µl SOC medium were added and bacteria were incubated at 37°C, 200rpm for 1h. Then 10-200µl of the transformation were spread on pre-warmed LB agar plates containing the appropriate antibiotic. When using the TOPO TA Cloning Kit Dual Promoter LB agar plates were coated beforehand with 40µl IPTG stock and 40µl X-Gal stock to allow blue/white selection. LB agar plates were incubated o/n at 37°C. If bacteria colonies were present, some were selected and analysed for the integration of the correct plasmid by colony PCR or miniprep culture and subsequent plasmid mapping using RE digest.

4.2.3.10 Cultivation of bacteria and plasmid DNA isolation

Depending on the subsequent application, plasmids were isolated at a different scale and purity.
For miniprep isolation of plasmids 3-5ml of LB medium containing the appropriate antibiotics were inoculated with a single clone and incubated at 37°C, 200rpm, o/n. In parallel a LB agar masterplate with all single clones used was done. Plasmid DNA was isolated as described in the NucleoSpin Plasmid protocol. The concentration was determined with a NanoDrop device. Samples were stored at -20°C. Plasmids were mapped by RE digest and/or sequenced by GATC.
For midiprep isolation of plasmids 200ml of LB medium containing the appropriate antibiotics were inoculated with a single clone and incubated at 37°C, 200rpm, o/n. Plasmid DNA was isolated as described in the NucleoBond Xtra Midi protocol and dissolved in 200µl sterile dH_2O. The concentration was determined with a NanoDrop device and plasmid solutions were stored at -20°C. Plasmids were control sequenced by GATC and deposited to the Schmid laboratory plasmid database. Additionally, a sample for the glycerol stock collection was set aside. 800µl of midiprep LB culture were mixed with 200µl 80% glycerol in DEPC H_2O and stored as a glycerol stock at -80°C.

4.2.3.11 Restriction endonuclease digest

RE digest was used for plasmid mapping, plasmid linearisation, and screening/genotyping. Plasmid mapping was performed on plasmid DNA from minipreps. 1µl plasmid DNA was digested in 11µl RE solution. RE were used as recommended in the manufacturer's manual in the most suitable buffer (https://www.neb.com/tools-and-resources/interactive-tools/double-digest-finder) . The digested products were analysed by agarose gel electrophoresis.
20µg ZFN plasmids were linearised in 100µl as described in the manufacturer's instruction but with an excess of RE for at least 2h. For all other linearisations 5µg or 10µg plasmid DNA were linearised in a 20µl or 50µl reaction. Agarose gel electrophoresis was used to examine if the plasmid was successfully linearised.
For screening/genotyping 10µl mastermix were added to 5µl PCR product.

Mastermix / reaction	1.5µl buffer
	0.3µl RE
	8.2µl sterile dH_2O

The samples were incubated for at least 2h at the temperature indicated in the manufacturer's manual and examined by agarose gel electrophoresis.

4.2.3.12 DNA purification and precipitation

Linearised plasmids were purified prior to *in vitro* mRNA synthesis according to the following different but similar protocols.
Protocol 1: To remove any residual RNase A activity, PK treatment was performed. This was done at 55°C for 30min in a solution containing 0.5µg/µl PK and 0.5% SDS. Then the liquid was transferred to a phase lock gel tube. An equal volume of phenol/chloroform/isoamylalcohol was added and microcentrifuge tubes were mixed 3min by vigorous inverting. Then the microcentrifuge tube was centrifuged for 5min at full speed and an equal volume of chloroform/isoamylalcohol was added to the supernatant. The microcentrifuge tube was vigorously inverted for 1min and centrifuged for 5min at full speed. The supernatant ready for precipitation was transferred to a new microcentrifuge tube (precipitation see below).
Protocol 2 (for ZFN): Steril dH_2O was added ad 250µl and transferred to a phase lock gel tube. 125µl phenol and 125µl chloroform were added and the liquid was mixed by vigorous inverting. Then the samples were centrifuged for 5min at full speed and an equal volume of chloroform was added to the supernatant. The microcentrifuge tube was vigorously inverted and centrifuged for 5min at full speed. The supernatant was transferred to a new microcentrifuge tube.

For precipitation $\frac{1}{10}$vol% 3M NaOAc pH4.5 and $2\frac{1}{2}$vol% 100% ethanol were added and incubated for 15min at -20°C. Then the samples were centrifuged for 20min at 4°C at 13000rpm and the supernatant was discarded. 300µl 75% ethanol were added and samples were centrifuged for 5-10min at 4°C at 13000rpm. The supernatant was removed. The pellet was dried at RT, dissolved in 20µl DEPC H_2O and used for mRNA synthesis.

4.2.3.13 *In vitro* mRNA synthesis and purification

mRNAs for microinjections require a 5'-cap and a polyA tail to enhance the stability and efficient translation. mRNA was synthesized *in vitro* from linearised plasmids with two different kits. *grnb* ZFN mRNAs were transcribed using the MessageMAX T7 mRNA transcription kit and *grna* ZFN mRNAs with the mMESSAGE mMACHINE T7 kit. During the plasmid linearisation the BGH polyA site following the ZFN coding sequence is cut of by the RE suggested in the manufacturer's manual. Therefore it was necessary to add a polyA tail by a polyA tailing reaction. The A-Plus Poly(A) Polymerase Tailing Kit was used as described in the instructions. *grna* and *grnb* ZFN mRNAs were purified using the MEGAClear Kit as described in the manufacturer's manual.
All other mRNAs for microinjections were synthesized with the mMESSAGE mMACHINE T7 or SP6 kit according to the manufacturer's protocol. For the purification lithium chloride precipitation was performed as described in the manufacturer's manual. All *in vitro* synthesised mRNAs were controlled by agarose gel electrophoresis and the concentration was determined using a NanoDrop device. mRNA was stored at -80°C.

4.2.3.14 *In vitro* transcription and translation

The TNT Coupled Reticulocyte Lysate Systems (SP6) was used for *in vitro* transcription and translation according to the technical bulletin. 0.5µg circular DNA templates were used for each reaction. RiboLock was applied as ribonuclease inhibitor and radiolabelled [^{35}S]-labelled methionine (Met) was used. Once the translation reaction was completed 4x Lämmli buffer was added and samples were boiled at 95°C for 5min to denature the proteins. Denatured samples were separated and analysed by SDS-PAGE.

4.2.3.15 Determination of protein concentration

For the determination of protein concentrations in cell culture lysates a BC Assay was applied as described in the protocol of the BC Assay Protein Quantitation Kit. BSA was used for the standard curve. The reaction was measured with a plate reader at 562nm.

4.2.3.16 SDS-polyacrylamide gel electrophoresis

SDS-polyacrylamide gel electrophoresis (SDS-PAGE) was done to separate proteins according to their molecular weight (MW). The percentage of the running gel was chosen depending on the expected MW of the protein of interest (http://www.thermoscientificbio.com/uploadedFiles/Resources/general-recommendations-for-sds-page.pdf) . Running gel (25ml for three times 1.5mm or 6-times 0.75mm gels) and stacking gel (6ml for 3 gels):

	7%	8%	12%	15%	St. gel
40% acrylamide	4.43ml	5.03ml	7.58ml	9.45ml	563µl
Running buffer	12.5ml	12.5ml	12.5ml	12.5ml	-
Stacking buffer	-	-	-	-	750µl
10% SDS	250µl	250µl	250µl	250µl	60µl
dH_2O	7.57ml	6.97ml	4.42ml	3.15ml	4.913ml
10% APS	250µl	250µl	250µl	250µl	60µl
TEMED	5µl	5µl	5µl	5µl	6µl

The PAGE equipment including denaturing gels was assembled and SDS running buffer was added. Wells were rinsed with SDS running buffer prior to loading of samples as well as protein standard to the wells. Electrophoresis was started with 80V, increased to 120-150V after the protein standard began to separate and was stopped when the region of interest showed a clear separation. Gels were subsequently used for Western Blotting or those containing radioactively labelled proteins for autoradiography.

4.2.3.17 Autoradiography

Polyacrylamide gels containing radioactively labelled proteins were fixed in destain solution for 30min on an orbital shaker. Then the solution was poured off and the gel was washed with H_2O until the acetic acid smell was gone. Subsequently, the gel was soaked in Amplify-Solution (Amplify Fluorographic Reagent) for 30min on an orbital shaker covered with aluminium foil to protect the light-sensitive solution. After that, the gel was dried with a vacuum dryer at 75°C for 1h:30min. X-ray films were put on the dried polyacrylamide gel, were exposed for 2-14h and were developed.

4.2.3.18 Protein transfer to PVDF-membrane (Western blotting)

Wet tank Western blotting was used to transfer and immobilize proteins on a membrane. Prior to blotting on PVDF-membranes, pre-wetting (activation) of the PVDF-membrane in methanol or isopropanol was performed. Afterwards, the membrane was washed in dH_2O and was put in 1x transfer buffer. Membrane and gel were assembled between foam pads and Whatman paper in a holder cassette. Then the proteins were transferred onto the PVDF-membrane in 1x transfer buffer at 400mA for 70min (90min for Grna). Membranes were subsequently used for immunodetection.

4.2.3.19 Immunodetection of proteins

After Western blotting, membranes were incubated at RT for 1h on an orbital shaker in i-Block, PBST milk, or TBST milk. Then the primary antibody was added in i-Block, PBST milk, or TBST milk, 0.05% NaN_3 and the membrane was incubated on a shaker at 4°C o/n. The next day the primary antibody was removed and kept for further use at 4°C. Afterwards the membrane was rinsed with PBST or TBST, was washed two times for 15min in PBST or TBST and then for two times for 15min in PBST milk or TBST milk on a shaker at RT. The secondary antibody was applied in PBST milk or TBST milk for 1h at RT. After removal of the secondary antibody the membrane was rinsed with PBST or TBST, was washed four times for 15min and three times for 10min in PBST or TBST. For immunodetection ECL Plus was used as indicated in the manual. The HRP moiety of the secondary antibody or direct conjugated antibody induces the emission of light from the substrate that can be detected upon exposure of X-ray films. After immunodetection the membrane was washed three times for 5min in PBST or TBST and either dried for storage or reused. Before a second immunodetection the membrane was stripped using one of the following protocols.
Stripping protocol 1: The membrane was incubated in 50ml stripping buffer plus 350µl β-mercaptoethanol at 50°C in a horizontally shaking water bath for 1.5h. Then the membrane was rinsed in PBST or TBST and washed six times for 5min in PBST or TBST. Afterwards the membrane was ready for the second immunodetection which was performed like the first immunodetection (see above).
Stripping protocol 2 (Yeung and Stanley, 2009): The membrane was incubated horizontally shaking in 10ml GuHCl-stripping buffer plus 70µl β-mercaptoethanol (0.1M) at RT for 5min. Then the membrane was washed two times for 5min in PBST or TBST. A second round of 5min incubation in 10ml GuHCl-stripping buffer plus 70µl β-mercaptoethanol followed. Afterwards, the membrane was rinsed in PBST or TBST and washed five times for 5min in PBST or TBST. After that, the membrane was

ready for the second immunodetection which was performed according to the first immunodetection (see above).

4.2.4 Others

4.2.4.1 Custom zinc finger nucleases

Custom ZFNs targeting *grna* and *grnb* designed according to the CompoZrTM algorithms were obtained from Sigma-Aldrich. *grna* and *grnb* were partially sequenced to determine the exact sequences of *grna* and *grnb* in our AB wildtype-line. In the pre-evaluation phase 16 pairs of possible ZFN DNA binding sites suggested by Sigma-Aldrich were aligned to the determined wildtype sequences and these with a perfect match were approved. After pre-evaluation the following ZFN sets summarised below were obtained from Sigma-Aldrich (ZFN binding sites capital letters; spacer/cut site small, italic letters). The *in vivo* evaluation of the ZFN sets and their usage for genome editing are described in detail in the results section.

ZFN sets	**binding and cut site**
grna PZFN1/PZFN2	TTTGCTCGCAGTGCCCCA*ataat*GAAGTCTGTGAAGCAGGC
grna PZFN3/PZFN4	CTGACAGTCTGCCTCGCT*gtggtg*ACCCTGGTTATTTGCT
grnb PZFN1/PZFN2	TACCACCTGCTGCCAG*atgcctg*ATGGGGGCTGGGGCT
grnb PZFN3/PZFN4	TACCACCTGCTGCCAG*atgcc*tgATGGGGGCTGGG
grnb PZFN5/PZFN6	ACCTGCTGCCAGATG*cctgat*GGGGGCTGGGGCTGCT

4.2.4.2 Generation of zebrafish specific monoclonal antibodies

Zebrafish specific monoclonal antibodies (mAb's) detecting Grna, Grnb, Grn1, and Grn2 were generated by the service unit monoclonal antibodies at the IMI, Helmholtz Center Munich. Peptides for immunization of mice and rats were synthesized and conjugated N- or C-terminally with ovalbumin (OVA) by Peptide Specialty Laboratories GmbH. The same peptides, also synthesized by Peptide Specialty Laboratories GmbH, were N- or C-terminally conjugated with BSA or biotin for the enzyme-linked immunosorbent assay (ELISA). The screening process for mAb's is described in the results section.

4.2.4.3 Databases, alignments and primer design

Databases used in this study are Ensembl Genome Browser (http://www.ensembl.org/index.html) and several resources provided by NCBI (http://www.ncbi.nlm.nih.gov/). CLC Main Workbench was used for alignments, assemblies, sequence analysis of DNA,

RNA and protein, calculation of the theoretical MW, RE mapping and construction of plasmid maps. Oligonucleotides were designed with CLC Main Workbench or Primer3 (http://primer3.ut.ee/). Primer specificity was evaluated using Primer-BLAST (http://www.ncbi.nlm.nih.gov/tools/primer-blast/). BLAST searches were performed on the Ensembl (http://www.ensembl.org/Multi/blastview) and NCBI (http://blast.ncbi.nlm.nih.gov/Blast.cgi) web pages.

4.2.4.4 Image processing and analysis

Images from microscopy were processed with ZEN blue, ZEN black, AxioVison, ImageJ, or Adobe Photoshop. In Adobe Photoshop the image size and levels were adjusted. Manual tracking of immune cells was done with the ImageJ plugin mTrackJ (Meijering et al., 2012) and images were stitched using the ImageJ plugin Image Stitching (Preibisch et al., 2009). Films from autoradiography or Western blotting were scanned with 600dpi resolution, converted to greyscale and image size as well as levels were adjusted with Adobe Photoshop. Bands on Western blot films were quantified by their density/intensity using ImageJ.

4.2.4.5 Statistics

Means, standard deviation (SD), and standard error of the mean (S.E.M.) were calculated using Graph Pad Prism. Graphs shown in this thesis were generated with the Graph Pad Prism software. The statistical analysis and test used are indicated in the respective figure legend.

5 Results

5.1 Characterization of zebrafish *granulins*

5.1.1 Four *granulins* in zebrafish

A database search in Ensembl (http://www.ensembl.org/index.html) identified four zf-*grns* - *grna*, *grnb*, *grn1* and *grn2* - annotated in the *Danio rerio* genome. Of these *grna* and *grnb* are listed to be orthologues of the mammalian *GRN*. *grn1* and *grn2* are paralogues of *grna* and *grnb* but lack a mammalian orthologue. The existence of four zf-*grns* was previously described (Cadieux et al., 2005). *grna* is located on chromosome 3 and due to its synthenic conservation potentially the true orthologue of the $7\frac{1}{2}$ granulin domain containing human GRN (Fig. 5.1) (Cadieux et al., 2005). I amplified *grna* from cDNA of 5dpf larvae and adult fin tissue. Its open reading frame (ORF) is 3147bp and it is translated into a 1049 amino acid (aa) protein, containing 12 granulin domains (Fig. 5.1) with a theoretical molecular weight (MW) of 112kDa. *grnb*, which is on chromosome 24, was amplified from cDNA of 4dpf larvae previously in

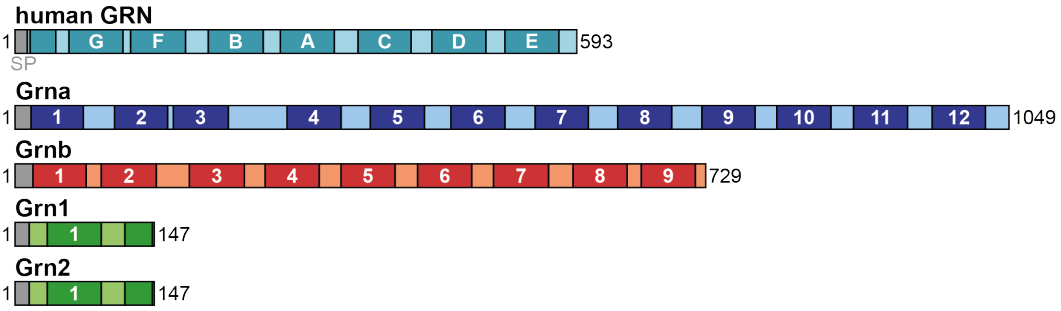

Figure 5.1 – Schematic illustration of human GRN and zf-Grns. Human GRN has $7\frac{1}{2}$ granulin domains, while 12 granulin domains were found in Grna, 9 in Grnb, and $1\frac{1}{2}$ in Grn1 and Grn2. Grey and SP: signal peptide. Black numbers: aa. Darker color and white letters/numbers: granulin domains.

the laboratory. Its ORF is 2187bp and translates into a 729aa protein with 9 granulin domains (Fig. 5.1). The calculated MW is 78kDa. *grn1* and *grn2* are both located side by side on chromosome 19 and are highly homologous (85% identity on aa level) (Fig. 10.1 and 10.2). I amplified both 441bp protein coding ORFs from expressed sequence tag (EST) clones. Both proteins are 147aa, with a theoretical MW of 16kDa and contain $1\frac{1}{2}$ granulin domains (Fig. 5.1).

5.1.2 Expression profile of zf-*grns*

The expression of the distinct zf-*grn* transcripts during development and in certain adult tissues was determined by RT-PCR. *grna* was expressed at very low levels from 1dpf to 5dpf. It was also expressed in brain, fin, and kidney with the highest expression in the kidney sample (Fig. 5.2 *grna*). In contrast, *grnb* was expressed from 1dpf to 5dpf

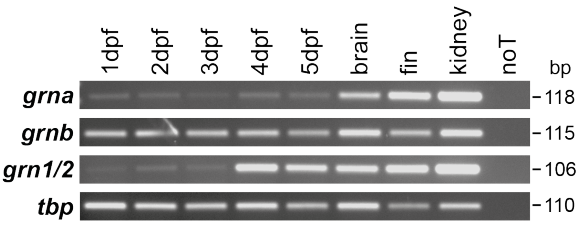

Figure 5.2 – Expression of zf-*grns* during development and in selected adult tissues. *grna* was expressed from 1dpf to 5dpf at very low levels. It was expressed stronger in brain, fin, and kidney. *grnb* was expressed throughout development and in all adult tissues analysed. *grn1/grn2* were expressed at very low levels from 1dpf to 3dpf. At 4dpf and 5dpf as well as in brain, fin, and kidney *grn1/grn2* were clearly expressed. *tbp* is used as reference. Semiquantitative RT-PCR. NoT: no template. 30 cycles.

as well as in samples derived from brain, fin, and kidney at levels comparable to the reference gene *tbp* (Fig. 5.2 *grnb*). Due to their high homology (Fig. 10.1) *grn1* and *grn2* were analysed with a primer pair that amplifies both, *grn1* and *grn2*, in one PCR reaction. From 1dpf to 3dpf *grn1/grn2* expression was almost absent, but at 4dpf and 5dpf they were clearly expressed, even higher than *grna* and *grnb*. In adult tissue the *grn1/grn2* expression resembled that of *grna*, being the highest in the kidney (Fig. 5.2 *grn1/grn2*).

grna and *grn1/grn2* expression was very high in kidney tissue, which is the main haematopoietic tissue in adult zebrafish, and *grn1/grn2* expression was high from 4dpf onward. At that stage of development the number of immune cells is increasing in zebrafish larvae. Moreover, it was shown that fish *granulins* are enriched in haematiopoietic tissue and cells of the myeloid lineage (Barreda et al., 2004; Belcourt et al., 1993, 1995; Craig et al., 2008; Hanington et al., 2006; Sakai et al., 2005; Zakrzewska et al., 2010). Therefore, I addressed if zf-*grn* transcripts are differentially expressed in macrophages or neutrophils. In a collaboration with Julien Rougeot from the laboratory of Annemarie Meijer at Leiden University, total mRNA was isolated from FACS sorted *mpeg1*:mCherry-positive cells, which are mainly macrophages, or *mpx*:GFP-positive cells, which are mainly neutrophils, and qPCRs were performed. *grna* and *grn1/grn2* mRNA transcripts were significantly enriched in the *mpeg1*:mCherry-positive cells from 6dpf old zebrafish larvae in comparison to *mpeg1*:mCherry-negative cells. *grna* expression was approx. 200-fold higher ($p = 0.0005$) and *grn1/grn2* expression was ap-

prox. 80-fold higher ($p = 0.003$) than in the corresponding *mpeg1*:mCherry-negative cells (Fig. 5.3A,C). In contrast, *mpeg1*:mCherry-positive cells and *mpeg1*:mCherry-negative cells from 6dpf larvae showed similar expression levels of *grnb* ($p = 0.2583$) (Fig. 5.3B). In *mpx*:GFP-positive cells *grna* and *grn1/grn2* mRNA transcripts were approx. 4-5-fold ($p = 0.0609$; $p = 0.0144$) higher than in *mpx*:GFP-negative cells (Fig. 5.3A,C). Whereas

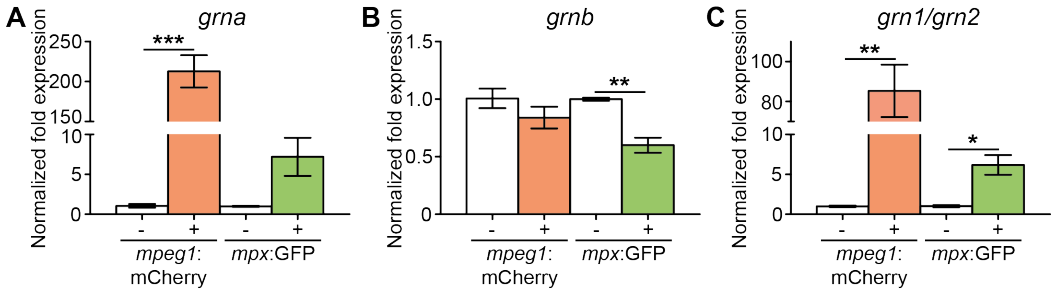

Figure 5.3 – mRNA expression levels of zf-*grns* in macrophages and neutrophils. **A**: *grna* mRNA was strongly enriched in *mpeg1*:mCherry-positive and to some degree in*mpx*:GFP-positive cells from 6dpf old larvae. $^{***}p = 0.0005$. **B**: *grnb* mRNA expression levels were indistinguishable in *mpeg1*:mCherry-positive and -negative cells and reduced in *mpx*:GFP-positive cells from 6dpf old larvae. $^{**}p = 0.0039$. **C**: *grn1/grn2* mRNAs in *mpeg1*:mCherry- and *mpx*:GFP-positive cells from 6dpf larvae were enriched. $^{**}p = 0.0030$. $^{*}p = 0.0144$. Normalized to *tbp*, *eif4a1b* and *eif5*. qPCR. $n = 3$. S.E.M. Unpaired t-test (two-tailed). **-** : *mpeg1*:mCherry- or *mpx*:GFP-negative. + : *mpeg1*:mCherry- or *mpx*:GFP-positive.

grnb mRNA was significantly depleted in *mpx*:GFP-positive cells ($p = 0.0039$) when compared to the *mpx*:GFP-negative cells (Fig. 5.3B).

In summary, zf-*grns* are expressed during development at different levels and in various tissues. Furthermore, *grna* and *grn1/grn2* expression is increased in haematopoietic tissue, particularly in macrophages, whereas *grnb* is not enriched in haematopoietic tissue.

5.1.3 Screening for zf-Grn specific antibodies

To detect zf-Grn proteins for example by Western blotting, monoclonal antibodies (mAbs) were generated. Epitopes in the zf-Grn proteins were selected that are located in the linker region close to the border of the granulin domains, to reduce the likelihood that the epitope is cleaved e.g. by elastase. The selected peptides and their conjugates are listed in table 5.1. These conjugated peptides were used by the service unit monoclonal antibodies (IMI, Helmholtz Center Munich) for the immunization of rats and mice. For the generation of mAbs, antibody producing lymphocytes, from the immunized animals, were fused with myeloma cells to hybridomas (Milstein, 1999). Supernatants from hybridoma cell pools were assayed by an ELISA using BSA or biotin-conjugated peptides at the service unit monoclonal antibodies (IMI, Helmholtz Center Munich).

Table 5.1 – Peptides for mAb generation and summary of hybridoma pools tested. Peptides for immunisation were conjugated N- or C-terminally to OVA via an endogenous (C) or added cysteine (-C-). Internal cysteines were replaced by the isosteric aa α-aminobutyric acid (AABA).

Peptide name	peptide sequence and conjugates	No. of positive / No. of all hybridoma pools tested
grb1	KEPALRETQRVEDRHMC-OVA	5/25
grb2	OVA-CTKSSSSTWWNNSL	10/30
gra1	KDLT[AABA]TNATHTQPLAD-C-OVA	4/45
gra2	LRRRS[AABA]VKTTRLYV-C-OVA	0/2
GRN1 / GRN2	VETVDTSASVIYC-OVA/ METEDVSASVIHC-OVA	3/145
grna_03	KQKRPETQRTTARPTGTTS-C-OVA	23/90
grna_04	GQRPSGKVK[AABA]NATHGC-OVA	2/13

Pools with a positive result were then tested in a first screen using immunoblotting of MYC- or V5-tagged zf-Grn proteins. These tagged zf-Grn proteins were derived from overexpression of zf-*grn* coding vectors in cell culture. While confirming the expression of the tagged proteins by Western blotting using tag-specific antibodies, I found Grna-MYC migrating on a SDS-PAGE between 150-250kDa at a MW of approx. 200kDa (Fig. 5.4A), Grnb-MYC at approx. 110kDa (Fig. 5.4B), and Grn1-V5 and Grn2-V5 at about 22kDa (Fig. 5.4C,D). Table 5.1 summarizes the number of tested

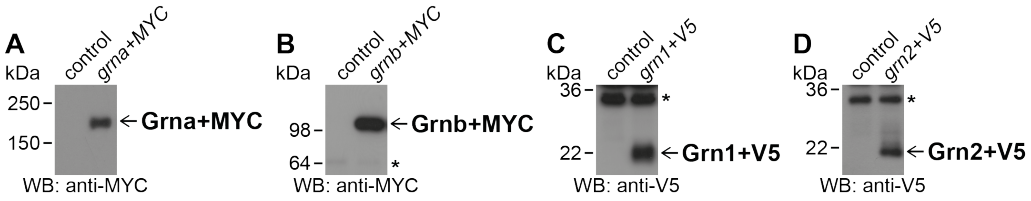

Figure 5.4 – Overexpression of tagged zf-Grn proteins in HEK293T cell culture. **A**: Grna+MYC did migrate on a SDS-PAGE at approx. 200kDa and was not detectable in the untransfected control. **B**: Grnb+MYC was detected on a SDS-PAGE at approx. 110kDa and was absent in the untransfected control. An unspecific band at 64kDa marked with an asterisk (*) served as loading control. **C-D**: Grn1+V5 and Grn2+V5 did migrate at about 22kDa on a SDS-PAGE and were not detected in the untransfected control. The asterisk (*) marks an unspecific band slightly below 36kDa that served as loading control.

hybridoma supernatant pools and the number of these having the ability to detect the overexpressed protein. The peptides selected to detect specifically Grn1 and Grn2 were very similar (Table 5.1), as Grn1 and Grn2 have a high homology (Fig. 10.2). Therefore, all hybridoma supernatant pools from immunizations with peptides GRN1 or

GRN2 were tested on Grn1+V5 and Grn2+V5 for Grn1 and/or Grn2 immuno-reactivity. Single clones from up to four positive tested hybridoma supernatant pools were then isolated by the service unit monoclonal antibodies (IMI, Helmholtz Center Munich). Media from these isolated single clones were tested in a second screen by immunoblotting using cell culture samples to isolate positive monoclonal Abs. By testing media from isolated single clones, no mAb for Grn1 and Grn2 could be established. For Grna clone grna_03 12E7-111 and for Grnb clone grb2 11F4-11 were positive. To confirm that these two mAbs do also recognize native zebrafish Grna or Grnb, *grna* and *grnb* mRNA were injected with and without a tag at one cell stage in fertilized zebrafish eggs. Overexpression of *grnb* in zebrafish embryos led to an increased intensity of the band above 98kDa at approx. 110kDa using mAb Grnb 11F4-11 for detection (Fig. 5.15). The detection of overexpressed Grna in embryos by Western blotting was not feasible. To confirm the specificity of mAb Grna 12E7-111, Grna was *in vitro* transcribed and translated from a vector coding for the ORF of *grna* using the TNT Coupled Reticulocyte Lysate System. [^{35}S]-labelled Grna protein from *in vitro* transcription and

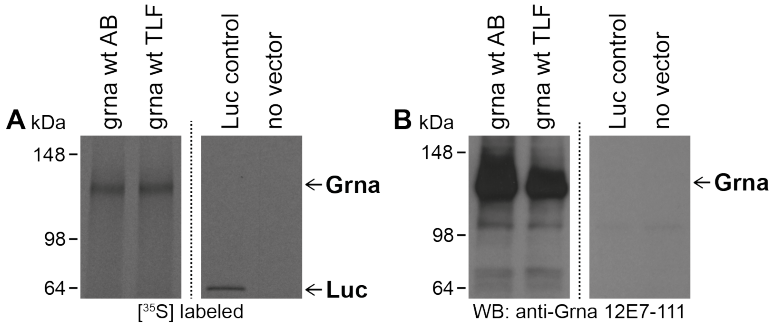

Figure 5.5 – The mAb Grna 12E7-111 detected *in vitro* transcribed and translated Grna. **A**: Autoradiography of *in vitro* transcribed and translated *grna* cDNA from wildtype (wt) AB and wt TLF zebrafish labelled with [^{35}S]-Met. Luciferase (Luc) control DNA labelled with [^{35}S]-Met. No vector control. **B**: *In vitro* transcribed and translated *grna* cDNA from wt AB and wt TLF zebrafish detected with mAb Grna 12E7-111. Luc control DNA and no vector control show no signal.

translation was detected on an autoradiography (Fig. 5.5A) and by mAb Grna 12E7-111 (Fig. 5.5B) at the same MW. In this assay Grna migrated at a lower MW than *in vivo* since post-translational modifications are not added to the protein in the *in vitro* assay. Therefore, this assay confirmed indirectly the specificity of mAb Grna 12E7-111.
Taken together, zebrafish specific mAbs detecting Grna and Grnb were successfully generated.

5.1.4 Grna and Grnb expression throughout development

Immunoblotting was performed with the Grna and Grnb specific mAbs to determine the protein expression of Grna and Grnb during development. No Grna specific band could

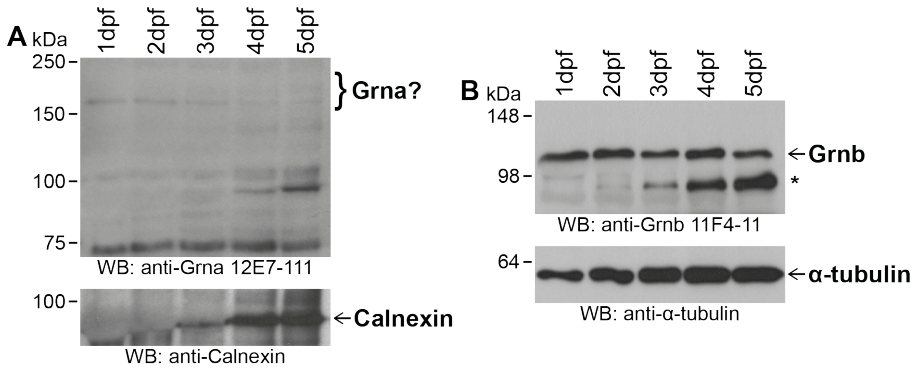

Figure 5.6 – Protein expression of Grna and Grnb during development. **A**: Grna protein levels were below the detection limit from 1dpf to 5dpf. All lanes contained protein (partially masked by yolk proteins) as confirmed by the Calnexin Ab. Two embryos per lane. **B**: Grnb was expressed from 1dpf to 5dpf as visualized by a band above 98kDa marked by a black arrow. The α-tubulin blot served as control. One embryo per lane. * unspecific band.

be detected between 150-250kDa (Fig. 5.6A), the range where Grna was expected since Grna+MYC derived from cell culture overexpression was migrating at approx. 200kDa (see also Fig. 5.15). This might be due to very low expression levels of *grna* at these stages of development (see Fig. 5.2). The Calnexin blot showed that the blotting was successful, even though the Calnexin band was masked at 1dpf to 3dpf by yolk proteins (Fig. 5.6A). When immunodetection with the Grnb specific mAb was performed a distinct Grnb signal above 98kDa was clearly detectable at all stages analysed (Fig. 5.6B). Also α-tubulin expression was detected throughout development. From 1dpf to 5dpf the amount of α-tubulin was increasing as the embryos/larvae were growing (Fig. 5.6B). In contrast to α-tubulin, Grnb expression was not increasing from 1dpf to 5dpf, which could be a hint that the Grnb expression is decreasing throughout development.
It can be concluded that Grna expression is below the detection limit from 1dpf to 5dpf and that Grnb protein is expressed from 1dpf through 5dpf.

5.2 Generation of Grna and Grnb loss of function mutants

Since it is published that patient mutations in GRN in FTLD-TDP/*GRN* and NCL/*GRN* lead to a partial or complete loss of functional protein (Cruts et al., 2012; Smith et al., 2012), I decided to generate Grna and Grnb loss of function zebrafish. I selected these two genes because of their orthology to human GRN. Like GRN, they

are composed of several granulin domains and would most likely allow to study the full length function of GRN. Loss of protein function studies can either be performed by KD or KO of a gene of interest. I chose a KO approach for this study, since it is more stable, inheritable, and additionally allows analyses in adult zebrafish. Moreover, unspecific phenotypes due to toxicity of the KD reagents are no longer an issue in KO zebrafish. One possibility to perform genome editing in a gene of interest in zebrafish is the application of ZFNs (Doyon et al., 2008; Meng et al., 2008).

5.2.1 ZFNs targeting *grna* and *grnb*

CompoZr Custom ZFNs from Sigma Aldrich targeting *grna* and *grnb* were obtained to generate mutations, which can lead to a stable and inheritable loss of protein function. The ZFNs were designed to target the first coding exons. Mutations in the very 5'

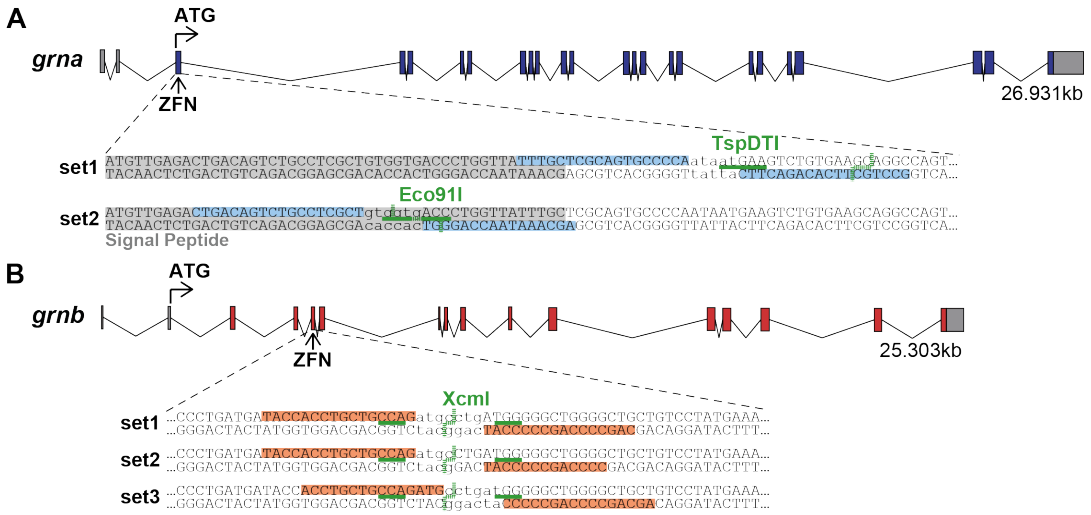

Figure 5.7 – Localisation of ZFN target sequences in *grna* and *grnb*. **A**: Schematic illustration of the genomic structure of *grna*. *grna* ZFN set1 and set2 target the first coding exon. *grna* ZFN set1 induced mutations can be detected with RE TspDTI and these of set2 using RE Eco91I. **B**: Schematic illustration of the genomic structure of *grnb*. All *grnb* ZFN sets are located in the third coding exon and ZFN induced mutations can be detected with RE XcmI. Grey boxes: untranslated region (UTR). Coloured boxes: coding region. Light red and light blue boxes: ZFN target sites. Green lines: binding and cut sites of RE.

region of the ORF, leading to a preTT codon, increase the likelihood for loss of function mutations, as such mRNAs are recognized by the NMD machinery (Vicente-Crespo and Palacios, 2010). Moreover, possible truncated proteins are very short and lose functional domains. I obtained two sets of ZFNs for *grna*, both targeting the first coding exon (Fig. 5.7A), and three sets for *grnb*, all targeting the third coding exon (Fig. 5.7B). For all targeting regions a BLAST search (http://blast.ncbi.nlm.nih.gov/Blast.cgi) with the target sites of the ZFN DNA binding domains was performed to evaluate the specificity

of the ZFN sets. *grna* and *grnb* were always the top hits and the only ones with a query cover of 100%. This indicates that the target sites of all ZFN sets are unique in the zebrafish genome and most likely highly specific for the respective gene of interest. Next,

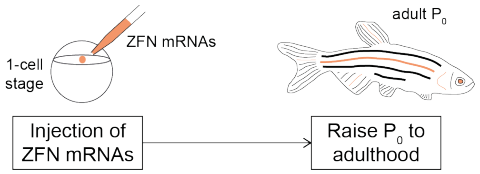

Figure 5.8 – Schematic illustration of mRNA injections of *grna* and *grnb* ZFNs and the resulting P0 generation.

the ZFN sets were injected as mRNAs by microinjection into fertilized zebrafish eggs at one cell stage (Fig. 5.8). Since all ZFNs contain a FLAG-tag in their coding sequence the translation of the ZFN mRNAs into proteins could be controlled by immunoblotting using an antibody detecting the FLAG-tag. In all samples injected with ZFNs bands at approx. 50kDa were present, that were absent in the uninjected siblings (Fig. 5.9). For most ZFN sets the two bands, which are derived from the ZFN that binds on the forward strand and the ZFN that binds on the reverse strand appeared as one band. The MW of the single ZFN is very similar. Nevertheless, the aa composition of the DNA binding site is unique for each ZFN and can result in a minor shift to a higher or lower MW (e.g. Fig. 5.9 ZFN *grna* set2). With these immunoblots I confirmed, that all

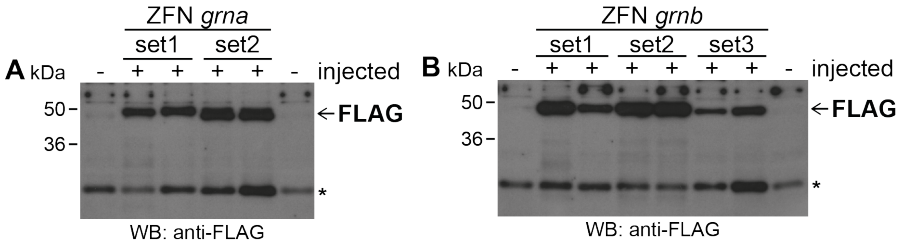

Figure 5.9 – All ZFN mRNAs were translated into FLAG-tagged proteins. **A**: Anti-FLAG immunoblot on control and *grna* ZFN mRNA injected samples. **B**: Anti-FLAG immunoblot on control and *grnb* ZFN mRNA injected samples. The asterisk (*) marks an unspecific band that served as loading control.

ZFN mRNAs were successfully translated into proteins.

The expression of proteins did not provide any information about the functionality of the ZFNs. To be functional the ZFNs need to form a nuclease heterodimer, that is able to cut double-strand DNA. Therefore, screening assays for all ZFN sets were established, which allow the detection of mutations induced by the cell's error-prone repair mechanism NHEJ, while repairing DSBs caused by active ZFNs. Thus, the screening assays are a read-out for ZFNs functionality and can additionally be used for genotyping of the established mutants afterwards. I amplified genomic DNA containing

Table 5.2 – Summary of screening assays for ZFN induced mutations in *grna* and *grnb*.

ZFN set	PCR product [bp]	RE (No. of cut sites)	band pattern in digested wt [bp]	band pattern in digested mut [bp]
grna set1	392	TspDTI (4)	46, 56, 79, 98, 113	46, 56, 79, **211**
grna set2	392	Eco91I (1)	159, 233	**392**
grnb set1-3	582	XcmI (1)	325, 257	**582**

the target sites of the ZFNs by PCR and digested the PCR product with the respective RE (Table 5.2). PCR product and RE digest were separated side by side by agarose gelelectrophoresis (Fig. 5.10). In a wildtype situtation, the PCR product is completely digested, which is represented by a complete shift to digested, smaller MW bands in the samples treated with RE. If the RE cuts once in the PCR product, two smaller bands are present in the sample digested with the RE (Fig. 5.10B,C uninjected), whereas if a RE cuts multiple times, several smaller bands are the result (Fig. 5.10A uninjected). Mutations altering the RE recognition site may prevent the digest and therefore, the

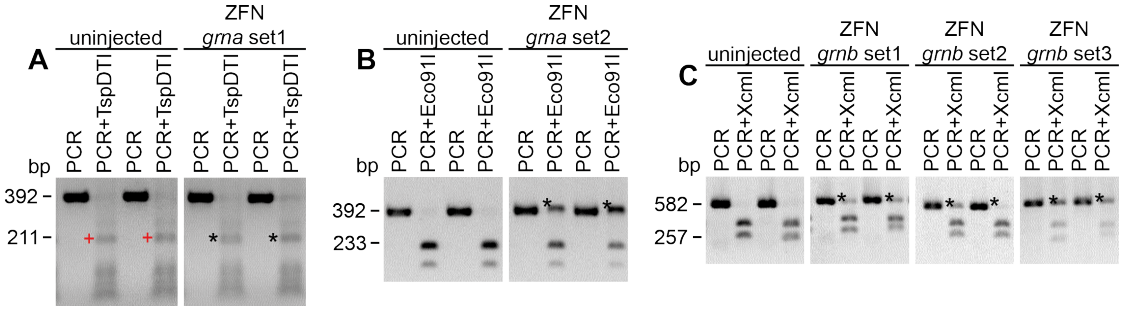

Figure 5.10 – Screening assays for ZFN-induced mutations in *grna* and *grnb*. Uninjected and injected P0 embryos were tested. PCR product and RE-digested PCR product were separated on agarose gels. **A**: Injection with ZFN *grna* set1 mRNAs. RE: TspDTI. The red plus mark the 211bp band that should be absent in RE-digested uninjected samples. **B**: Injection with ZFN *grna* set2 mRNAs. RE: Eco91I. **C**: Injection with ZFN *grnb* set1-3 mRNAs. RE: XcmI. **A-C**: The black asterisks (*) mark the band size in the RE-digested samples that remained in ZFNs injected samples only.

PCR product is digested only partially. The REs used for the screening assay and the expected band patterns are summarized in table 5.2. Since the RE, TspDTI, used for ZFN *grna* set1 cut four times in the *grna* PCR product, this screening assay was more complex compared to the other screening assays. Moreover, TspDTI led only to a partial digest in uninjected wildtype samples as the 211bp band, which corresponds to the band of ZFN induced mutations, was also visible in samples that were not injected with ZFNs (Fig. 5.10A). Therefore, it was difficult to discriminate with this screening assay between an incomplete digest and a partial digest due to ZFN induced mutations. Because of the lack of a suitable, robust screening assay ZFN *grna* set1 was no longer

pursued. In embryos injected with ZFN *grna* set2 mRNA (Fig. 5.10B) or ZFN *grnb* set1-3 mRNAs (Fig. 5.10C) (P0) the PCR bands at 392bp or 582bp were only partially digested and it can be concluded, that some cells of the P0 embryos carry mutations in *grna* or *grnb*, respectively. These P0 embryos are mosaic mutation carriers. They carry mutations in some somatic cells and most likely also in some germ cells. Several P0 siblings from positively tested ZFN mRNA microinjections were raised to adulthood for further screenings (Fig. 5.8).
In summary, I obtained two sets of ZFNs for *grna* and three sets of ZFNs for *grnb*. All ZFNs are successfully translated into proteins and it was shown that set2 of ZFNs targeting *grna* and all sets of ZFNs targeting *grnb* do cut double strand DNA in the ZFN targeting regions leading to induction of mutations in *grna* and *grnb* by the cellular repair mechanism NHEJ.

5.2.2 Screen for *grna* and *grnb* mutants

Injected P0 founder fish are still mosaic, meaning that they carry distinct mutations in randomly distributed cells throughout their bodies. To identify F1 zebrafish that carry a single mutation in every cell, the following screen (Fig. 5.11) was performed: Adult

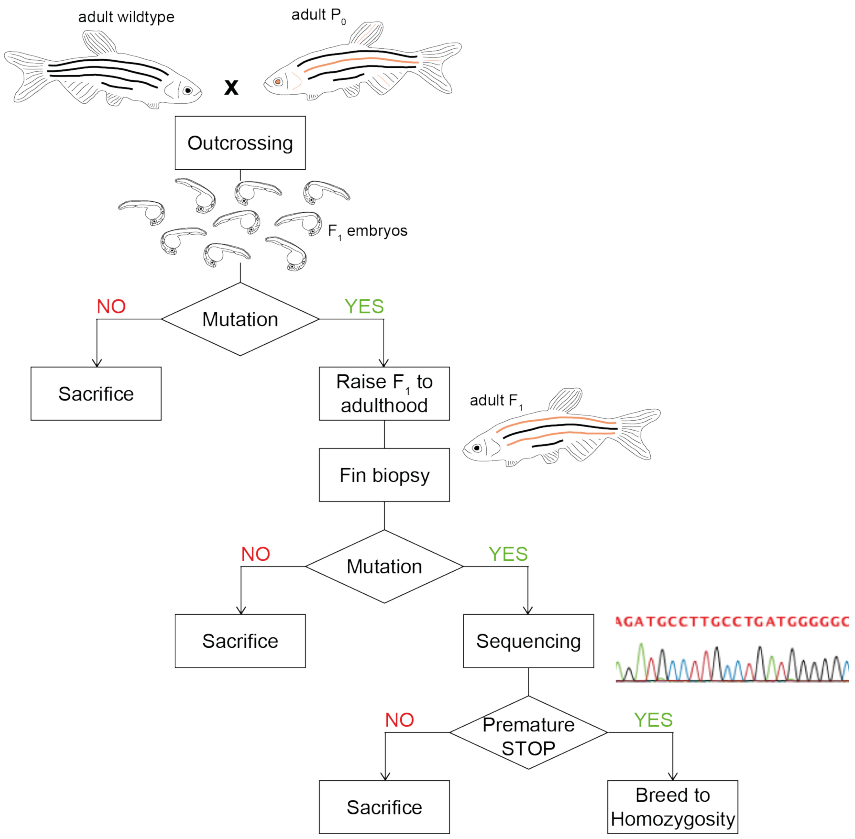

Figure 5.11 – Schematic illustration of the screening performed to establish Grna and Grnb loss of function mutants by ZFN-mediated genome editing.

ZFNs injected P0 zebrafish were mated to wildtype zebrafish (Fig. 5.11), to obtain a F1 generation that carries one single mutation in every somatic cell and 50% of the germ cells. At least 12 F1 offspring were sacrificed as embryos and were analysed using the screening assay (see Fig. 5.10). If mutations were detected, the siblings (F1) were raised to adulthood (Fig. 5.11). Fin biopsy were taken from these adult F1 zebrafish and the samples were analysed for mutations using the screening assay (Fig. 5.11). Sequencing was performed with samples from mutation carrier to determine the sequence of the mutation. Amongst the mutations - deletion, insertion, or indels - these were selected that result in a preTT codon in the same coding exon (Fig. 5.11). F1 mutation carrier with a preTT mutation were bred to homozygosity (Fig. 5.11).
For all sets of ZFNs, except *grnb* set3, more than 50% of the F1 clutches analysed carried mutations (Fig. 5.12). Consequently, more than 50% of the injected P0 fish had mutations in the germline, which were transmittable to the next generation. As all *grnb*

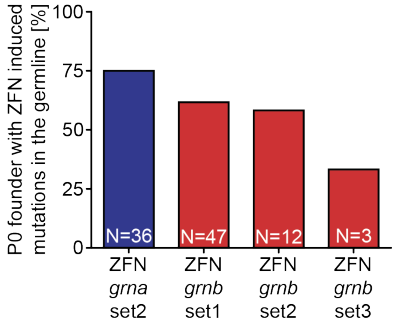

Figure 5.12 – ZFN induced mutations were transmitted through the germline with a high frequency. The percentages of germline transmission were 75%, 62%, 58%, and 33% for *grna* set2, *grnb* set1, set2, and set3, respectively. White numbers (N) are for the number of P0 founders analysed.

ZFN sets target almost the same genomic site, I decided to proceed only with zebrafish that carry ZFN *grnb* set1-induced mutations.
For *grna* offsprings from 13 P0 founder fish were analysed and up to five distinct mutations were detected that originate from one founder. This means that distinct mutations were present in the germ cell population of the P0 founder that were inherited to the F1 generation. These mutations trace back to various ZFN cutting events and subsequent DSB repair by the cells error-prone repair mechanism NHEJ. This explains why the mutations are slightly different from each other. All mutations induced by the *grna* ZFN set2 are summarized in Fig. 10.5A. In total 13 different mutations were detected and 6 of these result in a frameshift in the ORF. For *grnb* offsprings from 8 P0 founder fish were analysed and as much as three different mutations were detected in adult fish that descend from one founder. All mutations that emerged from this set of ZFN are summarized in Fig. 10.5B. All together 15 different mutations were detected

among which 11 result in a frameshift in the ORF. Four distinct *grna* and three distinct *grnb* mutations were selected that code for a preTT codon when translated into protein (Fig. 5.13). These four and three alleles were used in further experiments and carriers were bred to homozygosity.

In summary, ZFNs induced mutations in the germline, that were transmitted to the next generation. Mutations that result in a preTT codon were identified, likely leading to loss of protein function.

Figure 5.13 – Sequences of selected alleles that carry a preTT codon and lead to a preTT when translated into protein. **A**: *grna* wildtype and the four selected *grna* mutation alleles as well as their translation into proteins are shown. **B**: *grnb* wildtype and the three selected *grnb* mutation alleles as well as their translation into proteins are shown. wt: wildtype. Δ: deletion. +: insertion. *: Stop.

5.2.3 *grna* and *grnb* mutants are protein null mutants

In a KO animal model it is essential to confirm that the mRNA levels are reduced and even more important that the protein is no longer produced. Therefore, I performed qPCR experiments at 5dpf. *grna* mRNA levels in homozygous *grna* mutants carrying presumptive loss of function alleles were significantly reduced to approx. 50% of the mRNA expression levels detected in wildtype larvae (Fig. 5.14A). In *grnb* mutants homozygous for the presumptive loss of function alleles the reduction in mRNA levels was even more pronounced. Here the mRNA levels were reduced to approx. 10% of the expression levels detected in wildtype larvae (Fig. 5.14B).

The mutated mRNAs containing a preTT codon are most likely degraded via NMD. This endogenous RNA quality control mechanisms of cells hampers the synthesis of truncated, non-functional proteins by enhancing the degradation rate of mRNAs with preTT codons intensely (Garneau et al., 2007). Consequently, these mRNAs are not

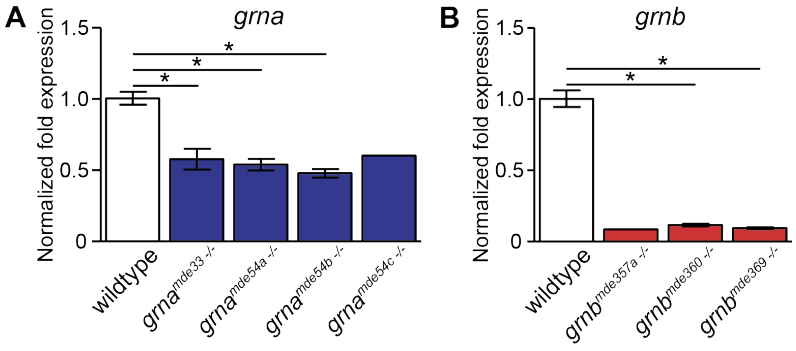

Figure 5.14 – The mRNA levels were reduced in all selected *grna*$^{-/-}$ and *grnb*$^{-/-}$ mutants. **A**: mRNA levels of *grna* were significantly reduced in *grna* mutants. **B**: *grnb* mRNA levels were significantly reduced in *grnb* mutants. 5dpf. Normalized to *actb1* and *tbp*. qPCR. S.E.M. Mann-Whitney test (one-tailed). $*$ $p = 0.05$. $n = 3$. No statistical analysis for $grna^{mde54c-/-}$ and $grnb^{mde357a-/-}$ since $n = 1$.

translated anymore leading to a loss of the associated protein. To show that Grna and Grnb protein is absent in *grna*$^{-/-}$ and *grnb*$^{-/-}$ mutants, respectively, immunoblots of either adult kidney samples or 1.5dpf embryos, using Grna and Grnb specific mAbs were performed. Grna protein was absent in all homozygous mutants analysed. The Grna specific band present in wildtype samples at approx. 200kDa was no longer detectable (Fig. 5.15A) in all adult kidney samples from *grna*$^{-/-}$ mutants. I used adult

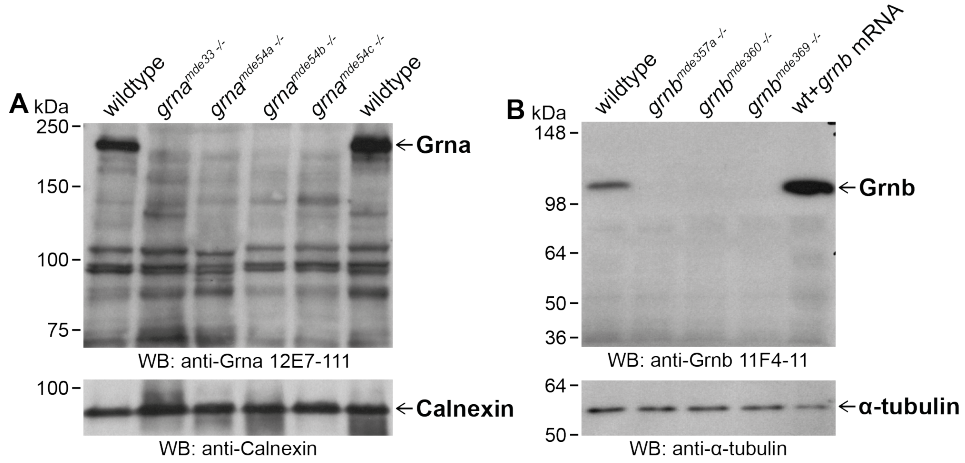

Figure 5.15 – Grna and Grnb protein was absent in all *grna*$^{-/-}$ and *grnb*$^{-/-}$ mutant alleles analysed. **A**: The Grna specific band was absent in all adult kidney samples derived from *grna*$^{-/-}$ mutants, whereas a Grna specific signal was detectable in wildtype samples. Calnexin served as a loading control. **B**: The Grnb specific band observed in wildtype samples was absent in all 1.5dpf samples from different *grnb*$^{-/-}$ mutants. Injection of *grnb* mRNA led to an increase in signal intensity of the Grnb specific band. The loading control α-tubulin was present in all samples.

kidney samples for this experiment as this is the tissue with the highest *grna* expression (Fig. 5.2). Grna was not detectable by immunoblotting using any other larval (Fig. 5.6A)

or adult tissue. In samples from *grnb*$^{-/-}$ mutants the Grnb protein was absent. The Grnb specific signal, observed in wildtype samples, was not detectable in all *grnb*$^{-/-}$ mutants analysed (Fig. 5.15B). It can be stated that all mutant alleles of *grna* and *grnb* are no longer translated into proteins.
In summary, all selected *grna* and *grnb* alleles are loss of function alleles and result in a KO of the respective protein.

5.3 Basic characterization of Grna and Grnb KO zebrafish

One of the aims of this study was to establish stable mutant lines to study the *in vivo* function of zf-*grns*. With the Grna and Grnb KO zebrafish I now addressed the following questions: What are the consequences if Grna, Grnb, or both proteins are lost? What is the phenotype of *grna* and *grnb* single and double mutants?

5.3.1 Single and double mutants are viable and fertile

I started to bred single and double mutants to hetero- and homozygosity and examined them for viability until adulthood and possible reproductive phenotypes. In rats GRN is expressed in rat oocytes (Suzuki et al., 2000) and it is published to be an important factor for processes like blastocyst hatching, adhesion, and outgrowth (Qin et al., 2005). Additionally, GRN was detected in the acrosome of the sperm in guinea pig and mice (Baba et al., 1993) and a decreased ejaculation incidence in GRN-deficient mice was reported (Kayasuga et al., 2007). Based on these publications, it was possible that a KO of Grna, Grnb, or both could have an effect on fertility in *grna* and/or *grnb* mutant zebrafish. In all in- and outbreedings performed, fertilized eggs were obtained. Among these all possible genotypes were present in a ratio expected according to Mendelian laws (Table 5.3). Larvae could be raised to adulthood and the lifespan of mutants was undistinguishable from wildtype zebrafish.
Taken together, *grna* and *grnb* single and double mutants have a normal viability and fertility.

5.3.2 Single and double mutants have no obvious morphological phenotype

I next examined the single and double mutants for obvious morphological alterations. Body shape, yolk, eye, brain, notochord, and somites were morphologically examined and at all embryonic, larval, and adult stages analysed, *grna* and *grnb* single and double mutants could not be phenotypically distinguished from wildtype. Representative images of 1.5dpf old wildtype and mutant embryos are shown in Fig. 5.16. When the wildtype and mutant embryos/larvae grew older the heart started to beat, systemic

Table 5.3 – Mendelian laws apply for incrosses of *grna*$^{-/-}$, *grnb*$^{-/-}$, and *grna*$^{-/-}$;*grnb*$^{-/-}$mutants. The number of clutches analysed is indicated. Examined rations are mean values and the SD is given.

Incross of *grna*$^{+/-}$, ($n = 6$)			
Genotype	*grna*$^{+/+}$	*grna*$^{+/-}$	*grna*$^{-/-}$
Examined ratio	$25.2 \pm 7.1\%$	$51.1 \pm 6.3\%$	$23.8 \pm 4.7\%$
Theoretical ratio	25%	50%	25%

Incross of *grnb*$^{+/-}$, ($n = 8$)			
Genotype	*grnb*$^{+/+}$	*grnb*$^{+/-}$	*grnb*$^{-/-}$
Examined ratio	$21.6 \pm 8.3\%$	$53.6 \pm 9.8\%$	$24.8 \pm 7.9\%$
Theoretical ratio	25%	50%	25%

Incross of *grna*$^{-/-}$;*grnb*$^{-/-}$, ($n = 10$)									
Genotype	*a*$^{+/+}$; *b*$^{+/+}$	*a*$^{+/-}$; *b*$^{+/+}$	*a*$^{+/+}$; *b*$^{+/-}$	*a*$^{+/-}$; *b*$^{+/-}$	*a*$^{-/-}$; *b*$^{+/+}$	*a*$^{+/+}$; *b*$^{-/-}$	*a*$^{-/-}$; *b*$^{+/-}$	*a*$^{+/-}$; *b*$^{-/-}$	*a*$^{-/-}$; *b*$^{-/-}$
Examined ratio	$8.3 \pm 6.2\%$	$15.0 \pm 8.5\%$	$7.6 \pm 4.6\%$	$24.0 \pm 8.6\%$	$5.7 \pm 4.2\%$	$8.7 \pm 6.5\%$	$8.0 \pm 4.4\%$	$14.0 \pm 8.0\%$	$8.8 \pm 6.5\%$
Theoretical ratio	6.25%	12.5%	12.5%	25%	6.25%	6.25%	12.5%	12.5%	6.25%

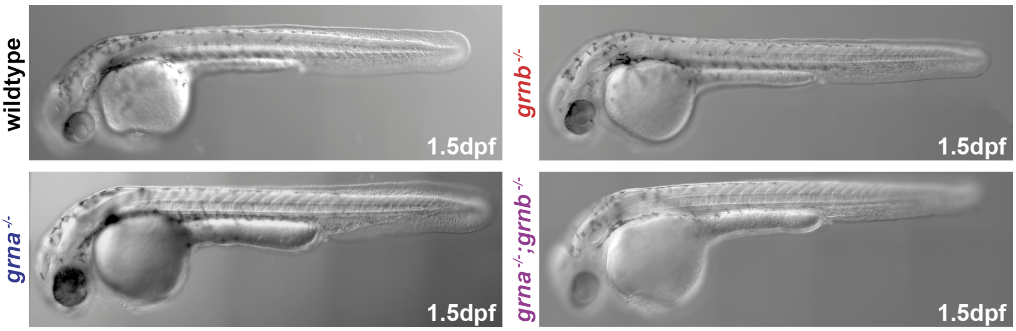

Figure 5.16 – Single and double mutants had no obvious morphological phenotype. Images of 1.5dpf old wildtype, *grna*$^{-/-}$, *grnb*$^{-/-}$ and *grna*$^{-/-}$;*grnb*$^{-/-}$ mutants. Lateral view. Anterior to the left. Single images were taken on a spinning disk microscope using transmitted light and were stitched using the Image Stiching plugin of ImageJ.

blood flow was initiated, pigmentation became visible and independent hatching was observed. Also juvenile and adult wildtype and mutants could not be discriminated according to their size, shape, or behaviour.

5.3.3 Single and double mutants lack compensation by paralogues

One possible explanation for the lack of a phenotype are compensatory mechanisms. Grnb could for example compensate the loss of Grna or Grn1 and Grn2 could compensate for the loss of Grna and Grnb. qPCR experiments were performed on total mRNA from 5dpf larvae to investigate possible compensatory mechanisms on the transcriptional level. First, *grnb* mRNA levels were examined in *grna*$^{-/-}$ mutants and these were alike in wiltype and *grna*$^{-/-}$ mutants (Fig. 5.17A). In the reverse experiment, the *grna* mRNA levels were equally expressed in wiltype and *grnb*$^{-/-}$ mutants (Fig. 5.17B). Therefore, it can be excluded that increased expression of the transcripts, *grna* and

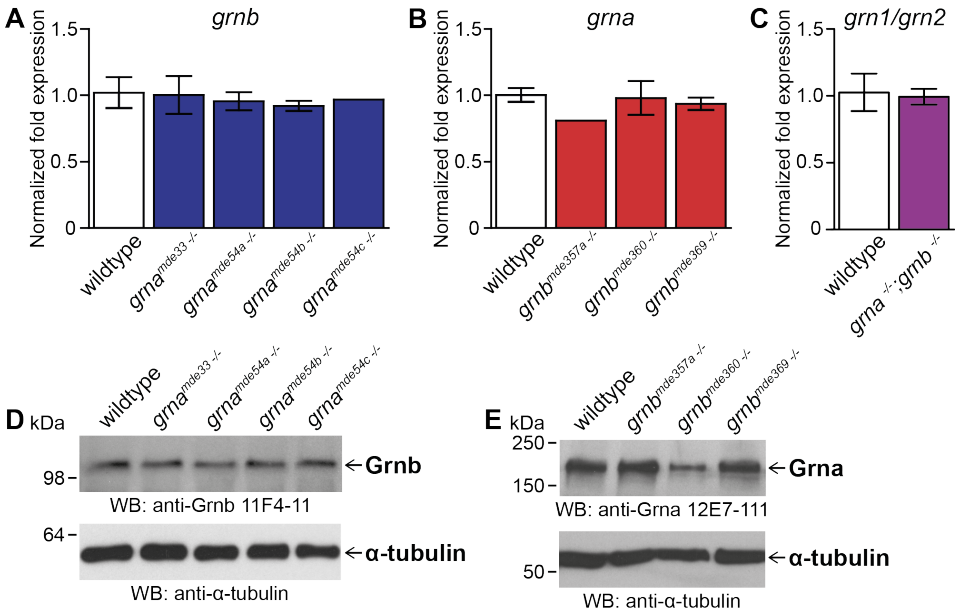

Figure 5.17 – Single and double mutants lacked compensatory upregulation of other zf-*grns*. **A**: mRNA levels of *grnb* were alike in wildtype and *grna*$^{-/-}$ mutants. $n = 3$, $n = 1$ $grna^{mde54c-/-}$. **B**: *grna* mRNA levels were the same in wildtype and *grnb*$^{-/-}$ mutants. $n = 3$, $n = 1$ $grnb^{mde357a-/-}$. **C**: *grn1/grn2* mRNA levels were unchanged in *grna*$^{-/-}$;*grnb*$^{-/-}$ mutants when compared to wildtype. $n = 4$. **A-C**: Normalized to *actb1* and *tbp*. 5dpf. qPCR. S.E.M. Mann-Whitney test (two-tailed). **D**: Grnb levels were indistinguishable in wildtype and *grna*$^{-/-}$ mutants samples from 3dpf old larvae. α-tubulin served as a loading control. **E**: Grna levels were about the same in adult kidney samples from wildtype and *grnb*$^{-/-}$ mutants. α-tubulin served as a loading control.

grnb, compensates for the loss of the paralogue. qPCR experiments detecting *grn1/grn2* in *grna*$^{-/-}$;*grnb*$^{-/-}$ mutants revealed that the loss of Grna and Grnb together did not lead to increased mRNA levels of *grn1/grn2* in comparison to wildtype (Fig. 5.17C).

Since it is possible that the KO of Grna or Grnb is compensated by an increased translation of the protein encoded by the paralogue, the Grnb protein expression levels were analysed by immunoblotting of 3dpf *grna*$^{-/-}$ mutants and the Grna levels were determined by immunoblotting of adult kidney samples from *grnb*$^{-/-}$ mutants. In none of the mutants analysed the protein levels of Grnb or Grna were increased. Therefore, it can be excluded that a KO of Grna or Grnb is compensated by enhanced translation of the protein encoded by the paralogue. Due to a lack of a Grn1/Grn2 specific antibody, a compensation of Grn1/Grn2 could not be addressed in *grna*$^{-/-}$*;grnb*$^{-/-}$ mutants.
In summary, compensatory upregulation of the paralogues in *grna* and *grnb* single and double mutants does not occur on the transcriptional level. Moreover, it can be excluded that Grna and Grnb compensated for the loss of each other on the translational level.

5.3.4 Single and double mutants are not developmentally delayed

GRN is published to be a growth factor (Bateman and Bennett, 2009), therefore, I asked if a KO of Grna, Grnb, or both could have an influence on the rate of development. Counting of the somites is a common staging parameter during development (Kimmel et al., 1995). Therefore, somites were counted in wildtype and single as well as double mutant embryos at 13-14 somite stage. The number of somites at that stage of

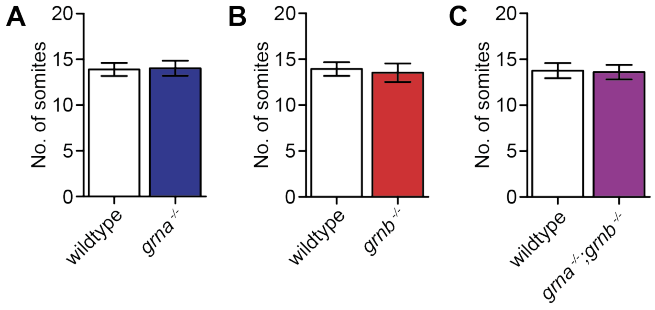

Figure 5.18 – *grna*$^{-/-}$, *grnb*$^{-/-}$, and *grna*$^{-/-}$*;grnb*$^{-/-}$ mutants were not developmentally delayed. **A**: The number of somites in *grna*$^{-/-}$ mutants and wildtype was indistinguishable. **B**: *grnb*$^{-/-}$ mutants and wildtype had about the same number of somites. **C**: The number of somites in *grna*$^{-/-}$*;grnb*$^{-/-}$ mutants and wildtype was alike at the stage analysed. SD. Mann-Whitney test (two-tailed). All n.s.. $n \geq 30$.

development was alike in *grna*$^{-/-}$ ($p = 0.3858$), *grnb*$^{-/-}$ ($p = 0.0627$), and *grna*$^{-/-}$*;grnb*$^{-/-}$ ($p = 0.2968$) mutants when compared to wildtype control embryos (Fig. 5.18). Thus, the pace of development is normal in single and double mutants also making comparisons of clutches from different matings possible.

5.4 Analysis of Grna;Grnb KO embryos for neuronal phenotypes

In the past, the analysis of SpMN axon outgrowth in the zebrafish trunk gained attention as a model for neurodegenerative diseases especially for MND. Loss of function embryos or transgenic zebrafish overexpressing neurodegenerative disease-associated genes were analysed for altered branching during axonal outgrowth or for SpMN axon truncation by quantifying the SpMN axon length (Chitramuthu et al., 2010; Ciura et al., 2013; Kabashi et al., 2010, 2011; Laird et al., 2010; Lemmens et al., 2007; McWhorter et al., 2003; Paquet et al., 2009; Schmid et al., 2013; Song and Pimplikar, 2012). Mutations in *GRN* are clearly linked to FTLD-TDP and *GRN* might be a minor risk factor for ALS (Del Bo et al., 2011; Sleegers et al., 2008). It is also published that *grna* (Chitramuthu et al., 2010; De Muynck et al., 2013; Laird et al., 2010) and *grnb* (Laird et al., 2010) morphants have defects in SpMN axon outgrowth and extended SpMN axon branching was demonstrated (Chitramuthu et al., 2010). To confirm that

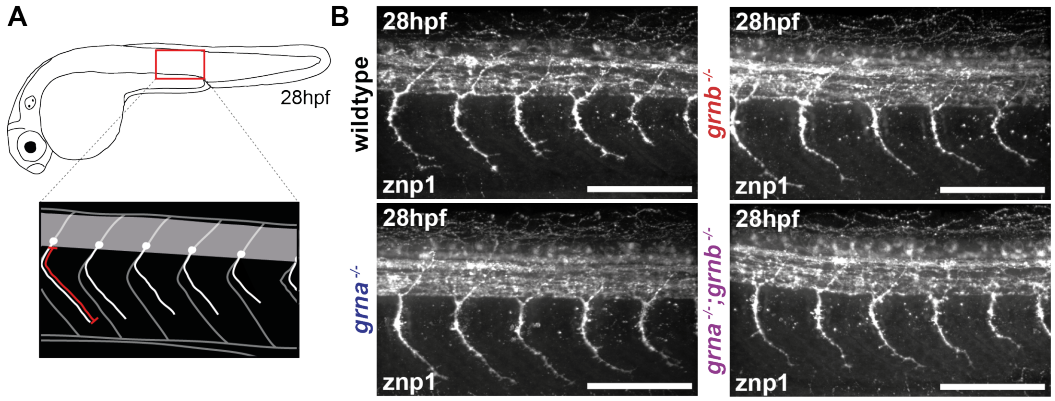

Figure 5.19 – *grna*$^{-/-}$, *grnb*$^{-/-}$, and *grna*$^{-/-}$;*grnb*$^{-/-}$ mutants did not have SpMN axon that show extended branching. **A**: Schematic illustration of a 28hpf embryo and a detail (red box) of the region analysed. SpMNs and their axons are depicted in white. The red line illustrates for SpMN axon 1 the measured SpMN axon length. Grey: spinal cord. **B**: Examples of whole-mount IF stainings of wildtype, *grna*$^{-/-}$, *grnb*$^{-/-}$, and *grna*$^{-/-}$;*grnb*$^{-/-}$ mutants at 28hpf stained with znp1 antibody. The five SpMN axons above the end of the yolk extension are displayed. Images taken by spinning disk confocal microscopy. Maximum projection. Lateral view. Anterior to the left. Scale bar: 100µm.

data, the SpMN axon outgrowth regarding length and branching was examined in *grna* and *grnb* single and double mutants by whole-mount IF stainings. Having made the experience that inter-clutch variations can result in slight but significant differences in the SpMN axon length (Fig. 5.20A), I did only compare embryos from one clutch. Briefly, I fixed the embryos at 28hpf, performed whole-mount IF stainings with the znp1 antibody, genotyped the anterior part of each stained embryo and imaged and analysed

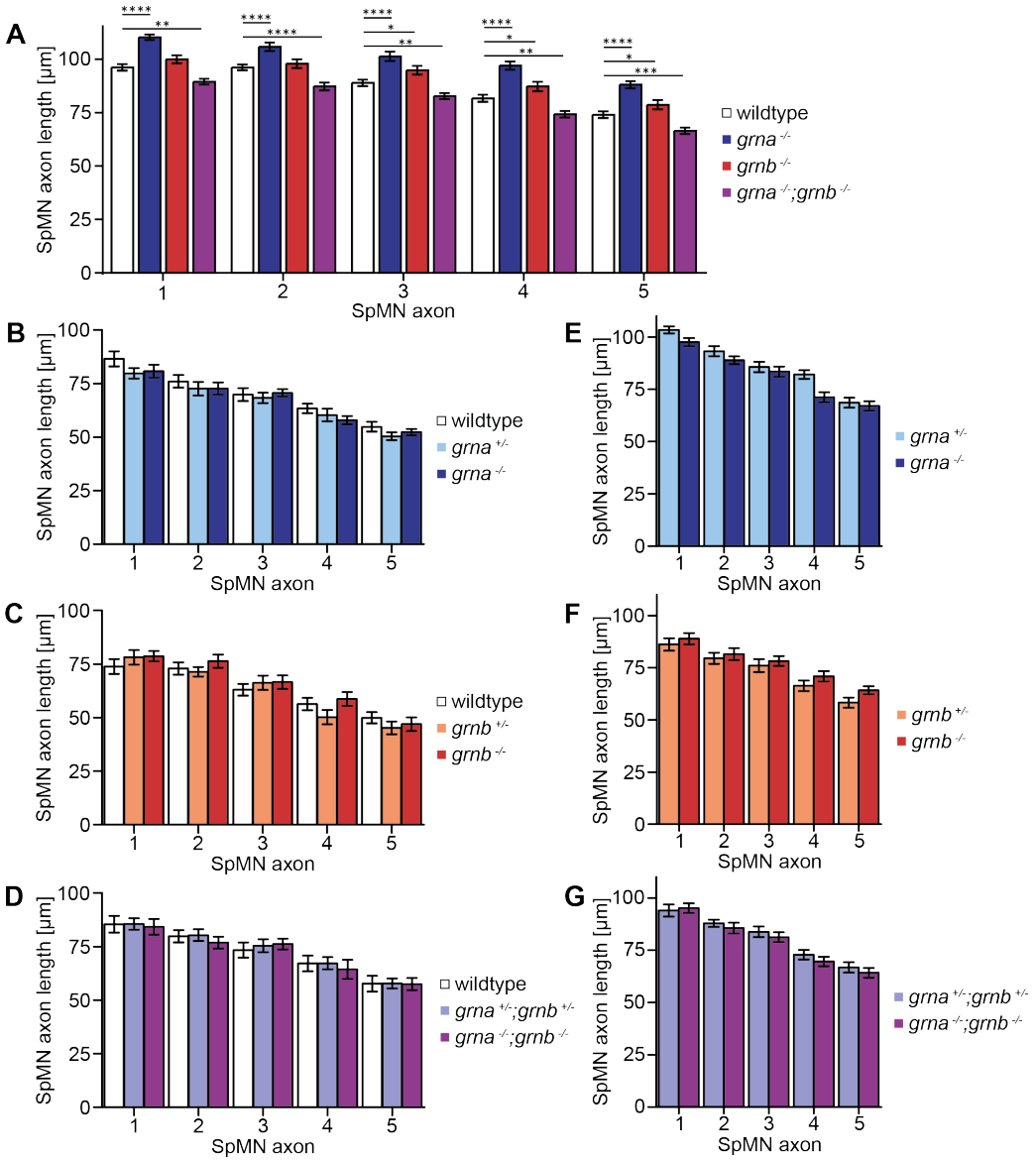

Figure 5.20 – The SpMN axon length of the five SpMN axons above the end of the yolk extension was normal. **A**: A comparison of the SpMN axon length of wildtype, *grna*$^{-/-}$, *grnb*$^{-/-}$, and *grna*$^{-/-}$*;grnb*$^{-/-}$ incrossings at 28hpf revealed a significant increase in the SpMN axon length in *grna*$^{-/-}$ mutants (****$p(1\text{-}5) < 0.0001$, $n = 66$), a partially significant increase in *grnb*$^{-/-}$ mutants ($p(1) = 0.1715$, $p(2) = 0.3425$, *$p(3) = 0.0378$, *$p(4) = 0.0350$, *$p(5) = 0.0447$, $65 \leq n \leq 67$), and a significantly reduced SpMN axon length in *grna*$^{-/-}$*;grnb*$^{-/-}$ mutants (**$p(1) = 0.0021$, ****$p(2) < 0.0001$, **$p(3) = 0.0029$, **$p(4) = 0.0032$, ***$p(5) = 0.0004$, $n = 64$) when compared to wiltype ($n = 63$). S.E.M. Mann-Whitney test (two-tailed). **B-D**: Wildtype, heterozygous, and homozygous embryos from spawnings of heterozygous mutants. **B**: *grna* mutants. $n = 30$. **C**: *grnb* mutants. $n = 30$. **D**: *grna;grnb* mutants. $n = 25$. **E-G**: Wildtype and homozygous embryos from spawnings of homozygous mutant females and heterozygous mutant males. **E**: *grna*. $n = 30$. **F**: *grnb* mutants. $n = 30$. **G**: *grna;grnb* mutants. $n = 30$. **B-G**: S.E.M. Two-way ANOVA. Bonferroni post-test. All n.s..

the five SpMN axons above the end of the yolk extension. From each clutch up to ten embryos from every genotype were imaged. To prevent that inter-clutch variations influence the results, I made sure that an equal number of wildtype, heterozygous, and homozygous embryos from each of the three independent experiments was included in the study. In none of the images taken, extended branching of the SpMN axons was observed (Fig. 5.19). Embryos for the first experiment derived from spawnings of heterozygous single and double mutant zebrafish. Consequently, wildtype, heterozygous, and homozygous embryos were compared. Measurements of the SpMN axon length, which is defined as the length of the SpMN axon from the ventral side of the spinal cord to its growth cone, revealed that the length was not altered in single and double heterozygous and homozygous embryos when compared to wildtype (Fig. 5.20B-D). This indicates that the SpMN axon outgrowth is normal in *grna*, *grnb*, and *grna;grnb* mutants. Still I had to exclude that maternal mRNA precludes SpMN axon outgrowth defects. Maternal mRNA, which is also targeted by translation inhibition KD technologies, is provided to the eggs by the mother and allows the embryos to synthesise proteins before the own transcription machinery is functional (Pelegri, 2003). To deplete maternal *grna* and/or *grnb* mRNA, a second experiment was set up with embryos originating in spawnings of homozygous mutant females and heteroyzgous mutant males. Herein, the SpMN axons also showed no extended branching and a comparison of the SpMN axon length in heterozygous and homozygous mutant embryos did not point to any differences in SpMN axon outgrowth (Fig. 5.20E-G).
In summary, the SpMN axons and their outgrowth are indistinguishable in Grna and Grnb single and double KO embryos compared to wildtype embryos and I could not confirm the data published from Laird and colleagues (Laird et al., 2010), Chitramuthu and colleagues (Chitramuthu et al., 2010) and De Muynck and colleagues (De Muynck et al., 2013) obtained in Grna and Grnb KD experiments.

5.5 Analysis of Grna;Grnb KO embryos for muscle phenotypes

It was also demonstrated that Grna has an influence on zebrafish muscle growth and regeneration (Li et al., 2013). Most of the study was done with *grna* morphants but also *grnb* morphants were used. Both morphants, but especially the *grna* morphants, showed a reduced number of Pax7-positive cells at 24hpf. At that stage of development Pax7 labels the nuclei of MPCs, which are located at the surface of the trunk musculature (Feng et al., 2006; Patterson et al., 2008) and therefore it was concluded that *grna* and *grnb* morphants have less MPCs (Li et al., 2013). With the observation from our laboratory that *tardbp*$^{-/-}$*;tardbpl*$^{-/-}$ double mutant zebrafish show muscle degeneration (Schmid et al., 2013), I asked if the *grna*$^{-/-}$*;grnb*$^{-/-}$ double mutants do also have a muscle phenotype. I

performed whole-mount IF stainings with the Pax7 antibody at 24hpf and quantified the number of Pax7-positive MPCs in the four somites above the end of the yolk extension (Fig. 5.21A). Pax7-positive MPCs can be distinguished from xanthophores, which are also Pax7-positive at that stage of development, by their localization at the lateral muscle surface, their roundish shape and their less intense labelling (Seger et al., 2011). In addition, I performed whole-mount IF stainings using α-actinin, F59-c, and ZE-BO

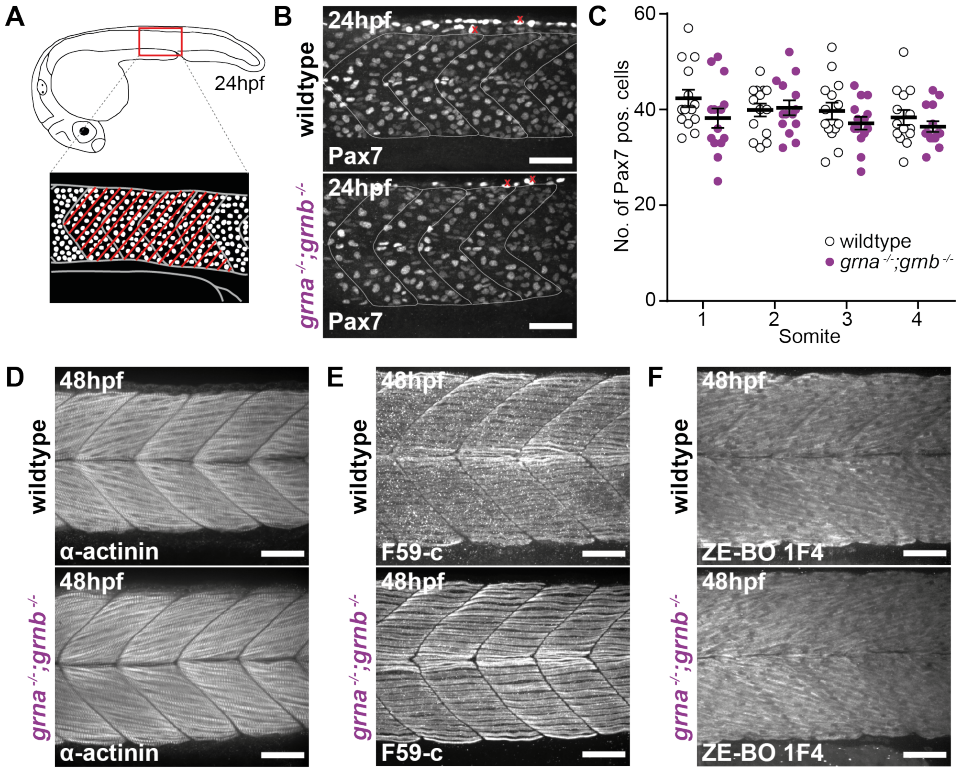

Figure 5.21 – The muscle in double mutants was normal. **A-C**: The number of Pax7-positive cells was not decreased in double mutant embryos. **A**: Schematic illustration of a 24hpf embryo and a detail (red box) of the region analysed. MPCs are represented as white dots. The crosshatched area marks the four somites, in which the Pax7-positive MPCs were quantified. **B**: IF stainings with Pax7 at 24hpf wildtype and *grna*$^{-/-}$;*grnb*$^{-/-}$ mutants. The somites are marked with white dashed lines. Pax7 did also label xanthophores at 24hpf, which can be distinguished from Pax7-positive MPCs by their elongated shape and intense staining. Examples are marked with a red 'x'. **C**: Quantification of Pax7-positive MPCs in the four somites above the end of the yolk extension. $n = 15$. S.E.M. Mann-Whitney test (two-tailed). **D-F**: The IF stainings of different muscle markers were alike in wildtype and double mutants at 48hpf.**D**: α-actinin. **E**: F59-c. **F**: ZE-BO 1F4. **B,D-F**: Lateral view. Anterior to the right. Maximum projection. Recorded by spinning disk confocal microscopy. Scale bar: 50µm.

1F4, to see, if the muscle is intact at 48hpf. α-actinin is a marker for Z-discs (Zhang et al., 2009), F59 binds to the myosin heavy chain of lateral adaxial slow-twitch muscle fibres (Zeller et al., 2002) and ZE-BO 1F4 detects smooth muscles as well as striated skeletal and heart muscles (fast-twitch muscle fibres) (Prengel, 2000). The Pax7-IF

did not show a different staining in wildtype and *grna*$^{-/-}$;*grnb*$^{-/-}$ mutants (Fig. 5.21B). Quantification of the number of Pax7-positive MPCs in the four somites above the end of the yolk extension revealed that the number of Pax7-positive MPCs was not significantly decreased in all somites analysed ($p(S1) = 0.0854$. $p(S2) = 0.7977$. $p(S3) = 0.3489$. $p(S4) = 0.2337$.) (Fig. 5.21C). No obvious differences in the muscle stainings using the α-actinin (Fig. 5.21D), F59-c (Fig. 5.21E), and ZE-BO 1F4 (Fig. 5.21F) antibodies at 48hpf were detectable in Grna;Grnb KO embryos when compared to age-matched wildtype. This indicates that the Z-discs and the slow- and fast-twitching muscle-fibres in the muscle are morphologically normal and intact at 48hpf in *grna*$^{-/-}$;*grnb*$^{-/-}$ mutants. Taken together there is no reduction in Pax7-positive MPCs in the *grna*$^{-/-}$;*grnb*$^{-/-}$ mutants as previously published in morphants (Li et al., 2013) and the truck muscles are morphologically intact at 48hpf.

5.6 Analysis of Grna;Grnb KO embryos for vascular phenotypes

It is published that administration of GRN increases the size and number of blood vessels in murine transcutaneous wounds and it was concluded that GRN has angiogenic properties (He et al., 2003). In a mouse model that expresses Grn in endothelial cells it was shown *in vivo* that Grn has an influence on growth and development of blood vessels (Toh et al., 2013). Moreover, *tardbp*$^{-/-}$;*tardbpl*$^{-/-}$ mutant zebrafish show a mispatterning of (intersegmental) blood vessels (Fig. 5.22C) (Schmid et al., 2013). I therefore analysed, if *grna*$^{-/-}$;*grnb*$^{-/-}$ mutants develop a vascular phenotype. I crossed *grna;grnb* mutants and wildtypes with the transgenic line Tg(*fli1a*:EGFP). In this line blood vessels can be visualized due to their expression of GFP under the blood vessel specific promoter *fli1a* (Lawson and Weinstein, 2002). Subsequently, I imaged the blood vessels above the end of the yolk extension in wildtype and Grna;Grnb double KO embryos at 48hpf by confocal microscopy (Fig. 5.22A). The images taken showed that the dorsal aorta (DA), which is located dorsal to the yolk, is present in wildtype and *grna*$^{-/-}$;*grnb*$^{-/-}$ double mutant embryos. The pattern of the intersegmental blood vessels (ISV) in *grna*$^{-/-}$;*grnb*$^{-/-}$ double mutant embryos and wildtype was indistinguishable and the dorsal longitudinal anastomotic vessels (DLAV) had connected the ISV in wildtype and mutants of 48hpf (Fig. 5.22B). Moreover, the circulation was established and the blood flow was indistinguishable in wildtype and *grna*$^{-/-}$;*grnb*$^{-/-}$ double mutant embryos. Therefore, I conclude that there is no vascular phenotype at 48hpf in *grna;grnb* mutants and that a KO of Grna and Grnb does not influence vasculogenesis.

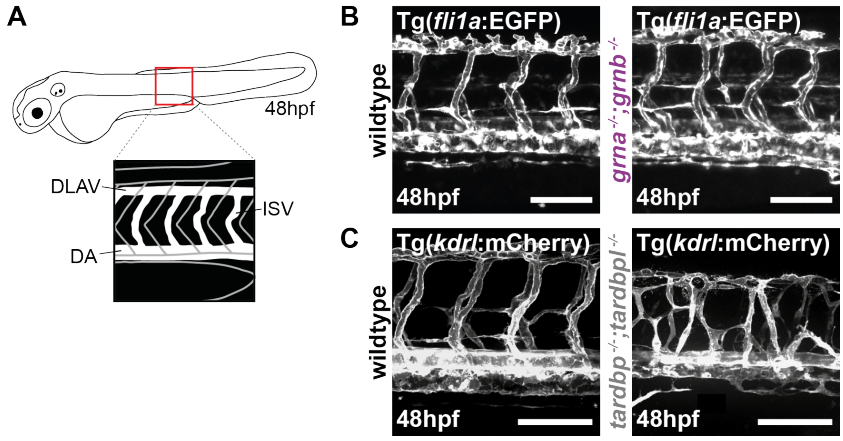

Figure 5.22 – The blood vessels in *grna*$^{-/-}$;*grnb*$^{-/-}$ double mutants above the end of the yolk extension were patterned normal. **A**: Schematic illustration of a 48hpf embryo and a detail (red box) of the region analysed. Blood vessel are represented in white. DLAV: dorsal longitudinal anastomotic vessel. DA: dorsal aorta. ISV: intersegmental blood vessels. **B**: Representative images of a Tg(*fli1a*:EGFP) wildtype and a Tg(*fli1a*:EGFP) *grna*$^{-/-}$;*grnb*$^{-/-}$ mutant at 48hpf. Lateral view. Anterior to the right. Maximum projection. Images recorded by confocal laser scanning microscopy. $n = 3$. Scale bar: 100µm. **C**: Representative images of a Tg(*kdrl*:mCherry) wildtype and a Tg(*kdrl*:mCherry) *tardbp*$^{-/-}$;*tardbpl*$^{-/-}$ mutant at 48hpf. Lateral view. Anterior to the right. Maximum projection. Images recorded by confocal laser scanning microscopy. Scale bar: 100µm. Recorded and kindly provided by Katrin Strecker.

5.7 Analysis of Grna;Grnb KO zebrafish for disease-related pathology

A partial and a complete loss of GRN lead to FTLD-TDP and NCL, respectively (Kleinberger et al., 2013; Smith et al., 2012) and Grn-deficient mice were shown to model some of the behavioural phenotypes, neuropathological as well as biochemical alterations (Filiano et al., 2013; Götzl et al., 2014; Kleinberger et al., 2013). As I aimed to establish a zebrafish model that could help to unravel the so far elusive pathomechanisms of FTLD-TDP/*GRN* and NCL/*GRN*, I investigated whether the Grna;Grnb KO zebrafish develop disease-related pathology. Thereby, I concentrated on neuropathological and biochemical alterations as well as behavioural phenotypes that have been reported in patients and/or mouse models before. Since Claire Russell and her colleagues have previously developed several assays to address NCL pathology in zebrafish (e.g. Mahmood et al., 2013a), I collaborated for a few of the following experiments with her and performed some of them in her laboratory at The Royal Veterinary College, University of London.

Amongst the most consistent neuropathological findings in Grn-deficient mammals are micro- and astrogliosis and increased lipofuscinosis (Kleinberger et al., 2013), of which

the latter is associated with lysosomal dysfunction. I asked if these neuropathological alterations or even neurodegeneration do occur in the Grna;Grnb KO zebrafish.

5.7.1 Analysis of Grna;Grnb KO larvae for neurodegeneration

In contrast to human FTLD-TDP/*GRN* and NCL/*GRN* patients (Rohrer et al., 2010; Smith et al., 2012), only one strain of Grn KO mice did develop neurodegeneration upon ageing (Ahmed et al., 2010) while all other Grn KO stains were devoid of neurodegeneration (Ghoshal et al., 2012; Wils et al., 2012). The vital dye acridine

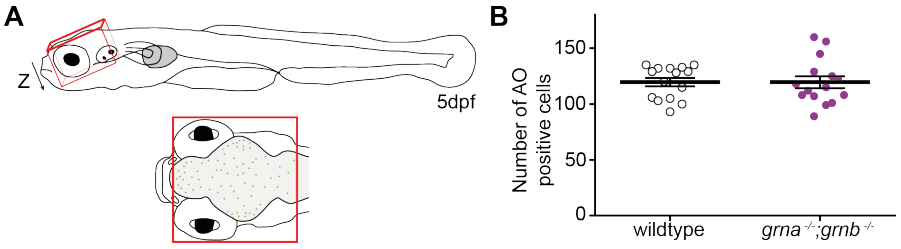

Figure 5.23 – There was no increased neurodegeneration in *grna*$^{-/-}$;*grnb*$^{-/-}$ mutants. **A**: Schematic illustration of a 5dpf larvae (lateral view) and a detail (red line) of the region analysed (dorsal view). The Z-Stack is indicated by the red rectangular prism. Dying cells are represented as green dots. **B**: Quantification of the number of acridine orange positive particle in the larval brain of wildtype and *grna*$^{-/-}$;*grnb*$^{-/-}$ mutants. $n = 15$. S.E.M. Mann-Whitney test (two-tailed).

orange was used previously as a marker to estimate the number of dying cells in zebrafish (Paquet et al., 2009). I applied this dye at 5dpf to analyse and quantify the number of acridine orange positive cells in the brain region indicated in the illustration (Fig. 5.23A) in *grna*$^{-/-}$;*grnb*$^{-/-}$ double mutants and wildtype controls. This quantification revealed that the number of acridine orange positive cells was not increased in the *grna*$^{-/-}$;*grnb*$^{-/-}$ double mutants, when compared to wildtype larvae ($p = 0.69$) (Fig. 5.23B). I concluded that there is no increased cell death in the brain of *grna*$^{-/-}$;*grnb*$^{-/-}$ larvae at 5dpf and most likely no neurodegeneration associated to loss of Grna and Grnb.

5.7.2 Analysis of Grna;Grnb KO larvae for microgliosis

In the murine brain *Grn* is expressed by neurons and microglia (Petkau et al., 2010). Moreover, it was shown that zebrafish *grna* is expressed by microglia and was even used as a microglial marker (Craig et al., 2008; Huang et al., 2012). As mentioned above, FTLD-TDP/*GRN* patients (Chen-Plotkin et al., 2010; Josephs et al., 2007; Mackenzie et al., 2006) and homozygous Grn KO mice (Ahmed et al., 2010; Ghoshal et al., 2012; Petkau et al., 2012; Wils et al., 2012; Yin et al., 2010a,b) develop micro- and astrogliosis. In contrast to mammals, zebrafish lack glia cells that resemble the mammalian astrocytes, while microglia are present already during larval stages. To

investigate, if *grna*$^{-/-}$;*grnb*$^{-/-}$ double mutant larvae develop microgliosis, I performed neutral red staining and approximated the number of microglia in the larval brain at 3dpf. Neutral red is a vital stain, that is incorporated in its red fluorescent form by macrophages and microglia and was used previously to label microglia in zebrafish (Herbomel et al., 2001). A quantification of the number of neutral red positive particles in the larval zebrafish brain (Fig. 5.24A) did not reveal a significant difference in wildtype and *grna*$^{-/-}$;*grnb*$^{-/-}$ double mutant larvae at 3dpf ($p = 0.2884$) (Fig. 5.24B). Therefore, it

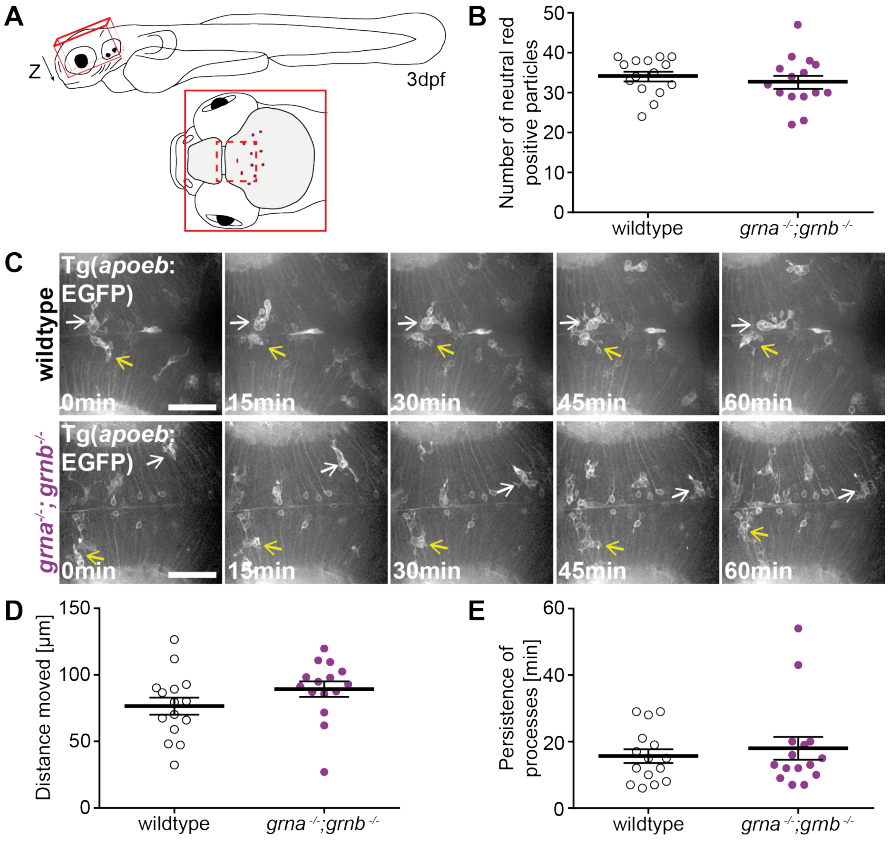

Figure 5.24 – There was no microgliosis in *grna*$^{-/-}$;*grnb*$^{-/-}$ mutant larvae. **A**: Schematic illustration of a 3dpf larvae (lateral view). The red square in the dorsal view below marks the region analysed in B and the red dashed line marks the region analysed in C-E. A Z-Stack is indicated by the red rectangular prism. Microglia are represented as dark red dots. **B**: Quantification of the number of neutral red positive particles in the larval brain of wildtype and *grna*$^{-/-}$;*grnb*$^{-/-}$ mutants. **C-E**: Microglia in wildtype and *grna*$^{-/-}$;*grnb*$^{-/-}$ mutants were similar. **C**: Still images from time-lapse recordings in the optic tectum of Tg(*apoeb*:lynEGFP) wildtype and Tg(*apoeb*:lynEGFP) *grna*$^{-/-}$;*grnb*$^{-/-}$ mutants. Two representative cells are marked with a yellow and white arrow. 3dpf. Recorded by spinning disk confocal microscopy. Orthogonal projection. Dorsal view. Anterior to the left. $n = 3$. Scale bar: 50µm. Recording time: 60min. 1frame/min. **D**: The distance microglia move within one hour was similar in wildtype and *grna*$^{-/-}$;*grnb*$^{-/-}$ mutants. **E**: Microglial processes persisted for about the same time in wildtype and *grna*$^{-/-}$;*grnb*$^{-/-}$ mutants. D-E: Quantification of the time-lapse recordings shown in C. 3dpf. B, D-E: $n = 15$. S.E.M. Mann-Whitney test (two-tailed).

can be concluded that the number of microglia is not increased in *grna*$^{-/-}$;*grnb*$^{-/-}$ double mutant larvae when compared to age-matched wildtype controls. Besides an increase in the number of microglia, activated microglia are indicative of microgliosis (Streit et al., 1999). During larval stages zebrafish microglia are still highly motile and phagocytic (amoeboid). Within the first weeks they mature to ramified microglia with a small cell body (Svahn et al., 2013). These ramified microglia can transform into morphologically different active microglia upon an injury (Baumgart et al., 2012) but the amoeboid microglia largely maintain their morphology even after an inflammatory stimulus (Sieger et al., 2012). Consequently, it is not informative to categorize microglia during larval development in active and inactive. Instead I compared wildtype and *grna*$^{-/-}$;*grnb*$^{-/-}$ mutant microglia according to their distance moved within one hour and the persistence of their processes, two parameters that were used before for the characterization of larval microglia (Svahn et al., 2013). For the visualisation of microglia, I crossed wildtype and *grna;grnb* double mutants in the transgenic line Tg(*apoeb*:lynEGFP) that labels some microglia (Peri and Nüsslein-Volhard, 2008). By *in vivo* time-lapse microscopy I recorded the microglia in the optic tectum of wildtype and *grna*$^{-/-}$;*grnb*$^{-/-}$ mutants at 3dpf and quantified the path or persistence of randomly selected microglia or processes, respectively. Still images of the *in vivo* time-lapse analysis demonstrate that microglia from wildtype and *grna*$^{-/-}$;*grnb*$^{-/-}$ mutants can not be discriminated due to their morphology (Fig. 5.24C). Moreover, the distance moved within one hour ($p = 0.0671$) (Fig. 5.24D) and the persistence of microglial processes ($p = 0.8296$) (Fig. 5.24E) was not statistically different in wildtype and *grna*$^{-/-}$;*grnb*$^{-/-}$ mutants indicating that amoeboid microglia in wildtype and *grna*$^{-/-}$;*grnb*$^{-/-}$ mutants are phenotypically similar. As the number of microglia was also not increased, I concluded that *grna*$^{-/-}$;*grnb*$^{-/-}$ double mutant larvae lack microgliosis. Additionally, my collaboration partner Rossella di Giaimo (Helmholtz Center Munich) performed a first staining on sections of adult zebrafish telencephali derived from wildtype and *grna*$^{-/-}$;*grnb*$^{-/-}$ double mutants with antibodies specific for microglia. These stainings did not reveal any obvious differences between microglial stainings in wildtype and Grna;Grnb KO brains. A quantification of active and ramified microglia in the adult zebrafish brains in an increased number of animals would be required to exclude effects on microglia at adult stages.
Taken together, brains from *grna*$^{-/-}$;*grnb*$^{-/-}$ zebrafish seem to be devoid of microgliosis in early development.

5.7.3 Analysis of Grna;Grnb KO zebrafish for lipofuscin aggregates

Another hallmark of FTLD-TDP and NCL but also other neurodegenerative diseases are aggregated proteins. In FTLD-TDP/*GRN* the main deposited protein is TDP-

43 (Eriksen and Mackenzie, 2008). In NCL/*GRN* the storage material in the brain is still unknown but an eccrine pale cell showed the typical NCL-lipofuscin fingerprint profile (Smith et al., 2012). As Grn-deficient mice are devoid of TDP-43 aggregates (Ahmed et al., 2010; Petkau et al., 2012; Wils et al., 2012), I did not perform stainings to detect TDP-43-positive inclusions in *grna*$^{-/-}$;*grnb*$^{-/-}$ mutants. The main storage material in aggregates of NCL is SCMAS or Saposin A and D (Jalanko and Braulke, 2009; Shacka, 2012) but by the time of analysis it was not clear if any of these two candidates is aggregating in NCL/*GRN*. Therefore, PAS stain was performed, a method that enables to stain aggregates of glycoproteins, including lipofuscin, and can be part of the examinations done to diagnose NCL in patients (Hall et al., 1989) and mice (Koike et al., 2005). It was shown previously, that PAS stain can stain lipofuscin in sections of aged zebrafish liver (Kishi et al., 2008). However, the existence of neurolipofuscin in zebrafish is controversially discussed (Kishi et al., 2003, 2008; Rosa et al., 2010). PAS stain was performed on 5dpf eye, forebrain, and optic tectum as well as 11mpf adult brain cryosections derived from wildtype and *grna*$^{-/-}$;*grnb*$^{-/-}$ mutants. Some dense pink

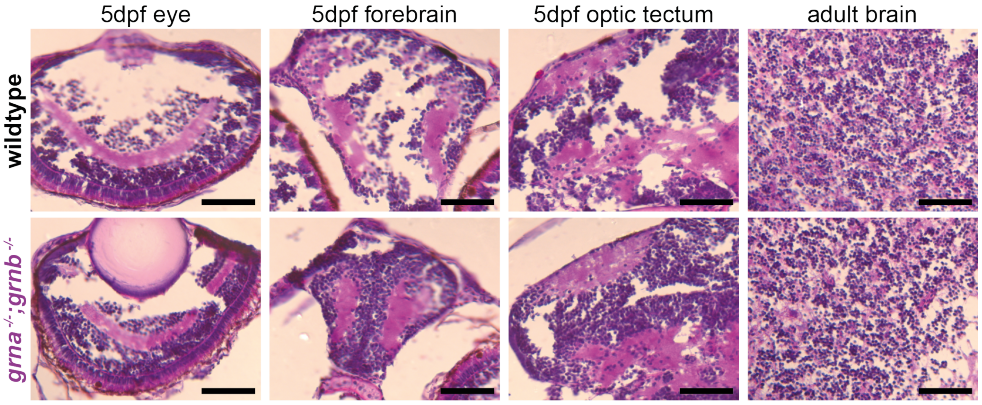

Figure 5.25 – PAS stain in wildtype and *grna*$^{-/-}$;*grnb*$^{-/-}$ mutants. Cryosections of 5dpf eye, forebrain, and optic tectum as well as 11mpf old adult brain, stained with PAS stain. The PAS stained sections of wildtype and *grna*$^{-/-}$;*grnb*$^{-/-}$ mutants are similar. Images by brightfield microscopy. Scale bar: 50µm.

structures were detected in the sections from larval and adult brain, but they were observed both in wildtype and *grna*$^{-/-}$;*grnb*$^{-/-}$ mutant samples (Fig. 5.25) and seemed to be too small for lipofuscin aggregates. Since the literature provides no images of neurolipofuscin in zebrafish (Rosa et al., 2010) and I and others could not come up with a zebrafish neurolipofuscin (positive) control, it is difficult to draw conclusions from this experiment. Consequently, it is not possible to provide a final answer to the issue whether increased neurolipofuscinosis is occurring in *grna*$^{-/-}$;*grnb*$^{-/-}$ mutant zebrafish. Moreover, the staining raises the question if lipofuscin deposits develop in the zebrafish brain at all.

5.7.4 Analysis of Grna;Grnb KO larvae for lysosomal dysfunction

NCL/*GRN* is per definition a lysosomal storage disorder with impaired lysosomal function (Kollmann et al., 2013; Smith et al., 2012) and there is now increasing evidence that lysosomal dysfunction plays a role in FTLD-TDP/*GRN* (Götzl et al., 2014). Moreover, studies in Grn-deficient mice point towards a lysosomal dysfunction as the protein expression levels of some lysosomal proteins were shown to be increased (Götzl et al., 2014; Tanaka et al., 2013; Wils et al., 2012). I first performed LysoTracker staining in wildtype and Grna;Grnb KO larvae. LysoTracker, an *in vivo* dye that was used in zebrafish before, labels acidic cell compartments e.g. lysosomes and phagolysosomes (Mahmood et al., 2013a; Peri and Nüsslein-Volhard, 2008). Consequently, this

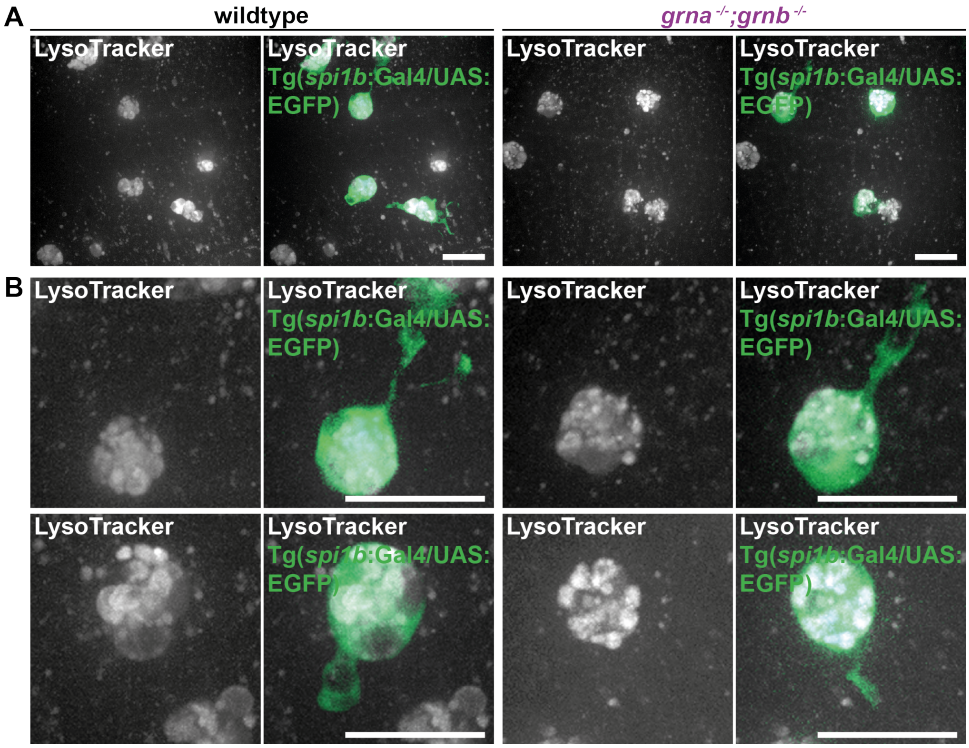

Figure 5.26 – Acidic cell compartments were present in wildtype and *grna*$^{-/-}$;*grnb*$^{-/-}$ microglia. LysoTracker staining at 3dpf in Tg(*spi1b*:Gal4;UAS:EGFP) wildtype and Tg(*spi1b*:Gal4;UAS:EGFP) *grna*$^{-/-}$;*grnb*$^{-/-}$ mutants. **A**: LysoTracker positive vesicles in microglia were detectable in wildtype and *grna*$^{-/-}$;*grnb*$^{-/-}$ mutant larval brains. **B**: Representative close-ups of two wildtype and two *grna*$^{-/-}$;*grnb*$^{-/-}$ mutant microglia. Maximum projections. Dorsal view. Images by spinning disk confocal microscopy. Scale bar: 20µm. Images are gamma corrected for better visualisation. $n = 6$.

staining would show if the acidic compartments in *grna*$^{-/-}$;*grnb*$^{-/-}$ mutants are still able to maintain an acidic pH, which is required for a proper function of lysosomal proteins. Moreover, a dramatic increase in the size of acidic compartments could be uncovered using this staining (Mahmood et al., 2013a). I applied LysoTracker at 3dpf and acidic

cell compartments in the optic tectum (see Fig. 5.24A) of Tg(*spi1b*:Gal4/UAS:GFP) wildtype and Tg(*spi1b*:Gal4/UAS:GFP) *grna*$^{-/-}$;*grnb*$^{-/-}$ mutants were visualized by confocal microscopy. In the transgenic line Tg(*spi1b*:Gal4/UAS:GFP) numerous microglia are labelled by GFP-expression (Peri and Nüsslein-Volhard, 2008) and it was demonstrated previously by LysoTracker staining that zebrafish microglia contain several acidic cell compartments of different size (Peri and Nüsslein-Volhard, 2008). In both wildtype and *grna*$^{-/-}$;*grnb*$^{-/-}$ mutants acidic vesicles could be visualized in microglia by LysoTracker staining indicating that acidic cell compartments were present in microglia of wildtype and *grna*$^{-/-}$;*grnb*$^{-/-}$ mutants (Fig. 5.26A,B). Moreover, the analysis revealed no obvious increase in the size of acidic vesicles in *grna*$^{-/-}$;*grnb*$^{-/-}$ mutants when compared to age-matched wildtype controls (Fig. 5.26A,B). Nevertheless, it was not possible to draw final conclusions regarding the number, size, or functionality of the lysosomes using LysoTracker staining.

To address whether lysosomal function in Grna;Grnb KOs is disturbed, I examined the expression levels of the lysosomal protease Ctsd (Benes et al., 2008) in *grna*$^{-/-}$;*grnb*$^{-/-}$ double mutants. CTSD is itself linked to NCL since homozygous loss of function mutations in *CTSD* are causative for congenital NCL (Siintola et al., 2006; Tyynelä et al., 2000). It was reported, that Grn-deficient mice exhibit elevated *Ctsd* mRNA expression and Ctsd protein levels (Götzl et al., 2014; Tanaka et al., 2013; Wils et al., 2012), suggesting an accumulation of lysosomal proteins due to lysosomal dysfunction in the Grn KO mice. Recent data indicate that also frontal cortex samples from FTLD-TDP/*GRN* patients show elevated CTSD levels (Götzl et al., 2014). Therefore I asked, if this increase in *ctsd* mRNA or Cstd protein does also occur in the *grna*$^{-/-}$;*grnb*$^{-/-}$ double mutants and performed qPCR experiments and immunoblotting of 5dpf whole zebrafish larvae and 7mpf and 22mpf adult brain samples, respectively. In contrast to the data in Grn-deficient mice, I could not detect differences in *ctsd* mRNA expression neither in larval stages nor in adult brain of Grna;Grnb KO zebrafish samples when compared to wildtype samples (p(5dpf) = 1.0, p(7mpf) = 0.4, p(22mpf) = 0.7) (Fig. 5.27A). The well characterized Ctsd antibody (a gift from Prof. Isidoro) (Follo et al., 2011) used for immunoblotting detected endogenous Ctsd at 5dpf and in 7mpf as well as 22mpf brain samples as a single band at 41kDa at about equal intensities in wildtype and *grna*$^{-/-}$;*grnb*$^{-/-}$ double mutant samples (Fig. 5.27B). In contrast to mammalian CTSD proprotein, which is cleaved into heavy- and light-chain, zebrafish Ctsd matures into a single-chain protein (Follo et al., 2013). Therefore, immunoblots from mammalian CTSD show two bands derived from proprotein and heavy-chain, whereas zebrafish Ctsd is represented by a single band (Follo et al., 2013; Götzl et al., 2014). A quantification of the Ctsd signals normalized to the loading control α-tubulin revealed no significant

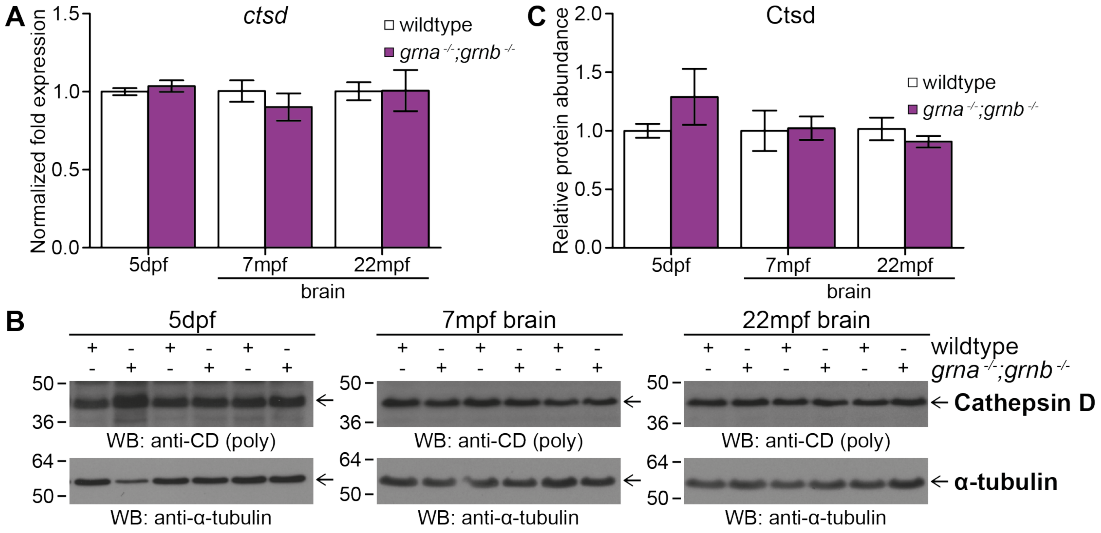

Figure 5.27 – *ctsd* mRNA and Ctsd protein levels were unchanged in *grna*$^{-/-}$;*grnb*$^{-/-}$ double mutants. **A**: *ctsd* mRNA expression in *grna*$^{-/-}$;*grnb*$^{-/-}$ mutants was not changed at 5dpf and in 7mpf as well as 22mpf brain samples when compared to wildtype samples. Normalized to *actb1* and *tbp*. qPCR. 5dpf: $n = 4$. 7mpf and 22mpf: $n = 3$. S.E.M. Mann-Whitney test (two-tailed). **B**: Immunoblots showing Ctsd and α-tubulin in 5dpf whole lysis samples as well as whole lysates from 7mpf and 22mpf brains. **C**: There was no increase in Ctsd levels in *grna*$^{-/-}$;*grnb*$^{-/-}$ double mutants. Quantification of Immunoblots displayed in B normalized to α-tubulin. 5dpf: $n = 4$. 7mpf and 22mpf: $n = 3$. S.E.M. Mann-Whitney test (two-tailed).

changes in the amount of Ctsd in *grna*$^{-/-}$;*grnb*$^{-/-}$ double mutant samples when compared to wildtype (p(5dpf) = 0.8857, p(7mpf) = 1.0, p(22mpf) = 0.7) (Fig. 5.27C). This data indicate that Ctsd is not accumulating in *grna*$^{-/-}$;*grnb*$^{-/-}$ double mutants.
In summary, *grna*$^{-/-}$;*grnb*$^{-/-}$ double mutants are capable to acidify acidic vesicles and do not accumulate the lysosomal protease Ctsd indicating a normal lysosomal function in *grna*$^{-/-}$;*grnb*$^{-/-}$ double mutants.

5.7.5 Analysis of Grna;Grnb KO samples for biochemical alterations

Apart from indications that GRN might have a lysosomal function (Götzl et al., 2014; Smith et al., 2012; Tanaka et al., 2013; Wils et al., 2012), the biological function of GRN and GRN-associated signaling mechanisms are still largely elusive. To provide information that could help to unravel the biological function of GRN I addressed the expression levels of genes that were differentially expressed in *Grn* KO mice and FTLD-TDP/*GRN* patients in the *grna*$^{-/-}$;*grnb*$^{-/-}$ double mutants. Amongst those genes, I selected *STAT3* and *FLNC*. In zebrafish there is one orthologue of *STAT3*, also named *stat3*, but two orthologues of *FLNC*, *flnca* and *flncb*. *stat3* was of interest since it is upregulated in the transcriptom and proteom analysis of *tardbp*$^{-/-}$;*tardbpl*$^{-/-}$ double mutant zebrafish (Schmid, unpublished; Schmid et al., 2013), seems to be upregulated

in *Grn* KO mice and was elevated in samples of FTLD-TDP/*GRN* patients (Janssens and Banzhaf-Strathmann, unpublished). *flnca* was upregulated in the transcriptom and proteom analysis of *tardbp*$^{-/-}$;*tardbpl*$^{-/-}$ double mutant zebrafish (Schmid, unpublished; Schmid et al., 2013). Therefore, *flnca* and *flncb* were chosen for analysis. Moreover, *FLNC* was elevated in brain samples of FTLD-TDP/*GRN* patients and Grn KO mice (Janssens, unpublished; Schmid et al., 2013). To determine the mRNA expression levels of *stat3*, *flnca*, and *flncb*, qPCR experiments were performed at 5dpf and in 7mpf as well as 22mpf brain samples from wildtype and Grna;Grnb KO zebrafish. The

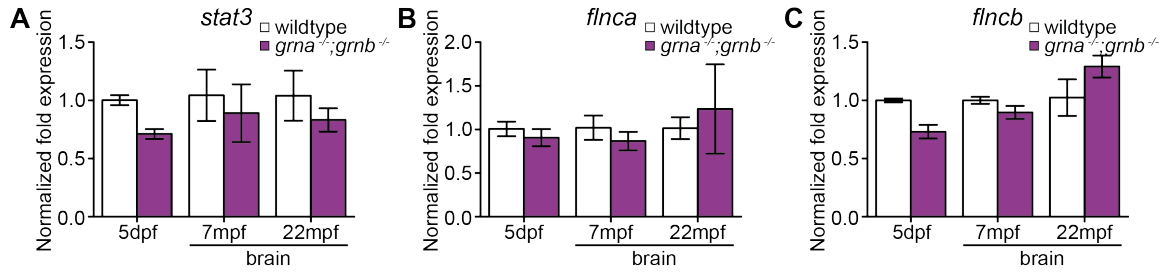

Figure 5.28 – *stat3*, *flnca*, and *flncb* mRNA levels were not significantly increased in *grna*$^{-/-}$;*grnb*$^{-/-}$ mutants. **A**: *stat3* mRNA levels were slightly decreased in *grna*$^{-/-}$;*grnb*$^{-/-}$ double mutants. **B**: The *flnca* mRNA levels were unchanged in *grna*$^{-/-}$;*grnb*$^{-/-}$ mutants. **C**: *flncb* mRNA was a little decreased in 5dpf *grna*$^{-/-}$;*grnb*$^{-/-}$ double mutants. Not altered at 7mpf and slightly increased in brain samples from *grna*$^{-/-}$;*grnb*$^{-/-}$ double mutants at 22mpf. Normalized to *actb1* and *tbp*. qPCR. 5dpf: $n = 4$. 7mpf and 22mpf: $n = 3$. S.E.M. Mann-Whitney test (two-tailed). All n.s.

qPCR experiments for *stat3* revealed, that the mRNA expression was slightly, but not significantly, decreased in whole larvea at 5dpf and brain from 7mpf or 22mpf old *grna*$^{-/-}$;*grnb*$^{-/-}$ double mutant zebrafish when compared to wildtype samples (p(5dpf) = 0.1, p(7mpf) = 0.4, p(22mpf) = 0.4) (Fig. 5.28A). *flnca* mRNA levels were unchanged, comparing wildtype and Grna;Grnb double KO samples of 5dpf larvae and 7mpf as well as 22mpf brains (p(5dpf) = 0.4, p(7mpf) = 0.7, p(22mpf) = 0.7) (Fig. 5.28B). *flncb* mRNA levels appeared to be decreased at 5dpf, unchanged at 7mpf and slightly increased at 22mpf in *grna*$^{-/-}$;*grnb*$^{-/-}$ double mutants in comparison to wildtype samples. However, these changes were not statistically significant (p(5dpf) = 0.1, p(7mpf) = 0.4, p(22mpf) = 0.4) (Fig. 5.28C).
Taken together, biochemical alterations namely increased expression levels of *STAT3* or *FLNC* observed in FTLD-TDP/*GRN* patients and Grn-deficient mice were not observed in *grna*$^{-/-}$;*grnb*$^{-/-}$ double mutant zebrafish.

5.7.6 Analysis of Grna;Grnb KO zebrafish for behavioural phenotypes

Clinical symptoms of FTLD are behavioural abnormalities and language dysfunction (Rademakers et al., 2012), of which especially the latter is not feasible to ex-

amine in zebrafish. Due to massive neurodegeneration, NCL patients suffer from seizures (Jalanko and Braulke, 2009; Shacka, 2012). Seizures were also described to occur in NCL/*GRN* patients (Smith et al., 2012). Seizure-like behaviour or abnormal bouts are documented in zebrafish larvae as quick, roundish spinning (Mahmood et al., 2013a,b) and can be induced by chemicals like pentylenetetrazole (PTZ) (Baraban et al., 2005). Despite a lack of neurodegeneration in the *grna*$^{-/-}$;*grnb*$^{-/-}$ double mutant larvae (see above), I did track the swim behaviour in *grna*$^{-/-}$;*grnb*$^{-/-}$ double mutants to exclude seizure-like behaviour. After an adaptation time of 30min, the swim path was recorded for 5min in 5dpf wildtype, *grna*$^{-/-}$;*grnb*$^{-/-}$ mutants as well as DMSO-, and PTZ-treated wildtype larvae. The PTZ-treated samples served as a positive control. I additionally extracted from the 5min-trackings the total distance moved, the mean velocity, and the percentage of time larvae spent on movements with a velocity above 2mm/s. In contrast to wildtype, *grna*$^{-/-}$;*grnb*$^{-/-}$ mutants, and DMSO-treated larvae, the PTZ-treated larvae were much more active (Fig. 5.29A). This is also reflected in the total distance moved, which was significantly increased in the PTZ-treated larvae (p(wt-*grna*$^{-/-}$;*grnb*$^{-/-}$) = 0.2386, p(wt-DMSO) = 0.0534, ***p(wt-PTZ) = 0.0002) (Fig. 5.29B). The mean velocity and the percental time larvae spent for movements faster than 2mm/s was comparable in wildtype, *grna*$^{-/-}$;*grnb*$^{-/-}$ mutants, and DMSO-treated larvae but significantly elevated in PTZ-treated wildtype larvae (Mean velocity: p(wt-*grna*$^{-/-}$;*grnb*$^{-/-}$) = 0.5657, p(wt-DMSO) = 0.8081, *p(wt-PTZ) = 0.0137. Movements > 2mm/s: p(wt-*grna*$^{-/-}$;*grnb*$^{-/-}$) = 0.2585, p(wt-DMSO) = 0.0668, **p(wt-PTZ) = 0.0016.) (Fig. 5.29C-D). This data suggests that swimming in 5dpf wildtype and *grna*$^{-/-}$;*grnb*$^{-/-}$ mutant larvae is very similar and devoid of seizure-like behaviour as observed upon PTZ-treatment.

The age at onset is very diverse in FTLD-TDP/*GRN* (Seelaar et al., 2008; van Swieten and Heutink, 2008) and it is believed that a second hit is required to trigger the disease (Dormann and Haass, 2011; Seelaar et al., 2008). To test if *grna*$^{-/-}$;*grnb*$^{-/-}$ mutants respond differently to a stressful stimulus, wildtype and *grna*$^{-/-}$;*grnb*$^{-/-}$ mutants were exposed to abrupt changes in illumination, which induces a photomotor response (Burgess and Granato, 2007; Vignet et al., 2013). Especially when facing abrupt darkness, a stimulus that is avoided by zebrafish larvae (Chen and Engert, 2014), zebrafish larvae tend to be more active (de Esch et al., 2012; MacPhail et al., 2009; Vignet et al., 2013). After an adaptation of 40min, 100% light in the recording device the 5dpf larvae were first exposed to 100% light for 5min and then two cycles of 5min darkness, 5min 100% light followed (Fig. 5.30). Within the time frames of 5min, the movies were analysed with respect to the total distance moved, the mean velocity, and the percental time spent for movement with a velocity above 2mm/s. Both wildtype and *grna*$^{-/-}$;*grnb*$^{-/-}$ mutants re-

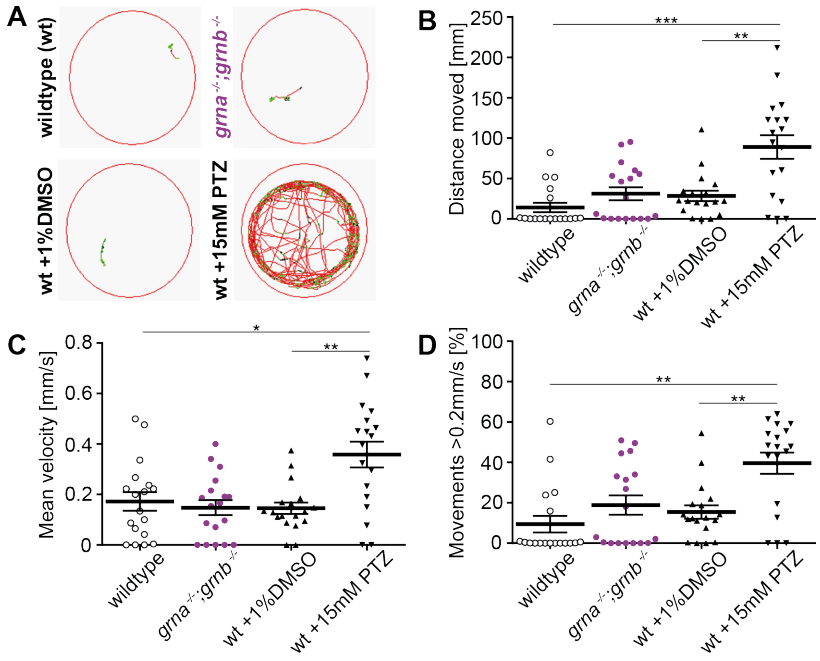

Figure 5.29 – The swim tracks of wildtype and *grna*$^{-/-}$;*grnb*$^{-/-}$ mutants revealed no abnormal swim behaviour. **A**: In contrast to PTZ-treated wildtype larvae the swim path of wildtype, *grna*$^{-/-}$;*grnb*$^{-/-}$ mutants, and DMSO-treated controls lacked abnormal bouts and bursts. 5dpf. Movements < 2mm/s: black lines. Movements 2mm/s – 6mm/s: green lines. Movements > 6mm/s: red lines. Adaptation time: 30min. Recording time: 5min. Recorded by a digital camera (30 frames/s). **B**: The total distance moved within 5min was equal in wildtype, *grna*$^{-/-}$;*grnb*$^{-/-}$ mutants, and DMSO-treated larvae but significantly increased in PTZ-treated larvae. ***p(wt-PTZ) = 0.0002. **p(DMSO-PTZ) = 0.004. **C**: The mean velocity was equal in wildtype, *grna*$^{-/-}$;*grnb*$^{-/-}$ mutants, and DMSO-treated larvae but significantly increased in PTZ-treated larvae. *p(wt-PTZ) = 0.0137. **p(DMSO-PTZ) = 0.0014. **D**: The time spent for movements with a velocity above 2mm/s was significantly more in PTZ-treated larvae when compared to wildtype, *grna*$^{-/-}$;*grnb*$^{-/-}$ mutant, and DMSO-treated larvae. **p(wt-PTZ) = 0.0016. **p(DMSO-PTZ) = 0.0037. B-D: Quantification from the movies recorded in A. $n = 18$. S.E.M. Mann-Whitney test (two-tailed).

sponded to the stimulus darkness with a significant increase in the total distance moved, the mean velocity, and the percentage of movements faster than 2mm/s (Fig. 5.30A-C). Upon abrupt reillumination all parameters analysed declined significantly in wildtype and *grna*$^{-/-}$;*grnb*$^{-/-}$ mutants to a similar extent (Fig. 5.30A-C). In the second round of stimulation the response was still occurring but it was less pronounced (Fig. 5.30A-C). In the mutants the photomotor response seemed to be less pronounced than in wildtype but this did not reach statistical significance when wildtype and *grna*$^{-/-}$;*grnb*$^{-/-}$ mutants are compared within the same time frame (Fig. 5.30A-C) (Distance moved: $p(1) = 0.4463$, $p(2) = 0.2626$, $p(3) = 0.3347$, $p(4) = 0.2366$, $p(5) = 0.2173$. Mean velocity: $p(1) = 0.5612$, $p(2) = 0.3852$, $p(3) = 0.1404$, $p(4) = 0.2493$, $p(5) = 0.3517$. Movements > 2mm/s: $p(1) = 0.3496$, $p(2) = 0.2366$, $p(3) = 0.4204$, $p(4) = 0.4761$,

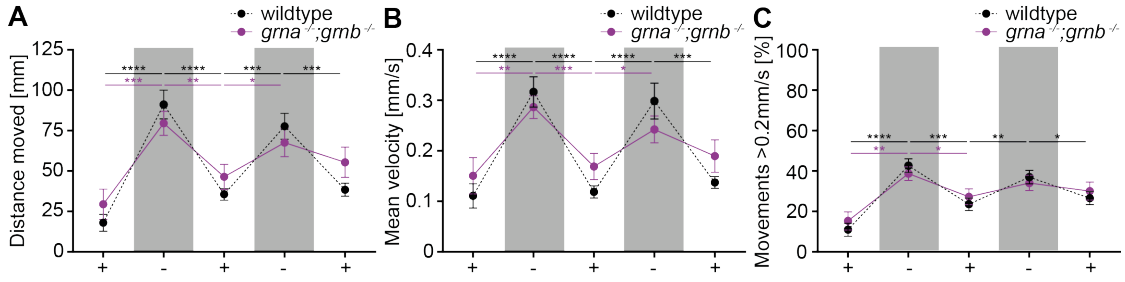

Figure 5.30 – Wildtype and *grna*$^{-/-}$;*grnb*$^{-/-}$ mutants showed a similar photomotor response. **A-C**: Quantification of movies recording the photomotor response in wildtype and *grna*$^{-/-}$;*grnb*$^{-/-}$ mutants. The following protocol has been applied: 40min adaptation time, 5min light (+) (1), 5min darkness (-) (2), 5min light (+) (3), 5min darkness (-) (4), 5min light (+) (5). **A**: The distance moved was significantly increased during the periods of darkness in wildtype and *grna*$^{-/-}$;*grnb*$^{-/-}$ mutants. **B**: The mean velocity of wildtype and *grna*$^{-/-}$;*grnb*$^{-/-}$ mutants was significantly elevated in darkness. **C**: Wildtype and *grna*$^{-/-}$;*grnb*$^{-/-}$ mutant larvae spent significantly more time with movements faster than 2mm/s when they were exposed to darkness. A-C: Periods of darkness are indicated in grey. 5dpf. $n = 18$. S.E.M. Mann-Whitney test (two-tailed). $^{*}p < 0.05$. $^{**}p < 0.01$. $^{***}p < 0.001$. $^{****}p < 0.0001$.

$p(5) = 0.6000$.). Therefore I concluded that the photomotor response is alike in wildtype and Grna;Grnb KO larvae at 5dpf and that Grna:Grnb KO larvae seem to show a normal reaction to stressful stimuli.

In summary, neuropathological alterations like neurodegeneration and microgliosis or biochemical alterations observed in Grn-deficient men or mice are absent in Grna;Grnb KO zebrafish. Moreover, their swim bahaviour as well as their photomotor response is normal indicating that Grna;Grnb KO zebrafish lack disease-related pathological phenotypes.

5.8 Wound healing and regeneration in Grna;Grnb KOs

Due to the lack of a phenotypes in healthy Grna;Grnb KO zebrafish, I next hypothesise that the *grna*$^{-/-}$;*grnb*$^{-/-}$ double mutants need to be challenged to exhibit phenotypes. Several publications demonstrated that GRN is involved in wound healing and inflammation (He et al., 2003; Qu et al., 2013; Tanaka et al., 2012; Zhu et al., 2002) and there are some reports suggesting a contribution of zf-Grns in injury and inflammation (Lien et al., 2006; Mathew et al., 2009; van der Sar et al., 2009). Moreover, I could show within this study that *grna* and *grn1/grn2* expression is enriched in haematopoietic tissue and macrophages. Therefore, I selected injuries and the induction of inflammation as a challenge for Grna;Grnb KOs.

5.8.1 Analysis of wound healing and regeneration in Grna;Grnb KO larvae

One advantage of the zebrafish as a model organism is that numerous larvae are obtained from one single spawning. Additionally, it is possible to keep zebrafish larvae optically transparent allowing *in vivo* imaging during development. To take these advantages into consideration I first analysed wound healing and regeneration in Grna;Grnb KO larvae.

5.8.1.1 Identifying a larval injury model with zf-Grn involvement

To increase the likelihood of a phenotype in challenged Grna;Grnb mutants, I evaluated larval injuries models and inducers of inflammation for increased zf-*grn* expression levels after the challenge. Previously, it has been reported that *grna* is upregulated after tail fin amputation in zebrafish larvae (Mathew et al., 2009), a well established assay in the field (Yoshinari and Kawakami, 2011). To confirm these findings, I performed qPCR for *grna*, *grnb*, *grn1/grn2*, and *apoeb* in wildtype zebrafish samples that were prepared according to the following procedure: The tail fin was amputated at 48hpf and embryos were fixed in RNAlater at the indicated time points - 3hpa, 24hpa, 48hpa, and 72hpa. By cutting the fixed larvae after the yolk extension, tail fin tissue was enriched. This tissue was then used for qPCR analysis. *apoeb* was used as a positive control, as it was shown before to increase after an injury in zebrafish (Lien et al., 2006; Mathew et al., 2009; Monnot et al., 1999). At 3hpa the *grna* levels were unchanged (p(3hpa) = 1.000), but *grna* was significantly increased to 1.5-fold in the tail fin tissue of injured embryos at 24hpa when compared to uninjured tail fin tissue ($^*p$(24hpa) = 0.0313). At 48hpa the levels were still slightly elevated (p(48hpa) = 0.3125) and at 72hpa there was no difference in the mRNA expression levels between injured and uninjured control tail fin samples (p(72hpa) = 0.8438) (Fig. 5.31A). *grnb* levels remained unchanged at all time points analysed. There was no increase after injury in comparison to uninjured fin tissue (p(3hpa) = 1.000, p(24hpa) = 0.4375, p(48hpa) = 0.5625, p(72hpa) = 1.000) (Fig. 5.31B). *grn1/grn2* levels showed a large variance at all time points examined in injured and uninjured samples. There might be a tendency to an increase in injured tissue, when compared to uninjured control samples, but this did not reach statistical significance (p(3hpa) = 0.1563, p(24hpa) = 0.0938, p(48hpa) = 0.5625, p(72hpa) = 1.000) (Fig. 5.31C). The positive control *apoeb* showed the first significant increase in injured tail fin tissue compared to uninjured tissue at 24hpa (p(3hpa) = 0.4375, $^*p$(24hpa) = 0.0313). At 48hpa *apoeb* was still elevated but to a lower extent (p(48hpa) = 0.0625) and at 72hpa there was a further decline in *apoeb* levels (p(72hpa) = 0.1563) (Fig. 5.31D). In summary, *grna* expression is elevated after

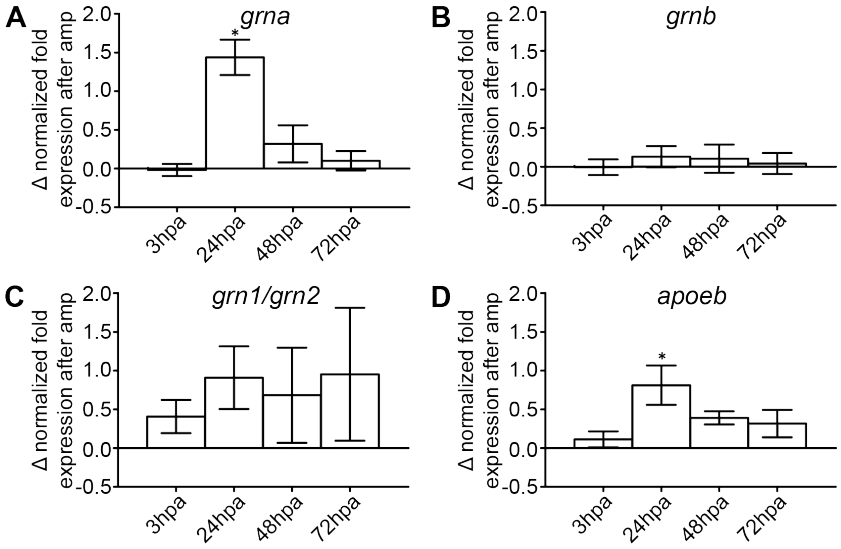

Figure 5.31 – *grna* was increased after tail fin amputation in zebrafish embryos/larvae. **A**: *grna* expression was significantly elevated in the injured tail fin tissue at 24hpa and mildly at 48hpa. $^*p(3\text{hpa}) = 0.0313$. **B**: *grnb* mRNA levels were the same in injured and uninjured control tail fin tissue at all time points analysed. **C**: *grn1/grn2* expression had a tendency to be increased in all tail fin tissue samples after amputation but the expression was highly variable. **D**: *apoeb* was increased significantly at 24hpa and slightly higher at 48hpa and 72hpa in injured tail fin tissue. $^*p = 0.0313$. A-D: $n = 6$. Normalized to *actb1* and *tbp*. qPCR. The difference (Δ) between cut and uncut fin tissue samples are diagrammed. S.E.M. Wilcoxon signed-rank test (two-tailed).

tail fin amputation in zebrafish embryos/larvae, similar to the positive control *apoeb*. *grn1/grn2* might be augmented after larval fin injury whereas *grnb* expression is not changed at all.

As a second independent assay I performed chemically induced wounding using $CuSO_4$. This inflammation assay is also suitable for in high-throughput (d'Alençon et al., 2010) and does not require time-consuming manual amputation of tiny larval fins. Groups of wildtype larvae were exposed at 3dpf for 1h to $CuSO_4$. Whole zebrafish larvae were fixed directly after 1h of $CuSO_4$ treatment and after additional 3h as well as 6h of recovery. In contrast to the tail fin amputation in zebrafish larvae, there was no increase of *grna* at any of the time points analysed, when compared to untreated samples ($p(1\text{h}) = 1.0$, $p(1{+}3\text{h}) = 0.5$, $p(1{+}6\text{h}) = 0.5$) (Fig. 5.32A). *grnb* and *grn1/grn2* expression were unchanged, as well (*grnb*: $p(1\text{h}) = 0.25$, $p(1{+}3\text{h}) = 1.0$, $p(1{+}6\text{h}) = 0.75$. *grn1/grn2)*: $p(1\text{h}) = 0.5$, $p(1{+}3\text{h}) = 0.5$, $p(1{+}6\text{h}) = 0.75$) (Fig. 5.32B,C). Also *apoeb*, which was used as a positive control in the tail fin amputation assay, remained unchanged in all $CuSO_4$-treated samples analysed ($p(1\text{h}) = 0.75$, $p(1{+}3\text{h}) = 0.75$, $p(1{+}6\text{h}) = 0.5$) (Fig. 5.32D). *mmp9* expression, which served as a positive control in this assay (d'Alençon et al., 2010), was strongly increased after 1h of $CuSO_4$ treatment ($p(1\text{h}) = 0.25$), remained slightly

upregulated after 3h of recovery when compared to untreated samples ($p(1+3h) = 0.25$) and decreased further after 6h of recovery (Fig. 5.32F), confirming that the $CuSO_4$-induced wounding itself did work. As a consequence of these experiments it can be summarized that chemical wounding with $CuSO_4$ has no effect on zf-*grn* expression levels in wildtype larvae and that is not a promising inflammation assay for the purpose pursued in the following.

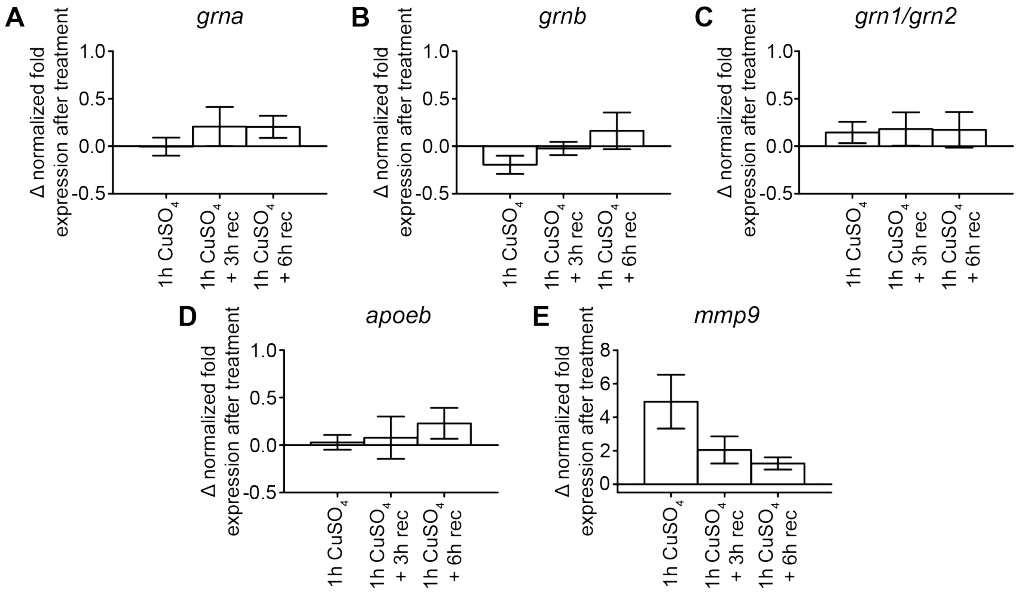

Figure 5.32 – $CuSO_4$ induced wounding at 3dpf did not lead to increased zf-*grn* expression levels at any of the time points analysed. **A**: *grna* mRNA levels remained unchanged in all samples analysed. **B**: *grnb* mRNA levels remained unchanged in all samples. **C**: *grn1/grn2* were not increased in any samples analysed. **D**: *apoeb* was unchanged after $CuSO_4$ treatment. **E**: *mmp9* raised 5-fold after 1h $CuSO_4$ treatment compared to untreated samples. After 3h of recovery the mRNA levels were still elevated by 2-fold. A-E: Normalized to *actb1* and *tbp*. The difference (Δ) between cut and uncut fin tissue samples are diagrammed. qPCR. $n = 3$. S.E.M. Wilcoxon signed-rank test (two-tailed). Rec: recovery.

5.8.1.2 Regeneration of the tail fin in Grna;Grnb KO larvae

After demonstrating that *grna* is significantly increased after a tail fin amputation I asked if the KO of Grna and Grnb has an influence on the regeneration of the larval tail fin. For the analysis of the regenerative capacity in *grna*$^{-/-}$;*grnb*$^{-/-}$ mutants, the tail fins of wildtype and *grna*$^{-/-}$;*grnb*$^{-/-}$ double mutant embryos were dissected with microscissors at 48hpf and images were taken by brightfield microscopy at 0hpa, 24hpa, 48hpa, and 72hpa. A comparison of the regenerating tail fins at the selected time points after injury in wildtype and *grna*$^{-/-}$;*grnb*$^{-/-}$ double mutant embryos/larvae showed that there was no obvious difference between the two genotypes, as illustrated in representative images

(Fig. 5.33A). In both, wildtype and *grna*$^{-/-}$;*grnb*$^{-/-}$ double mutant embryos/larvae the wound was first sealed and then the amputated fin was restored in size and shape within three days (Fig. 5.33A). To approximate if the larval fin was restored in the same size in wildtype and *grna*$^{-/-}$;*grnb*$^{-/-}$ double mutants, I quantified the length growth in the regenerating larval fin tissue. The length is defined as the minimal distance from

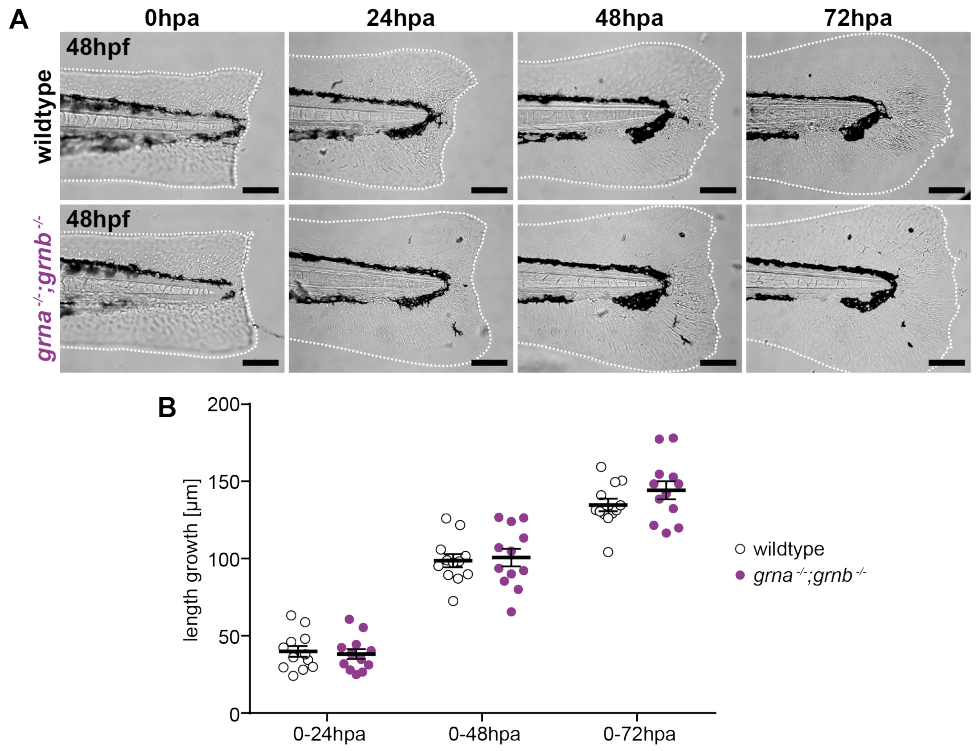

Figure 5.33 – *grna*$^{-/-}$;*grnb*$^{-/-}$ mutants regenerated the tail fin after amputation like wildtype. **A**: Representative images of wildtype and *grna*$^{-/-}$;*grnb*$^{-/-}$ mutant embryos/larvae after amputation are shown. $n = 12$. Scale bar: 100µm. The white dashed line highlights the border of the fin. Lateral view. Anterior to the left. Images by brightfield microscopy. **B**: Quantification of the length growth after tail fin amputation. The length growth was alike in wildtype and *grna*$^{-/-}$;*grnb*$^{-/-}$ double mutants. $n = 12$. S.E.M. Mann-Whitney test (two-tailed).

the caudal border of pigmentation to the most distal part of the fin and represents the length growth in caudal direction. This analysis revealed that the length growth in caudal direction was comparable in wildtype and *grna*$^{-/-}$;*grnb*$^{-/-}$ double mutants within all intervals analysed (p(0-24) = 0.7430, p(0-48) = 0.7430, p(0-72) = 0.2876) (Fig. 5.33B) indicating that the regeneration of the tail fin after amputation is not affected by a KO of Grna and Grnb.

5.8.1.3 Myeloid cell response in Grna;Grnb KO larvae after tail fin amputations

I showed that *grna* and *grn1/grn2* expression is enriched in macrophages and in the kidney, which is the main haematopoietic tissue in zebrafish. Therefore, I asked if myeloid cells, including macrophages, in *grna*$^{-/-}$;*grnb*$^{-/-}$ double mutants are still able to react normally to an injury by migrating to the wound margin. Moreover, it was suggested that macrophages from Grn-deficient mice are more active (Kao et al., 2011; Yin et al., 2010a). To visualize myeloid cells, I raised wildtype and *grna;grnb* double mutants with fluorescently labelled myeloid cells by using the transgenic line Tg(*spi1b*:Gal4;/UAS:EGFP) (Peri and Nüsslein-Volhard, 2008). At 3dpf the number of myeloid cells is higher than at 48hpf, therefore, I dissected the tail fin for this experiment at 3dpf and imaged the migration of myeloid cells to the wound *in vivo* for the subsequent 16h by time-lapse recordings using confocal microscopy. Representative still images from the *in vivo* time-lapse recordings in Tg(*spi1b*:Gal4/UAS:GFP) wildtype and Tg(*spi1b*:Gal4/UAS:GFP) *grna*$^{-/-}$;*grnb*$^{-/-}$ double mutants illustrate that the cells of the myeloid lineage, of which a subset was GFP-positive, migrated towards the wound margin after tail fin amputation (Fig. 5.34A). These cells seemed to react similarly in wildtype and *grna*$^{-/-}$;*grnb*$^{-/-}$ double mutant larvae (Fig. 5.34A).
To obtain a better insight in the myeloid cell migration after tail fin amputation in wildtype and Grna;Grnb KO larvae, the first five GFP-positive cells that arrived at the wound edge in the recordings described above (Fig 5.34A) were manually tracked and quantified using the ImageJ plugin mTrackJ (Meijering et al., 2012). The parameters were chosen according to a previous publication that quantified the macrophage- and neutrophil-response after tail fin amputation (Ellett et al., 2011). I extracted the migration path, the mean velocity, the meandering index (direct path length/actual path length), the time to the wound, and the percentage of time the cells spent in the wound. All cell migration paths obtained from the four wildtype and four *grna*$^{-/-}$;*grnb*$^{-/-}$ mutants looked similar (Fig 5.34B) and could not be assigned to a respective genotype. There was no difference in the mean velocity of the tracked myeloid cells in wildtype and Grna;Grnb KO larvae ($p = 0.2734$) (Fig. 5.34C) and the meandering index showed a slight but not significant reduction in the *grna*$^{-/-}$;*grnb*$^{-/-}$ double mutants compared to wildtype ($p = 0.1124$) (Fig. 5.34D). In both wildtype and Grna;Grnb double KOs the time to the wound margin was about the same ($p = 0.5638$) (Fig. 5.34E) and the percentage of time the myeloid cells spent in the wound was a bit but not significantly reduced in *grna*$^{-/-}$;*grnb*$^{-/-}$ double mutant larvae in comparison to wildtype larvae ($p = 0.1146$) (Fig. 5.34F). This suggests that myeloid cells do respond similarly to a tail fin amputation in wildtype and Grna;Grnb double KO larvae.

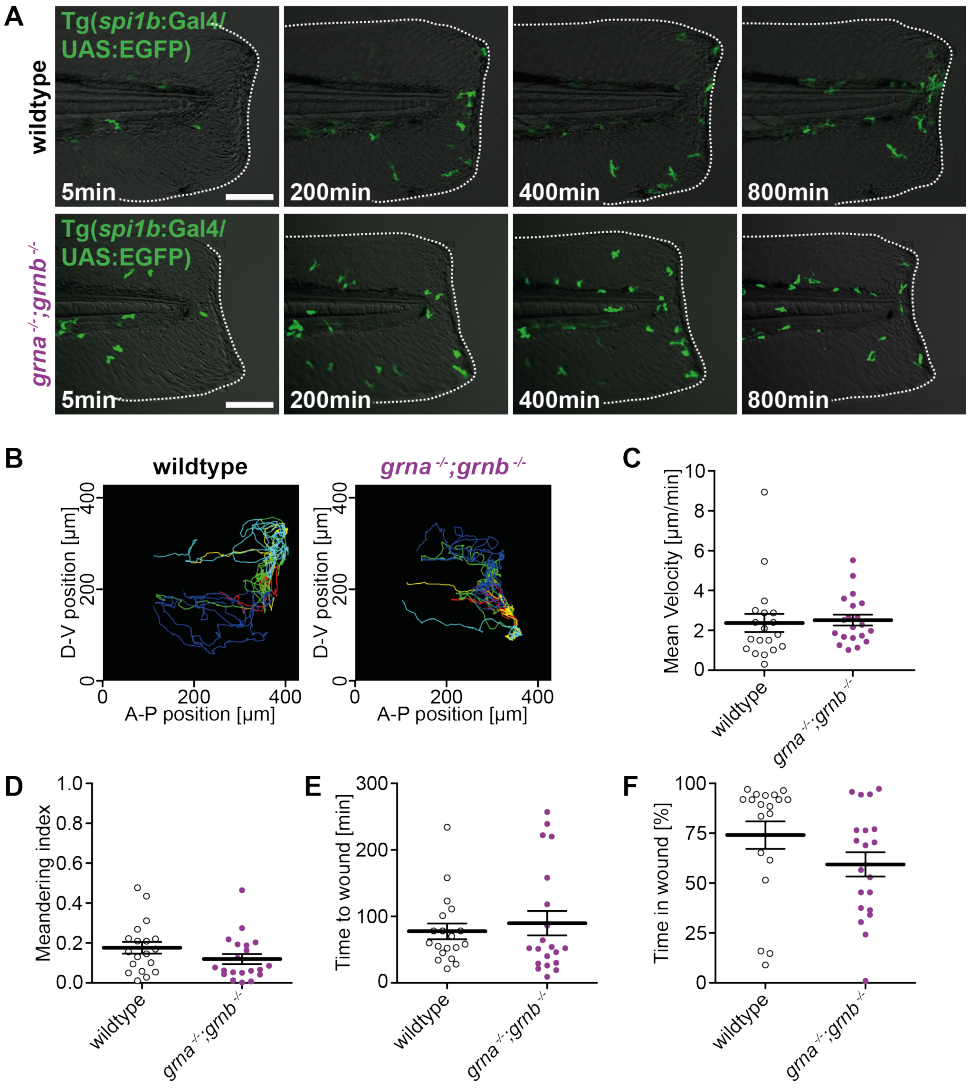

Figure 5.34 – The myeloid cell reponse in *grna*$^{-/-}$;*grnb*$^{-/-}$ larvae after tail fin amputation at 72hpf was like that in wildtype. **A**: Representative images from *in vivo* time-lapse recordings of cells of the myeloid linage that did respond to a tail fin amputation in wildtype and *grna*$^{-/-}$;*grnb*$^{-/-}$ double mutant Tg(*spi1b*:Gal4/UAS:EGFP). Recording time: 16h. 1frame/min. Scale bar: 100µm. $n = 4$. Overlays of DIC and green fluorescence channels. The white dashed line highlights the margin of the larval fin. Single plane. Lateral view. Anterior to the left. Recorded by spinning disk confocal microscopy. **B**: Cell migration paths for the first five GFP-postive cells that arrived at the wound, followed for 16 hours after tail fin amputation. Extracted from the movies illustrated in A. Manual tracking. **C-F**: Quantitative analysis of the migration path after tail fin amputation from the manual trackings in B. **C**: The mean velocity of myeloid cells over the whole time of recording was about the same in wildtype and *grna*$^{-/-}$;*grnb*$^{-/-}$ double mutant larvae. **D**: Myeloid cells in wildtype and Grna;Grnb KO larvae had a similar meandering index (direct path length/actual path length). **E**: The time myeloid cells needed to migrate to the wound was alike. **F**: In wildtype and *grna*$^{-/-}$;*grnb*$^{-/-}$ mutants myeloid cells spent about the same time at the wound edge. $n = 4x5$. S.E.M. Mann-Whitney test (two-tailed).

Taken together, I confirmed increased *grna* expression levels after tail fin amputation, but a lack of Grna and Grnb does not affect the regeneration of the larval tail fin and does not disturb the recruitment of myeloid cells to the wound.

5.8.2 First steps towards an analysis of wound healing and regeneration in adult Grna;Grnb KO brains

Developmental processes are characterized by a massive proliferation and selective cell death. Signaling pathways involved during development are sometimes unlike those in adulthood. Despite the fact that zebrafish grow throughout their life (Kishi et al., 2003) and have a tremendous regenerative capacity (Gemberling et al., 2013), it is possible that such differences between larval and adult tissue could prevent the manifestation of phenotypes in Grna;Grnb KO embryos and larvae even after a challenge like an injury. Moreover, phenotypes caused by Grn-deficiency seem to require ageing, as it was demonstrated in Grn-deficient mice that Grn-related phenotypes become more prominent upon ageing (Götzl et al., 2014; Wils et al., 2012). This is also supported by the fact that NCL/*GRN* patients, which are homozygous for a loss of function mutation in *GRN*, have an age at onset in young adulthood (Smith et al., 2012). Both NCL/*GRN* and FTLD-TDP/*GRN* are diseases of the brain and additionally *Grn* is upregulated in mice after a traumatic brain injury (Tanaka et al., 2012). To examine if the zf-*grn* levels are also upregulated after an injury in adult zebrafish brains and with the aim to analyse the Grna;Grnb KO mutant brains after an injury in the future, I initiated a collaboration with Rossella di Giaimo and Jovica Ninkovic at the Helmholtz Center Munich. Their group has established stab wound injuries in the adult zebrafish telencephalon (Baumgart et al., 2012). Interestingly, a microarray approach, performed on samples from stab wound injured zebrafish telencephali in this laboratory, indicates an upregulation of zf-*grns* after such kind of injury (di Giaimo, unpublished). To confirm their findings and determine which zf-*grns* are upregulated after a stab wound injury in the adult telencephalon I performed qPCRs for *grna*, *grnb*, and *grn1/grn2* in wildtype telencephali two days after a telencephalic stab wound injury (dpi) and compared them to uninjured wildtype telencephalon samples. I found *grna* to be approx. 40-fold upregulated after 2dpi in injured telencephalon samples, when compared to uninjured controls ($^*p = 0.05$) (Fig. 5.35A) whereas *grnb* mRNA remained unchanged ($p = 0.35$) (Fig. 5.35B). *grn1/grn2* expression levels were increased 35-times in comparison to uninjured samples in response to a stab wound injury ($^*p = 0.05$) (Fig. 5.35C). Interestingly, both, *grna* and *grn1/grn2*, did respond stronger to the injury than the positive controls *apoeb* ($^*p = 0.05$) and *mmp9* ($^*p = 0.05$), which were significantly elevated to approx. 30-fold in telencephali from injured samples, when

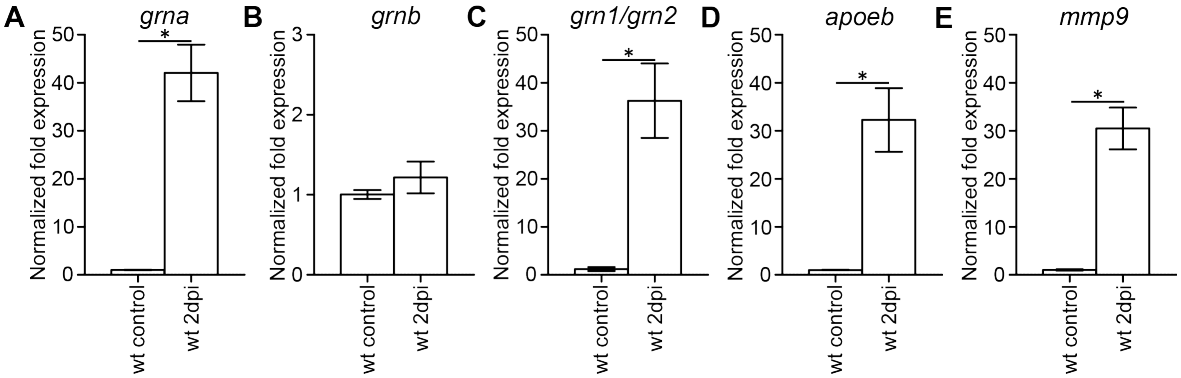

Figure 5.35 – *grna* and *grn1/grn2* were increased after stab wound injury in wildtype adult telencephalon. **A**: *grna* was increased 2dpi in injured telencephalon samples. **B**: *grnb* levels were comparable in injured and uninjured telencephali. **C**: *grn1/grn2* was strongly elevated at 2dpi in injured telencephali. **D**: 2dpi *apoeb* was enhanced in samples from injured telencephali. **E**: *mmp9* rose at 2dpi in response to an injury in the adult telencephalon. A-E: Normalized to *tbp*. mRNA isolated from adult zebrafish telencephali. $n = 3$. qPCR. S.E.M. Mann-Whitney test (one-tailed). $^*p = 0.05$.

compared to uninjured controls (Fig. 5.35D,E). In summary, *grna* and *grn1/grn2* were upregulated strongly after stab wound injury in the adult telencephalon, whereas *grnb* did not respond to the injury.

Because of these promising results a first test experiment was performed comparing wildtype and Grna;Grnb KO brains after a stab wound injury. These imply that the number of proliferating cells in the subventricular zone might be increased in Grna;Grnb KO telencephali when compared to wildtype. For a further detailed analysis and for quantifications a larger sample size is required. These animals are currently growing and ageing in the fish facility.

6 Discussion

6.1 GRN function split onto four zebrafish genes

In contrast to the single *GRN* gene in mammals, there are four zf-*grns* encoded in the zebrafish genome (Cadieux et al., 2005). The existence of *grna* and *grnb*, the *GRN* orthologues with several granulin domains can be explained by the hypothesis that the zebrafish underwent an additional round of whole-genome duplication during evolution, the so-called teleost-specific genome duplication (TSD) (Cadieux et al., 2005; Howe et al., 2013; Meyer and Schartl, 1999; Taylor et al., 2003). Due to the TSD, one human gene is frequently represented by two orthologues in the zebrafish genome. Interestingly, the carp and goldfish genome seem to contain only shorter Granulins, as long Granulins were not described so far in those species (Belcourt et al., 1993, 1995). Therefore, it is possible, that the shorter zf-*grns*, *grn1* and *grn2*, are encoding Granulins that are specific to non-mammalian vertebrates. This is supported by the fact that there are no orthologues of *grn1* and *grn2* in mammals. It is likely that the shorter zf-Grns were lost in mammals during evolution due to functional redundancy (Meyer and Schartl, 1999). The existence of the two shorter zf-*grns* in zebrafish is likely to derive from a single gene duplication in zebrafish, since *grn1* and *grn2* are located in tandem on the same chromosome (Meyer and Schartl, 1999). Moreover, other related fish species, like medaka, harbour only one shorter *granulin* in their genome. The function of all zf-Grns and reasons why the zebrafish has in contrast to carp and goldfish also long zf-Grns is elusive. The zf-Grns with several granulin domains resemble more the mammalian full-length protein, GRN, and the shorter zf-Grns could function similar to the cleaved mammalian granulin peptides. In mammals both GRN and the granulin peptides are bioactive and it was shown that they can have opposing functions. GRN antagonizes for example inflammation and the granulin peptides boost inflammation (Zhu et al., 2002). Whether Grna and Grnb are also proteolytically processed in zebrafish is unclear. I hypothesise that Grn1 and Grn2 perform the function of the mammalian granulin peptides superseding the proteolytical processing of Grna and Grnb. Taken together, the coexpression of long and short zf-Grns suggest a functional diversification of the Granulins in zebrafish.

6.1.1 Different splice variants of *grna*?

For the generation of zf-Grn-specific tools the full length cDNAs of *grna* and *grnb* transcripts were cloned and *grn1* and *grn2* were amplified from ESTs. For *grnb* the transcript deposited at the Ensembl database and published previously was confirmed (Cadieux et al., 2005). For *grna* a splice variant was amplified that is deposited at the Ensembl

database and encodes a 1049aa protein with 12 granulin domains. This *grna* transcript is longer and encodes two more granulin domains than the *grna* transcript, which was published previously and is also deposited in the Ensembl database (Cadieux et al., 2005). It is possible that the two splice variants are transcribed in distinct tissues, but within this study I did only obtain the longer splice variant from zebrafish of different age and from different tissues. In mouse *Grn*, skipping of one exon results in a transcript, that encodes a Grn protein lacking one granulin domain (He and Bateman, 2003). Moreover, the previous published *grna* was amplified from an EST (Cadieux et al., 2005), that was no longer commercially available. For human GRN 21 splice variants are listed in the Ensembl database and a transcript coding for a 593aa protein seems to be the most abundant. Since I could only isolate the *grna* transcript coding for Grna with 12 granulin domains, I conclude, that this is, even if other transcripts might be present, the main *grna* transcript. Consistent with the human cells, one major splice variant was isolated for *grna* and *grnb*, respectively.

6.1.2 zf-Grns seem to be posttranslationally modified

All tagged zf-Grns, derived from cell culture overexpression, migrate in SDS-PAGE at a higher MW than the calculated MW. GRNs are complex glycosylated glycoproteins. Among other factors glycosylation can prevent efficient binding of SDS to the protein, leading to a slower migration in SDS-PAGE (Lottspeich and Engels, 2012; Songsrirote et al., 2010). Human GRN has a calculated MW of 68.5kDa, but is migrating in SDS-PAGE due to heavy glycosylation at approximately 75-90kDa (Capell et al., 2011; Songsrirote et al., 2010). Similar to human GRN, zf-Grns contain predicted glycosylation sites and are likely to also migrate at a higher MW in SDS-PAGE than calculated. Two laboratories described migration of Grna and Grnb at lower MW than the calculated MW using self-made polyclonal Grna as well as Grnb peptide antibodies (Baranowski, 2008; Chitramuthu et al., 2010; Li et al., 2010, 2013). Unfortunately, both laboratories did not provide a detailed characterization of their antibodies, raising concerns about the specificity of these antibodies. It is possible, that Grna and Grnb are proteolytically processed and that specific cleaving products do migrate at a lower MW. However, in my hands zf-Grns did migrate at a higher MW similar to the running behaviour observed for human GRN and I did not observe Grna or Grnb specific bands at the MW suggested in the published literature (Baranowski, 2008; Chitramuthu et al., 2010; Li et al., 2010, 2013).

Since there were no antibodies commercially available that detect zf-Grns, zebrafish-specific mAbs detecting Grna and Grnb as well as Grn1/Grn2 were generated. In mammals it was shown that the full-length GRN can be proteolytically cleaved in

the linker region (Kleinberger et al., 2013). This was taken into consideration for the selection of the peptide for the generation of the mAb. Moreover, it is very difficult to generate antibodies detecting the granulin peptides themselves (personal communication A. Capell; Nguyen et al., 2013). Therefore, peptides chosen for the mAb generation are located partially in the linker region and partially in the granulin domain. Additionally it was evaluated if the selected peptides are suitable antigenes. Zebrafish-specific mAb were successfully generated for Grna and Grnb but not for Grn1 and Grn2. The latter two proteins are highly homologous and only one peptide sequence almost identical in Grn1 and Grn2 did fulfil the requirements for antigene selection. It is possible that exactly this region in Grn1 and Grn2 is posttranslationally modified masking the epitope and preventing recognition by mAbs. Furthermore, generation of antibodies detecting granulin peptides proved to be very difficult in the past (personal communication A. Capell; Nguyen et al., 2013). As Grn1 and Grn2 resemble the granulin peptides it is possible that a generation of Grn1 and Grn2 specific mAbs is facing the same limitations as the generation of antibodies raised against the granulin peptides. In contrast to previous publications (Baranowski, 2008; Chitramuthu et al., 2010; Li et al., 2010, 2013) the specificity of the Grna and Grnb mAb used in this study was demonstrated with different independent approaches e.g. overexpression in cell culture and dose dependent detection in samples from homo- and heterozygous mutants strengthening the validity of the mAbs generated within this study. Proper determination of antibody specificity using different independent experiments like performed herein prevents pitfalls like the confirmation of a KD and an antibody specificity in the same experiment. Since our Grna and Grnb mAb are clearly specific for either protein, they provide a great, novel tool for the analysis of zebrafish Grna and Grnb.

6.1.3 *grna* and *grn1/grn2* expression is enriched in macrophages

During development all four zf-*grns* are expressed (Cadieux et al., 2005). However, the expression levels at different developmental stages are distinct. *grna* and *grnb* are expressed throughout development (Cadieux et al., 2005) and *grnb* is expressed at much higher levels than *grna*. This was not described in a previous characterization of zf-*grns* (Cadieux et al., 2005). On the protein level, Grnb levels are higher as well. Grnb is detectable throughout development, while Grna is only expressed below the detection limit. However, it can not be excluded, that the Grnb mAb is more sensitive than the Grna mAb precluding Grna detection. Since *grn1* and *grn2* are highly homologous (ORF: 92% identity), they were analysed together. In the first days of zebrafish development *grn1/grn2* is almost absent, in line with previous findings (Cadieux et al., 2005).

In contrast all zf-*grns* are expressed in adult brain, fin, and kidney. Interestingly, the expression of *grna* and *grn1/grn2* was very strong in the kidney, which was not described previously (Cadieux et al., 2005). Moreover, the adult zebrafish kidney was the only tissue were Grna was detectable on protein level. The kidney is the main haematopoietic tissue in zebrafish (Jing and Zon, 2011) and previous data from other fish species indicated a role of Granulins in haematopoiesis and macrophage differentiation as well as maturation (Barreda et al., 2004; Belcourt et al., 1993, 1995; Hanington et al., 2006). Interestingly, the increase of *grn1/grn2* expression seems to coincide with the developmental timeframe in which the number of leukocytes is rising, indicating that *grn1/grn2* might be enriched in leukocytes (Jing and Zon, 2011).
In a collaboration with Julien Rougeot from the laboratory of Annemarie Meijer at Leiden University, the expression levels of zf-*grns* in FACS sorted leukocyte cell populations were analysed and revealed a strong enrichment of *grna* and *grn1/grn2* in macrophages. Also in the *mpx*:GFP-positive cells, which are mainly neutrophils and a subpopulation of inflammatory macrophages (Mathias et al., 2009), there was a minor enrichment of *grna* and *grn1/grn2*. This can be assigned to the macrophages in the *mpx*:GFP-positive cell population. This data is supported by publications that found an enrichment of *GRN* in cells of the human and mouse myeloid lineage, e.g. in macrophages and (activated) microglia (Chantry et al., 1998; Hashimoto et al., 1999, 2003; Martens et al., 2012; Ong et al., 2006; Petkau et al., 2010; Tanaka et al., 2012). Since zebrafish microglia derive from primitive macrophages, it can be speculated that *grna* and *grn1/grn2* expression levels are also elevated in this cell type in zebrafish. Moreover, *in situ* data during zebrafish development revealed that the zf-*grns* are expressed in haematopoietic tissues (Cadieux et al., 2005) and *grna* was used as a marker for microglia (Craig et al., 2008; Huang et al., 2012). This data indicate that zf-*grns*, but especially *grna* and *grn1/grn2*, are involved in haematopoiesis and possibly in macrophages and microglia function (Craig et al., 2008; Huang et al., 2012). Macrophages and microglia are phagocytic cells and especially in activated macrophages and microglia phagosomes fuse with lysosomes, to degrade the ingested material (Murphy et al., 2008). There is now increasing evidence for a possible role of GRN in lysosomal function (Belcastro et al., 2011; Hu et al., 2010; Kollmann et al., 2005; Nykjaer and Willnow, 2012; Qian et al., 2008; Tanaka et al., 2013; Zheng et al., 2011) and recently a lysosomal dysfunction in Grn-deficient men and mice was proposed (Götzl et al., 2014; Tanaka et al., 2013). Additionally, it is known that treatment of cells with compounds that alkalize the pH of the lysosome or inhibit the vacuolar ATPase, like Bafilomycin-A1, increase GRN levels (Capell et al., 2011). Therefore, I speculate that GRN's lysosomal function could be to sense and balance the amount of functional

lysosomes. It is also possible that GRN is involved in the regulation of macrophage and microglia activation, as it was demonstrated that macrophages and microglia from Grn KO mice are more phagocytic (Kao et al., 2011; Yin et al., 2010a). Moreover it is likely that Grna and Grn1 as well as Grn2 have an important function in balancing the inflammatory response, as it was published that GRN exhibits anti-inflammatory, whereas the granulin peptides exhibits pro-inflammatory properties (Zhu et al., 2002). According to my data Grnb seems to have a different expression pattern and it is possible, that Grnb is bioactive in distinct processes within different tissues. It was recently published that GRN is important for a functional blood brain barrier since it is needed for a normal endothelial tight junction structure (Jackman et al., 2013). At least in the larval brain, *grnb* expression (Cadieux et al., 2005) resembles that of *claudin 5a* and *claudin 5b*, which are components of the tight junction in zebrafish (Xie et al., 2010). It would therefore be interesting to examine if *grnb* plays a role in tight junction integrity in zebrafish.

6.2 zf-Grns and a role in the inflammatory response

Due to the enrichment of *grna* and *grn1/grn2* expression in macrophages and haematopoietic tissues as well as previous observations that *grna* is, for example, increased after a tail fin amputation in zebrafish larvae (Mathew et al., 2009) or after ventricular resection of the adult zebrafish heart (Lien et al., 2006), the expression levels of zf-*grns* were analysed after three different stimuli that trigger an inflammatory response. First, tail fin amputation, second, chemically induced wounding with $CuSO_4$, and third, a stab wound injury in the adult zebrafish telencephalon.
After a tail fin amputation in zebrafish larvae *grna* but not *grn1/grn2* is significantly increased, confirming previously published data (Mathew et al., 2009). Even though the effect was less pronounced and did not last as long as described before (Mathew et al., 2009), it was statistically significant. Since *grn1* and *grn2* are expressed at very low level during the larval stages analysed, it is possible that a minor differential *grn1/grn2* expression after tail fin amputation is not detectable due to the poor signal to noise ratio that can interfere with the analysis of low abundant transcripts. This is also a possible explanation of the striking divergences in the analysis of *grn1/grn2* after larval tail fin amputation.
Despite successful wounding, $CuSO_4$ treatment in zebrafish larvae did not have an influence on the expression of any of the zf-*grns* It is described that $CuSO_4$ treatment leads to the recruitment of neutrophils to the injured neuromasts (d'Alençon et al., 2010; Wittmann et al., 2012). Whether macrophages are also involved in the inflammatory response to $CuSO_4$ is not analysed so far. Therefore, it is possible that only neutrophils

are responsive to $CuSO_4$ treatment and macrophages, including an activation of *grna* and/or *grn1/grn2*, are not.

After an injury in the adult zebrafish telencephalon, *grna* and *grn1/grn2* are strongly increased at 2dpi. Since it was demonstrated before that the number of microglia is increased at 2dpi and that the microglia are in an activated state (Baumgart et al., 2012) it is possible that the increase of *grna* and *grn1/grn2* is a direct consequence of an increase in microglia.

It is still unclear why *grna* and *grn1/grn2* expression levels are increased after injury. They are expressed in macrophages and most likely in microglia, as well. The number of macrophages and microglia is increased around the wound site at the fin fold or in the telencephalon, respectively (Baumgart et al., 2012; Ellett et al., 2011), and after both injuries, tail fin amputation and stab wound injury, I did selectively analyse the injured tissue and not the whole larvae or whole zebrafish, as it was done after the $CuSO_4$ treatment. It is unclear if the number of cells expressing *grna* as well as *grn1/grn2*, most likely macrophages or microglia, increases or if the expression of *grna* and *grn1/grn2* per cell is increased upon injury. It is also possible that both scenarios are occurring simultaneously. Furthermore, it is of interest, if a wound is needed or if also degenerative processes as seen in neurodegenerative diseases in the absence of a wound, can trigger increased *grna* and *grn1/grn2* expression. GRN was demonstrated to be involved in wound healing (He et al., 2003) and in mice it was shown that *Grn* is upregulated for example after a traumatic brain injury (Tanaka et al., 2012) or after spinal contusion (Naphade et al., 2010). Moreover, *GRN* was shown to be upregulated in several neurodegenerative diseases, like in the spinal cord of ALS patients and around amyloid plaques in AD patients (Ahmed et al., 2007). Consequently, it would be interesting to examine the zf-*grns* levels in zebrafish models of neurodegenerative diseases.

Taken together, the observations made within this study in zebrafish strengthen previous data describing an involvement of *GRN* in the inflammatory response to an injury and confirm previous data in zebrafish. It is likely that the increase in GRN expression in these processes is conserved in vertebrates, including zebrafish, making the zebrafish an excellent model organism to study the role of GRN upon injury. It still remains unclear why GRNs accross different species are increased after an inflammatory stimulus and during chronic inflammation. Therefore, it still needs to be further established, how GRN is involved in inflammation and why a lack of GRN is connected to neurodegenerative diseases.

6.3 Consequences of Grna and Grnb KO in zebrafish

FTLD-TDP/*GRN* patients suffer from GRN haploinsufficiency (Hardy and Rogaeva, 2013) and NCL/*GRN* patients have no GRN (Smith et al., 2012). Therefore, I decided to generate zebrafish loss of function mutants, to model aspects of the here mentioned neurodegenerative diseases in zebrafish. Moreover, Grna and Grnb KO zebrafish provide an excellent model to elucidate the physiological function of these two proteins. Zebrafish mutants, in contrast to morphants, allow the analysis of phenotypic alterations also in adult zebrafish. This is of special interest since NCL/*GRN* patients become symptomatic in their twenties and FTLD-TDP/*GRN* patients usually above 50 (Fujioka and Wszolek, 2011; Smith et al., 2012). Additionally, mutations are stable and can be inherited. Among the four zf-*grns*, *grna* and *grnb*, the two *GRN* orthologues were chosen for the generation of loss of function mutants. *grna* is believed to be the true orthologue of *GRN*, due to it synthenic conversation (Cadieux et al., 2005) and *grnb* is of interest because of its expression in the brain during development (Cadieux et al., 2005; Shankaran et al., 2008). Moreover, a deficiency of both *grn* orthologues in zebrafish would exclude a possible compensation for the loss of the paralogue, which was observed before for example in the single *tardbp*$^{-/-}$ mutants, where alternative splicing of *tardbpl* compensates for the loss of *tardbp* (Schmid et al., 2013).

6.3.1 Generation of KO alleles in Grna and Grnb using ZFNs

For targeted mutagenesis in *grna* and *grnb* ZFNs were used, which were at the beginning of my thesis the state-of-the-art technology for genome editing in zebrafish (Doyon et al., 2008; Meng et al., 2008; Schmid et al., 2013; van Bebber et al., 2013). The CompoZr Custom ZFN from Sigma Aldrich for *grna* and *grnb* were targeting the first and third coding exon, respectively, and mRNAs carrying mutations leading to a preTT codon that could escape the NMD, would result in very short, most likely not functional, truncated proteins. All analysed ZFN sets were demonstrated to be functional and did induce mutations at the preselected target sites in *grna* and *grnb*. These mutations were heritable, as it was shown before for other ZFN-induced mutations (Doyon et al., 2008; Meng et al., 2008; Schmid et al., 2013; van Bebber et al., 2013). Among all frameshift mutations generated, a subset (four for *grna* and three for *grnb*) was selected that caused a preTT codon. mRNAs with a preTT codon are normally eliminated by NMD (Vicente-Crespo and Palacios, 2010), leading to a loss of functional protein. To determine if Grna and Grnb are absent in the respective mutants, *grna* and *grnb* mRNA expression and Grna and Grnb protein levels were determined. I could show that *grna* and *grnb* mRNAs are significantly reduced. Despite the fact that the NMD

machinery enhances the degradation rate of mRNAs containing a preTT codon resulting in a decreased amount of preTT codon containing transcripts, such transcripts are still detectable. In the Grna and Grnb mutants the residual mRNA expression of *grna* reached a plateau at 50% of the wildtype mRNA expression levels and *grnb* plateaued at 10%. I speculate that the *grna* mRNA is stabilized by an antisense RNA (Cadieux et al., 2005) slowing down the degradation rate of mutated *grna* mRNA by NMD. The Grna and Grnb proteins are not detectable in all Grna and Grnb KO samples analysed. Therefore, it can be concluded that all *grna* and *grnb* mutant alleles selected in this study are resulting in a loss of functional proteins and that all homozygous Grna and Grnb mutants are Grna or Grnb KO zebrafish.

6.3.2 zf-Grns do not compensate for each other's loss

Due to an additional round of genome duplication in the teleost lineage, there are two orthologues of GRN in zebrafish, Grna and Grnb (Howe et al., 2013; Meyer and Schartl, 1999; Taylor et al., 2003). Furthermore, zebrafish have retained smaller Granulins, Grn1 and Grn2, which seem to be absent in mammals. It is likely that the loss of function of one of the zf-Grns is compensated by the upregulation of the other(s), as observed for example in the *tardbp* mutant zebrafish (Schmid et al., 2013). Interestingly, neither in *grna* nor *grnb* single mutants the other zf-*grn* is differentially expressed. On the protein level Grna or Grnb also do not compensate for the loss of the paralogue. *grn1/grn2* mRNAs do not compensate for the loss of Grna and Grnb. If they compensate for the loss of Grna and Grnb by increased translation remains to be determined upon availability of specific antibodies. Despite their structural similarities *grna* and *grnb* have quite different expression patterns (Cadieux et al., 2005) and the lack of compensation suggests also that they might have distinct functions and are regulated differentially, pointing to a functional diversification or a gain of new functions during evolution (Meyer and Schartl, 1999). According to the expression pattern (Cadieux et al., 2005) and the data obtained within this study, Grn1 and Grn2 are more likely to compensate a lack of Grna than Grnb. Grn1 and Grn2 are structurally different from Grna and do resemble more the processed granulin peptides. Since Grn was demonstrated to be anti-inflammatory and the granulin peptides to be pro-inflammatory (Zhu et al., 2002), it is difficult to imagine that Grn1 and Grn2, which do only have $1\frac{1}{2}$ granulin domains take over the function of the presumably anti-inflammatory Grna, which has 12 granulin domains in zebrafish. But this remains to be answered. Moreover, it is possible that zf-Grns are not essential in the healthy developing zebrafish larvae making compensation not necessary. Maybe functional zf-Grns are only needed in special conditions such as injury, inflammation or other insults. Additionally, other less related proteins could

compensate for the loss of Grna and Grnb. Taken together, a loss of Grna and Grnb seems to cause no compensatory upregulation of the paralogue, indicating different functions.

6.3.3 No need of Grna and Grnb for reproduction and development

Grn was identified in rodents in the reproductive system (Bateman and Bennett, 2009). Therefore, it was of interest if Grna and Grnb KO zebrafish are fertile. Matings did provide information that even the *grna*$^{-/-}$;*grnb*$^{-/-}$ double mutants are fertile and capable to produce viable offsprings according to Mendelian ratios. Single and double homozygous mutant offsprings did not show any obvious morphological changes either. This is consistent with observations in rodents where Grn KO mice are viable and fertile and do not have obvious morphological phenotypes (Ahmed et al., 2010; Ghoshal et al., 2012; Petkau et al., 2012; Wils et al., 2012; Yin et al., 2010a,b).
Since GRN is a growth factor (Bateman and Bennett, 2009), it was of interest if the lack of Grna or Grnb or both has an effect on the rate of development of zebrafish embryos. I showed that a KO of Grna and Grnb does not lead to a delay in development. It is possible that other growth factors are more important for a proper zebrafish development (Eivers et al., 2004) or that Grna and Grnb do not have a function as a growth factor during development. Growth factors can have specific functions and can act therefore tissue specific (Rentzsch et al., 2004). Even though zf-Grns are secreted proteins it is possible that they can only influence the growth of distinct cell types at distinct developmental stage. Whether Grna or Grnb display growth factor like properties in certain tissues or in adult zebrafish remains to be answered. In summary, reproductive phenotypes and a reduced developmental rate due to a lack of Grna and/or Grnb can be excluded.

6.4 Different phenotypes in Grna and Grnb KO and KD

KD is a powerful tool to study genes in zebrafish, especially during development (Eisen and Smith, 2008) and also for the zf-Grns a few KD studies are published (Chitramuthu et al., 2010; De Muynck et al., 2013; Laird et al., 2010; Li et al., 2010, 2013). With the *grna* and *grnb* single and double mutants in hands, I aimed to confirm some of the previously published findings. In the following the strikingly different results obtained in Grna and Grnb KO and KD zebrafish are discussed.

6.4.1 SpMN axon outgrowth in Grna and Grnb KO embryos

Even though *GRN* is only a minor risk factor for ALS (Del Bo et al., 2011; Sleegers et al., 2008), two laboratories did analyse the SpMN axon outgrowth in zebrafish morphants and could show that *grna* and *grnb* morphants have SpMN axons outgrowth defects (Chitramuthu et al., 2010; De Muynck et al., 2013; Laird et al., 2010). Here I would like to point to a discrepancy reported by one laboratory (Cadieux et al., 2005; Chitramuthu et al., 2010). *grna* and *grnb*, which code for presumably secreted proteins, do not seem to be expressed in SpMNs or the tissue surrounding the SpMN axons in a study published in 2005 (Cadieux et al., 2005). But in a follow-up study *grna* expression was stated to be observed at the somite boundaries, in the spinal cord, and in SpMN axons. Interestingly, whole-mount IF using an antibody apparently specific for Grna showed immunoreactivity at the somite boundaries, in the spinal cord, and in the SpMN as well (Chitramuthu et al., 2010). According to the literature available, I aimed to confirm the published data and analysed the SpMN axon outgrowth in *grna* and *grnb* single and double mutants. In these, the SpMN axons showed no signs of truncation or extended branching, when compared to wildtype controls. The analyses performed in this study were very carefully controlled, meaning that always the five SpMN axons above the end of the yolk extension were analysed and are shown as single bars in the graph. This clear definition of the region analysed was partially done in the KD studies published (Chitramuthu et al., 2010; De Muynck et al., 2013; Laird et al., 2010). When the length of still growing SpMN axons is determined a clear regional definition is essential as the more ventral SpMN axons are longer than more caudal ones at that stage of development. After I experienced SpMN axon length variations due to minor inter-clutch variations, I compared only siblings and included from each clutch the same quantity of embryos in the dataset. If inter- or intra-clutch comparisons were made in the KD studies is not stated (Chitramuthu et al., 2010; De Muynck et al., 2013; Laird et al., 2010). In the KD publications I observed that some of the KD embryos appeared morphologically abnormal (Chitramuthu et al., 2010). Including such kind of embryos in the analysis of the SpMN length could easily reveal a significantly reduced SpMN length because of reduced growth or developmental delay in general. To exclude an influence of maternal mRNA, which is also reduced when translation inhibition MO are used, the SpMN axon outgrowth analysis was repeated with matings of homozygous females and heterozygous males. The heterozygous embryos served as controls in this experimental setup, since it was shown before that the SpMN axons in heterozygous *grna* and *grnb* single and double mutants do not have any SpMN axon outgrowth defects. Also in this experimental setup, in the absence of maternal and zygotic mRNA, the embryos are devoid of any SpMN axon outgrowth defects. Contradictory results

obtained from morphants and mutants regarding SpMN axon outgrowth phenotypes, have been described previously in zebrafish (den Broeder et al., 2009; Kabashi et al., 2010; Schmid et al., 2013; Tucker et al., 2006) and raise the question if a MO-induced off-target effect or neurotoxicity is responsible for the SpMN axon outgrowth phenotypes observed in morphants. Both Grna and Grnb KD studies are done carefully, however important controls are missing or are unclear (Chitramuthu et al., 2010; Laird et al., 2010). Western blot analysis with a specific antibody are necessary to control the effectivity of a translation inhibition MO (Eisen and Smith, 2008). Chitramuthu and colleagues used an anti-Grna antibody to confirm the KD, but they detected Grna and its KD-mediated reduction at a MW of 55kDa, which is smaller than the theoretically calculated MW of Grna (112kDa) and far below the MW of Grna (approx. 200kDa) determined within this study, raising some doubts about the antibody specificity and the provided KD control. They also rescued the Grna KD by human *GRN* and *grna* mRNA overexpression. This was only possible for the MO-induced truncation of SpMN axons but not the extended branching, indicating that the extended branching could be a toxic off-target effect of the MO- or mRNA-injections. For their Grnb KD they did not provide any KD control (Chitramuthu et al., 2010). Laird and colleagues showed a dose-dependent effect of two independent *grna* and *grnb* MOs on the SpMN axon length, of which they could rescue one *grna* MO-induced SpMN truncation by the expression of human *GRN* mRNA. For the other *grna* MO and the *grnb* MOs rescue experiments are not provided (Laird et al., 2010). Unfortunately, they did not show images of the MO-mediated KD and it is possible that the truncation of SpMN could be caused by MO-induced toxicity or developmental delay. Taken together, these observations raised serious questions about the specificity of the MOs used and the significance of those studies. In contrast, the *grna* and *grnb* mutants generated and used in this study were carefully characterized and every embryo used for the SpMN axon outgrowth analysis was genotyped. Therefore, I conclude that neither Grna nor Grnb is needed for a proper outgrowth of SpMN axons in zebrafish and that even a lack of both proteins does not result in SpMN axon outgrowth defects.

6.4.2 MPCs in Grna;Grnb double KO embryos

It was demonstrated that a KD of Grna leads to an impaired muscle growth and the authors showed that *grna* and *grnb* morphants have a reduced number of Pax7-positive MPCs (Li et al., 2013). In contrast, the number of Pax7-positive MPCs in $grna^{-/-};grnb^{-/-}$ double mutant embryos was not decreased and there was no effect on the differentiated slow and fast trunk muscles. There is one transverse section included in the study from Li and colleagues that shows the expression of Grna in the larval trunk myotome, but

negative or positive controls confirming the antibody specificity are missing (Li et al., 2013). Moreover, the expression pattern of *grna* and *grnb* described by others are not consistent with a muscle phenotype, since neither the muscle itself nor the surrounding tissue is expressing *grna* or *grnb* (Cadieux et al., 2005). Li and colleagues used a translation inhibition MO that was carefully validated in their laboratory before (Li et al., 2010). In the previous study they showed that the MO is able to silence a grna-GFP reporter construct, confirmed the KD on protein level (98kDa) and rescued the observed liver phenotype by overexpression of *grna* (Li et al., 2010). Also the number of Pax7-positive MPCs was rescued by overexpression of *grna* but in between the two studies of the same laboratory the MW of Grna dropped to 55kDa and therefore, the Grna KD was confirmed by the reduction of a signal at 55kDa (Li et al., 2013), raising serious doubts about the KD efficiency especially in the later study. Moreover, the Grna KD embryos shown in the publication have a massive increase in cell death, pointing towards toxicity and the Grnb KD embryos displayed seem to be developmentally younger than 24hpf. With the additional finding in the Grna;Grnb KOs I conclude that neither Grna nor Grnb has an influence on the muscle growth.

Taken together, the data obtained herein highlights that KD studies have to be analysed with great caution, since the phenotypes often cannot be confirmed by a genetic KO (Schmid and Haass, 2013).

6.5 Grna and Grnb are not required for proper vasculogenesis

GRN is published to be an angiogenic factor (He et al., 2003; Ho et al., 2008; Toh et al., 2013) and *tardbp*$^{-/-}$*;tardbpl*$^{-/-}$ double mutant zebrafish have mispatterned blood vessels (Schmid et al., 2013). I therefore analysed the blood vessels in *grna*$^{-/-}$*;grnb*$^{-/-}$ double mutants for proper vessel patterning. During embryonic stages the blood vessels in *grna*$^{-/-}$*;grnb*$^{-/-}$ double mutants had a wildtype pattern, suggesting that Grna and Grnb are not required for proper vasculogenesis during zebrafish development. Grn1 and Grn2 could be important for vascular patterning, but at the developmental stages analysed *grn1* and *grn2* expression is very low. In mice, *Grn* is expressed in the developing microvasculature (Daniel et al., 2003). In contrast to that, there is no clear evidence for an expression of zf-*grns* in the developing vasculature (Cadieux et al., 2005). Therefore, it is possible that blood vessels in zebrafish do not need zf-Grns for proper vasculogenesis. Whether zf-Grns have angiogenic capacities at all, similar to mammalian GRN (He et al., 2003; Ho et al., 2008), remains to be determined. Recent data suggested that GRN is needed for a proper functional blood brain barrier (Jackman

et al., 2013). Therefore, it would be interesting to examine the blood brain barrier integrity (Nishimura et al., 2013) in *grna*$^{-/-}$;*grnb*$^{-/-}$ double mutant zebrafish.

6.6 Grna;Grnb KO zebrafish lack disease-related phenotypes

After the discovery in 2006 that mutations in *GRN* are causative for FTLD-TDP (Baker et al., 2006; Cruts et al., 2006) and in 2012 that a complete absence of GRN leads to NCL (Smith et al., 2012), the major challenge in the field was and still is to unravel the underlying pathomechanisms. In the recent years patient material from FTLD-TDP/*GRN* patients was analysed in detail and experiments using cell culture systems as well as animal models were performed. Some of the phenotypes described in GRN patients and Grn KO mice were addressed in the *grna*$^{-/-}$;*grnb*$^{-/-}$ double mutant zebrafish and the results are discussed hereafter.

6.6.1 No neurodegeneration in Grna;Grnb KO larvae

Both FTLD-TDP/*GRN* and NCL/*GRN* are neurodegenerative diseases and animal models mimicking these diseases should develop neurodegeneration as well. Interestingly, neurodegeneration was only reported in one aged Grn KO mouse strain (Ahmed et al., 2010) but not in others (Ghoshal et al., 2012; Petkau et al., 2012; Wils et al., 2012). Consistent with the findings in most Grn-deficient mice, also Grna;Grnb KO larvae lack an increase in neurodegeneration. The dying cells observed in brains of 5dpf Grna;Grnb KO and wildtype larvae are mostly undergoing programmed cell death through developmental pruning processes (Eyo and Dailey, 2013). Neurodegeneration in the brain of adult Grna;Grnb KO fish was not examined, but is rather unlikely based on the observations in rodents. Why neurodegeneration observed in Grn-deficient humans is not seen in mice and zebrafish that lack Grn is still elusive. It was postulated that a longer lifespan in humans might play a role (Götzl et al., 2014). Moreover, it is possible that characteristics specific to human beings, e.g. human specific sialic acid biology (Varki, 2009), promote neurodegeneration upon GRN-deficiency in men.

6.6.2 No microgliosis in Grna;Grnb KO larvae

In contrast to FTLD-TDP/*GRN* patients (Chen-Plotkin et al., 2010; Josephs et al., 2007; Mackenzie et al., 2006) and homozygous Grn KO mice (Ahmed et al., 2010; Ghoshal et al., 2012; Petkau et al., 2012; Wils et al., 2012; Yin et al., 2010a,b) the *grna*$^{-/-}$;*grnb*$^{-/-}$ double mutant zebrafish do not develop microgliosis in the larval brain. One possible explanation for this finding are the time points of analysis, which might have been too early. But also preliminary examinations in sections of adult Grna;Grnb

KO brains were not indicative of microgliosis in *grna*$^{-/-}$;*grnb*$^{-/-}$ double mutant zebrafish. Moreover, it would be of interest to examine the phagocytic behaviour of microglia in Grna;Grnb KOs, since it was demonstrated that macrophages and microglia of Grn KO mice are more active (Kao et al., 2011; Martens et al., 2012; Tanaka et al., 2012, 2013). Heterozygous Grn KO mice also lack gliosis (Ahmed et al., 2010; Filiano et al., 2013). Similar to the remaining wildtype Grn in heterozygous mice, the presence of Grn1 as well as Grn2 might be sufficient to prevent microgliosis in Grna;Grnb KOs. In general, microglia are present in zebrafish (Sieger et al., 2012; Svahn et al., 2013) and microgliosis including activated microglia, has been detected after an injury in the adult zebrafish brain (Baumgart et al., 2012). Parenchymal astrocytes are not present in zebrafish and therefore Grna;Grnb KO zebrafish were not examined for astrogliosis. Radial ependymoglia located at the ventricle seem to have functions attributed to parenchymal astrocytes (Baumgart et al., 2012). But after an injury in the adult zebrafish telencephalon there are for example no or very few cells positive for glial fibrillary acidic protein (Gfap) detectable in the parenchyma around the injury site. Instead Gfap-positive radial glia at the ventricle start to proliferate (Baumgart et al., 2012; März et al., 2011). These data indicate that the cellular response to an injury in zebrafish is different to the observations made in mammals. This might also be an explanation for the lack of scar formation and the tremendous regenerative capacity of the zebrafish brain (Baumgart et al., 2012). To my knowledge, there is no model so far describing adult onset neurodegeneration in the zebrafish brain. Therefore, it remains to be seen if microgliosis comparable to that observed in FTLD-TDP/*GRN* patients and homozygous Grn KO mice can occur at all in the uninjured adult zebrafish brain.

6.6.3 Are Grna;Grnb KOs devoid of aggregates?

Another hallmark of neurodegenerative diseases including FTLD and NCL are protein deposits (Kleinberger et al., 2013). FTLD-TDP/*GRN* patients as well as Grn KO mice show increased SCMAS and Saposin D staining (Götzl et al., 2014) and FTLD-TDP/*GRN* patients do additionally possess ubiquitin-positive TDP-43 deposits (Neumann et al., 2006) of which the latter were not observed in Grn KO mice (Ahmed et al., 2010; Ghoshal et al., 2012; Petkau et al., 2012; Wils et al., 2012). NCL/*GRN* patients and mice lacking Grn have consistently shown an increase in autofluorescent lipofuscin deposits (Ahmed et al., 2010; Petkau et al., 2012; Smith et al., 2012; Wils et al., 2012). The "ageing pigment" lipofuscin can be found in postmitotic cells of nearly every ageing organism (Jung et al., 2010). In zebrafish lipofuscin was demonstrated by PAS stain in the liver of 3.8 year old animals and autofluorescent material was detected in the eye after 4.8 years of birth (Kishi et al., 2008). Interestingly, one group mentioned the

observation of neurolipofuscin in 2.5 year old zebrafish, but did not show images (Rosa et al., 2010). My collaboration partner Claire Russell has, however, never observed autofluorescent deposits in zebrafish. Lipofuscin can also be visualized by PAS stain. Abnormal big dense, pinkish aggregates reminiscent of lipofuscin deposits in zebrafish, were detectable in CLN2 mutant zebrafish upon PAS staining (C. Russell, personal communication). The PAS stain in brains of larval and 11mpf adult Grna;Grnb KO zebrafish were devoid of any obvious abnormalities when compared to wildtype controls indicating absence of lipofuscin deposits. Whether lipofuscin deposits accumulate in the brain of Grna;Grnb KO zebrafish and if neurolipofuscin does occur in zebrafish in general could not be clarified within this study due to a lack of a positive control for aged brains. Possibly the time points of analysis were scheduled too early, as even pathological lipofuscin is only accumulating over time (Ahmed et al., 2010; Petkau et al., 2012; Smith et al., 2012; Wils et al., 2012). Additionally, the high regenerative capacity of zebrafish might have an influence. Lipofuscin-containing cells are maybe less functional and therefore quickly removed and replaced (Gemberling et al., 2013). Nevertheless, it was shown before, that protein deposits do form in zebrafish cells and can be detected before being removed (Paquet et al., 2009; Schiffer et al., 2007). However, both studies relied on strong overexpression of the aggregating protein. It might be worth to analyse the brains of more aged Grna;Grnb KO zebrafish with focus on brain regions that have been reported to contain neurolipofuscin in zebrafish or are primarily affected in humans and mice. Moreover, it would be interesting to examine the aged *grna*$^{-/-}$*;grnb*$^{-/-}$ double mutant zebrafish brains for TDP-43- and p62-positive deposits or elevated Saposin D and SCMAS levels, which have been detected in FTLD-TDP/*GRN* patients and/or Grn-deficient mice (Götzl et al., 2014; Neumann et al., 2006), to clarify if protein deposits do form in zebrafish that lack Grna and Grnb.

6.6.4 No indications for lysosomal dysfunction in Grna;Grnb KOs

NCL is a lysosomal storage disorder (Smith et al., 2012) and there is now increasing evidence of a lysosomal dysfunction in FTLD-TDP/*GRN* and Grn KO mice (Götzl et al., 2014). Consequently, I asked if the lysosomes in Grna;Grnb KO larvae are functional. Stainings with the *in vivo* dye LysoTracker that is incorporated in its fluorescent form in acidic subcellular compartments including lysosomes indicate that *grna*$^{-/-}$*;grnb*$^{-/-}$ double mutant larvae are able to establish vesicular acidic cell compartments. This acidic pH is required for an efficient function of lysosomal proteins. LysoTracker staining was demonstrated to be functional in zebrafish before (Donà et al., 2013; He et al., 2009; Mahmood et al., 2013a; Peri and Nüsslein-Volhard, 2008), but the detailed structure and appearance of zebrafish lysosomes is not characterized very

well. Therefore conclusions regarding the size, number, and localization of lysosomes in cells of Grna;Grnb KOs cannot be drawn. Additionally, it would be of interest to examine the lysosomes in the adult brain of *grna*$^{-/-}$;*grnb*$^{-/-}$ double mutants, as aberrant lysosomal staining becomes more prominent in aged Grn KO mice (Götzl et al., 2014). Both analyses require a lysosome specific labelling method. This could be realized either in a transgenic zebrafish line that labels lysosomes selectively and seems to be available in the laboratory of John Rawls (J. Rawls, personal communication) or by immunohistochemical stainings on whole larvae or sections using lysosome specific antibodies like the LAMP1 antibody (Drerup and Nechiporuk, 2013). Unfortunately, the latter still lacks a detailed validation in zebrafish. Furthermore, it would be interesting to analyse lysosomal size, number, and localization in sections from Grna;Grnb KO mutants and controls by electron microscopy best suited for the small size of zebrafish lysosomes, especially in neurons.

Lysosomal proteins and also some transcripts encoding lysosomal proteins, e.g. CTSD, accumulate in Grn KO mice and FTLD-TDP/*GRN* patients (Götzl et al., 2014; Tanaka et al., 2013; Wils et al., 2012). Unlike CTSD in Grn-deficient men and mammals (Götzl et al., 2014; Tanaka et al., 2013; Wils et al., 2012), the *ctsd* mRNA and Ctsd protein levels are unchanged in *grna*$^{-/-}$;*grnb*$^{-/-}$ double mutant zebrafish. In Grna;Grnb KO larvae this can be explained by the fact that *Ctsd* mRNA and Ctsd protein levels increase with age in Grn-deficent mice (Götzl et al., 2014; Wils et al., 2012) and that larvae are simply too young to show differences. The factor ageing was considered in the analysis of aged zebrafish brains from Grna;Grnb KOs and no difference in the Ctsd mRNA or protein expression levels were detectable. Zebrafish Ctsd and its processing is slightly different to mammalian CTSD. The zebrafish Ctsd is mono-glycosylated and matures into a single-chain protein, whereas CTSD is di-glycosylated and cleaved into light and heavy chain (Follo et al., 2011, 2013). However, both the proprotein and the heavy chain are increased in Grn KO mice (Götzl et al., 2014), thus the minor differences between CTSDs should be of no consequence in these experiments. Another reason for stable Ctsd levels in the Grna;Grnb KOs might be the tremendous regenerative capacity of the zebrafish even in the adult brain (Gemberling et al., 2013; Kizil et al., 2012). It is possible that cells with elevated Ctsd levels have a decreased lysosomal function and are eliminated and replaced. Furthermore, it could be that Ctsd is unexceptionally not affected but other lysosomal proteins are. Hence, it would be interesting to analyse other lysosomal proteins that have been reported to be elevated in Grn KO mice like for example Saposin D or TMEM106B (Götzl et al., 2014). Since zebrafish regenerate much better than mammals (Gemberling et al., 2013), ageing in general could be fundamentally distinct precluding the accumulation of lysosomal

proteins. A higher turnover capacity could also prevent an accumulation of lysosomal proteins in zebrafish, however there are no indications so far that lysosomal biology in zebrafish is very different to that in mammals. Nevertheless, it cannot be excluded that minor differences exist and that these could have had an effect on the analysis of Ctsd levels in the Grna;Grnb KO zebrafish. To learn more about the lysosomal biology in zebrafish in general and possible difference in *grna*$^{-/-}$*;grnb*$^{-/-}$ double mutant zebrafish, it would be of interest to analyse the lysosomal dynamics in zebrafish larvae by *in vivo* imaging. It was demonstrated that the lysosomal biogenesis is increased in Grn KO mice especially after an injury (Götzl et al., 2014; Tanaka et al., 2013) indicating a decreased lysosomal function upon Grn-deficiency. For the further characterization of the lysosomal dysfunction, lysosomal dynamics and turnover should be compared in Grn-deficient and control model systems.

6.6.5 No biochemical alterations in Grna;Grnb KOs

Besides lysosomal proteins that were linked to Grn-deficiency, there are also others e.g. STAT3 and FLNC that seem to be differentially expressed upon a partial or complete loss of GRN (J. Janssens and J. Banzhaf-Strathmann, unpublished; Schmid et al., 2013). In contrast to the increased *Stat3* levels in Grn KO mice and FTLD-TDP/*GRN* patients, the *stat3* levels in all Grna;Grnb KO samples were not statistically significantly altered. The increase in *Stat3* expression was becoming more obvious in aged Grn KO mice. Therefore, it might be worth to analyse *stat3* in aged *grna*$^{-/-}$*;grnb*$^{-/-}$ double mutant brain samples. The mechanisms that lead to the *STAT3* increase in mammals and the cell types involved are not examined so far. STAT3, which is a transcription factor, is involved in many processes, amongst others neuroinflammation. Oxidative stress or anti- and pro-inflammatory cytokines can activate STAT3 and it is discussed as a factor that promotes on the one hand cell death and on the other hand neuronal survival (Nicolas et al., 2013). Possibly *Stat3* is increased as a result of micro- and astrogliosis observed in Grn KO mice and FTLD-TDP/*GRN* patients (Ahmed et al., 2010; Ghoshal et al., 2012; Petkau et al., 2012; Wils et al., 2012; Yin et al., 2010a,b). If so, it would explain the lack of a *stat3* increase in *grna*$^{-/-}$*;grnb*$^{-/-}$ double mutants which are devoid of microgliosis.

The expression of the two *FLNC* orthologues, *flnca* and *flncb*, was not changed when compared to wildtype controls. Interestingly, there is a slight increase in *flncb* at 22mpf in *grna*$^{-/-}$*;grnb*$^{-/-}$ double mutant brains. Of the two orthologues *flncb* is related more closely to *FLNC* (Ruparelia et al., 2012) and it would be interesting to see if *flncb* expression in even older Grna;Grnb KO brains is further increasing. Mutations in *FLNC* are linked to myofibrillar myopathies and *flnca* and *flncb* expression in zebrafish embryos

is mainly observed in the muscle (Ruparelia et al., 2012). Interestingly, there seems to be one patient with a mutation in *FLNC* who developed also cerebellar atrophy (Tasca et al., 2012). But the exact reasons of increased *FLNC* levels in FTLD-TDP/*GRN* remain to be determined. The unaltered expression of *stat3*, *flnca*, and *flncb* in the *grna*$^{-/-}$*;grnb*$^{-/-}$ double mutants could be based on the presence of Grn1 and Grn2 that might be sufficient to compensate for the loss of Grna and Grnb. Consequently, it would be worth to repeat the analysis of *stat3*, *flnca*, and *flncb* expression levels in aged brains derived from zebrafish mutant that lack all zf-*grns*. STAT3 and FLNC are also of interest, since an upregulation of Stat3 and Flnca was originally discovered in the proteom analysis of the *tardbp*$^{-/-}$*;tardbpl*$^{-/-}$ double mutants (Schmid et al., 2013). Tardbp and Tardbpl are the orthologues of TDP-43, which is typically found in intracellular deposits of FTLD-TDP/*GRN* patients and it is unclear so far if a lack of soluble TDP-43 or a TDP-43-aggregate-mediated toxicity is harmful to neurons. The identification of increased *STAT3* and *FLNC* levels in Grn-deficient mammals and Tardbp;Tardbpl KO zebrafish provides now a connection between a loss of GRN and TDP-43 and it is of great interest to solve the underlying pathomechanisms.

6.6.6 No behavioural phenotypes in Grna;Grnb KO larvae

One of the symptoms in NCL/*GRN* are epileptic seizures due to massive neurodegeneration (Smith et al., 2012). I could show before that Grna;Grnb KO larvae show no signs of neurodegeneration and I aimed to exclude seizure-like swimming behaviour, as well. In contrast to PTZ-treated wildtype and CLN2 mutant larvae (Mahmood et al., 2013a) the *grna*$^{-/-}$*;grnb*$^{-/-}$ double mutants swim like wildtype and do not suffer from seizure-like swim episodes. NCL/*GRN* patients became symptomatic in their twenties (Smith et al., 2012). If Grna;Grnb KOs develop neurodegeneration as aged adults and if this leads occasionally to seizure-like swim episodes remains to be answered. This could be addressed by long-term recording of the swimming behaviour of adult zebrafish. FTLD-TDP/*GRN* patients develop very diverse phenotypes ranging from behavioural abnormalities to comprehension and speech problems (Bonvicini et al., 2014) and also the behavioural analysis of Grn KO mice reveal very diverse results (Kleinberger et al., 2013). Since FTLD-TDP/*GRN* typically has an age at onset above 50, it would be interesting to analyse the Grna;Grnb KO zebrafish for example in a behavioural test that has been established for the aggression-boldness syndrome (Norton et al., 2011). The analysis of the motor performance in Grn-deficient mice revealed a reduced swim speed in some strains (Ghoshal et al., 2012; Wils et al., 2012). Additionally the touch response and avoidance swimming behaviour was reported to be reduced in Grna KD embryos (Chitramuthu et al., 2010). On the contrary, the Grna;Grnb KO zebrafish

larvae did not respond differently in a photomotor response experiment. This demonstrates that cognition of a stimulus, processing of the information, and response to a stimulus are similar in *grna*$^{-/-}$;*grnb*$^{-/-}$ double mutant larvae and wildtype controls and also indicates no motor deficits in the double mutants as suggested by others (Chitramuthu et al., 2010). Therefore, it can be concluded that the Grna;Grnb KO larvae show a normal response to a visual stimulus.

It was demonstrated before that zebrafish larvae can serve as a model for neurodegenerative diseases like NCL (Follo et al., 2011; Mahmood et al., 2013a), however zebrafish larvae that lack Grna and Grnb are clearly devoid of any phenotypic alterations that were described in Grn-deficient mammals before. First analysis in adult *grna*$^{-/-}$;*grnb*$^{-/-}$ brains did not provide any indications for disease-associated phenotypes or biochemical alterations. A more detailed examination of aged Grna;Grnb KO zebrafish will determine if ageing might affect these parameters in mutants. Since for example heterozygous Grn KO mice were devoid of signatures of lysosomal impairment (Filiano et al., 2013; Götzl et al., 2014), it is possible that Grn1 and Grn2 are sufficient to preclude phenotypes and it would be interesting to analyse if Grna;Grnb KO zebrafish that additionally lack Grn1 and Grn2 develop disease-related pathologies described in Grn-deficient men and mice.

6.7 Normal wound healing in Grna and Grnb KO larvae

It was confirmed in this study that especially *grna* expression is increased after an injury. Therefore, I asked whether a lack of Grna and Grnb could have an influence on the inflammatory response or the regeneration in Grna;Grnb KOs revealing a long-awaited phenotype in the mutants. Tail fin amputations, a well accepted model to study the inflammatory response and regeneration in the larval zebrafish (Ellett et al., 2011; Yoshinari and Kawakami, 2011), were performed in *grna*$^{-/-}$;*grnb*$^{-/-}$ double mutant zebrafish larvae. In the experiments it was shown that the regeneration of the tail fin is comparable in Grna;Grnb KO and wildtype larvae. The regeneration time and the morphological shape of the regenerate are not distinguishable. Moreover, the response of cells of the myeloid lineage to a larval tail fin amputation was similar. There was a slight reduction of the time the cell spent in the wound but this was not statistically significant and can be explained by the different cell types, neutrophils and macrophages, that could have been selected for the single cell tracking (Ellett et al., 2011). As *grna* and *grn1/grn2* are enriched in macrophages it would be interesting to examine the response of macrophages to an injury selectively. The transgenic line used in this study,

Tg(*spi1b*:Gal4/UAS:EGFP), labels all cell types of myeloid origin, which are at the developmental stage of analysis mainly macrophages and neutrophils, and it would be worth to repeat the cell tracking in a transgenic line that labels only macrophages for example the Tg(*mpeg1*:mCherry). Due to the findings that macrophages and microglia from Grn KO mice have an enhanced phagocytic activity and show an exaggerated inflammatory response after e.g. a traumatic brain injury (Kao et al., 2011; Martens et al., 2012; Tanaka et al., 2012), the phagocytic activity would be of special interest. Additionally, it is possible that Grn1 and Grn2 compensate for the lack of Grna and Grnb after a tail fin amputation. Unfortunately, the determination of the *grn1/grn2* expression levels is challenging at that specific time of development, since they are close to the detection limit. Already in the expression analysis conducted in tail fin amputated wildtype larvae, a very high variance between the single experiments was observed. Consequently, it would be important to use a robust assay, that would allow to answer the question if Grn1 and Grn2 compensate for the lack of Grna and Grnb after an injury. One possibility is to compare the response to a stab wound injury in adult zebrafish telencephali of wildtype and $grna^{-/-};grnb^{-/-}$ mutant brains. These experiments could be realized in a collaboration with a group at the Helmholtz Center Munich, which has extensive experience, performing this kind of injury experiments in adult zebrafish. In the larval zebrafish, however, there are so far no indications that a loss of Grna and Grnb leads to an increased inflammatory response after a tail fin amputation. In Grn KO mice in contrast an exaggerated inflammatory response after a traumatic brain injury was reported (Tanaka et al., 2012). Cells of the myeloid lineage in Grna;Grnb KO larvae are responsive to inflammatory cues and show no irregular migration path after a tail fin amputation. It is possible, that the injury model chosen herein is affecting the wrong tissue at the wrong developmental stage and that an injury in the (adult) zebrafish brain would give insights into underlying pathomechanisms. One should also keep in mind, that the restoration of a fin is different to the replacement of neurons in the brain and it is quite likely that different signaling pathways and mechanisms are involved in these two processes (Lenkowski and Raymond, 2014). Moreover, zebrafish have a high regenerative capacity (Gemberling et al., 2013) and it should be considered that the pathways that caused an exaggerated inflammatory response in Grn KO mice might not be conserved in zebrafish.

7 Outlook

So far the examinations of Grna;Grnb KO zebrafish embryos and larvae did not reveal any phenotypic alterations. Since NCL/*GRN* and FTLD-TDP/*GRN* patients as well as Grn KO mice become symptomatic and develop phenotypes as adults (Fujioka and Wszolek, 2011; Kleinberger et al., 2013; Smith et al., 2012) it remains to be answered if Grna;Grnb KO zebrafish develop phenotypic alterations upon ageing. The disease onset in FTLD-TDP/*GRN* patients is frequently asymmetric, therefore, it was hypothesized that a second hit, a small traumatic injury or a microhemorrhage, is needed to trigger the disease (Hardy and Rogaeva, 2013). To consider such aspects, one should analyse Grna;Grnb KO zebrafish after a stab wound injury in the adult telencephalon. Preliminary data already indicate a difference between wildtype and Grna;Grnb KOs. It is published that an acute inflammation in the adult zebrafish brain enhances its regenerative capacity after an injury (Kyritsis et al., 2012). Moreover, it was demonstrated that the inflammatory response after a traumatic brain injury is increased in Grn KO mice (Tanaka et al., 2012). I hypothesize that Grna;Grnb KO zebrafish, which provide a unique model to study this issue, respond with increased inflammation to an injury in the adult telencephalon when compared to wildtype, leading to an increase in the regenerative response to the injury, indicated by an elevated number of proliferative cells in the subventricular zone.

Even though *grn1/grn2* expression is not increased in Grna;Grnb KO larvae, it is possible that Grn1 and Grn2 are capable to compensate for the lack of Grna and Grnb, especially after an injury. To test this hypothesis, either a *grn1* and *grn2* KD or KO would be required. A MO KD is easy to perform but would allow only a temporal analysis in larvae. *grn1/grn2* expression becomes first prominent at 3dpf to 4dpf, a time where a MO is already very diluted. Consequently, a KO would be the better choice. For a KO the CRISPR/Cas9 system would be used, which is the method-of-choice for genome editing (Hruscha et al., 2013; Schmid and Haass, 2013). The generation of *grn1* and *grn2* mutants was already initiated and is on the way. A special challenge of this approach is the fact that *grn1* and *grn2* are in tandem on the same chromosome. Therefore, either the whole locus needs to be deleted at once or the mutants need to be generated successively. Once the *granulin* quadruple mutants are available, it would be of great interest to analyse them for phenotypic alterations. These models hold the unique potential to functionally analyse the physiological function of the full-length-like GRN with the Grna;Grnb KOs and the physiological function of the processed granulin peptides with the quadruple mutants.

8 References

Z. Ahmed, I. R. A. Mackenzie, M. L. Hutton, and D. W. Dickson. Progranulin in frontotemporal lobar degeneration and neuroinflammation. *Journal of neuroinflammation*, 4:7, 2007.

Z. Ahmed, H. Sheng, Y.-f. Xu, W.-L. Lin, A. E. Innes, J. Gass, X. Yu, C. A. Wuertzer, H. Hou, S. Chiba, K. Yamanouchi, M. Leissring, L. Petrucelli, M. Nishihara, M. L. Hutton, E. McGowan, D. W. Dickson, and J. Lewis. Accelerated lipofuscinosis and ubiquitination in granulin knockout mice suggest a role for progranulin in successful aging. *American Journal Of Pathology*, 177(1):311–324, July 2010.

G. W. Anderson, H. H. Goebel, and A. Simonati. Human pathology in NCL. *Biochimica et biophysica acta*, 1832(11): 1807–1826, Nov. 2013.

P. E. A. Ash, K. F. Bieniek, T. F. Gendron, T. Caulfield, W.-L. Lin, M. Dejesus-Hernandez, M. M. van Blitterswijk, K. Jansen-West, J. W. Paul, R. Rademakers, K. B. Boylan, D. W. Dickson, and L. Petrucelli. Unconventional translation of C9ORF72 GGGGCC expansion generates insoluble polypeptides specific to c9FTD/ALS. *Neuron*, 77 (4):639–646, Feb. 2013.

B. Ayari, K. H. El Hachimi, C. Yanicostas, A. Landoulsi, and N. Soussi-Yanicostas. Prokineticin 2 expression is associated with neural repair of injured adult zebrafish telencephalon. *Journal of neurotrauma*, 27(5):959–972, May 2010.

T. Baba, H. Nemoto, K. Watanabe, Y. Arai, and G. L. Gerton. Exon/intron organization of the gene encoding the mouse epithelin/granulin precursor (acrogranin). *FEBS letters*, 322(2):89–94, May 1993.

C. A. Baker and L. Manuelidis. Unique inflammatory RNA profiles of microglia in Creutzfeldt-Jakob disease. *Proceedings of the National Academy of Sciences of the United States of America*, 100(2):675–679, Jan. 2003.

M. Baker, I. R. Mackenzie, S. M. Pickering-Brown, J. Gass, R. Rademakers, C. Lindholm, J. Snowden, J. Adamson, A. D. Sadovnick, S. Rollinson, A. Cannon, E. Dwosh, D. Neary, S. Melquist, A. Richardson, D. Dickson, Z. Berger, J. Eriksen, T. Robinson, C. Zehr, C. A. Dickey, R. Crook, E. McGowan, D. Mann, B. Boeve, H. Feldman, and M. Hutton. Mutations in progranulin cause tau-negative frontotemporal dementia linked to chromosome 17. *Nature*, 442(7105):916–919, Aug. 2006.

S. C. Baraban, M. R. Taylor, P. A. Castro, and H. Baier. Pentylenetetrazole induced changes in zebrafish behavior, neural activity and c-fos expression. *Neuroscience*, 131(3):759–768, 2005.

D. C. Baranowski. *Investigation of the function and protein-protein interaction of zberafish progranulin-A during development*. PhD thesis, Montreal, Jan. 2008.

D. R. Barreda, P. C. Hanington, C. K. Walsh, P. Wong, and M. Belosevic. Differentially expressed genes that encode potential markers of goldfish macrophage development in vitro. *Developmental and comparative immunology*, 28 (7-8):727–746, June 2004.

A. Bateman and H. P. J. Bennett. The granulin gene family: from cancer to dementia. *BioEssays : news and reviews in molecular, cellular and developmental biology*, 31(11):1245–1254, Nov. 2009.

A. Bateman, D. Belcourt, H. Bennett, C. Lazure, and S. Solomon. Granulins, a novel class of peptide from leukocytes. *Biochemical and biophysical research communications*, 173(3):1161–1168, Dec. 1990.

E. V. Baumgart, J. S. Barbosa, L. Bally-Cuif, M. Götz, and J. Ninkovic. Stab wound injury of the zebrafish telencephalon: a model for comparative analysis of reactive gliosis. *Glia*, 60(3):343–357, Mar. 2012.

V. M. Bedell, Y. Wang, J. M. Campbell, T. L. Poshusta, C. G. Starker, R. G. Krug, W. Tan, S. G. Penheiter, A. C. Ma, A. Y. H. Leung, S. C. Fahrenkrug, D. F. Carlson, D. F. Voytas, K. J. Clark, J. J. Essner, and S. C. Ekker. In vivo genome editing using a high-efficiency TALEN system. *Nature*, 491(7422):114–118, Nov. 2012.

V. Belcastro, V. Siciliano, F. Gregoretti, P. Mithbaokar, G. Dharmalingam, S. Berlingieri, F. Iorio, G. Oliva, R. Polishchuck, N. Brunetti-Pierri, and D. di Bernardo. Transcriptional gene network inference from a massive dataset elucidates transcriptome organization and gene function. *Nucleic acids research*, 39(20):8677–8688, Nov. 2011.

D. R. Belcourt, C. Lazure, and H. P. Bennett. Isolation and primary structure of the three major forms of granulin-like peptides from hematopoietic tissues of a teleost fish (Cyprinus carpio). *The Journal of biological chemistry*, 268(13): 9230–9237, May 1993.

D. R. Belcourt, Y. Okawara, J. N. Fryer, and H. P. Bennett. Immunocytochemical localization of granulin-1 to mononuclear phagocytic cells of the teleost fish Cyprinus carpio and Carassius auratus. *Journal of leukocyte biology*, 57(1): 94–100, Jan. 1995.

P. Benes, V. Vetvicka, and M. Fusek. Cathepsin D–many functions of one aspartic protease. *Critical reviews in oncology/hematology*, 68(1):12–28, Oct. 2008.

C. M. Bennett, J. P. Kanki, J. Rhodes, T. X. Liu, B. H. Paw, M. W. Kieran, D. M. Langenau, A. Delahaye-Brown, L. I. Zon, M. D. Fleming, and A. T. Look. Myelopoiesis in the zebrafish, Danio rerio. *Blood*, 98(3):643–651, Aug. 2001.

D. Bhaya, M. Davison, and R. Barrangou. CRISPR-Cas systems in bacteria and archaea: versatile small RNAs for adaptive defense and regulation. *Annual review of genetics*, 45:273–297, 2011.

B. R. Bill, A. M. Petzold, K. J. Clark, L. A. Schimmenti, and S. C. Ekker. A primer for morpholino use in zebrafish. *Zebrafish*, 6(1):69–77, Mar. 2009.

J. Boch, H. Scholze, S. Schornack, A. Landgraf, S. Hahn, S. Kay, T. Lahaye, A. Nickstadt, and U. Bonas. Breaking the code of DNA binding specificity of TAL-type III effectors. *Science (New York, NY)*, 326(5959):1509–1512, Dec. 2009.

C. Bonvicini, E. Milanesi, A. Pilotto, N. Cattane, E. Premi, S. Archetti, A. Padovani, M. Gennarelli, and B. Borroni. Understanding phenotype variability in frontotemporal lobar degeneration due to granulin mutation. *Neurobiology of aging*, 35(5):1206–1211, May 2014.

B. Borroni, F. Ferrari, D. Galimberti, B. Nacmias, C. Barone, S. Bagnoli, C. Fenoglio, I. Piaceri, S. Archetti, C. Bonvicini, M. Gennarelli, M. Turla, E. Scarpini, S. Sorbi, and A. Padovani. Heterozygous TREM2 mutations in frontotemporal dementia. *Neurobiology of aging*, 35(4):934.e7–934.e10, Apr. 2014.

L. B. Borst, S. K. Patterson, S. Lanka, M. M. Suyemoto, and C. W. Maddox. Zebrafish (Danio rerio) as a screen for attenuation of Lancefield group C streptococci and a model for streptococcal pathogenesis. *Veterinary pathology*, 50 (3):457–467, May 2013.

P. Bossù, F. Salani, A. Alberici, S. Archetti, G. Bellelli, D. Galimberti, E. Scarpini, G. Spalletta, C. Caltagirone, A. Padovani, and B. Borroni. Loss of function mutations in the progranulin gene are related to pro-inflammatory cytokine dysregulation in frontotemporal lobar degeneration patients. *Journal of neuroinflammation*, 8(1):65, June 2011.

N. Brouwers, K. Sleegers, S. Engelborghs, S. Maurer-Stroh, I. Gijselinck, J. van der Zee, B. A. Pickut, M. Van den Broeck, M. Mattheijssens, K. Peeters, J. Schymkowitz, F. Rousseau, J.-J. Martin, M. Cruts, P. P. De Deyn, and C. Van Broeckhoven. Genetic variability in progranulin contributes to risk for clinically diagnosed Alzheimer disease. *Neurology*, 71(9):656–664, Aug. 2008.

M. Bucan, B. Gatalica, T. Baba, and G. L. Gerton. Mapping of Grn, the gene encoding the granulin/epithelin precursor (acrogranin), to mouse chromosome 11. *Mammalian genome : official journal of the International Mammalian Genome Society*, 7(9):704–705, Sept. 1996.

H. A. Burgess and M. Granato. Modulation of locomotor activity in larval zebrafish during light adaptation. *The Journal of experimental biology*, 210(Pt 14):2526–2539, July 2007.

B. Cadieux, B. P. Chitramuthu, D. Baranowski, and H. P. J. Bennett. The zebrafish progranulin gene family and antisense transcripts. *BMC genomics*, 6:156, 2005.

A. Capell, S. Liebscher, K. Fellerer, N. Brouwers, M. Willem, S. Lammich, I. Gijselinck, T. Bittner, A. M. Carlson, F. Sasse, B. Kunze, H. Steinmetz, R. Jansen, D. Dormann, K. Sleegers, M. Cruts, J. Herms, C. Van Broeckhoven, and C. Haass. Rescue of Progranulin Deficiency Associated with Frontotemporal Lobar Degeneration by Alkalizing Reagents and Inhibition of Vacuolar ATPase. *Journal of Neuroscience*, 31(5):1885–1894, Feb. 2011.

A. M. Carlson, M. J. Maurer, K. M. Goergen, K. R. Kalli, C. L. Erskine, M. D. Behrens, K. L. Knutson, and M. S. Block. Utility of progranulin and serum leukocyte protease inhibitor as diagnostic and prognostic biomarkers in ovarian cancer. *Cancer epidemiology, biomarkers & prevention : a publication of the American Association for Cancer Research, cosponsored by the American Society of Preventive Oncology*, July 2013.

T. Cathomen and J. K. Joung. Zinc-finger nucleases: the next generation emerges. *Molecular therapy : the journal of the American Society of Gene Therapy*, 16(7):1200–1207, July 2008.

B. Cenik, C. F. Sephton, B. K. Cenik, J. Herz, and G. Yu. Progranulin: a proteolytically processed protein at the crossroads of inflammation and neurodegeneration. *Journal of Biological Chemistry*, Aug. 2012.

N. Chang, C. Sun, L. Gao, D. Zhu, X. Xu, X. Zhu, J.-W. Xiong, and J. J. Xi. Genome editing with RNA-guided Cas9 nuclease in zebrafish embryos. *Cell research*, 23(4):465–472, Apr. 2013.

D. Chantry, A. J. DeMaggio, H. Brammer, C. J. Raport, C. L. Wood, V. L. Schweickart, A. Epp, A. Smith, J. T. Stine, K. Walton, L. Tjoelker, R. Godiska, and P. W. Gray. Profile of human macrophage transcripts: insights into macrophage biology and identification of novel chemokines. *Journal of leukocyte biology*, 64(1):49–54, July 1998.

S. Chen, G. Oikonomou, C. N. Chiu, B. J. Niles, J. Liu, D. A. Lee, I. Antoshechkin, and D. A. Prober. A large-scale in vivo analysis reveals that TALENs are significantly more mutagenic than ZFNs generated using context-dependent assembly. *Nucleic acids research*, 41(4):2769–2778, Feb. 2013a.

X. Chen and F. Engert. Navigational strategies underlying phototaxis in larval zebrafish. *Frontiers in systems neuroscience*, 8:39, 2014.

X. Chen, J. Chang, Q. Deng, J. Xu, T. A. Nguyen, L. H. Martens, B. Cenik, G. Taylor, K. F. Hudson, J. Chung, K. Yu, P. Yu, J. Herz, R. V. Farese, T. Kukar, and M. G. Tansey. Progranulin Does Not Bind Tumor Necrosis Factor (TNF) Receptors and Is Not a Direct Regulator of TNF-Dependent Signaling or Bioactivity in Immune or Neuronal Cells. *Journal of Neuroscience*, 33(21):9202–9213, May 2013b.

A. S. Chen-Plotkin, J. Xiao, F. Geser, M. Martinez-Lage, M. Grossman, T. Unger, E. M. Wood, V. M. Van Deerlin, J. Q. Trojanowski, and V. M.-Y. Lee. Brain progranulin expression in GRN-associated frontotemporal lobar degeneration. *Acta Neuropathologica*, 119(1):111–122, Jan. 2010.

A. S. Chen-Plotkin, T. L. Unger, M. D. Gallagher, E. Bill, L. K. Kwong, L. Volpicelli-Daley, J. I. Busch, S. Akle, M. Grossman, V. Van Deerlin, J. Q. Trojanowski, and V. M.-Y. Lee. TMEM106B, the risk gene for frontotemporal dementia, is regulated by the microRNA-132/212 cluster and affects progranulin pathways. *Journal of Neuroscience*, 32(33):11213–11227, Aug. 2012.

N. C. Chi, R. M. Shaw, S. De Val, G. Kang, L. Y. Jan, B. L. Black, and D. Y. R. Stainier. Foxn4 directly regulates tbx2b expression and atrioventricular canal formation. *Genes & development*, 22(6):734–739, Mar. 2008.

B. P. Chitramuthu, D. C. Baranowski, D. G. Kay, A. Bateman, and H. P. Bennett. Progranulin modulates zebrafish motoneuron development in vivo and rescues truncation defects associated with knockdown of Survival motor neuron 1. *Molecular neurodegeneration*, 5:41, 2010.

S. W. Cho, S. Kim, J. M. Kim, and J.-S. Kim. Targeted genome engineering in human cells with the Cas9 RNA-guided endonuclease. *Nature biotechnology*, 31(3):230–232, Mar. 2013.

S. W. Cho, S. Kim, Y. Kim, J. Kweon, H. S. Kim, S. Bae, and J.-S. Kim. Analysis of off-target effects of CRISPR/Cas-derived RNA-guided endonucleases and nickases. *Genome research*, 24(1):132–141, Jan. 2014.

M. Christian, T. Cermak, E. L. Doyle, C. Schmidt, F. Zhang, A. Hummel, A. J. Bogdanove, and D. F. Voytas. Targeting DNA double-strand breaks with TAL effector nucleases. *Genetics*, 186(2):757–761, Oct. 2010.

S. Ciura, S. Lattante, I. Le Ber, M. Latouche, H. Tostivint, A. Brice, and E. Kabashi. Loss of function of C9orf72 causes motor deficits in a zebrafish model of Amyotrophic Lateral Sclerosis. *Annals of Neurology*, May 2013.

L. Cong, F. A. Ran, D. Cox, S. Lin, R. Barretto, N. Habib, P. D. Hsu, X. Wu, W. Jiang, L. A. Marraffini, and F. Zhang. Multiplex genome engineering using CRISPR/Cas systems. *Science (New York, NY)*, 339(6121):819–823, Feb. 2013.

S. E. L. Craig, A.-A. Calinescu, and P. F. Hitchcock. Identification of the molecular signatures integral to regenerating photoreceptors in the retina of the zebra fish. *Journal of ocular biology, diseases, and informatics*, 1(2-4):73–84, Dec. 2008.

M. Cruts, I. Gijselinck, J. van der Zee, S. Engelborghs, H. Wils, D. Pirici, R. Rademakers, R. Vandenberghe, B. Dermaut, J.-J. Martin, C. van Duijn, K. Peeters, R. Sciot, P. Santens, T. De Pooter, M. Mattheijssens, M. Van den Broeck, I. Cuijt, K. Vennekens, P. P. De Deyn, S. Kumar-Singh, and C. Van Broeckhoven. Null mutations in progranulin cause ubiquitin-positive frontotemporal dementia linked to chromosome 17q21. *Nature*, 442(7105):920–924, Aug. 2006.

M. Cruts, J. Theuns, and C. Van Broeckhoven. Locus-specific mutation databases for neurodegenerative brain diseases. *Human mutation*, 33(9):1340–1344, Sept. 2012.

A. Cvejic, C. Hall, M. Bak-Maier, M. V. Flores, P. Crosier, M. J. Redd, and P. Martin. Analysis of WASp function during the wound inflammatory response–live-imaging studies in zebrafish larvae. *Journal of Cell Science*, 121(Pt 19):3196–3206, Oct. 2008.

C. A. d'Alençon, O. A. Peña, C. Wittmann, V. E. Gallardo, R. A. Jones, F. Loosli, U. Liebel, C. Grabher, and M. L. Allende. A high-throughput chemically induced inflammation assay in zebrafish. *BMC Biology*, 8(1):151, 2010.

R. Daniel, Z. He, K. P. Carmichael, J. Halper, and A. Bateman. Cellular localization of gene expression for progranulin. *The journal of histochemistry and cytochemistry : official journal of the Histochemistry Society*, 48(7):999–1009, July 2000.

R. Daniel, E. Daniels, Z. He, and A. Bateman. Progranulin (acrogranin/PC cell-derived growth factor/granulin-epithelin precursor) is expressed in the placenta, epidermis, microvasculature, and brain during murine development. *Developmental dynamics : an official publication of the American Association of Anatomists*, 227(4):593–599, Aug. 2003.

C. de Esch, H. van der Linde, R. Slieker, R. Willemsen, A. Wolterbeek, R. Woutersen, and D. De Groot. Locomotor activity assay in zebrafish larvae: influence of age, strain and ethanol. *Neurotoxicology and teratology*, 34(4):425–433, July 2012.

L. De Muynck and P. Van Damme. Cellular Effects of Progranulin in Health and Disease. *Journal of molecular neuroscience : MN*, May 2011.

L. De Muynck, S. Herdewyn, S. Beel, W. Scheveneels, L. Van Den Bosch, W. Robberecht, and P. Van Damme. The neurotrophic properties of progranulin depend on the granulin E domain but do not require sortilin binding. *Neurobiology of aging*, May 2013.

M. Dejesus-Hernandez, I. R. Mackenzie, B. F. Boeve, A. L. Boxer, M. Baker, N. J. Rutherford, A. M. Nicholson, N. A. Finch, H. Flynn, J. Adamson, N. Kouri, A. Wojtas, P. Sengdy, G.-Y. R. Hsiung, A. Karydas, W. W. Seeley, K. A. Josephs, G. Coppola, D. H. Geschwind, Z. K. Wszolek, H. Feldman, D. S. Knopman, R. C. Petersen, B. L. Miller, D. W. Dickson, K. B. Boylan, N. R. Graff-Radford, and R. Rademakers. Expanded GGGGCC hexanucleotide repeat in noncoding region of C9ORF72 causes chromosome 9p-linked FTD and ALS. *Neuron*, 72(2):245–256, Oct. 2011.

R. Del Bo, S. Corti, D. Santoro, I. Ghione, C. Fenoglio, S. Ghezzi, M. Ranieri, D. Galimberti, M. Mancuso, G. Siciliano, C. Briani, L. Murri, E. Scarpini, J. C. Schymick, B. J. Traynor, N. Bresolin, and G. P. Comi. No major progranulin genetic variability contribution to disease etiopathogenesis in an ALS Italian cohort. *Neurobiology of aging*, 32(6): 1157–1158, June 2011.

S. DeMorrow. Progranulin: a novel regulator of gastrointestinal cancer progression. *Translational gastrointestinal cancer*, 2(3):145–151, July 2013.

M. J. den Broeder, H. van der Linde, J. R. Brouwer, B. A. Oostra, R. Willemsen, and R. F. Ketting. Generation and characterization of FMR1 knockout zebrafish. *PloS one*, 4(11):e7910, 2009.

H.-X. Deng, W. Chen, S.-T. Hong, K. M. Boycott, G. H. Gorrie, N. Siddique, Y. Yang, F. Fecto, Y. Shi, H. Zhai, H. Jiang, M. Hirano, E. Rampersaud, G. H. Jansen, S. Donkervoort, E. H. Bigio, B. R. Brooks, K. Ajroud, R. L. Sufit, J. L. Haines, E. Mugnaini, M. A. Pericak-Vance, and T. Siddique. Mutations in UBQLN2 cause dominant X-linked juvenile and adult-onset ALS and ALS/dementia. *Nature*, 477(7363):211–215, Sept. 2011.

Q. Deng and A. Huttenlocher. Leukocyte migration from a fish eye's view. *Journal of Cell Science*, 125(Pt 17): 3949–3956, Sept. 2012.

E. Donà, J. D. Barry, G. Valentin, C. Quirin, A. Khmelinskii, A. Kunze, S. Durdu, L. R. Newton, A. Fernandez-Minan, W. Huber, M. Knop, and D. Gilmour. Directional tissue migration through a self-generated chemokine gradient. *Nature*, 503(7475):285–289, Nov. 2013.

D. Dormann and C. Haass. TDP-43 and FUS: a nuclear affair. *Trends in neurosciences*, 34(7):339–348, July 2011.

Y. Doyon, J. M. McCammon, J. C. Miller, F. Faraji, C. Ngo, G. E. Katibah, R. Amora, T. D. Hocking, L. Zhang, E. J. Rebar, P. D. Gregory, F. D. Urnov, and S. L. Amacher. Heritable targeted gene disruption in zebrafish using designed zinc-finger nucleases. *Nature biotechnology*, 26(6):702–708, June 2008.

C. M. Drerup and A. V. Nechiporuk. JNK-interacting protein 3 mediates the retrograde transport of activated c-Jun N-terminal kinase and lysosomes. *PLoS genetics*, 9(2):e1003303, 2013.

Y. Egashira, Y. Suzuki, Y. Azuma, T. Takagi, K. Mishiro, S. Sugitani, K. Tsuruma, M. Shimazawa, S. Yoshimura, M. Kashimata, T. Iwama, and H. Hara. The growth factor progranulin attenuates neuronal injury induced by cerebral ischemia-reperfusion through the suppression of neutrophil recruitment. *Journal of neuroinflammation*, 10 (1):105, 2013.

J. S. Eisen and J. C. Smith. Controlling morpholino experiments: don't stop making antisense. *Development (Cambridge, England)*, 135(10):1735–1743, May 2008.

E. Eivers, K. McCarthy, C. Glynn, C. M. Nolan, and L. Byrnes. Insulin-like growth factor (IGF) signalling is required for early dorso-anterior development of the zebrafish embryo. *The International journal of developmental biology*, 48(10):1131–1140, Dec. 2004.

F. Ellett and G. J. Lieschke. Zebrafish as a model for vertebrate hematopoiesis. *Current opinion in pharmacology*, 10 (5):563–570, Oct. 2010.

F. Ellett, L. Pase, J. W. Hayman, A. Andrianopoulos, and G. J. Lieschke. mpeg1 promoter transgenes direct macrophage-lineage expression in zebrafish. *Blood*, 117(4):e49–56, Jan. 2011.

J. L. Eriksen and I. R. A. Mackenzie. Progranulin: normal function and role in neurodegeneration. *Journal of neurochemistry*, 104(2):287–297, Jan. 2008.

R. Esterberg, A. B. Coffin, H. Ou, J. A. Simon, D. W. Raible, and E. W. Rubel. Fish in a Dish: Drug Discovery for Hearing Habilitation. *Drug discovery today. Disease models*, 10(1), 2013.

N. Etemadi, A. Webb, A. Bankovacki, J. Silke, and U. Nachbur. Progranulin does not inhibit TNF and lymphotoxin-α signalling through TNF receptor 1. *Immunology and cell biology*, 91(10):661–664, Nov. 2013.

U. B. Eyo and M. E. Dailey. Microglia: key elements in neural development, plasticity, and pathology. *Journal of neuroimmune pharmacology : the official journal of the Society on NeuroImmune Pharmacology*, 8(3):494–509, June 2013.

X. Feng, E. G. Adiarte, and S. H. Devoto. Hedgehog acts directly on the zebrafish dermomyotome to promote myogenic differentiation. *Developmental Biology*, 300(2):736–746, Dec. 2006.

Y. Feng, C. Santoriello, M. Mione, A. Hurlstone, and P. Martin. Live imaging of innate immune cell sensing of transformed cells in zebrafish larvae: parallels between tumor initiation and wound inflammation. *PLoS biology*, 8 (12):e1000562, 2010.

A. J. Filiano, L. H. Martens, A. H. Young, B. A. Warmus, P. Zhou, G. Diaz-Ramirez, J. Jiao, Z. Zhang, E. J. Huang, F.-B. Gao, R. V. Farese, and E. D. Roberson. Dissociation of frontotemporal dementia-related deficits and neuroinflammation in progranulin haploinsufficient mice. *Journal of Neuroscience*, 33(12):5352–5361, Mar. 2013.

C. Follo, M. Ozzano, V. Mugoni, R. Castino, M. Santoro, and C. Isidoro. Knock-down of cathepsin D affects the retinal pigment epithelium, impairs swim-bladder ontogenesis and causes premature death in zebrafish. *PloS one*, 6(7): e21908, 2011.

C. Follo, M. Ozzano, C. Montalenti, M. Ekkapongpisit, and C. Isidoro. Similarities and differences in the biogenesis, processing and lysosomal targeting between zebrafish and human pro-Cathepsin D: functional implications. *The international journal of biochemistry & cell biology*, 45(2):273–282, Feb. 2013.

G. Frampton, P. Invernizzi, F. Bernuzzi, H. Y. Pae, M. Quinn, D. Horvat, C. Galindo, L. Huang, M. McMillin, B. Cooper, L. Rimassa, and S. DeMorrow. Interleukin-6-driven progranulin expression increases cholangiocarcinoma growth by an Akt-dependent mechanism. *Gut*, 61(2):268–277, Feb. 2012.

W. Fujii, K. Kawasaki, K. Sugiura, and K. Naito. Efficient generation of large-scale genome-modified mice using gRNA and CAS9 endonuclease. *Nucleic acids research*, 41(20):e187, Nov. 2013.

S. Fujioka and Z. K. Wszolek. Clinical aspects of familial forms of frontotemporal dementia associated with parkinsonism. *Journal of molecular neuroscience : MN*, 45(3):359–365, Nov. 2011.

T. Gaj, C. A. Gersbach, and C. F. Barbas. ZFN, TALEN, and CRISPR/Cas-based methods for genome engineering. *Trends in biotechnology*, 31(7):397–405, July 2013.

X. Gao, A. P. Joselin, L. Wang, A. Kar, P. Ray, A. Bateman, A. M. Goate, and J. Y. Wu. Progranulin promotes neurite outgrowth and neuronal differentiation by regulating GSK-3β. *Protein & cell*, 1(6):552–562, June 2010.

N. L. Garneau, J. Wilusz, and C. J. Wilusz. The highways and byways of mRNA decay. *Nature Reviews Molecular Cell Biology*, 8(2):113–126, Feb. 2007.

J. Gass, W. C. Lee, C. Cook, N. Finch, C. Stetler, K. Jansen-West, J. Lewis, C. D. Link, R. Rademakers, A. Nykjaer, and L. Petrucelli. Progranulin regulates neuronal outgrowth independent of Sortilin. *Molecular neurodegeneration*, 7(1):33, July 2012.

M. Gemberling, T. J. Bailey, D. R. Hyde, and K. D. Poss. The zebrafish as a model for complex tissue regeneration. *Trends in genetics : TIG*, 29(11):611–620, Nov. 2013.

G. F. Gerlach, L. N. Schrader, and R. A. Wingert. Dissection of the adult zebrafish kidney. *Journal of visualized experiments : JoVE*, (54), 2011.

N. Ghoshal, J. T. Dearborn, D. F. Wozniak, and N. J. Cairns. Core features of frontotemporal dementia recapitulated in progranulin knockout mice. *Neurobiology of disease*, 45(1):395–408, Jan. 2012.

J. K. Götzl, K. Mori, M. Damme, K. Fellerer, S. Tahirovic, G. Kleinberger, J. Janssens, J. van der Zee, C. M. Lang, E. Kremmer, J.-J. Martin, S. Engelborghs, H. A. Kretzschmar, T. Arzberger, C. Van Broeckhoven, C. Haass, and A. Capell. Common pathobiochemical hallmarks of progranulin-associated frontotemporal lobar degeneration and neuronal ceroid lipofuscinosis. *Acta Neuropathologica*, Mar. 2014.

R. Guerreiro, B. Bilgic, G. Guven, J. Bras, J. Rohrer, E. Lohmann, H. Hanagasi, H. Gurvit, and M. Emre. A novel compound heterozygous mutation in TREM2 found in a Turkish frontotemporal dementia-like family. *Neurobiology of aging*, 34(12):2890.e1–5, Dec. 2013.

Z. Guo, Q. Li, Y. Han, Y. Liang, Z. Xu, and T. Ren. Prevention of LPS-induced acute lung injury in mice by progranulin. *Mediators of inflammation*, 2012:540794, 2012.

A. Gupta, X. Meng, L. J. Zhu, N. D. Lawson, and S. A. Wolfe. Zinc finger protein-dependent and -independent contributions to the in vivo off-target activity of zinc finger nucleases. *Nucleic acids research*, 39(1):381–392, Jan. 2011.

T. Gupta and M. C. Mullins. Dissection of organs from the adult zebrafish. *Journal of visualized experiments : JoVE*, (37), 2010.

A. Gutierrez, L. Pan, R. W. J. Groen, F. Baleydier, A. Kentsis, J. Marineau, R. Grebliunaite, E. Kozakewich, C. Reed, F. Pflumio, S. Poglio, B. Uzan, P. Clemons, L. VerPlank, F. An, J. Burbank, S. Norton, N. Tolliday, H. Steen, A. P. Weng, H. Yuan, J. E. Bradner, C. Mitsiades, A. T. Look, and J. C. Aster. Phenothiazines induce PP2A-mediated apoptosis in T cell acute lymphoblastic leukemia. *The Journal of clinical investigation*, 124(2):644–655, Feb. 2014.

M. Hafez and G. Hausner. Homing endonucleases: DNA scissors on a mission. *Genome / National Research Council Canada = Génome / Conseil national de recherches Canada*, 55(8):553–569, Aug. 2012.

C. Hall, M. V. Flores, T. Storm, K. Crosier, and P. Crosier. The zebrafish lysozyme C promoter drives myeloid-specific expression in transgenic fish. *BMC developmental biology*, 7:42, 2007.

N. A. Hall, B. D. Lake, D. N. Palmer, R. D. Jolly, and A. D. Patrick. Glycoconjugates in storage cytosomes from ceroid-lipofuscinosis (Batten's disease) and in lipofuscin from old-age brain. *Advances in experimental medicine and biology*, 266:225–41– discussion 242, 1989.

C. L. Hammond, Y. Hinits, D. P. S. Osborn, J. E. N. Minchin, G. Tettamanti, and S. M. Hughes. Signals and myogenic regulatory factors restrict pax3 and pax7 expression to dermomyotome-like tissue in zebrafish. *Developmental Biology*, 302(2):504–521, Feb. 2007.

J. J. Han, M. Yu, N. Houston, S. M. Steinberg, and E. C. Kohn. Progranulin is a potential prognostic biomarker in advanced epithelial ovarian cancers. *Gynecologic oncology*, 120(1):5–10, Jan. 2011.

D. Hanahan. Studies on transformation of Escherichia coli with plasmids. *Journal of molecular biology*, 166(4):557–580, June 1983.

P. C. Hanington, D. R. Barreda, and M. Belosevic. A novel hematopoietic granulin induces proliferation of goldfish (Carassius auratus L.) macrophages. *The Journal of biological chemistry*, 281(15):9963–9970, Apr. 2006.

J. Hardy and E. Rogaeva. Motor neuron disease and frontotemporal dementia: sometimes related, sometimes not. *Experimental neurology*, Nov. 2013.

S. Hashimoto, T. Suzuki, H. Y. Dong, S. Nagai, N. Yamazaki, and K. Matsushima. Serial analysis of gene expression in human monocyte-derived dendritic cells. *Blood*, 94(3):845–852, Aug. 1999.

S.-i. Hashimoto, S. Nagai, J. Sese, T. Suzuki, A. Obata, T. Sato, N. Toyoda, H.-Y. Dong, M. Kurachi, T. Nagahata, K.-i. Shizuno, S. Morishita, and K. Matsushima. Gene expression profile in human leukocytes. *Blood*, 101(9):3509–3513, May 2003.

C. He and D. J. Klionsky. Analyzing autophagy in zebrafish. *Autophagy*, 6(5):642–644, July 2010.

C. He, C. R. Bartholomew, W. Zhou, and D. J. Klionsky. Assaying autophagic activity in transgenic GFP-Lc3 and GFP-Gabarap zebrafish embryos. *Autophagy*, 5(4):520–526, May 2009.

Z. He and A. Bateman. Progranulin (granulin-epithelin precursor, PC-cell-derived growth factor, acrogranin) mediates tissue repair and tumorigenesis. *Journal of molecular medicine (Berlin, Germany)*, 81(10):600–612, Oct. 2003.

Z. He, A. Ismail, L. Kriazhev, G. Sadvakassova, and A. Bateman. Progranulin (PC-cell-derived growth factor/acrogranin) regulates invasion and cell survival. *Cancer research*, 62(19):5590–5596, Oct. 2002.

Z. He, C. H. P. Ong, J. Halper, and A. Bateman. Progranulin is a mediator of the wound response. *Nature Medicine*, 9(2):225–229, Feb. 2003.

P. Herbomel, B. Thisse, and C. Thisse. Zebrafish early macrophages colonize cephalic mesenchyme and developing brain, retina, and epidermis through a M-CSF receptor-dependent invasive process. *Developmental Biology*, 238(2): 274–288, Oct. 2001.

J. C. Ho, Y. C. Ip, S. T. Cheung, Y. T. Lee, K. F. Chan, S. Y. Wong, and S. T. Fan. Granulin-epithelin precursor as a therapeutic target for hepatocellular carcinoma. *Hepatology (Baltimore, Md.)*, 47(5):1524–1532, May 2008.

J. R. Hodges, R. Davies, J. Xuereb, J. Kril, and G. Halliday. Survival in frontotemporal dementia. *Neurology*, 61(3): 349–354, Aug. 2003.

I. E. Holm, E. Englund, I. R. A. Mackenzie, P. Johannsen, and A. M. Isaacs. A reassessment of the neuropathology of frontotemporal dementia linked to chromosome 3. *Journal of neuropathology and experimental neurology*, 66(10): 884–891, Oct. 2007.

K. Howe, M. D. Clark, C. F. Torroja, J. Torrance, C. Berthelot, M. Muffato, J. E. Collins, S. Humphray, K. McLaren, L. Matthews, S. McLaren, I. Sealy, M. Caccamo, C. Churcher, C. Scott, J. C. Barrett, R. Koch, G.-J. Rauch, S. White, W. Chow, B. Kilian, L. T. Quintais, J. A. Guerra-Assunção, Y. Zhou, Y. Gu, J. Yen, J.-H. Vogel, T. Eyre, S. Redmond, R. Banerjee, J. Chi, B. Fu, E. Langley, S. F. Maguire, G. K. Laird, D. Lloyd, E. Kenyon, S. Donaldson, H. Sehra, J. Almeida-King, J. Loveland, S. Trevanion, M. Jones, M. Quail, D. Willey, A. Hunt, J. Burton, S. Sims, K. McLay, B. Plumb, J. Davis, C. Clee, K. Oliver, R. Clark, C. Riddle, D. Eliott, G. Threadgold, G. Harden, D. Ware, B. Mortimer, G. Kerry, P. Heath, B. Phillimore, A. Tracey, N. Corby, M. Dunn, C. Johnson, J. Wood, S. Clark, S. Pelan, G. Griffiths, M. Smith, R. Glithero, P. Howden, N. Barker, C. Stevens, J. Harley, K. Holt, G. Panagiotidis, J. Lovell, H. Beasley, C. Henderson, D. Gordon, K. Auger, D. Wright, J. Collins, C. Raisen, L. Dyer, K. Leung, L. Robertson, K. Ambridge, D. Leongamornlert, S. McGuire, R. Gilderthorp, C. Griffiths, D. Manthravadi, S. Nichol, G. Barker, S. Whitehead, M. Kay, J. Brown, C. Murnane, E. Gray, M. Humphries, N. Sycamore, D. Barker, D. Saunders, J. Wallis, A. Babbage, S. Hammond, M. Mashreghi-Mohammadi, L. Barr, S. Martin, P. Wray, A. Ellington, N. Matthews, M. Ellwood, R. Woodmansey, G. Clark, J. Cooper, A. Tromans, D. Grafham, C. Skuce, R. Pandian, R. Andrews, E. Harrison, A. Kimberley, J. Garnett, N. Fosker, R. Hall, P. Garner, D. Kelly, C. Bird, S. Palmer, I. Gehring, A. Berger, C. M. Dooley, Z. Ersan-Ürün, C. Eser, H. Geiger, M. Geisler, L. Karotki, A. Kirn, J. Konantz, M. Konantz, M. Oberländer, S. Rudolph-Geiger, M. Teucke, K. Osoegawa, B. Zhu, A. Rapp, S. Widaa, C. Langford, F. Yang, N. P. Carter, J. Harrow, Z. Ning, J. Herrero, S. M. J. Searle, A. Enright, R. Geisler, R. H. A. Plasterk, C. Lee, M. Westerfield, P. J. de Jong, L. I. Zon, J. H. Postlethwait, C. Nüsslein-Volhard, T. J. P. Hubbard, H. Roest Crollius, J. Rogers, and D. L. Stemple. The zebrafish reference genome sequence and its relationship to the human genome. *Nature*, 496(7446):498–503, Apr. 2013.

A. Hruscha, P. Krawitz, A. Rechenberg, V. Heinrich, J. Hecht, C. Haass, and B. Schmid. Efficient CRISPR/Cas9 genome editing with low off-target effects in zebrafish. *Development (Cambridge, England)*, 140(24):4982–4987, Dec. 2013.

F. Hu, T. Padukkavidana, C. B. Vægter, O. A. Brady, Y. Zheng, I. R. Mackenzie, H. H. Feldman, A. Nykjaer, and S. M. Strittmatter. Sortilin-mediated endocytosis determines levels of the frontotemporal dementia protein, progranulin. *Neuron*, 68(4):654–667, Nov. 2010.

P. Huang, A. Xiao, M. Zhou, Z. Zhu, S. Lin, and B. Zhang. Heritable gene targeting in zebrafish using customized TALENs. *Nature biotechnology*, 29(8):699–700, Aug. 2011.

T. Huang, J. Cui, L. Li, P. F. Hitchcock, and Y. Li. The role of microglia in the neurogenesis of zebrafish retina. *Biochemical and biophysical research communications*, 421(2):214–220, May 2012.

W. Y. Hwang, Y. Fu, D. Reyon, M. L. Maeder, P. Kaini, J. D. Sander, J. K. Joung, R. T. Peterson, and J.-R. J. Yeh. Heritable and Precise Zebrafish Genome Editing Using a CRISPR-Cas System. *PloS one*, 8(7):e68708, 2013a.

W. Y. Hwang, Y. Fu, D. Reyon, M. L. Maeder, S. Q. Tsai, J. D. Sander, R. T. Peterson, J.-R. J. Yeh, and J. K. Joung. Efficient genome editing in zebrafish using a CRISPR-Cas system. *Nature biotechnology*, 31(3):227–229, Mar. 2013b.

H. Ito, M. Nakamura, O. Komure, T. Ayaki, R. Wate, H. Maruyama, Y. Nakamura, K. Fujita, S. Kaneko, Y. Okamoto, M. Ihara, T. Konishi, K. Ogasawara, A. Hirano, H. Kusaka, R. Kaji, R. Takahashi, and H. Kawakami. Clinicopathologic study on an ALS family with a heterozygous E478G optineurin mutation. *Acta Neuropathologica*, 122(2): 223–229, Aug. 2011.

K. Jackman, T. Kahles, D. Lane, L. Garcia-Bonilla, T. Abe, C. Capone, K. Hochrainer, H. Voss, P. Zhou, A. Ding, J. Anrather, and C. Iadecola. Progranulin deficiency promotes post-ischemic blood-brain barrier disruption. *Journal of Neuroscience*, 33(50):19579–19589, Dec. 2013.

A. Jalanko and T. Braulke. Neuronal ceroid lipofuscinoses. *Biochimica et biophysica acta*, 1793(4):697–709, Apr. 2009.

J. Jian, J. Konopka, and C. Liu. Insights into the role of progranulin in immunity, infection, and inflammation. *Journal of leukocyte biology*, Oct. 2012.

J. Jian, S. Zhao, Q. Tian, E. Gonzalez-Gugel, J. J. Mundra, S. M. Z. Uddin, B. Liu, B. Richbourgh, R. Brunetti, and C.-J. Liu. Progranulin directly binds to the CRD2 and CRD3 of TNFR extracellular domains. *FEBS letters*, 587 (21):3428–3436, Nov. 2013.

M. Jinek, K. Chylinski, I. Fonfara, M. Hauer, J. A. Doudna, and E. Charpentier. A programmable dual-RNA-guided DNA endonuclease in adaptive bacterial immunity. *Science (New York, NY)*, 337(6096):816–821, Aug. 2012.

M. Jinek, A. East, A. Cheng, S. Lin, E. Ma, and J. Doudna. RNA-programmed genome editing in human cells. *eLife*, 2:e00471, 2013.

L. Jing and L. I. Zon. Zebrafish as a model for normal and malignant hematopoiesis. *Disease Models & Mechanisms*, 4(4):433–438, July 2011.

K. A. Josephs, Z. Ahmed, O. Katsuse, J. F. Parisi, B. F. Boeve, D. S. Knopman, R. C. Petersen, P. Davies, R. Duara, N. R. Graff-Radford, R. J. Uitti, R. Rademakers, J. Adamson, M. Baker, M. L. Hutton, and D. W. Dickson. Neuropathologic features of frontotemporal lobar degeneration with ubiquitin-positive inclusions with progranulin gene (PGRN) mutations. *Journal of neuropathology and experimental neurology*, 66(2):142–151, Feb. 2007.

M. E. Judy, A. Nakamura, A. Huang, H. Grant, H. McCurdy, K. F. Weiberth, F. Gao, G. Coppola, C. Kenyon, and A. W. Kao. A shift to organismal stress resistance in programmed cell death mutants. *PLoS genetics*, 9(9):e1003714, Sept. 2013.

T. Jung, A. Höhn, and T. Grune. Lipofuscin: detection and quantification by microscopic techniques. *Methods in molecular biology (Clifton, NJ)*, 594:173–193, 2010.

E. Kabashi, L. Lin, M. L. Tradewell, P. A. Dion, V. Bercier, P. Bourgouin, D. Rochefort, S. Bel Hadj, H. D. Durham, C. Vande Velde, G. A. Rouleau, and P. Drapeau. Gain and loss of function of ALS-related mutations of TARDBP (TDP-43) cause motor deficits in vivo. *Human Molecular Genetics*, 19(4):671–683, Feb. 2010.

E. Kabashi, V. Bercier, A. Lissouba, M. Liao, E. Brustein, G. A. Rouleau, and P. Drapeau. FUS and TARDBP but not SOD1 interact in genetic models of amyotrophic lateral sclerosis. *PLoS genetics*, 7(8):e1002214, Aug. 2011.

M. Kamada, Y. Izumi, T. Ayaki, M. Nakamura, S. Kagawa, E. Kudo, W. Sako, H. Maruyama, Y. Nishida, H. Kawakami, H. Ito, and R. Kaji. Clinicopathologic features of autosomal recessive amyotrophic lateral sclerosis associated with optineurin mutation. *Neuropathology : official journal of the Japanese Society of Neuropathology*, July 2013.

M. Kanther and J. F. Rawls. Host-microbe interactions in the developing zebrafish. *Current opinion in immunology*, 22(1):10–19, Feb. 2010.

A. W. Kao, R. J. Eisenhut, L. H. Martens, A. Nakamura, A. Huang, J. A. Bagley, P. Zhou, A. de Luis, L. J. Neukomm, J. Cabello, R. V. Farese, and C. Kenyon. A neurodegenerative disease mutation that accelerates the clearance of apoptotic cells. *Proceedings of the National Academy of Sciences of the United States of America*, 108(11):4441–4446, Mar. 2011.

J. Karlsson, J. von Hofsten, and P. E. Olsson. Generating transparent zebrafish: a refined method to improve detection of gene expression during embryonic development. *Marine biotechnology (New York, N.Y.)*, 3(6):522–527, Nov. 2001.

A. Kawakami, T. Fukazawa, and H. Takeda. Early fin primordia of zebrafish larvae regenerate by a similar growth control mechanism with adult regeneration. *Developmental dynamics : an official publication of the American Association of Anatomists*, 231(4):693–699, Dec. 2004.

Y. Kayasuga, S. Chiba, M. Suzuki, T. Kikusui, T. Matsuwaki, K. Yamanouchi, H. Kotaki, R. Horai, Y. Iwakura, and M. Nishihara. Alteration of behavioural phenotype in mice by targeted disruption of the progranulin gene. *Behavioural brain research*, 185(2):110–118, Dec. 2007.

K. Kessenbrock, T. Dau, and D. E. Jenne. Tailor-made inflammation: how neutrophil serine proteases modulate the inflammatory response. *Journal of molecular medicine (Berlin, Germany)*, 89(1):23–28, Jan. 2011.

Y. G. Kim, J. Cha, and S. Chandrasegaran. Hybrid restriction enzymes: zinc finger fusions to Fok I cleavage domain. *Proceedings of the National Academy of Sciences of the United States of America*, 93(3):1156–1160, Feb. 1996.

C. B. Kimmel, W. W. Ballard, S. R. Kimmel, B. Ullmann, and T. F. Schilling. Stages of embryonic development of the zebrafish. *Developmental dynamics : an official publication of the American Association of Anatomists*, 203(3): 253–310, July 1995.

S. Kishi, J. Uchiyama, A. M. Baughman, T. Goto, M. C. Lin, and S. B. Tsai. The zebrafish as a vertebrate model of functional aging and very gradual senescence. *Experimental gerontology*, 38(7):777–786, July 2003.

S. Kishi, P. E. Bayliss, J. Uchiyama, E. Koshimizu, J. Qi, P. Nanjappa, S. Imamura, A. Islam, D. Neuberg, A. Amsterdam, and T. M. Roberts. The identification of zebrafish mutants showing alterations in senescence-associated biomarkers. *PLoS genetics*, 4(8):e1000152, 2008.

C. Kizil, J. Kaslin, V. Kroehne, and M. Brand. Adult neurogenesis and brain regeneration in zebrafish. *Developmental neurobiology*, 72(3):429–461, Mar. 2012.

G. Kleinberger, A. Capell, C. Haass, and C. Van Broeckhoven. Mechanisms of granulin deficiency: lessons from cellular and animal models. *Molecular neurobiology*, 47(1):337–360, Feb. 2013.

M. Koike, M. Shibata, S. Waguri, K. Yoshimura, I. Tanida, E. Kominami, T. Gotow, C. Peters, K. von Figura, N. Mizushima, P. Saftig, and Y. Uchiyama. Participation of autophagy in storage of lysosomes in neurons from mouse models of neuronal ceroid-lipofuscinoses (Batten disease). *The American journal of pathology*, 167(6):1713–1728, Dec. 2005.

Y. Kojima, K. Ono, K. Inoue, Y. Takagi, K.-i. Kikuta, M. Nishimura, Y. Yoshida, Y. Nakashima, H. Matsumae, Y. Furukawa, N. Mikuni, M. Nobuyoshi, T. Kimura, T. Kita, and M. Tanaka. Progranulin expression in advanced human atherosclerotic plaque. *Atherosclerosis*, 206(1):102–108, Sept. 2009.

K. Kollmann, K. E. Mutenda, M. Balleininger, E. Eckermann, K. von Figura, B. Schmidt, and T. Lübke. Identification of novel lysosomal matrix proteins by proteome analysis. *Proteomics*, 5(15):3966–3978, Oct. 2005.

K. Kollmann, K. Uusi-Rauva, E. Scifo, J. Tyynelä, A. Jalanko, and T. Braulke. Cell biology and function of neuronal ceroid lipofuscinosis-related proteins. *Biochimica et biophysica acta*, 1832(11):1866–1881, Nov. 2013.

V. Kroehne, D. Freudenreich, S. Hans, J. Kaslin, and M. Brand. Regeneration of the adult zebrafish brain from neurogenic radial glia-type progenitors. *Development (Cambridge, England)*, 138(22):4831–4841, Nov. 2011.

N. Kyritsis, C. Kizil, S. Zocher, V. Kroehne, J. Kaslin, D. Freudenreich, A. Iltzsche, and M. Brand. Acute inflammation initiates the regenerative response in the adult zebrafish brain. *Science (New York, NY)*, 338(6112):1353–1356, Dec. 2012.

A. S. Laird, A. Van Hoecke, L. De Muynck, M. Timmers, L. Van Den Bosch, P. Van Damme, and W. Robberecht. Progranulin is neurotrophic in vivo and protects against a mutant TDP-43 induced axonopathy. *PloS one*, 5(10): e13368, 2010.

C. M. Lang, K. Fellerer, B. M. Schwenk, P.-H. Kuhn, E. Kremmer, D. Edbauer, A. Capell, and C. Haass. Membrane orientation and subcellular localization of transmembrane protein 106B (TMEM106B), a major risk factor for frontotemporal lobar degeneration. *Journal of Biological Chemistry*, 287(23):19355–19365, June 2012.

N. D. Lawson and B. M. Weinstein. In vivo imaging of embryonic vascular development using transgenic zebrafish. *Developmental Biology*, 248(2):307–318, Aug. 2002.

N. D. Lawson and S. A. Wolfe. Forward and reverse genetic approaches for the analysis of vertebrate development in the zebrafish. *Developmental cell*, 21(1):48–64, July 2011.

I. Le Ber, A. Camuzat, R. Guerreiro, K. Bouya-Ahmed, J. Bras, G. Nicolas, A. Gabelle, M. Didic, A. De Septenville, S. Millecamps, T. Lenglet, M. Latouche, E. Kabashi, D. Campion, D. Hannequin, J. Hardy, A. Brice, and French

Clinical and Genetic Research Network on FTD/FTD-ALS. SQSTM1 mutations in French patients with frontotemporal dementia or frontotemporal dementia with amyotrophic lateral sclerosis. *JAMA neurology*, 70(11):1403–1410, Nov. 2013.

M.-J. Lee, T.-F. Chen, T.-W. Cheng, and M.-J. Chiu. rs5848 variant of progranulin gene is a risk of Alzheimer's disease in the Taiwanese population. *Neuro-degenerative diseases*, 8(4):216–220, 2011.

Y.-B. Lee, H.-J. Chen, J. N. Peres, J. Gomez-Deza, J. Attig, M. Stalekar, C. Troakes, A. L. Nishimura, E. L. Scotter, C. Vance, Y. Adachi, V. Sardone, J. W. Miller, B. N. Smith, J.-M. Gallo, J. Ule, F. Hirth, B. Rogelj, C. Houart, and C. E. Shaw. Hexanucleotide Repeats in ALS/FTD Form Length-Dependent RNA Foci, Sequester RNA Binding Proteins, and Are Neurotoxic. *Cell reports*, 5(5):1178–1186, Dec. 2013.

R. Lemmens, A. Van Hoecke, N. Hersmus, V. Geelen, I. D'Hollander, V. Thijs, L. Van Den Bosch, P. Carmeliet, and W. Robberecht. Overexpression of mutant superoxide dismutase 1 causes a motor axonopathy in the zebrafish. *Human Molecular Genetics*, 16(19):2359–2365, Oct. 2007.

J. R. Lenkowski and P. A. Raymond. Müller glia: Stem cells for generation and regeneration of retinal neurons in teleost fish. *Progress in retinal and eye research*, Jan. 2014.

I. U. S. Leong, D. Lai, C.-C. Lan, R. Johnson, D. R. Love, R. Johnson, and D. R. Love. Targeted mutagenesis of zebrafish: use of zinc finger nucleases. *Birth defects research. Part C, Embryo today : reviews*, 93(3):249–255, Sept. 2011.

L. Li, B. Yan, Y.-Q. Shi, W.-Q. Zhang, and Z.-L. Wen. Live imaging reveals differing roles of macrophages and neutrophils during zebrafish tail fin regeneration. *Journal of Biological Chemistry*, 287(30):25353–25360, July 2012.

Y. H. Li, M. H. C. Chen, H. Y. Gong, S. Y. Hu, Y. W. Li, G. H. Lin, C. C. Lin, W. Liu, and J. L. Wu. Progranulin A-mediated MET Signaling Is Essential for Liver Morphogenesis in Zebrafish. *Journal of Biological Chemistry*, 285 (52):41001–41009, Dec. 2010.

Y.-H. Li, H.-Y. Chen, Y.-W. Li, S.-Y. Wu, Wangta-Liu, G.-H. Lin, S.-Y. Hu, Z.-K. Chang, H.-Y. Gong, C.-H. Liao, K.-Y. Chiang, C.-W. Huang, and J.-L. Wu. Progranulin regulates zebrafish muscle growth and regeneration through maintaining the pool of myogenic progenitor cells. *Scientific reports*, 3:1176, 2013.

C.-L. Lien, M. Schebesta, S. Makino, G. J. Weber, and M. T. Keating. Gene expression analysis of zebrafish heart regeneration. *PLoS biology*, 4(8):e260, Aug. 2006.

G. J. Lieschke, A. C. Oates, M. O. Crowhurst, A. C. Ward, and J. E. Layton. Morphologic and functional characterization of granulocytes and macrophages in embryonic and adult zebrafish. *Blood*, 98(10):3087–3096, Nov. 2001.

G. J. Lieschke, A. C. Oates, B. H. Paw, M. A. Thompson, N. E. Hall, A. C. Ward, R. K. Ho, L. I. Zon, and J. E. Layton. Zebrafish SPI-1 (PU.1) marks a site of myeloid development independent of primitive erythropoiesis: implications for axial patterning. *Developmental Biology*, 246(2):274–295, June 2002.

H.-Y. Lim, B. Albuquerque, A. Häussler, T. Myrczek, A. Ding, and I. Tegeder. Progranulin contributes to endogenous mechanisms of pain defense after nerve injury in mice. *Journal of cellular and molecular medicine*, 16(4):708–721, Apr. 2012.

F. Liu and Z. Wen. Cloning and expression pattern of the lysozyme C gene in zebrafish. *Mechanisms of development*, 113(1):69–72, Apr. 2002.

F. Lottspeich and J. W. Engels. *Bioanalytik*. Spektrum Akademischer Verlag Gmbh, Apr. 2012.

R. G. MacDonald, S. R. Pfeffer, L. Coussens, M. A. Tepper, C. M. Brocklebank, J. E. Mole, J. K. Anderson, E. Chen, M. P. Czech, and A. Ullrich. A single receptor binds both insulin-like growth factor II and mannose-6-phosphate. *Science (New York, NY)*, 239(4844):1134–1137, Mar. 1988.

I. R. A. Mackenzie. The neuropathology and clinical phenotype of FTD with progranulin mutations. *Acta Neuropathologica*, 114(1):49–54, July 2007.

I. R. A. Mackenzie, M. Baker, S. Pickering-Brown, G.-Y. R. Hsiung, C. Lindholm, E. Dwosh, J. Gass, A. Cannon, R. Rademakers, M. Hutton, and H. H. Feldman. The neuropathology of frontotemporal lobar degeneration caused by mutations in the progranulin gene. *Brain : a journal of neurology*, 129(Pt 11):3081–3090, Nov. 2006.

R. C. MacPhail, J. Brooks, D. L. Hunter, B. Padnos, T. D. Irons, and S. Padilla. Locomotion in larval zebrafish: Influence of time of day, lighting and ethanol. *Neurotoxicology*, 30(1):52–58, Jan. 2009.

F. Mahmood, S. Fu, J. Cooke, S. W. Wilson, J. D. Cooper, and C. Russell. A zebrafish model of CLN2 disease is deficient in tripeptidyl peptidase 1 and displays progressive neurodegeneration accompanied by a reduction in proliferation. *Brain : a journal of neurology*, 136(Pt 5):1488–1507, May 2013a.

F. Mahmood, M. Mozere, A. A. Zdebik, H. C. Stanescu, J. Tobin, P. L. Beales, R. Kleta, D. Bockenhauer, and C. Russell. Generation and validation of a zebrafish model of EAST (Epilepsy, ataxia, sensorineural deafness and tubulopathy) syndrome. *Disease Models & Mechanisms*, Feb. 2013b.

A. Malaspina, N. Kaushik, and J. de Belleroche. Differential expression of 14 genes in amyotrophic lateral sclerosis spinal cord detected using gridded cDNA arrays. *Journal of neurochemistry*, 77(1):132–145, Apr. 2001.

P. Mali, L. Yang, K. M. Esvelt, J. Aach, M. Guell, J. E. DiCarlo, J. E. Norville, and G. M. Church. RNA-guided human genome engineering via Cas9. *Science (New York, NY)*, 339(6121):823–826, Feb. 2013.

M. S. Marks, H. F. G. Heijnen, and G. Raposo. Lysosome-related organelles: unusual compartments become mainstream. *Current opinion in cell biology*, 25(4):495–505, Aug. 2013.

L. H. Martens, J. Zhang, S. J. Barmada, P. Zhou, S. Kamiya, B. Sun, S.-W. Min, L. Gan, S. Finkbeiner, E. J. Huang, and R. V. Farese. Progranulin deficiency promotes neuroinflammation and neuron loss following toxin-induced injury. *The Journal of clinical investigation*, Oct. 2012.

M. März, R. Schmidt, S. Rastegar, and U. Strähle. Regenerative response following stab injury in the adult zebrafish telencephalon. *Developmental dynamics : an official publication of the American Association of Anatomists*, 240 (9):2221–2231, Sept. 2011.

L. K. Mathew, S. Sengupta, J. A. Franzosa, J. Perry, J. La Du, E. A. Andreasen, and R. L. Tanguay. Comparative expression profiling reveals an essential role for raldh2 in epimorphic regeneration. *Journal of Biological Chemistry*, 284(48):33642–33653, Nov. 2009.

J. R. Mathias, B. J. Perrin, T.-X. Liu, J. Kanki, A. T. Look, and A. Huttenlocher. Resolution of inflammation by retrograde chemotaxis of neutrophils in transgenic zebrafish. *Journal of leukocyte biology*, 80(6):1281–1288, Dec. 2006.

J. R. Mathias, M. E. Dodd, K. B. Walters, S. K. Yoo, E. A. Ranheim, and A. Huttenlocher. Characterization of zebrafish larval inflammatory macrophages. *Developmental and comparative immunology*, 33(11):1212–1217, Nov. 2009.

M. L. McWhorter, U. R. Monani, A. H. M. Burghes, and C. E. Beattie. Knockdown of the survival motor neuron (Smn) protein in zebrafish causes defects in motor axon outgrowth and pathfinding. *The Journal of Cell Biology*, 162(5): 919–931, Sept. 2003.

A. H. Meijer, F. J. Verbeek, E. Salas-Vidal, M. Corredor-Adámez, J. Bussman, A. M. van der Sar, G. W. Otto, R. Geisler, and H. P. Spaink. Transcriptome profiling of adult zebrafish at the late stage of chronic tuberculosis due to Mycobacterium marinum infection. *Molecular immunology*, 42(10):1185–1203, June 2005.

E. Meijering, O. Dzyubachyk, and I. Smal. Methods for cell and particle tracking. *Methods in enzymology*, 504:183–200, 2012.

X. Meng, M. B. Noyes, L. J. Zhu, N. D. Lawson, and S. A. Wolfe. Targeted gene inactivation in zebrafish using engineered zinc-finger nucleases. *Nature biotechnology*, 26(6):695–701, June 2008.

A. Meyer and M. Schartl. Gene and genome duplications in vertebrates: the one-to-four (-to-eight in fish) rule and the evolution of novel gene functions. *Current opinion in cell biology*, 11(6):699–704, Dec. 1999.

J. C. Miller, M. C. Holmes, J. Wang, D. Y. Guschin, Y.-L. Lee, I. Rupniewski, C. M. Beausejour, A. J. Waite, N. S. Wang, K. A. Kim, P. D. Gregory, C. O. Pabo, and E. J. Rebar. An improved zinc-finger nuclease architecture for highly specific genome editing. *Nature biotechnology*, 25(7):778–785, July 2007.

J. C. Miller, S. Tan, G. Qiao, K. A. Barlow, J. Wang, D. F. Xia, X. Meng, D. E. Paschon, E. Leung, S. J. Hinkley, G. P. Dulay, K. L. Hua, I. Ankoudinova, G. J. Cost, F. D. Urnov, H. S. Zhang, M. C. Holmes, L. Zhang, P. D. Gregory, and E. J. Rebar. A TALE nuclease architecture for efficient genome editing. *Nature biotechnology*, 29(2):143–148, Dec. 2010.

C. Milstein. The hybridoma revolution: an offshoot of basic research. *BioEssays : news and reviews in molecular, cellular and developmental biology*, 21(11):966–973, Nov. 1999.

C. B. Moens, T. M. Donn, E. R. Wolf-Saxon, and T. P. Ma. Reverse genetics in zebrafish by TILLING. *Briefings in functional genomics & proteomics*, 7(6):454–459, Nov. 2008.

K. Moisse, K. Volkening, C. Leystra-Lantz, I. Welch, T. Hill, and M. J. Strong. Divergent patterns of cytosolic TDP-43 and neuronal progranulin expression following axotomy: implications for TDP-43 in the physiological response to neuronal injury. *Brain research*, 1249:202–211, Jan. 2009.

G. Monami, E. M. Gonzalez, M. Hellman, L. G. Gomella, R. Baffa, R. V. Iozzo, and A. Morrione. Proepithelin promotes migration and invasion of 5637 bladder cancer cells through the activation of ERK1/2 and the formation of a paxillin/FAK/ERK complex. *Cancer research*, 66(14):7103–7110, July 2006.

M. J. Monnot, P. J. Babin, G. Poleo, M. Andre, L. Laforest, C. Ballagny, and M. A. Akimenko. Epidermal expression of apolipoprotein E gene during fin and scale development and fin regeneration in zebrafish. *Developmental dynamics : an official publication of the American Association of Anatomists*, 214(3):207–215, Mar. 1999.

F. E. Moore, D. Reyon, J. D. Sander, S. A. Martinez, J. S. Blackburn, C. Khayter, C. L. Ramirez, J. K. Joung, and D. M. Langenau. Improved somatic mutagenesis in zebrafish using transcription activator-like effector nucleases (TALENs). *PloS one*, 7(5):e37877, 2012.

K. Mori, S.-M. Weng, T. Arzberger, S. May, K. Rentzsch, E. Kremmer, B. Schmid, H. A. Kretzschmar, M. Cruts, C. Van Broeckhoven, C. Haass, and D. Edbauer. The C9orf72 GGGGCC repeat is translated into aggregating dipeptide-repeat proteins in FTLD/ALS. *Science (New York, NY)*, 339(6125):1335–1338, Mar. 2013.

M. J. Moscou and A. J. Bogdanove. A simple cipher governs DNA recognition by TAL effectors. *Science (New York, NY)*, 326(5959):1501, Dec. 2009.

M. C. Mullins, M. Hammerschmidt, P. Haffter, and C. Nüsslein-Volhard. Large-scale mutagenesis in the zebrafish: in search of genes controlling development in a vertebrate. *Current biology : CB*, 4(3):189–202, Mar. 1994.

P. Murawala, E. M. Tanaka, and J. D. Currie. Regeneration: the ultimate example of wound healing. *Seminars in cell & developmental biology*, 23(9):954–962, Dec. 2012.

K. P. Murphy, P. Travers, M. Walport, and C. Janeway. *Janeway's immunobiology*. Garland Pub, 2008.

C. Mussolino, R. Morbitzer, F. Lütge, N. Dannemann, T. Lahaye, and T. Cathomen. A novel TALE nuclease scaffold enables high genome editing activity in combination with low toxicity. *Nucleic acids research*, 39(21):9283–9293, Nov. 2011.

S. B. Naphade, K. A. Kigerl, L. B. Jakeman, S. K. Kostyk, P. G. Popovich, and J. Kuret. Progranulin expression is upregulated after spinal contusion in mice. *Acta Neuropathologica*, 119(1):123–133, Jan. 2010.

T. Nedachi, T. Kawai, T. Matsuwaki, K. Yamanouchi, and M. Nishihara. Progranulin enhances neural progenitor cell proliferation through glycogen synthase kinase 3β phosphorylation. *Neuroscience*, pages 1–10, Apr. 2011.

M. Neumann, D. M. Sampathu, L. K. Kwong, A. C. Truax, M. C. Micsenyi, T. T. Chou, J. Bruce, T. Schuck, M. Grossman, C. M. Clark, L. F. McCluskey, B. L. Miller, E. Masliah, I. R. Mackenzie, H. Feldman, W. Feiden, H. A. Kretzschmar, J. Q. Trojanowski, and V. M.-Y. Lee. Ubiquitinated TDP-43 in frontotemporal lobar degeneration and amyotrophic lateral sclerosis. *Science (New York, NY)*, 314(5796):130–133, Oct. 2006.

M. Neumann, L. K. Kwong, E. B. Lee, E. Kremmer, A. Flatley, Y. Xu, M. S. Forman, D. Troost, H. A. Kretzschmar, J. Q. Trojanowski, and V. M.-Y. Lee. Phosphorylation of S409/410 of TDP-43 is a consistent feature in all sporadic and familial forms of TDP-43 proteinopathies. *Acta Neuropathologica*, 117(2):137–149, Feb. 2009.

A. D. Nguyen, T. A. Nguyen, L. H. Martens, L. L. Mitic, and R. V. Farese. Progranulin: at the interface of neurodegenerative and metabolic diseases. *Trends in endocrinology and metabolism: TEM*, 24(12):597–606, Dec. 2013.

C. S. Nicolas, M. Amici, Z. A. Bortolotto, A. Doherty, Z. Csaba, A. Fafouri, P. Dournaud, P. Gressens, G. L. Collingridge, and S. Peineau. The role of JAK-STAT signaling within the CNS. *JAK-STAT*, 2(1):e22925, Jan. 2013.

P. Niethammer, C. Grabher, A. T. Look, and T. J. Mitchison. A tissue-scale gradient of hydrogen peroxide mediates rapid wound detection in zebrafish. *Nature*, 459(7249):996–999, June 2009.

Y. Nishimura, K. Yata, T. Nomoto, T. Ogiwara, K. Watanabe, T. Shintou, A. Tsuboyama, M. Okano, N. Umemoto, Z. Zhang, M. Kawabata, B. Zhang, J. Kuroyanagi, Y. Shimada, T. Miyazaki, T. Imamura, H. Tomimoto, and T. Tanaka. Identification of a novel indoline derivative for in vivo fluorescent imaging of blood-brain barrier disruption in animal models. *ACS chemical neuroscience*, 4(8):1183–1193, Aug. 2013.

W. H. J. Norton, K. Stumpenhorst, T. Faus-Kessler, A. Folchert, N. Rohner, M. P. Harris, J. Callebert, and L. Bally-Cuif. Modulation of Fgfr1a signaling in zebrafish reveals a genetic basis for the aggression-boldness syndrome. *Journal of Neuroscience*, 31(39):13796–13807, Sept. 2011.

A. Nykjaer and T. E. Willnow. Sortilin: a receptor to regulate neuronal viability and function. *Trends in neurosciences*, 35(4):261–270, Apr. 2012.

K. Ohmi, D. S. Greenberg, K. S. Rajavel, S. Ryazantsev, H. H. Li, and E. F. Neufeld. Activated microglia in cortex of mouse models of mucopolysaccharidoses I and IIIB. *Proceedings of the National Academy of Sciences of the United States of America*, 100(4):1902–1907, Feb. 2003.

H. Okura, S. Yamashita, T. Ohama, A. Saga, A. Yamamoto-Kakuta, Y. Hamada, N. Sougawa, R. Ohyama, Y. Sawa, and A. Matsuyama. HDL/apolipoprotein A-I binds to macrophage-derived progranulin and suppresses its conversion into proinflammatory granulins. *Journal of atherosclerosis and thrombosis*, 17(6):568–577, June 2010.

C. H. P. Ong and A. Bateman. Progranulin (granulin-epithelin precursor, PC-cell derived growth factor, acrogranin) in proliferation and tumorigenesis. *Histology and histopathology*, 18(4):1275–1288, Oct. 2003.

C. H. P. Ong, Z. He, L. Kriazhev, X. Shan, R. G. E. Palfree, and A. Bateman. Regulation of progranulin expression in myeloid cells. *American journal of physiology Regulatory, integrative and comparative physiology*, 291(6):R1602–12, Dec. 2006.

D. N. Palmer, L. A. Barry, J. Tyynelä, and J. D. Cooper. NCL disease mechanisms. *Biochimica et biophysica acta*, 1832(11):1882–1893, Nov. 2013.

X.-D. Pan and X.-C. Chen. Clinic, neuropathology and molecular genetics of frontotemporal dementia: a mini-review. *Translational neurodegeneration*, 2(1):8, 2013.

D. Paquet, R. Bhat, A. Sydow, E.-M. Mandelkow, S. Berg, S. Hellberg, J. Fälting, M. Distel, R. W. Köster, B. Schmid, and C. Haass. A zebrafish model of tauopathy allows in vivo imaging of neuronal cell death and drug evaluation. *The Journal of clinical investigation*, 119(5):1382–1395, May 2009.

S. Partanen, A. Haapanen, C. Kielar, C. Pontikis, N. Alexander, T. Inkinen, P. Saftig, T. H. Gillingwater, J. D. Cooper, and J. Tyynelä. Synaptic changes in the thalamocortical system of cathepsin D-deficient mice: a model of human congenital neuronal ceroid-lipofuscinosis. *Journal of neuropathology and experimental neurology*, 67(1):16–29, Jan. 2008.

S. E. Patterson, L. B. Mook, and S. H. Devoto. Growth in the larval zebrafish pectoral fin and trunk musculature. *Developmental dynamics : an official publication of the American Association of Anatomists*, 237(2):307–315, Feb. 2008.

F. Pelegri. Maternal factors in zebrafish development. *Developmental dynamics : an official publication of the American Association of Anatomists*, 228(3):535–554, Nov. 2003.

E. M. Pera, S. Hou, I. Strate, O. Wessely, and E. M. De Robertis. Exploration of the extracellular space by a large-scale secretion screen in the early Xenopus embryo. *The International journal of developmental biology*, 49(7):781–796, 2005.

F. Peri and C. Nüsslein-Volhard. Live imaging of neuronal degradation by microglia reveals a role for v0-ATPase a1 in phagosomal fusion in vivo. *Cell*, 133(5):916–927, May 2008.

T. L. Petkau, S. J. Neal, P. C. Orban, J. L. MacDonald, A. M. Hill, G. Lu, H. H. Feldman, I. R. A. Mackenzie, and B. R. Leavitt. Progranulin expression in the developing and adult murine brain. *The Journal of comparative neurology*, 518(19):3931–3947, Oct. 2010.

T. L. Petkau, S. J. Neal, A. Milnerwood, A. Mew, A. M. Hill, P. Orban, J. Gregg, G. Lu, H. H. Feldman, I. R. A. Mackenzie, L. A. Raymond, and B. R. Leavitt. Synaptic dysfunction in progranulin-deficient mice. *Neurobiology of disease*, 45(2):711–722, Feb. 2012.

E. Petoukhov, S. Fernando, F. Mills, F. Shivji, D. Hunter, C. Krieger, M. A. Silverman, and S. X. Bamji. Activity-dependent secretion of progranulin from synapses. *Journal of Cell Science*, 126(Pt 23):5412–5421, Dec. 2013.

M. Pikkarainen, P. Hartikainen, and I. Alafuzoff. Neuropathologic features of frontotemporal lobar degeneration with ubiquitin-positive inclusions visualized with ubiquitin-binding protein p62 immunohistochemistry. *Journal of neuropathology and experimental neurology*, 67(4):280–298, Apr. 2008.

M. Polymenidou, C. Lagier-Tourenne, K. R. Hutt, S. C. Huelga, J. Moran, T. Y. Liang, S.-C. Ling, E. Sun, E. Wancewicz, C. Mazur, H. Kordasiewicz, Y. Sedaghat, J. P. Donohue, L. Shiue, C. F. Bennett, G. W. Yeo, and D. W. Cleveland. Long pre-mRNA depletion and RNA missplicing contribute to neuronal vulnerability from loss of TDP-43. *Nature Neuroscience*, 14(4):459–468, Apr. 2011.

M. H. Porteus and D. Carroll. Gene targeting using zinc finger nucleases. *Nature biotechnology*, 23(8):967–973, Aug. 2005.

S. Preibisch, S. Saalfeld, and P. Tomancak. Globally optimal stitching of tiled 3D microscopic image acquisitions. *Bioinformatics (Oxford, England)*, 25(11):1463–1465, June 2009.

E. Premi, A. Padovani, and B. Borroni. Frontotemporal Lobar Degeneration. *Advances in experimental medicine and biology*, 724:114–127, 2012.

I. Prengel. *Entwicklung und immunmorphologische Charakterisierung monoklonaler Antikörper gegen Proteine des Zebrabärblings (Danio rerio)*. PhD thesis, Munich, Jan. 2000.

M. Qian, D. E. Sleat, H. Zheng, D. Moore, and P. Lobel. Proteomics analysis of serum from mutant mice reveals lysosomal proteins selectively transported by each of the two mannose 6-phosphate receptors. *Molecular & Cellular Proteomics*, 7(1):58–70, Jan. 2008.

J. Qin, L. Diaz-Cueto, J.-E. Schwarze, Y. Takahashi, M. Imai, K. Isuzugawa, S. Yamamoto, K.-T. Chang, G. L. Gerton, and K. Imakawa. Effects of progranulin on blastocyst hatching and subsequent adhesion and outgrowth in the mouse. *Biology of reproduction*, 73(3):434–442, Sept. 2005.

F. Qiu, L. Song, F. Ding, H. Liu, Q. Shu, N. Yang, W. Liu, and X. Li. Expression level of the growth factor progranulin is related with development of systemic lupus erythematosus. *Diagnostic pathology*, 8:88, 2013.

H. Qu, H. Deng, and Z. Hu. Plasma progranulin concentrations are increased in patients with type 2 diabetes and obesity and correlated with insulin resistance. *Mediators of inflammation*, 2013:360190, 2013.

R. Rademakers, M. Neumann, and I. R. Mackenzie. Advances in understanding the molecular basis of frontotemporal dementia. *Nature reviews. Neurology*, 8(8):423–434, Aug. 2012.

G. S. Ralph, P. A. Radcliffe, D. M. Day, J. M. Carthy, M. A. Leroux, D. C. P. Lee, L.-F. Wong, L. G. Bilsland, L. Greensmith, S. M. Kingsman, K. A. Mitrophanous, N. D. Mazarakis, and M. Azzouz. Silencing mutant SOD1

using RNAi protects against neurodegeneration and extends survival in an ALS model. *Nature Medicine*, 11(4): 429–433, Apr. 2005.

S. A. Renshaw and N. S. Trede. A model 450 million years in the making: zebrafish and vertebrate immunity. *Disease Models & Mechanisms*, 5(1):38–47, Jan. 2012.

S. A. Renshaw, C. A. Loynes, D. M. I. Trushell, S. Elworthy, P. W. Ingham, and M. K. B. Whyte. A transgenic zebrafish model of neutrophilic inflammation. *Blood*, 108(13):3976–3978, Dec. 2006.

A. E. Renton, E. Majounie, A. Waite, J. Simón-Sánchez, S. Rollinson, J. R. Gibbs, J. C. Schymick, H. Laaksovirta, J. C. van Swieten, L. Myllykangas, H. Kalimo, A. Paetau, Y. Abramzon, A. M. Remes, A. Kaganovich, S. W. Scholz, J. Duckworth, J. Ding, D. W. Harmer, D. G. Hernandez, J. O. Johnson, K. Mok, M. Ryten, D. Trabzuni, R. J. Guerreiro, R. W. Orrell, J. Neal, A. Murray, J. Pearson, I. E. Jansen, D. Sondervan, H. Seelaar, D. Blake, K. Young, N. Halliwell, J. B. Callister, G. Toulson, A. Richardson, A. Gerhard, J. Snowden, D. Mann, D. Neary, M. A. Nalls, T. Peuralinna, L. Jansson, V.-M. Isoviita, A.-L. Kaivorinne, M. Hölttä-Vuori, E. Ikonen, R. Sulkava, M. Benatar, J. Wuu, A. Chiò, G. Restagno, G. Borghero, M. Sabatelli, ITALSGEN Consortium, D. Heckerman, E. Rogaeva, L. Zinman, J. D. Rothstein, M. Sendtner, C. Drepper, E. E. Eichler, C. Alkan, Z. Abdullaev, S. D. Pack, A. Dutra, E. Pak, J. Hardy, A. Singleton, N. M. Williams, P. Heutink, S. Pickering-Brown, H. R. Morris, P. J. Tienari, and B. J. Traynor. A hexanucleotide repeat expansion in C9ORF72 is the cause of chromosome 9p21-linked ALS-FTD. *Neuron*, 72(2):257–268, Oct. 2011.

F. Rentzsch, J. Bakkers, C. Kramer, and M. Hammerschmidt. Fgf signaling induces posterior neuroectoderm independently of Bmp signaling inhibition. *Developmental dynamics : an official publication of the American Association of Anatomists*, 231(4):750–757, Dec. 2004.

J. D. Rohrer, G. R. Ridgway, M. Modat, S. Ourselin, S. Mead, N. C. Fox, M. N. Rossor, and J. D. Warren. Distinct profiles of brain atrophy in frontotemporal lobar degeneration caused by progranulin and tau mutations. *NeuroImage*, 53(3):1070–1076, Nov. 2010.

C. E. d. Rosa, R. Y. Kuradomi, D. V. Almeida, C. F. C. Lannes, M. d. A. Figueiredo, A. G. Dytz, D. B. Fonseca, and L. F. Marins. GH overexpression modifies muscle expression of anti-oxidant enzymes and increases spinal curvature of old zebrafish. *Experimental gerontology*, 45(6):449–456, June 2010.

E. Rubino, I. Rainero, A. Chiò, E. Rogaeva, D. Galimberti, P. Fenoglio, Y. Grinberg, G. Isaia, A. Calvo, S. Gentile, A. C. Bruni, P. H. St George-Hyslop, E. Scarpini, S. Gallone, L. Pinessi, and TODEM Study Group. SQSTM1 mutations in frontotemporal lobar degeneration and amyotrophic lateral sclerosis. *Neurology*, 79(15):1556–1562, Oct. 2012.

A. A. Ruparelia, M. Zhao, P. D. Currie, and R. J. Bryson-Richardson. Characterization and investigation of zebrafish models of filamin-related myofibrillar myopathy. *Human Molecular Genetics*, 21(18):4073–4083, Sept. 2012.

M. Sakai, T. Kono, and R. Savan. Identification of expressed genes in carp (Cyprinus carpio) head kidney cells after in vitro treatment with immunostimulants. *Developments in biologicals*, 121:45–51, 2005.

J. D. Sander, L. Cade, C. Khayter, D. Reyon, R. T. Peterson, J. K. Joung, and J.-R. J. Yeh. Targeted gene disruption in somatic zebrafish cells using engineered TALENs. *Nature biotechnology*, 29(8):697–698, Aug. 2011.

M. Sardiello, M. Palmieri, A. di Ronza, D. L. Medina, M. Valenza, V. A. Gennarino, C. Di Malta, F. Donaudy, V. Embrione, R. S. Polishchuk, S. Banfi, G. Parenti, E. Cattaneo, and A. Ballabio. A gene network regulating lysosomal biogenesis and function. *Science (New York, NY)*, 325(5939):473–477, July 2009.

A. F. Schier. Genomics: Zebrafish earns its stripes. *Nature*, 496(7446):443–444, Apr. 2013.

N. W. Schiffer, S. A. Broadley, T. Hirschberger, P. Tavan, H. A. Kretzschmar, A. Giese, C. Haass, F. U. Hartl, and B. Schmid. Identification of anti-prion compounds as efficient inhibitors of polyglutamine protein aggregation in a zebrafish model. *The Journal of biological chemistry*, 282(12):9195–9203, Mar. 2007.

T. Schlegelmilch, K. Henke, and F. Peri. Microglia in the developing brain: from immunity to behaviour. *Current opinion in neurobiology*, 21(1):5–10, Feb. 2011.

B. Schmid and C. Haass. Genomic editing opens new avenues for zebrafish as a model for neurodegeneration. *Journal of neurochemistry*, 127(4):461–470, Nov. 2013.

B. Schmid, A. Hruscha, S. Hogl, J. Banzhaf-Strathmann, K. Strecker, J. van der Zee, M. Teucke, S. Eimer, J. Hegermann, M. Kittelmann, E. Kremmer, M. Cruts, B. Solchenberger, L. Hasenkamp, F. van Bebber, C. Van Broeckhoven, D. Edbauer, S. F. Lichtenthaler, and C. Haass. Loss of ALS-associated TDP-43 in zebrafish causes muscle degeneration, vascular dysfunction, and reduced motor neuron axon outgrowth. *Proceedings of the National Academy of Sciences of the United States of America*, 110(13):4986–4991, Mar. 2013.

A. Schulz, A. Kohlschütter, J. Mink, A. Simonati, and R. Williams. NCL diseases - clinical perspectives. *Biochimica et biophysica acta*, 1832(11):1801–1806, Nov. 2013.

H. Seelaar, W. Kamphorst, S. M. Rosso, A. Azmani, R. Masdjedi, I. de Koning, J. A. Maat-Kievit, B. Anar, L. Donker Kaat, G. J. Breedveld, D. Dooijes, J. M. Rozemuller, I. F. Bronner, P. Rizzu, and J. C. van Swieten. Distinct genetic forms of frontotemporal dementia. *Neurology*, 71(16):1220–1226, Oct. 2008.

C. Seger, M. Hargrave, X. Wang, R. J. Chai, S. Elworthy, and P. W. Ingham. Analysis of Pax7 expressing myogenic cells in zebrafish muscle development, injury, and models of disease. *Developmental dynamics : an official publication of the American Association of Anatomists*, 240(11):2440–2451, Nov. 2011.

D. J. Selkoe. Alzheimer's disease. *Cold Spring Harbor perspectives in biology*, 3(7), July 2011.

R. E. Seltman and B. R. Matthews. Frontotemporal lobar degeneration: epidemiology, pathology, diagnosis and management. *CNS drugs*, 26(10):841–870, Oct. 2012.

G. Serrero, D. M. Hawkins, B. Yue, O. Ioffe, P. Bejarano, J. T. Phillips, J. F. Head, R. L. Elliott, K. R. Tkaczuk, A. K. Godwin, J. Weaver, and W. E. Kim. Progranulin (GP88) tumor tissue expression is associated with increased risk of recurrence in breast cancer patients diagnosed with estrogen receptor positive invasive ductal carcinoma. *Breast cancer research : BCR*, 14(1):R26, 2012.

J. J. Shacka. Mouse models of neuronal ceroid lipofuscinoses: useful pre-clinical tools to delineate disease pathophysiology and validate therapeutics. *Brain research bulletin*, 88(1):43–57, May 2012.

S. S. Shankaran, A. Capell, A. T. Hruscha, K. Fellerer, M. Neumann, B. Schmid, and C. Haass. Missense mutations in the progranulin gene linked to frontotemporal lobar degeneration with ubiquitin-immunoreactive inclusions reduce progranulin production and secretion. *The Journal of biological chemistry*, 283(3):1744–1753, Jan. 2008.

C. E. Shiau, K. R. Monk, W. Joo, and W. S. Talbot. An anti-inflammatory NOD-like receptor is required for microglia development. *Cell reports*, 5(5):1342–1352, Dec. 2013.

D. Sieger and F. Peri. Animal models for studying microglia: The first, the popular, and the new. *Glia*, 61(1):3–9, Jan. 2013.

D. Sieger, C. Moritz, T. Ziegenhals, S. Prykhozhij, and F. Peri. Long-range Ca2+ waves transmit brain-damage signals to microglia. *Developmental cell*, 22(6):1138–1148, June 2012.

E. Siintola, S. Partanen, P. Strömme, A. Haapanen, M. Haltia, J. Maehlen, A.-E. Lehesjoki, and J. Tyynelä. Cathepsin D deficiency underlies congenital human neuronal ceroid-lipofuscinosis. *Brain : a journal of neurology*, 129(Pt 6): 1438–1445, June 2006.

K. Sleegers, N. Brouwers, S. Maurer-Stroh, M. A. van Es, P. Van Damme, P. W. J. van Vught, J. van der Zee, S. Serneels, T. De Pooter, M. Van den Broeck, M. Cruts, J. Schymkowitz, P. De Jonghe, F. Rousseau, L. H. van den Berg, W. Robberecht, and C. Van Broeckhoven. Progranulin genetic variability contributes to amyotrophic lateral sclerosis. *Neurology*, 71(4):253–259, July 2008.

K. R. Smith, J. Damiano, S. Franceschetti, S. Carpenter, L. Canafoglia, M. Morbin, G. Rossi, D. Pareyson, S. E. Mole, J. F. Staropoli, K. B. Sims, J. Lewis, W.-L. Lin, D. W. Dickson, H.-H. Dahl, M. Bahlo, and S. F. Berkovic. Strikingly different clinicopathological phenotypes determined by progranulin-mutation dosage. *American journal of human genetics*, 90(6):1102–1107, June 2012.

P. Song and S. W. Pimplikar. Knockdown of amyloid precursor protein in zebrafish causes defects in motor axon outgrowth. *PloS one*, 7(4):e34209, 2012.

K. Songsrirote, Z. Li, D. Ashford, A. Bateman, and J. Thomas-Oates. Development and application of mass spectrometric methods for the analysis of progranulin N-glycosylation. *Journal of proteomics*, 73(8):1479–1490, June 2010.

R. Sood and P. Liu. Novel insights into the genetic controls of primitive and definitive hematopoiesis from zebrafish models. *Advances in hematology*, 2012:830703, 2012.

U. Strähle and C. Grabher. The zebrafish embryo as a model for assessing off-target drug effects. *Disease Models & Mechanisms*, 3(11-12):689–692, Nov. 2010.

W. J. Streit, S. A. Walter, and N. A. Pennell. Reactive microgliosis. *Progress in neurobiology*, 57(6):563–581, Apr. 1999.

M. Suzuki, M. Bannai, M. Matsumuro, Y. Furuhata, R. Ikemura, E. Kuranaga, Y. Kaneda, M. Nishihara, and M. Takahashi. Suppression of copulatory behavior by intracerebroventricular infusion of antisense oligodeoxynucleotide of granulin in neonatal male rats. *Physiology & behavior*, 68(5):707–713, Mar. 2000.

A. J. Svahn, M. B. Graeber, F. Ellett, G. J. Lieschke, S. Rinkwitz, M. R. Bennett, and T. S. Becker. Development of ramified microglia from early macrophages in the zebrafish optic tectum. *Developmental neurobiology*, 73(1):60–71, Jan. 2013.

Y. Tanaka, T. Matsuwaki, K. Yamanouchi, and M. Nishihara. Exacerbated inflammatory responses related to activated microglia after traumatic brain injury in progranulin-deficient mice. *Neuroscience*, 231C:49–60, Nov. 2012.

Y. Tanaka, T. Matsuwaki, K. Yamanouchi, and M. Nishihara. Increased Lysosomal Biogenesis in Activated Microglia and Exacerbated Neuronal Damage after Traumatic Brain Injury in Progranulin-Deficient Mice. *Neuroscience*, 250 (C):8–19, July 2013.

W. Tang, Y. Lu, Q. Y. Tian, Y. Zhang, F. J. Guo, G. Y. Liu, N. M. Syed, Y. Lai, E. A. Lin, L. Kong, J. Su, F. Yin, A. H. Ding, A. Zanin-Zhorov, M. L. Dustin, J. Tao, J. Craft, Z. Yin, J. Q. Feng, S. B. Abramson, X. P. Yu, and C. j. Liu. The Growth Factor Progranulin Binds to TNF Receptors and Is Therapeutic Against Inflammatory Arthritis in Mice. *Science (New York, NY)*, 332(6028):478–484, Apr. 2011.

L. Tapia, A. Milnerwood, A. Guo, F. Mills, E. Yoshida, C. Vasuta, I. R. Mackenzie, L. Raymond, M. Cynader, W. Jia, and S. X. Bamji. Progranulin deficiency decreases gross neural connectivity but enhances transmission at individual synapses. *Journal of Neuroscience*, 31(31):11126–11132, Aug. 2011.

G. Tasca, Z. Odgerel, M. Monforte, S. Aurino, N. F. Clarke, L. B. Waddell, B. Udd, E. Ricci, and L. G. Goldfarb. Novel FLNC mutation in a patient with myofibrillar myopathy in combination with late-onset cerebellar ataxia. *Muscle & nerve*, 46(2):275–282, Aug. 2012.

J. S. Taylor, I. Braasch, T. Frickey, A. Meyer, and Y. Van de Peer. Genome duplication, a trait shared by 22000 species of ray-finned fish. *Genome research*, 13(3):382–390, Mar. 2003.

H. Toh, B. P. Chitramuthu, H. P. J. Bennett, and A. Bateman. Structure, Function, and Mechanism of Progranulin; the Brain and Beyond. *Journal of molecular neuroscience : MN*, June 2011.

H. Toh, M. Cao, E. Daniels, and A. Bateman. Expression of the growth factor progranulin in endothelial cells influences growth and development of blood vessels: a novel mouse model. *PloS one*, 8(5):e64989, 2013.

B. Trevarrow, D. L. Marks, and C. B. Kimmel. Organization of hindbrain segments in the zebrafish embryo. *Neuron*, 4(5):669–679, May 1990.

B. Tucker, R. I. Richards, and M. Lardelli. Contribution of mGluR and Fmr1 functional pathways to neurite morphogenesis, craniofacial development and fragile X syndrome. *Human Molecular Genetics*, 15(23):3446–3458, Dec. 2006.

J. Tyynelä, I. Sohar, D. E. Sleat, R. M. Gin, R. J. Donnelly, M. Baumann, M. Haltia, and P. Lobel. A mutation in the ovine cathepsin D gene causes a congenital lysosomal storage disease with profound neurodegeneration. *The EMBO Journal*, 19(12):2786–2792, June 2000.

M. J. Ungurs, N. J. Sinden, and R. A. Stockley. Progranulin is a substrate for neutrophil-elastase and proteinase-3 in the airway and its concentration correlates with mediators of airway inflammation in COPD. *American journal of physiology. Lung cellular and molecular physiology*, 306(1):L80–7, Jan. 2014.

F. D. Urnov, E. J. Rebar, M. C. Holmes, H. S. Zhang, and P. D. Gregory. Genome editing with engineered zinc finger nucleases. *Nature reviews Genetics*, 11(9):636–646, Sept. 2010.

F. van Bebber, A. Hruscha, M. Willem, B. Schmid, and C. Haass. Loss of Bace2 in zebrafish affects melanocyte migration and is distinct from Bace1 knock out phenotypes. *Journal of neurochemistry*, 127(4):471–481, Nov. 2013.

P. Van Damme, A. Van Hoecke, D. Lambrechts, P. Vanacker, E. Bogaert, J. van Swieten, P. Carmeliet, L. Van Den Bosch, and W. Robberecht. Progranulin functions as a neurotrophic factor to regulate neurite outgrowth and enhance neuronal survival. *The Journal of Cell Biology*, 181(1):37–41, Apr. 2008.

A. M. van der Sar, H. P. Spaink, A. Zakrzewska, W. Bitter, and A. H. Meijer. Specificity of the zebrafish host transcriptome response to acute and chronic mycobacterial infection and the role of innate and adaptive immune components. *Molecular immunology*, 46(11-12):2317–2332, July 2009.

J. van der Zee, T. Van Langenhove, G. Kleinberger, K. Sleegers, S. Engelborghs, R. Vandenberghe, P. Santens, M. Van den Broeck, G. Joris, J. Brys, M. Mattheijssens, K. Peeters, P. Cras, P. P. De Deyn, M. Cruts, and C. Van Broeckhoven. TMEM106B is associated with frontotemporal lobar degeneration in a clinically diagnosed patient cohort. *Brain : a journal of neurology*, 134(3):808–815, Feb. 2011.

J. C. van Swieten and P. Heutink. Mutations in progranulin (GRN) within the spectrum of clinical and pathological phenotypes of frontotemporal dementia. *Lancet neurology*, 7(10):965–974, Oct. 2008.

A. Varki. Multiple changes in sialic acid biology during human evolution. *Glycoconjugate journal*, 26(3):231–245, Apr. 2009.

M. Vercellino, S. Grifoni, A. Romagnolo, S. Masera, A. Mattioda, C. Trebini, C. Chiavazza, L. Caligiana, E. Capello, G. L. Mancardi, D. Giobbe, R. Mutani, M. T. Giordana, and P. Cavalla. Progranulin expression in brain tissue and cerebrospinal fluid levels in multiple sclerosis. *Multiple Sclerosis Journal*, May 2011.

M. Vicente-Crespo and I. M. Palacios. Nonsense-mediated mRNA decay and development: shoot the messenger to survive? *Biochemical Society transactions*, 38(6):1500–1505, Dec. 2010.

C. Vignet, M.-L. Bégout, S. Péan, L. Lyphout, D. Leguay, and X. Cousin. Systematic screening of behavioral responses in two zebrafish strains. *Zebrafish*, 10(3):365–375, Sept. 2013.

H. Wang, Y. Sun, S. Liu, H. Yu, W. Li, J. Zeng, C. Chen, and J. Jia. Upregulation of progranulin by Helicobacter pylori in human gastric epithelial cells via p38MAPK and MEK1/2 signaling pathway: role in epithelial cell proliferation and migration. *FEMS immunology and medical microbiology*, June 2011.

A. C. Ward, D. O. McPhee, M. M. Condron, S. Varma, S. H. Cody, S. M. N. Onnebo, B. H. Paw, L. I. Zon, and G. J. Lieschke. The zebrafish spi1 promoter drives myeloid-specific expression in stable transgenic fish. *Blood*, 102(9): 3238–3240, Nov. 2003.

V. Warrier, M. Vieira, and S. E. Mole. Genetic basis and phenotypic correlations of the neuronal ceroid lipofusinoses. *Biochimica et biophysica acta*, 1832(11):1827–1830, Nov. 2013.

G. D. J. Watts, J. Wymer, M. J. Kovach, S. G. Mehta, S. Mumm, D. Darvish, A. Pestronk, M. P. Whyte, and V. E. Kimonis. Inclusion body myopathy associated with Paget disease of bone and frontotemporal dementia is caused by mutant valosin-containing protein. *Nature Genetics*, 36(4):377–381, Apr. 2004.

E. Wienholds, S. Schulte-Merker, B. Walderich, and R. H. A. Plasterk. Target-selected inactivation of the zebrafish rag1 gene. *Science (New York, NY)*, 297(5578):99–102, July 2002.

T. E. Willnow, C. M. Petersen, and A. Nykjaer. VPS10P-domain receptors - regulators of neuronal viability and function. *Nature reviews Neuroscience*, 9(12):899–909, Dec. 2008.

H. Wils, G. Kleinberger, S. Pereson, J. Janssens, A. Capell, D. Van Dam, I. Cuijt, G. Joris, P. P. De Deyn, C. Haass, C. Van Broeckhoven, and S. Kumar-Singh. Cellular ageing, increased mortality and FTLD-TDP-associated neuropathology in progranulin knockout mice. *The Journal of pathology*, 228(1):67–76, Sept. 2012.

A. Wimo, L. Jönsson, A. Gustavsson, D. McDaid, K. Ersek, J. Georges, L. Gulácsi, K. Karpati, P. Kenigsberg, and H. Valtonen. The economic impact of dementia in Europe in 2008-cost estimates from the Eurocode project. *Int J Geriatr Psychiatry*, 26(8):825–832, Aug. 2011.

N. Wittkopp, E. Huntzinger, C. Weiler, J. Saulière, S. Schmidt, M. Sonawane, and E. Izaurralde. Nonsense-mediated mRNA decay effectors are essential for zebrafish embryonic development and survival. *Molecular and Cellular Biology*, 29(13):3517–3528, July 2009.

C. Wittmann, M. Reischl, A. H. Shah, R. Mikut, U. Liebel, and C. Grabher. Facilitating drug discovery: an automated high-content inflammation assay in zebrafish. *Journal of visualized experiments : JoVE*, (65):e4203, 2012.

A. Xiao, Z. Wang, Y. Hu, Y. Wu, Z. Luo, Z. Yang, Y. Zu, W. Li, P. Huang, X. Tong, Z. Zhu, S. Lin, and B. Zhang. Chromosomal deletions and inversions mediated by TALENs and CRISPR/Cas in zebrafish. *Nucleic acids research*, June 2013.

J. Xie, E. Farage, M. Sugimoto, and B. Anand-Apte. A novel transgenic zebrafish model for blood-brain and blood-retinal barrier development. *BMC developmental biology*, 10:76, 2010.

J. Xu, M. Xilouri, J. Bruban, J. Shioi, Z. Shao, I. Papazoglou, K. Vekrellis, and N. K. Robakis. Extracellular progranulin protects cortical neurons from toxic insults by activating survival signaling. *Neurobiology of aging*, 32(12):2326.e5–16, Dec. 2011.

J. Xu, L. Du, and Z. Wen. Myelopoiesis during zebrafish early development. *Journal of genetics and genomics = Yi chuan xue bao*, 39(9):435–442, Sept. 2012.

Y.-G. Yeung and E. R. Stanley. A solution for stripping antibodies from polyvinylidene fluoride immunoblots for multiple reprobing. *Analytical biochemistry*, 389(1):89–91, June 2009.

F. Yin, R. Banerjee, B. Thomas, P. Zhou, L. Qian, T. Jia, X. Ma, Y. Ma, C. Iadecola, M. F. Beal, C. Nathan, and A. Ding. Exaggerated inflammation, impaired host defense, and neuropathology in progranulin-deficient mice. *Journal of Experimental Medicine*, 207(1):117–128, Jan. 2010a.

F. Yin, M. Dumont, R. Banerjee, Y. Ma, H. Li, M. T. Lin, M. F. Beal, C. Nathan, B. Thomas, and A. Ding. Behavioral deficits and progressive neuropathology in progranulin-deficient mice: a mouse model of frontotemporal dementia. *The FASEB journal : official publication of the Federation of American Societies for Experimental Biology*, 24(12): 4639–4647, Dec. 2010b.

N. Yoshinari and A. Kawakami. Mature and juvenile tissue models of regeneration in small fish species. *The Biological bulletin*, 221(1):62–78, Aug. 2011.

N. Yoshinari, T. Ishida, A. Kudo, and A. Kawakami. Gene expression and functional analysis of zebrafish larval fin fold regeneration. *Developmental Biology*, 325(1):71–81, Jan. 2009.

B.-S. Youn, S.-I. Bang, N. Klöting, J. W. Park, N. Lee, J.-E. Oh, K.-B. Pi, T. H. Lee, K. Ruschke, M. Fasshauer, M. Stumvoll, and M. Blüher. Serum progranulin concentrations may be associated with macrophage infiltration into omental adipose tissue. *Diabetes*, 58(3):627–636, Mar. 2009.

A. Zakrzewska, C. Cui, O. W. Stockhammer, E. L. Benard, H. P. Spaink, and A. H. Meijer. Macrophage-specific gene functions in Spi1-directed innate immunity. *Blood*, 116(3):e1–11, July 2010.

T. Zanocco-Marani, A. Bateman, G. Romano, B. Valentinis, Z. H. He, and R. Baserga. Biological activities and signaling pathways of the granulin/epithelin precursor. *Cancer research*, 59(20):5331–5340, Oct. 1999.

J. Zeller, V. Schneider, S. Malayaman, S.-i. Higashijima, H. Okamoto, J. Gui, S. Lin, and M. Granato. Migration of zebrafish spinal motor nerves into the periphery requires multiple myotome-derived cues. *Developmental Biology*, 252(2):241–256, Dec. 2002.

R. Zhang, J. Yang, J. Zhu, and X. Xu. Depletion of zebrafish Tcap leads to muscular dystrophy via disrupting sarcomere-membrane interaction, not sarcomere assembly. *Human Molecular Genetics*, 18(21):4130–4140, Nov. 2009.

Y.-P. Zhao, Q.-Y. Tian, S. Frenkel, and C.-J. Liu. The promotion of bone healing by progranulin, a downstream molecule of BMP-2, through interacting with TNF/TNFR signaling. *Biomaterials*, 34(27):6412–6421, Sept. 2013.

Y. Zheng, O. A. Brady, P. S. Meng, Y. Mao, and F. Hu. C-terminus of progranulin interacts with the beta-propeller region of sortilin to regulate progranulin trafficking. *PloS one*, 6(6):e21023, 2011.

J. Zhu, C. Nathan, W. Jin, D. Sim, G. S. Ashcroft, S. M. Wahl, L. Lacomis, H. Erdjument-Bromage, P. Tempst, C. D. Wright, and A. Ding. Conversion of proepithelin to epithelins: roles of SLPI and elastase in host defense and wound repair. *Cell*, 111(6):867–878, Dec. 2002.

Y. Zu, X. Tong, Z. Wang, D. Liu, R. Pan, Z. Li, Y. Hu, Z. Luo, P. Huang, Q. Wu, Z. Zhu, B. Zhang, and S. Lin. TALEN-mediated precise genome modification by homologous recombination in zebrafish. *Nature Methods*, 10(4): 329–331, Apr. 2013.

9 Danksagung

Vielen Dank ...

... Prof. Christian Haass für die wissenschaftliche Betreuung meiner Doktorarbeit. Ich finde es immer wieder beeindruckend, wie Sie das ganze Institut mit Ihrem Enthusiasmus und Ihrer Freude an der Forschung anstecken und motivieren. Vielen Dank für Ihre Unterstützung und die Möglichkeit an Ihrem Institut zu promovieren.

... Dr. Bettina Schmid für die direkte wissenschaftliche Betreuung meiner Doktorarbeit. Vielen Dank für all Deine Unterstützung und deine Korrekturarbeit. Danke, dass Du es mir ermöglicht hast, Konferenzen zu besuchen. Das war für dieses Projekt sehr wertvoll.

... den derzeit noch unbekannten Gutachtern dieser Doktorarbeit und den Mitgliedern der zukünftigen Prüfungskommission.

... Prof. Thomas Misgeld und Dr. Dieter Jenne, für die Zeit, die Sie in meine TAC-Meetings investiert haben, und Ihre hilfreichen Ratschläge.

... allen meinen Kooperationspartnern, Dr. Claire Russell, Kim Weger, Dr. Annemarie Meijer, Julien Rougeot, Dr. Rossella Di Giaimo, Dr. Jovica Ninkovic, Dr. Elisabeth Kremmer, Prof. Ciro Isidoro, Dr. Carlo Follo und Dr. Francesca Peri, für die erfolgreiche Zusammenarbeit und die Bereitstellung von Fischlinien und Reagenzien.

... allen derzeitigen und ehemaligen Mitgliedern der Zebrafisch-Gruppe für den Zusammenhalt und die angenehme Arbeitsatmosphäre. Es hat Spaß gemacht mit euch zusammenzuarbeiten. Den Tierpflegern, Daniela und Roberto, danke ich für die exzellente Versorgung der Zebrafische, und den TAs, Mathias und Kathi sowie dem PostDoc-TA 'Herr' Alex, für die Einweisung ins Labor, fachliche Diskussionen, ihre Unterstüzung bei Experimenten und ihre Fischarbeit. Den Hiwis, 'Frau' Alex, Rielana, Michi und Hanne, danke ich für diverse Genotypisierungen. Außerdem möchte ich Alexandra Rechenberg für ihre tolle Bachelorarbeit an *grn1* und *grn2* danken und meinen Praktikantinnen Elisabeth und Camilla für ihre Unterstüzung bei diesem Projekt. Meinen 'Büro'kollegen Dominik, Frauke, Katrin, Laura, Sophie und Yu danke ich für fachliche Diskussionen, jegliche Unterstützung und Spaß und Ratschereien zwischendrin und außerhalb des Instituts. Danke Frauke für die Korrektur dieser Arbeit.

... allen derzeitigen und ehemaligen Mitgliedern des Haass Labors, insbesonders natürlich allen aus dem 7. Stock für die gute Stimmung, fachliche Diskussionen, abwechslungsreiche Mittagspausen und spontane Partys. Ein besonderer Dank gilt Eva und Denise, die für Fragen zur Dissertation immer ein offenes Ohr hatten.

... Dr. Anja Capell und Dr. Sven Lammich für die Betreuung des Radioaktiv-Labors und die zugehörige Einweisung und Dr. Anja Capell und Kathrin Fellerer für die Hilfe bei den Zellkultur-Experimenten und für Zellkulturproben.

... Sabine Odoy für das exzellente Service und Barbara Kassner und Annette Schell für Rat und Tat mit Verträgen und allem was dazugehört.

... der Universität Bayern e.V. für das Stipendium, dem COST scientific program on EuFishBioMed für die Short Term Scientific Mission Fellowship und IMPRS-LS für die finanzielle Unterstützung. Sie hat mir den Besuch von Konferenzen und Workshops ermöglicht. Besonders möchte ich mich beim Koordinationsbüro von IMPRS-LS für die Organisation von erstklassigen und lehrreichen Workshops und Retreats bedanken. Das hat immer viel Spaß gemacht.

... all meinen Freunden, dafür das es euch gibt und wir so viel Schönes zusammen erleben dürfen. Ganz besonders möchete ich mich bei meinen Mädels aus der Schulzeit für unsere langjährigen Freundschaften bedanken. Ihr seid, jede für sich und alle zusammen, einzigartig.

... meinen Eltern, meiner Schwester und der erweiterten Familie, für den Rückhalt, die Unterstützung und die schöne gemeinsame Zeit, die wir immer wieder miteinander verbringen können.

10 Appendix

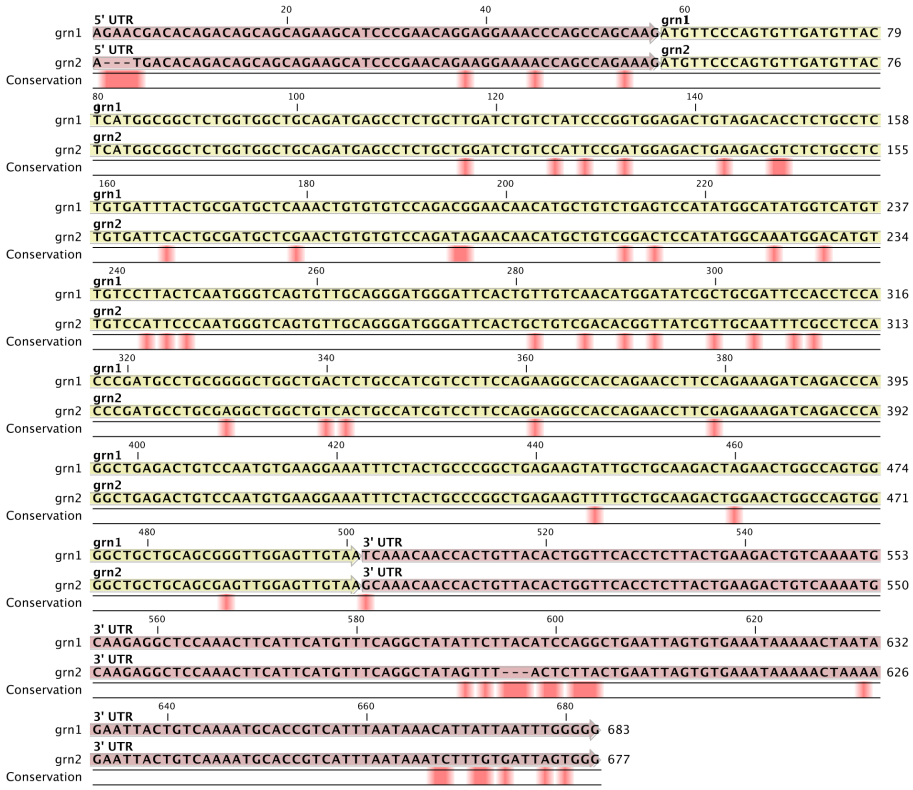

Figure 10.1 – *grn1* (ENSDART00000051972) and *grn2* (ENSDART00000051970) aligned with CLC Main Workbench. Red: 5'UTR or 3'UTR. Yellow: ORF. Red in conservation line: bp that are different.

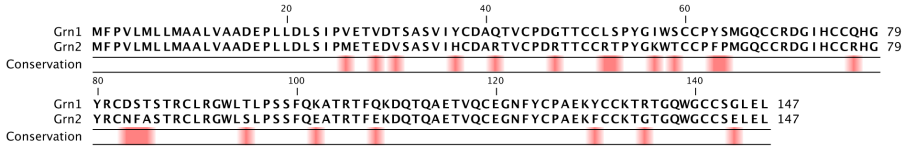

Figure 10.2 – Grn1 (ENSDARP00000051971) and Grn2 (ENSDARP00000051969) aligned with CLC Main Workbench. Red in conservation line: aa that are different.

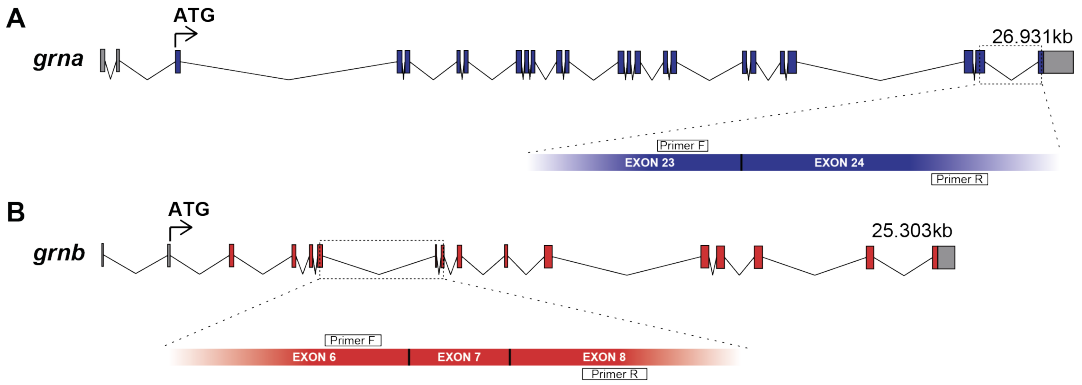

Figure 10.3 – Schematic representation of *grna* and *grnb* and the qPCR primer binding sites. The genomic structures of *grna* and *grnb* are depicted.

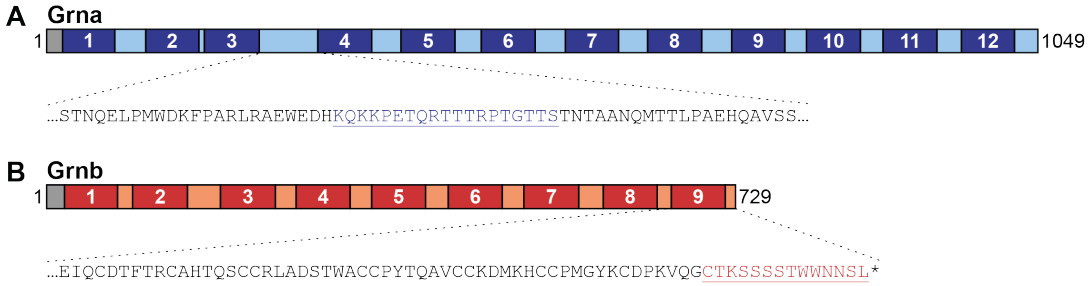

Figure 10.4 – Schematic representation of Grna and Grnb and the binding sites of the Grna and Grnb specific mAbs.

A *grna*

```
ATGTTGAGACTGACAGTCTGCCTCGCTGTGGTGACCCTGGTTATTTGCTCGCAGTGCCCCAATAATGAAGTCTGTGAAGCAGGCCAGT… WT
Founder_1752
ATGTTGAGACTGACAGTCTGCCTCGC:::::::::CCTGGTTATTTGCTCGCAGTGCCCCAATAATGAAGTCTGTGAAGCAGGCCAGT… Δ9
Founder_1755
ATGTTGAGACTGACAGTCa::::::::::::::GACCCTGGTTATTTGCTCGCAGTGCCCCAATAATGAAGTCTGTGAAGCAGGCCAGT… Δ13 (Δ14 and +1)
Founder_1758
ATGTTGAGACTGACAGTCTGCCTCGCTGTGGTtGACCCTGGTTATTTGCTCGCAGTGCCCCAATAATGAAGTCTGTGAAGCAGGCCAG… +1
Founder_1759
ATGTTGAGACTGACAGTCTGCCTCGC:::::::::CCTGGTTATTTGCTCGCAGTGCCCCAATAATGAAGTCTGTGAAGCAGGCCAGT… Δ9
ATGTTGAGACTGACAGTCTGCCTCGCTGgttatttGACCCTGGTTATTTGCTCGCAGTGCCCCAATAATGAAGTCTGTGAAGCAGGCC… +3 (Δ4 and +7)
ATGTTGAGACTGACAGTCTGCCTCGCTG::::::::::GTTATTTGCTCGCAGTGCCCCAATAATGAAGTCTGTGAAGCAGGCCAGT… Δ11
ATGTTGAGACTGACAGTCTGCCTCGCTGTG:TGACCCTGGTTATTTGCTCGCAGTGCCCCAATAATGAAGTCTGTGAAGCAGGCCAGT… Δ1
ATGTTGAGACTGACAGTCTGCCTCGCTGTG:::ACCCTGGTTATTTGCTCGCAGTGCCCCAATAATGAAGTCTGTGAAGCAGGCCAGT… Δ3
Founder_1760
ATGTTGAGACTGACAGTCTGCCTCGCTG::::::::::GTTATTTGCTCGCAGTGCCCCAATAATGAAGTCTGTGAAGCAGGCCAGT… Δ11
Founder_1761
ATGTTGAGACTGACAGTCTGCCTCGCTGTG:::ACCCTGGTTATTTGCTCGCAGTGCCCCAATAATGAAGTCTGTGAAGCAGGCCAGT… Δ3
Founder_1762
ATGTTGAGACTGACAGTCTGCC::::::::::ACCCTGGTTATTTGCTCGCAGTGCCCCAATAATGAAGTCTGTGAAGCAGGCCAGT… Δ11
ATGTTGAGACTGACAGTCTGCCT:::::::::GACCCTGGTTATTTGCTCGCAGTGCCCCAATAATGAAGTCTGTGAAGCAGGCCAGT… Δ9
ATGTTGAGACTGACAGTCTGCCTCGCTG::::::::::GTTATTTGCTCGCAGTGCCCCAATAATGAAGTCTGTGAAGCAGGCCAGT… Δ11
Founder_1765
ATGTTGAGACTGACAGTCTGCCTCGCTGTG:::ACCCTGGTTATTTGCTCGCAGTGCCCCAATAATGAAGTCTGTGAAGCAGGCCAGT… Δ3
Founder_1766
ATGTTGAGACTGACAGTCTGCCTCGCTGTG:::ACCCTGGTTATTTGCTCGCAGTGCCCCAATAATGAAGTCTGTGAAGCAGGCCAGT… Δ3
Founder_1767
ATGTTGAGACTGACAGTCTGCCTCG::::::::::CTGGTTATTTGCTCGCAGTGCCCCAATAATGAAGTCTGTGAAGCAGGCCAGT… Δ11
ATGTTGAGACTGACAGTCTGCCTCGCTGTG:::ACCCTGGTTATTTGCTCGCAGTGCCCCAATAATGAAGTCTGTGAAGCAGGCCAGT… Δ3
Founder_1768
ATGTTGAGACTGACAGTCTGCCTCGCTGTG:::ACCCTGGTTATTTGCTCGCAGTGCCCCAATAATGAAGTCTGTGAAGCAGGCCAGT… Δ3
Founder_1770
ATGTTGAGACTGACAGTCTGCCTg::::::::::::CCTGGTTATTTGCTCGCAGTGCCCCAATAATGAAGTCTGTGAAGCAGGCCAGT… Δ11 (Δ12 and +1)
ATGTTGAGACTGACAGTCTGCCTCGgttatttttacaCTGGTTATTTGCTCGCAGTGCCCCAATAATGAAGTCTGTGAAGCAGGCCAGT… +0 (Δ11 and +11)
ATGTTGAGACTGACAGTCTGCCTCGCTGTG:::ACCCTGGTTATTTGCTCGCAGTGCCCCAATAATGAAGTCTGTGAAGCAGGCCAGT… Δ3
Founder_1773
ATGTTGAGACTGACAGTCTGCCTCGCTGg:::GACCCTGGTTATTTGCTCGCAGTGCCCCAATAATGAAGTCTGTGAAGCAGGCCAGT… Δ3 (Δ4 and +1)
ATGTTGAGACTGACAGTCTGCCTCGCTGTG:TGACCCTGGTTATTTGCTCGCAGTGCCCCAATAATGAAGTCTGTGAAGCAGGCCAGT… Δ1
ATGTTGAGACTGACAGTCTGCCTCGCTGTG:::ACCCTGGTTATTTGCTCGCAGTGCCCCAATAATGAAGTCTGTGAAGCAGGCCAGT… Δ3
```

B *grnb*

```
…GATGATACCACCTGCTGCCAGATGCCTGATGGGGGGCTGGGGCTGCTGTCCTATGAAAAATGTAAAGCACTTTTTAAAAAAAAAATGC… WT
Founder_1620
…GATGATACCACCTGCTGCC:::::::TGATGGGGGGCTGGGGCTGCTGTCCTATGAAAAATGTAAAGCACTTTTTAAAAAAAAAATGC… Δ7
…GATGATACCACCTGCTGCCAGA:::::GATGGGGGGCTGGGGCTGCTGTCCTATGAAAAATGTAAAGCACTTTTTAAAAAAAAAATGC… Δ5
…GATGATACCACCTGCTGCCAGAT:::::::GGGGGGCTGGGGCTGCTGTCCTATGAAAAATGTAAAGCACTTTTTAAAAAAAAAATGC… Δ7
Founder_1621
…GATGATACCACCTGCTG:::::::::::::::GGGGGCTGGGGCTGCTGTCCTATGAAAAATGTAAAGCACTTTTTAAAAAAAAAATGC… Δ14
…GATGATACCACCTGCTGCCA:::::::::TGGGGGGCTGGGGCTGCTGTCCTATGAAAAATGTAAAGCACTTTTTAAAAAAAAAATGC… Δ9
…GATGATACCACCTGCTGCCAGATG::::ggggcagcaGGGGCTGCTGTCCTATGAAAAATGTAAAGCACTTTTTAAAAAAAAAATGC… Δ4(Δ13 and +9)
Founder_1622
…GATGATACCACCTGCTGCCAGAT:::::::GGGGGGCTGGGGCTGCTGTCCTATGAAAAATGTAAAGCACTTTTTAAAAAAAAAATGC… Δ7
…GATGATACCACCTGCTGCCAGAT::::::::::::::::::::::::::::::::::::::::::::::::::TTTTTAAAAAAAAAATGC… Δ46
Founder_1647
…GATGATACCACCTGCTGCCAG:::::::ATGGGGGCTGGGGCTGCTGTCCTATGAAAAATGTAAAGCACTTTTTAAAAAAAAAATGC… Δ7
…GATGATACCACCTGCTGCCAGATGC::::::::::::TGGGGCTGCTGTCCTATGAAAAATGTAAAGCACTTTTTAAAAAAAAAATGC… Δ11
Founder_1649
…GATGATA:::::::::::::::::::::::::GGGGCTGGGGCTGCTGTCCTATGAAAAATGTAAAGCACTTTTTAAAAAAAAAATGC… Δ24
…GATGATACCACCTGCTGCCAG::::::::::::::::::::::::::::::::::::::::::::::::::::::::AAAAAATGC… Δ57
Founder_1650
…GATGATACCACCTGCTGCC:::::::::::::::GGCTGGGGCTGCTGTCCTATGAAAAATGTAAAGCACTTTTTAAAAAAAAAATGC… Δ14
Founder_1654
…GATGATACCACCTGCTGCC::::::::::::::::::::::::::::::::::::::::::::::::::::::::::::::AAATGC… Δ62
…GATGATACCACCTGCTGCCAGAT:::::::GGGGGGCTGGGGCTGCTGTCCTATGAAAAATGTAAAGCACTTTTTAAAAAAAAAATGC… Δ7
Founder_1656
…GATGATACCACCTGCTGCCAcctgccacctgCTGATGGGGGGCTGGGGCTGCTGTCCTATGAAAAATGTAAAGCACTTTTTAAAAAAA… +6 (Δ5 and +11)
…GATGATACCACCTGCTGCCAGAT:::::::GGGGGCTGGGGCTGCTGTCCTATGAAAAATGTAAAGCACTTTTTAAAAAAAAAATGC… Δ7
…GATGATACCACCTGCTGCCAGATGCCTGgcctgATGGGGGCTGGGGCTGCTGTCCTATGAAAAATGTAAAGCACTTTTTAAAAAAAA… +5
```

Figure 10.5 – Sequences of ZFN-induced mutations that were detected in the F1 generation. **A**: Offsprings from 13 founder injected with ZFNs targeting *grna* were analysed and 13 different mutations were observed. **B**: Offsprings from 8 founder injected with ZFN targeting *grnb* were analysed and 15 different mutations were observed. **Δ**: deletion, **+**: insertion